Recent Trends in the Land Carbon Cycle

Submitted by
Guillermo Nicolas Murray-Tortarolo

To the University of Exeter as a thesis for the degree of Doctor of

Philosophy in Mathematics

In June 2015

I certify that all material in this thesis which is not my own work has been identified and that no material has previously been submitted and approved for the award of a degree by this or any other University.

Signature: .....

Abstract

Land ecosystems absorb about a quarter of all human emissions of carbon (C) by fossil fuel burning and land use change. This percentage varies greatly within years due to the land ecosystem response to climate variability and disturbance**.** Significant uncertainties remain in our knowledge of the magnitude and spatio-temporal changes in the land C sinks. The aims of my thesis are 1) to evaluate the capacity of different dynamic global vegetation models (DGVMs) to reproduce the fluxes and stocks of the land C cycle and 2) to analyse the drivers of change in the land C over the last two decades (1990-2009).

In the first part of this thesis I evaluated the DGVM results over two regions: the Northern Hemisphere (NH) and the Tropics. Over the NH DGVMs tend to simulate longer growing seasons and a greater positive leaf area index trend in response to warming than that observed from satellite data. For the tropical region we found a high spatial correlation between the DGVMs and the observations for C stocks and fluxes, but the models produced higher C stocks over the non-forested areas.

In the second part I studied the processes controlling the regional land C cycle. The findings can be summarized as: (1) the land CO_2 sink has increased over the study period, through increases in tropical and southern regions with negligible change in northern regions; (2) globally and in most regions, the land sinks are not increasing as fast as the growth rate of excess atmospheric CO_2 and (3) changes in water availability, particularly over the dry season, played a fundamental role in determining regional trends in NPP.

My work seeks to improve our understanding of the relationship between the C cycle and its drivers, however considerable research is needed to understand the role of additional processes such as land use change, nitrogen deposition, to mention just a few.

Acknowledgements

I am deeply thankful to my supervisors Prof. Pierre Friedlingstein and Prof. Stephen Sitch. They gave me this amazing opportunity and wisely guided me through the whole process. I will always be grateful for your guidance and support. I am privileged to have had you as my mentors and learned so much from you both.

I would not have been able to do this project without the multiple sources of funding I had. I am thankful to the Climate Change and Sustainable Futures research project at the University of Exeter, Consejo Nacional de Ciencia y Tecnologia (CONACyT), Consejo Estatal de Ciencia, Tecnologia e Industria de Michoacan (CECTI), Secretaria de Educacion Publica (SEP) and TERRABITES COST-ACTION for believing in me and funding my education.

I am also grateful with all my co-authors for their interest in my work and their valuable input. I would not have completed my PhD without their help along the way. Also I want to thank my fellow PhD students who share the office with me, for all the jokes and your friendship.

To my parents, whose love for knowledge fuelled my imagination and creativity.

To Victor, who made all of this possible.

Finally I will always be grateful to the two loves of my life. Fabiola, my beloved wife, and Guillermo, my beloved son, you are the motivation of my life and the only reason I try to be better everyday. Thank you for keeping me in the light.

Table of Contents

Abbreviations

C: Carbon

CH_4: Methane

CO_2: Carbon Dioxide

DGVMs: Dynamic Global Vegetation Models

DSI: Dry Season Intensity

DSL: Dry Season Length

ET: Evapotranspiration

ESM: Earth-System Models

ENSO: El Niño Southern Oscillation

FAPAR: Fraction of Active Photosintetically Radiation Absorbed

GPP: Gross Primary Productivity

GSL: Growing Season Length

IAV: interannual variability

ITCZ: Inter Tropical Conversion Zone

MCWD: Maximum Climatological Water Deficit

MRT: Mean Residence Time

MTE: Model Tree Ensemble

NH: Northern Hemisphere

NBP: Net Biome Productivity

NEP: Net Ecosystem Production

NPP: Net Primary Productivity

LAI: Leaf Area Index

LUC: Land Use Change

P: Precipitation

PDSI: Palmer Drought Severity Index

PFT: Plant Functional Type

Pg: Petagrams

RCP: Representative Concentration Pathway

Rh: Heterotopic Respiration

SPI: Standard Precipitation index

Tg: Teragrams

VOD: Vertical Optical Depth

WSI: Wet Season Intensity

WSL: Wet Season Length

INTRODUCTION

Chapter 1: Introduction

1.1 The Carbon Cycle on Earth

The recycling of elements is a key feature of our planet that allows the existence and continuation of life. All major nutrients cycle through the four components of the Earth system: air, land, water and living organisms. This is true for all elements, but particularly for the 6 main elements that constitute the building blocks of life: sulphur, hydrogen, oxygen, nitrogen, phosphorous and carbon (C).

C helps modulate atmospheric temperature and is fundamental to energy exchanges in living organisms. Firstly, it keeps the planet warm, the natural Earth's atmosphere has only about 0.3% (300 ppm) concentration of C, but this fraction, plus other greenhouse gases (such as water vapour and methane), are enough to keep the planet's temperature 15 degrees above what it would be in the absence of their presence in the atmosphere, allowing the existence of liquid water and life (Lovelock, 1987). The C components are responsible for 25% of this greenhouse effect (Rodhe, 1990). Secondly, C is fundamental to all living organisms, as part of their constitutive tissues (e.g. wood, leaves) and as a way to store and use energy.

The C cycles through the Earth system in three different components: the atmosphere, the ocean and the land. In its gaseous form, the primarily pool of C is in the inorganic form CO_2, with a burden of 760 PgC in the atmosphere (Ciais et al., 2013). This is also the most dynamic of all components, as it's natural lifetime –the time for a molecule to circulate through the atmosphere- is around 8 years, this short life-span of C in the atmosphere is primarily driven by the exchange of CO_2 with the oceans and the living organisms capturing and respiring it back (Moore and Braswell, 2012). However, it is important to note that the "residence time" of CO_2 in the atmosphere is much longer, a pulse of CO_2 in the atmosphere will be removed by the land and oceans owing multiple processes over centuries to millennia (Ciais et al. 2013)

In the oceans C has multiple forms (such as dissolved organic C, particulate organic C, and dissolved inorganic C), with up to 98% of all oceanic C in inorganic forms. The total pool of C in the ocean has been estimated at 38,000 PgC (Sarmiento and Gruber, 2006), out of which about 97% is concentrated in the deep oceans. In spite of representing a vast pool, the deep ocean C is relatively stable taking thousands of years to turnover. On the other

hand, the C exchange in the surface waters is more dynamic due to the quick exchange with the atmosphere. Finally, marine biota accounts for 3PgC but it is responsible for cycling 50-60PgCyr^{-1} due to is shorter lifetime of 5 weeks (Ciais et al., 2013).

Land C is contained mainly in organic forms, in the soil (1,500-2000 PgC) and the vegetation (360-650PgC) (Ciais et al., 2013; Liu et al. 2015). This C has a lifetime of about 10 years for the vegetation C and about 25 years for the soil C (Chapin et al. 2011). A large fraction of the land C is also contained in the frozen permafrost soils, with an estimated 1200 PgC in organic forms (Schuur et al., 2008), and also in peatlands and wetlands, with around 450 PgC.

The last pool of C is the soil contained on the Earth's crust and mantle. This represent at least 99% of all planetary C but its cycling, regulated by soil weathering, tectonic plate movement and volcanism makes it an extremely slow pool, with lifetimes of millions and thousand of millions of years (Chapin et al. 2011).

Over the shorter time periods (centuries, decades, inter and intra annual) the terrestrial C cycle is driven by photosynthesis and respiration by land vegetation (Keeling et al. 1995) and by the human activities (Le Quere et al., 2013, 2014). Human activities, in particular fossil fuel burning and land-use change, have altered the global C cycle. Changes in the C cycle in the atmosphere, oceans and land are shown in **Figure 1**. CO_2 in the atmosphere has increased from 280 at the onset of the industrial revolution to near 400 ppm today (that is an increase of 43%), which could be the highest concentration over the last 3-5 million years (Pearson & Palmer, 2000). The growth rate of atmospheric CO_2 has also gone up from 1% per year over 1990-1999 to 3% over 2001-2010 (Le Quere et al., 2013). The airborne fraction, the fraction of human emissions that remains in the atmosphere, is somewhere between 40-45% (Knorr, 2009).

Changes in the ocean C occurred mostly over the surface waters as an increase in dissolved inorganic C (Sarmiento et al., 1998). The process is driven by the difference in the partial pressure of CO_2 between the atmosphere and the oceanic water, through Henry's law. An increase of 1ppm of CO_2 in the atmosphere leads to a net uptake of 0.28ppm in the oceans, hence the ocean has been a net sink of C over the last 20 years, absorbing 28% of all human emissions (Le Quere et al., 2013) or about 2.4±0.7 PgCyr^{-1}. Based on modelling

work, the sink exhibits little interannual variability, mostly driven by changes in the sea surface temperature (Gruber et al., 2002).

The C stored in land ecosystems depends on the activity of plants and soil microbes but also on land use by humans. Before the industrial revolution, there was a balance between the biosphere and the atmosphere in the exchange of C: the entire flux of C that was captured through photosynthesis was eventually released back into the atmosphere via decomposition with a small fraction exported to oceans via the river system. As humans modified the system the tight balance was broken. The land began to absorb more C through mechanisms such as the CO_2 fertilization effect on photosynthesis, increases in nitrogen deposition stimulating plant growth, longer growing seasons due to warming and the reforestation of mid latitudes (Ciais et al., 2013). According to recent modelling estimtes, over the last two decades terrestrial ecosystems captured 1.6±1.0 $PgCyr^{-1}$ –different sources estimate similar values as detailed in the next section- or the equivalent to 22%-30% of total anthropogenic emissions (Le Quere et al. 2013). However, the human influence on the land-C is also negative, through deforestation and conversion of natural ecosystems into pastures and croplands, with emissions of 0.9 ± 0.8 $PgCyr^{-1}$ (Le Quere et al., 2013).

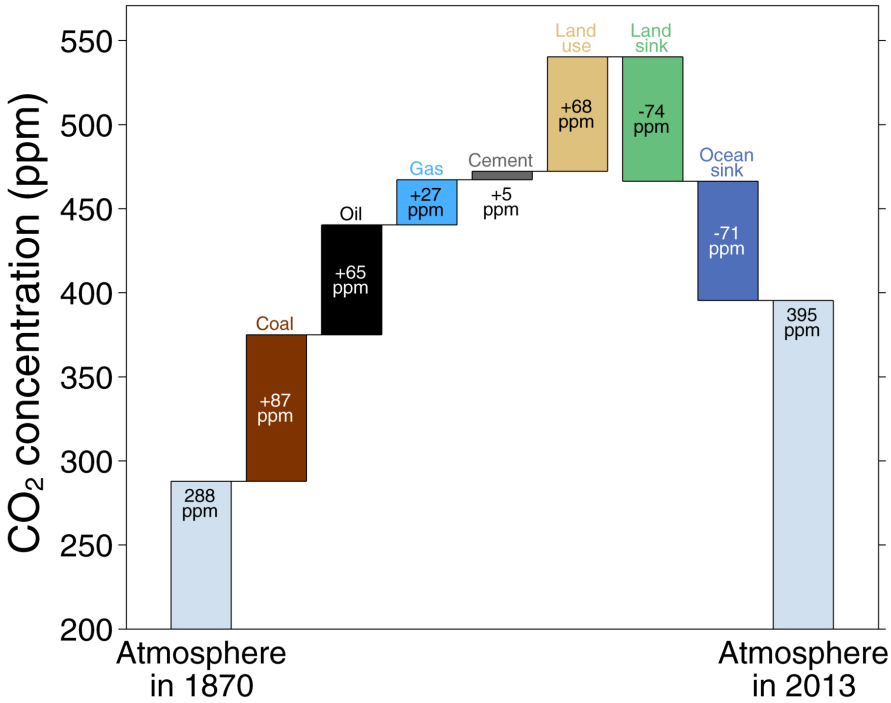

Figure 1.1. Global carbon emission and sinks from 1870-2013 in parts per million (ppm). Original image from the Global Carbon Budget 2014 (http://www.globalcarbonproject.org).

Considerable uncertainties remain in our knowledge of the magnitude and spatio-temporal changes in the land C sink (Ciais et al., 2013), particularly in the year-to-year variation. Modelling studies have suggested that the interannual variability (IAV) in atmospheric CO_2 is driven by the terrestrial ecosystems, which in turn is regulated by the variation in vegetation productivity -particularly over the semi-arid regions- (Keeling et al. 1995; Poulter et al. 2014, Ahlstrom et al. 2015). Several different drivers affect the land C at different scales and act in different directions: both increasing and decreasing CO_2 exchange between the land and atmosphere. Understanding the mechanisms behind variations in the IAV in the terrestrial C exchange, and its implications for the global C cycle for the future, are a key study for Earth-System science and the correct reproduction of future modelled scenarios (e.g. Cox et al. 2013).

1.2 Drivers of the terrestrial C cycle

In the absence of disturbance two main processes control the C dynamics in terrestrial ecosystems: photosynthesis and respiration. As much as 270 $PgCyr^{-1}$ passes through leaves each year, however only about 120 $PgCyr^{-1}$ are actually

fixed in the vegetation (Farquhar and Sharkey 1982). Half is then consumed by autotrophic respiration and the rest is used to sustain plant growth (leaves, roots and wood). The total uptake of C by the vegetation is the Net Primary Productivity (NPP), which accounts for about 60 $PgCyr^{-1}$; on the long-term virtually all of this returns to the atmosphere as heterotrophic respiration (Rh) or combustion by fires (Prentice et al., 2001) and a small fraction is lost as riverine fluxes (Regnier et al. 2014) –although this flux is not included in most global models-. The difference between NPP and Rh is called Net Ecosystem Production (NEP). When disturbance processes (natural such as fires or human induced such as land use change) are also considered, the Net Biome Productivity (NBP) represents the net exchange of C between the land and atmosphere usually applied at broader scales (Chapin et al. 2006).

$$NBP = NPP - Rh - LUC - Fire - other\ disturbances$$

Global NBP has been estimated from different sources. Recent modelling work estimate annual NBP between 1.6 ± 1.0 $PgCyr^{-1}$ (Le Quere et al., 2013; Ciais et al., 2013); results from atmospheric CO_2 inversions set the value at 1.65 ± 0.29 $PgCyr^{-1}$ (Gurney and Eckels, 2011; Pelyn et al., 2013); the flux can also be calculated indirectly from geophysical methods, using O_2/N_2 rations and the CO_2 concentration in the atmosphere Manning and Keeling (2006) estimated a value of 1.2 ± 0.8 $PgCyr^{-1}$; using mid-air vertical atmospheric CO_2 measurements the flux is estimated at 1.4 ± 1.4 $PgCyr^{-1}$ (Stephens et al., 2007); based on inventory-based data Pan et al. (2010) estimated a land uptake of 1.3 ± 0.2 $PgCyr^{-1}$; finally, the land-C flux can also be estimated by closing the C budget (as a reminder of the atmospheric CO_2 growth and the ocean uptake), thus resulting in an uptake of 1.5 ± 0.9 $PgCyr^{-1}$ (Sarmiento et al., 2010).

Altough some level of variation is found across estimates, all of them agree that land ecosystems generally had gained C over recent decades. However NBP shows high interannual and decadal variability. The interannual variations are driven by ecosystem response to climate variability (temperature, precipitation and radiation) and the decadal by changes in nutrient availability (e.g. nitrogen and phosphorus), land use and land cover changes (LUC) and disturbance (Ciais et al., 2013).

Change in atmospheric CO_2 concentration.

The main direct effect of CO_2 on land ecosystems is a boost in GPP, through increasing the photosynthetic rate of plants. On the leaf level, oxygen and CO_2 compete for the reaction place of RUBISCO, the carbon-fixing enzyme. As the relative partial pressure of CO_2 increases, the process becomes more efficient, reducing the oxygenase reaction rate (Farquhar and Sharkley, 1982). Through enhanced photosynthesis plants develop faster, and/or augmenting in size –or mass-, which ultimately translates into higher NPP, biomass and in addition more litter production. The process also enhances Rh as more C is available for decomposition, however the increase in NPP is faster than in Rh and the net C balance is a sink. In other words, rising atmospheric CO_2 translates to more C uptake by the terrestrial ecosystems. In the last 100 years, the CO_2 fertilization effect has been estimated to boots NPP by about 20-25% (Friedlingstein et al., 1995; Ainsworth and Long, 2005; Norby et al. 2005; Wang et al., 2012; Ciais et al., 2013).

Another impact of an increase in atmospheric CO_2 is a change in the water-carbon relationships of plants. The water-carbon trade-off is a basic metabolic feature of all plants, regulated by stomatal control. The central idea is that plants necessarily loose water in order to gain CO_2 for photosynthesis. A higher CO_2 concentration means that the plants gain more C per unit of water, in water-limited ecosystems this can result in longer growing seasons and higher annual NPP (Field et al. 1995). This may also lead to a small decrease in the evaporative fluxes and to a small increase in continental river runoff (Betts et al., 2007); however the effect of soil moisture limitation on evapotranspiration seems to have a larger role in controlling the land water fluxes (Jung et al., 2010).

The effects of climate variability and change

As a greenhouse gas, increasing atmospheric CO_2 leads to global warming and changes in the global water cycle. Temperature has increased by around 0.5-0.7 ºK during the last century, with higher values occurring over the land and the northern hemisphere (Ciais et al., 2013; Stocker et al., 2013) On the other hand, the increase in radiative forcing has accelerated the planetary water fluxes by 5% (or 8%/ºC) (Durack et al. 2012), leading to more extreme

seasonality (Chou et al. 2014) and a redistribution of global precipitation patterns (Zhang et al. 2007).

However the effects of climate change on the terrestrial C cycle are not fully understood. When the changes in the terrestrial C-cycle were attributed to the effects of changing temperature, precipitation and atmospheric CO_2 over recent decades (1980-2002), Piao et al (2009) found that CO_2 was responsible for at least 80% of the increase in both NPP and NBP. The effect of climate combined (temperature + precipitation change) was near zero, due to a balancing act of a positive precipitation effect and a negative from temperature. When analysing the effects of climate change in global NBP over the last century, as simulated by ESMs, Friedlingstein et al. (2006) found that the directional response was not clear, with models showing opposite trends.

Multiple contrary effects occur at the same time (e.g., an increase in T leads to enhanced RH, but also to longer growing seasons at high latitudes). As a consequence different model estimates produce contrasting results regarding the relative contribution of climate to the change in NBP in the long-term; however the increase in temperature usually leads to a loss of C from land ecosystems (Friedlingstein et al., 2006; Arora et al., 2013; Piao et al., 2013; Ciais et al., 2013). In addition the effect of climate change on land ecosystems –at least in the Northern Hemisphere- has lead to an increase in the atmospheric CO_2 amplitude, signalling a large change in ecosystem conditions (Graven et al., 2013).

Due to this uncertainty of terrestrial C cycle responses to climate in the historical period, it is not surprising that the simulated future response of land-C to climate change is also very different across models (Friedlingstein et al, 2006, 2014; Arora et al., 2013). The uncertainty arises from the strength of the climate-carbon feedbacks, but also from the strength of the CO_2 fertilization effect. There are at least four important global climate-C feedbacks that might alter current uptake trends: 1) The change in the rate of microbial respiration due to increased temperature, 2) the thawing of the permafrost and C release with global warming, 3) increases in regional drought and impact on land C cycle and 4) warming of the northern hemisphere (NH) and impact on the vegetation growing season.

The first happens because soil organic C decomposition depends on the activity of bacteria, which in turn depends on environmental conditions such as

temperature and moisture (Chapin et al. 2011). Under future scenarios warming may lead to faster respiration rates and quicker turnover times (Knorr et al. 2005). A warmer planet could potentially mean that the C residence time in soil is reduced. However, recent research has shown that ecosystem residence time also depend strongly on changes in the hydrological cycle (Carvalhais et al. 2014).

The second feedback is the thawing of the permafrost. As temperature increases the high latitude frozen soils start to thaw, allowing decomposition of previously frozen 'old carbon' stocks from the thawed soil. This could be a major C source in this century, since its estimated that the permafrost contains 1200 PgC (Schuur et al., 2008), from which approximately 50-250 PgC has been projected to be released by 2100 (Koven et al., 2011; Ciais et al., 2013; Stocker et al., 2013).

The third feedback concerns decreases in regional precipitation and/or warming, which would enhance surface and soil drying. Drought may also play an important role in the total C balance. Until recently drought trends were expected to increase in the future (Dai et al., 2012), contrary to the overall global precipitation trend, due to the fact that most of the 'new' rain will fall on the oceans (Sterl et al., 2008). As shown by Zeng et al. (2005), during the period 1998-2002 global NBP decreased by 0.9 PgC yr^{-1} due to several regional droughts in the Northern Hemisphere. A similar pattern was found for Amazon during 2005 and 2009 (Doughty et al. 2015). Additionally, this variation in the water cycle may induce enhanced plant mortality (Allen et al., 2010), which ultimately may change some ecosystems for being a C sink to a source. However there are still considerable uncertainties in our understanding of the relationship between the water and C cycles and recent publications suggest increasing drought may be largely driven by the natural variability of the climate system (Sheffield et al., 2013). In spite it seems that although drought may not increase in length due to climate change, it is likely that when it happens it will be quicker and more intense (Trenbeth et al., 2014)

The last feedback is an increase on the length of the growing season over the NH, due to early thawing of winter-snow, an early spring bud-burst and a later leaf shed, all consequences of global warming. Several model studies (e.g. Piao et al., 2007, Barichivich et al., 2013) and field data (Matsumoto et al., 2003) have found a lengthening of the growing season of about 1-4

days/decade over the northern hemisphere. The longer active period of plants could lead to increase C uptake, as leaves are able to photosynthesise for an extended period. Virtually all models agree that this increase in the NH growing season leads to more C uptake (Ciais et al., 2013), however it remains a challenge for DGVMs to represent the phenological cycle correctly (Richardson et al., 2011).

Fire

Fire in the Earth system is responsible for emitting ~2-3.2 PgC yr^{-1} (van der Werf et al. 2010), a quantity similar to total NBP. Due to this, it accounts for a significant proportion of the year-to-year variation in the land-atmosphere exchange (Prentice et al., 2011). The interannual variability of fire emissions is driven to changes in global temperature, precipitation, fuel load (Van der Werf et al., 2008; Pausas et al., 2012) and land-use change (Houghton et al., 2012). Interestingly the burned area and the total fire emissions are highly decoupled from year-to-year, total C emissions are driven primarily by forested areas, whereas burned area is largely controlled by savannah fires (Van der Werf et al., 2003), with both responding differently to human perturbation.

Nutrient control: nitrogen and phosphorus

Nitrogen (N) limits plant growth and microbial decomposition in most ecosystems worldwide (Vitousek et al., 1997), with phosphorous (P) playing a similar role over the savannahs (Reich and Olensky, 2004). Both nutrients are key regulators of the land C-balance and can drive plant productivity in nutrient-poor ecosystems (Fernandez-Martinez, et al., 2014). In spite most global models (DGVMs and ESMs) usually neglect their limiting effect and assume plant growth to be driven C-uptake trough photosynthesis (Reich et al., 2006), which leads to overestimating the land C-balance in future scenarios (Thorthon et al., 2007; Wieder et a., 2015). Recent studies have shown that when the full N and P cycles are taken into account, the C-uptake is reduced by 25% -19% due to N and 6% due to P- by the end of next century (Goll et al., 2012; Wieder et al., 2015).

On the other hand humans had more than doubled the amount of reactive N (Nr) that circulates the planet (Gruber and Galloway, 2008). This new Nr is likely to increase the C sink in terrestrial ecosystems to some extent (Sokolov et al., 2008). The effect is particularly important in grasslands (Felzer et al., 2011) and northern ecosystems (Kim et al., 2011) where cold conditions limit the rate of soil organic matter decomposition by microbes, i.e. the rate of N mineralization. Nonetheless, the widespread N-limitation is likely to reduce the land C uptake over future scenarios (Zaehle et al., 2010; Ciais et al., 2013).

Land use change

Land use change, through forest conversion into pastures and croplands, is one of the main drivers of the land C cycle (Hurtt et al. 2011). Presently, agriculture already covers 40% of the planet surface (Ramankutty and Foley, 1999). Current emissions from LUC represent 0.9±0.8 $PgCyr^{-1}$ (Friedlingstein et al., 2010; Le Quere et al., 2013). Land use change also has potential secondary effects such as: fire, change in species composition and nutrient depletion, which ultimately interact with vegetation, potentially decreasing its capacity to fix C.

Changes in all of these drivers have an anthropogenic component and while the global land C sink is estimated within well-known boundaries **(Figure 1.1)**, the regional differences in NBP and its drivers remains uncertain. One of

the possibilities to reduce this uncertainty is the usage of Dynamic Global Vegetation Models (DGVMs).

1.3 Dynamic Global Vegetation Models and the TRENDY initiative

Dynamic Global Vegetation Models (DGVMs) are process-based computer programs that simulate land fluxes of C, water fluxes and energy (in some cases also nitrogen) throughout the vegetation and the soil, as a response of changes in the climate, atmospheric CO_2 concentration, land use change and other disturbances (e.g. nitrogen deposition or fire). They do this based on a set of submodels representing key ecophysiological and disturbance processes (e.g. photosynthesis, allocation, soil C, vegetation competition, fire, etc.) that run at different time scales (e.g. photosynthesis is simulated typically every 30 seconds, fire every month) at a set spatial resolution (e.g. 0.5ºx0.5º).

DGVMs are widely employed in the literature to study different processes of the Earth system. For example they have been used to simulate the effect of volcanoes eruptions on plant productivity over the high-latitudes (Lucht et al. 2002), to measure the impacts of agriculture in the land C cycle (Bondeau et al. 2007) or to simulate fire dynamics and their impact on the vegetation (Thonicke et al. 2001). However possibly the main usage is to evaluate the terrestrial C cycle and its response to global climate change (e.g. McGuire et al., 2001, Sitch et al. 2008).

Modelling communities have developed their own DGVMs and while these models have many similarities in the way they represent some processes (e.g. most of them simulate photosynthesis based on the Farquar and Sharkey, 1982 or Collatz et al. 1991 equations), they differ in the way they represent different types of vegetation and their interaction, on parameterisations for many other processes (eg. phenology, allocation, mortality, litter and soil dynamics, etc) and in the number of processes they include (e.g. some include fire, nitrogen dynamics, vegetation dynamic and competition, etc) (Prentice et al. 2007; Sitch et al., 2008; Piao et al. 2013).

In order to better understand and constrain the response of the land-C cycle to climate change, agricultural usage and rising atmospheric CO_2, a consortium of modellers force their individual DGVMs under similar protocols. The “TRENDY” modelling group ran different DGVMs using the same forcing data and similar spin-up techniques to evaluate the change in terrestrial C cycle

over the last century. These results are central to my thesis as I evaluated and analysed these model output throughout my PhD.

1.4 Aims and research objectives

The first aim of my PhD thesis is to evaluate the results from the TRENDY project against observed data for particular processes of the land ecosystems and/or particular regions. This gives us a general overview of the underlying uncertainty of the models and the similarities and discrepancies between them.

The second aim is to analyse the processes driving the changes in the land C over the last decades. A particular focus has been paid to drought and changes in the dry season, as this was identified as a key driver of global vegetation processes and changes in NPP.

1.5 Specific Objectives

1. To evaluate the ability of the DGVMs to reproduce the phenological responses of the northern hemisphere to recent changes in temperature against observed satellite data.
2. To compare DGVM results with different observational data (e.g. forest inventories, satellite observations, fluxtower measurements) at continental (Africa) and regional (Mexico) scales, to produce estimates of change in NEP and NBP in the past and the possible implications for the future.
3. To investigate the evolution of the land C cycle over the past two decades and to attribute the relevant part to its drivers (e.g. climate variability and change) over the same time period.
4. To analyse the impacts of changing drought in the vegetation (NPP) over the last century, recent decades (1989-2005) and the reminder of the 21st century.

1.6 Thesis structure and main findings

My thesis is divided in six chapters, each containing four sections: introduction, model evaluation, process analysis and conclusions. The first chapter is a review of the relevant literature on the C cycle and the land component. Chapters 2 and 3 represent a compendium guided by the evaluation of the DGVMs, Chapter 4 and 5 are based on the analysis of different processes that drive the land C cycle, and chapter 6 are the general conclusions of the thesis.

Chapter 2 focuses on the changes in the growing season over the NH over a span of 20 years (1986-2005). This chapter raises the questions: how well can models reproduce changes in phenology over the NH? Is uncertainty DGVM structure (ie growth and phenology parametrisation) more important than uncertainty in simulated climate when aiming to reproduce LAI in the NH?

Chapter 3 consists of a comparison of model results with satellite and field data at two different spatial scales over the tropics (continental and country-level). We focused on targeting the questions of how well DGVMs reproduce continental (Africa) and country (Mexico) level estimates for the land C fluxes and pools? Can we improve current estimates by adding model-based information?

Chapter 4 contains results for recent trends (1990-2009) in the land C pools and fluxes. This chapter focuses on the main drivers for the land-C flux over this time period.

Chapter 5 investigates the link between changes in dryness and vegetation productivity globally over multiple time-scales, using novel dryness metrics.

Chapter 6 contains the conclusions and discussion of the thesis, with a particular emphasis on the key findings, limitations of my study and the opportunities for further research. I also included the main contribution of my work to the research field.

1.7 Contribution to co-authored papers

I led three papers and co-authored another three, relevant for my PhD Thesis.

Those are:

1. Murray-Tortarolo, Guillermo, Alessandro Anav, Pierre Friedlingstein, Stephen Sitch, Shilong Piao, Zaichun Zhu, Benjamin Poulter et al. "Evaluation of land surface models in reproducing satellite-derived LAI over the high-latitude Northern Hemisphere: Part I: Uncoupled DGVMs." *Remote Sensing* 5, no. 10 (2013): 4819-4838.

2. Anav, Alessandro, G Murray-Tortarolo, Pierre Friedlingstein, Stephen Sitch, Shilong Piao, and Zaichun Zhu. "Evaluation of Land Surface Models in Reproducing Satellite Derived Leaf Area Index over the High-Latitude Northern Hemisphere. Part II: Earth System Models." *Remote Sensing* 5, no. 8 (2013): 3637-3661.

3. Valentini, R., Arneth, A., Bombelli, A., Castaldi, S., Cazzolla Gatti, R., Chevallier, F., Ciais, P., Grieco, E., Hartmann, J., Henry, M., Houghton, R.A., Jung, M., Kutsch, W.L., Malhi, Y., Mayorga, E., Merbold, L., Murray-Tortarolo, G., Papale, D., Peylin, P., Poulter, B., Raymond, P.A., Santini, M., Sitch, S., Vaglio Laurin, G., van der Werf, G.R., Williams, C.A., Scholes, R.J., 2014. A full greenhouse gases budget of Africa: synthesis, uncertainties, and vulnerabilities. *Biogeosciences* 11, 381–407. doi:10.5194/bg-11-381-2014

4. Murray-Tortarolo, Guillermo, Victor J Jaramillo, Fabiola Murguia-Flores, Pierre Friedlingstein, Stephen Sitch and Alessandro Anav. “The Full Carbon Cycle of Mexico: Present, Past and Future”. In preparation.

5. Sitch, S., P. Friedlingstein, N. Gruber, S. D. Jones, G. Murray-Tortarolo, A. Ahlström, S. C. Doney et al. "Trends and drivers of regional sources and sinks of carbon dioxide over the past two decades." *Biogeosciences* (2015): 20113-20177.

6. Murray-Tortarolo, Guillermo, Brigitte Mueller, Imogen Fletcher, Sonia Seneviratne, Stephen Sitch, Pierre Friedlingstein, Alessandro Anav et al. “Changes in the Dry Season Intensity are a Key Driver of Global NPP Trends”. Submitted to Nature Geosciences.

The first two papers are contained in chapter 2, they represents part 1 and 2 of the same study. The study was designed by Alessandro Anav and myself with important contributions from Pierre Friedlingstein, Stephen Sitch, Shilong Piao and Zaichun Zhu. Additional co-authors were responsible for providing LAI data for the individual DGVMs and contributing to the writing of the papers. I was responsible for the execution and writing of the first part (uncoupled DGVMs)

and Alessandro Anav for the second part (coupled ESMs). Both papers have been published in the open access journal *Remote Sensing*.

Results from papers 3 and 4 are part of chapter 3. The greenhouse gas budget of Africa was designed and executed by Riccardo Valentini (University of Tuscia) as part of the Regional Carbon Cycle Assestement and Processes (RECCAP) initiative. I contributed with estimates and maps for individual models and ensemble for NEP and NPP (Figures 4 and 5 on the main paper), and the analyses of model results. The paper has been published in the open access journal *Biogeosciences.* An extraction of these results, comparing NEP with atmospheric inversions is contained in chapter 3. The fourth paper considers the full C cycle of Mexico for the present, past and future, and was designed and executed by myself. It benefits from ideas and analysis from the rest of the co-authors. It compares results from field, satellite, fluxtowers and DGVM data to give an estimate of the country's C stocks and fluxes. This paper is in progress and its included in chapter 3.

Co-authored paper number 5 is my chapter number 4. Stephen Sitch and Pierre Friedlingstein designed the original TRENDY experiments. I was involved in this study from the beginning of my PhD and throughout the first year. I contributed with the preparation of all the figures and partially in the analysis for trends and fluxes of individual models. The study has been published in the open-access journal *Biogeosciences*.

Finally, paper number 6 is chapter number 5. This study was designed and executed by myself, again with input from co-authors. I dedicated most of my PhD to the study of the impacts of drought on vegetation processes contained here. This paper is the culmination of these efforts and shows a clear link between changes in the length and intensity of the dry season and the trend in NPP. The paper has been submitted to the journal *Nature Geosciences*.

Furthermore I contributed to three additional studies as part of my PhD, however they were slightly beyond the mainscope of my thesis, hence I decided not to include them in the present manuscript. The papers are:

1. Anav A, Friedlingstein P, Beer C, Ciais P, Harper A, Jones C, Murray-Tortarolo G, Papale D, Parazoo NC, Peylin P et al (2015) Spatio-temporal patterns of terrestrial gross primary production: a review. Rev Geophys. doi:10. 1002/ 2015RG000483

2. Fletcher, I, et al. A novel index of potential fire based on the productivity-aridity gradient. *Submitted to Earth System Dynamics*.

3. Quijas, S, et al. Modelling Ecosystem Services Based on the LPJ-ml DGVM. Submitted to *Ecosystems.*

PART 1: MODEL EVALUATION

Chapter 2. Evaluation of DGVMs and ESMs in reproducing satellite derived LAI over the Northern Hemisphere

Chapter 3. Comparing model results against different observations at multiple spatial scales: the case of the pantropic.

Two chapters comprise part one of this thesis, guided by the need to evaluate the ability of DGVMs in reproducing observed data. Model evaluation usually consists of an assessment of individual models at different time and spatial scales. The temporal component comprises an analysis on seasonality, IAV and long-term trends, while the spatial component is based on anomaly maps and zonal averages (Anav et al. 2013).

There are several examples of model evaluation in the literature. For example Peng et al. (2015) evaluated the seasonality of CO_2 fluxes for nine DGVMs and found that most models tend to overestimate GPP and Rh when compared with 16 FLUXNET sites. As a result models tend to underestimate NBP and the seasonal amplitude. Anav et al. (2013) found a similar result when analysing the carbon component of ESMs, with higher GPP and LAI in the models than the observations. Another example is the paper by Cadule et al. (2010), here the authors evaluated the land component of three ESMs and found different strengths and weaknesses of each model depending on the time scale.

The second chapter follows the traditional model evaluation at different time scales (seasonal, IAV and long-term) on the ability of the models in reproducing LAI and growing season metric related over the Northern Hemisphere. I compared 8 models from the TRENDY ensemble and 11 ESM models for the period 1985-2005 with satellite observations of LAI for their seasonal amplitude, maximum LAI, growing season onset, offset and growing season length (GSL), and for the trend in LAI and the GSL.

For the third chapter I evaluated NEP over Africa, comparing the results from 9 DGVMs against CO_2 atmospheric inversions. However because inversions are calculated annually, only long-term trend and the spatial differences between products were analysed. For the second part of the chapter, I compared the C stored in Mexico (vegetation and soil) calculated from the models against field data from 4000 points. Again, because field sampling is complicated in terms of time and money, only one year of data is available (2000), so the evaluation was again centered only in spatial differences. The chapter then follows to an analisys on the changes in the C stocks over the last 60 years and over the reminder of the century based on modelled results.

Chapter 2: Evaluation of DGVMs and ESMs in reproducing satellite derived LAI over the Northern Hemisphere

2.1 Summary

Leaf Area Index (LAI) represents the number of leaf layers in an ecosystem and it is key in the coupling of the land surface to the atmosphere. LAI does not remain constant over the year, and its seasonality is driven by temperature over the Northern Hemisphere (NH) and by precipitation over the tropics (Anav et al. 2013). Recent climate change, particularly warming over the NH has led to changes in seasonal LAI. Generally, the warmer temperature leads to earlier spring budburst (Schwartz et al. 2006), i.e. leaf onset, which translates into longer growing seasons (Linderholm, 2006) and a higher mean annual LAI.

Models differ in the way they represent phenology and an integral evaluation over the NH is missing. The objective of this chapter was to fill this informationg gap. In particular, I wanted to know the role of structural uncertainty (i.e. differences in model parametrization and processes included) against the uncertainty induced by climate in the different ESMs. In order to do this, I compared different LAI metrics against satellite obserbations for the period 1985-2005 over the NH. I used 8 DGVMs from the TRENDY compendium and 11 ESMs from CMIP5.

The main results can by summarized as: 1) all models (ESMs and DGVMs) tend to overestimate GSL, onset and offset as well as the trend in LAI and GSL, particularly over the boreal forest and 2) errors introduced by DGVMs structure are greater than those introduced by different simulated climate by ESMs.

Remote Sens. **2013**, *5*, 1-x manuscripts; doi:10.3390/rs50x000x
OPEN ACCESS
Remote Sensing
ISSN 2072-4292
www.mdpi.com/journal/remotesensing
Article

Evaluation of Land Surface Models in Reproducing Satellite-Derived LAI over the High-Latitude Northern Hemisphere. Part I: Uncoupled DGVMs

Guillermo Murray-Tortarolo [1,*], Alessandro Anav [1], Pierre Friedlingstein [1], Stephen Sitch [2], Shilong Piao [3], Zaichun Zhu [4], Benjamin Poulter [5], Soenke Zaehle [6], Anders Ahlström [7], Mark Lomas [8], Sam Levis [9], Nicholas Viovy [5] and Ning Zeng [10]

[1] College of Engineering, Mathematics & Physical Sciences, University of Exeter, Harrison Building, North Park Road, Exeter EX4 4QF, UK; E-Mails: A.Anav@exeter.ac.uk (A.A.); P.Friedlingstein@exeter.ac.uk (P.F.)
[2] College of Life and Environmental Sciences, University of Exeter, Amory Building, Rennes Drive, Exeter EX4 4RJ, UK; E-Mail: S.A.Sitch@exeter.ac.uk
[3] Department of Ecology, Peking University, Beijing 100871, China; E-Mail: slpiao@pku.edu.cn
[4] Department of Earth and Environment, Boston University, 675 Commonwealth Avenue, Boston, MA 02215, USA; E-Mail: zhu.zaichun@gmail.com
[5] Laboratoire des Sciences du Climat et de l'Environnement, CEA CNRS UVSQ, Gif-sur-Yvette 91191, France; E-Mails: benjamin.poulter@lsce.ipsl.fr (B.P.); nicolas.viovy@lsce.ipsl.fr (N.V.)
[6] Max Planck Institute for Biogeochemistry, P.O. Box 10 01 64, Jena 07701, Germany;
E-Mail: szaehle@bgc-jena.mpg.de
[7] Department of Physical Geography and Ecosystem Science, Lund University, Sölvegatan 12, SE 22362, Lund; E-Mail: anders.ahlstrom@nateko.lu.se
[8] Department of Animal & Plant Sciences, University of Sheffield, Sheffield S10 2TN, UK;
E-Mail: m.r.lomas@sheffield.ac.uk
[9] National Center for Atmospheric Research, Boulder, CO80305, USA; E-Mail: slevis@ucar.edu
[10] Department of Atmospheric and Oceanic Science, University of Maryland, College Park,
MD 20740, USA; E-Mail: zeng@umd.edu

* Author to whom correspondence should be addressed; E-Mail: gnm202@ex.ac.uk;

Received: 15 August 2013; in revised form: 9 September 2013 / Accepted: 17 September 2013 /
Published: 18 September 2013

Abstract: Leaf Area Index (LAI) represents the total surface area of leaves above a unit area of ground and is a key variable in any vegetation model, as well as in climate models. New high resolution LAI satellite data is now available covering a period of several decades. This provides a unique opportunity to validate LAI estimates from multiple vegetation models. The objective of this paper is to compare new, satellite-derived LAI measurements with modeled output for the Northern Hemisphere. We compare monthly LAI output from eight land surface models from the TRENDY compendium with satellite data from an Artificial Neural Network (ANN) from the latest version (third generation) of GIMMS AVHRR NDVI data over the period 1986–2005. Our results show that all the models overestimate the mean LAI, particularly over the boreal forest. We also find that seven out of the eight models overestimate the length of the active vegetation-growing season, mostly due to a late dormancy as a result of a late summer phenology. Finally, we find that the models report a much larger positive trend in LAI over this period than the satellite observations suggest, which translates into a higher trend in the growing season length. These results highlight the need to incorporate a larger number of more accurate plant functional types in all models and, in particular, to improve the phenology of deciduous trees.

Keywords: LAI; land surface models; growing season; trendy; northern hemisphere; phenology

---

1. Introduction

Leaf Area Index (LAI) is the number of leaf layers per unit area in an ecosystem. It is widely used in the coupling of land surface and atmospheric processes, such as radiation, precipitation interception [1] and gas exchange [2]. There are several methods to estimate LAI [3], including direct observation and the use of modern radiometers. However, at global scale satellite products are arguably the most important. LAI is a key variable of energy and water balance

calculations in vegetation models [4]. It influences numerous model outputs such as net primary productivity (NPP), evapotranspiration (ET), the fraction of the light being absorbed by plants (FAPAR) and nutrient dynamics [5]. Land Surface Models (LSMs) have different approaches for calculating LAI, and while the use of plant functional types (PFTs) is widespread [6], there are important differences in the number of simulated PFTs, their spatial distribution and the representation of vegetation dynamics [7].

LSMs differ in the number of PFTs they include [8], and typically divide vegetation into between 4 and 16 PFTs. The number of PFTs and their parameterization leads to important discrepancies in the distribution of the vegetation types [9]. In addition, models vary in their representation of functional trade-offs and plant responses to the environment [10]. The former creates a trade-off between the number of modeled PFTs and their correct representation: using many PFTs leads to an increased uncertainty due to their parameterizations, while an insufficient number results in a misrepresentation of vegetation dynamics. One example of this is the ratio of evergreen to deciduous boreal forest in the Northern Hemisphere, or the ratio of evergreen forests to grasslands over the tropics; the distribution of these have important implications for future climate prediction, as shown by Sitch *et al.* [7,11].

There are several studies that have compared model results with satellite data [11–13].

Buermann *et al.* [12] compared the NCAR-CC3 model with satellite data and found that the model partitioning of latent and sensible heat fluxes create discrepancies in the CO_2 fluxes, which lead to an overestimation of the modeled growing season length (GSL). In another example, Richardson *et al.* [14] compared phenology measurements of ten forests sites in USA with fourteen vegetation models; they found that the models overestimated the length of the growing season, while correctly reproducing the CO_2 fluxes due to an underestimation of the LAI peak. Finally, Randerson *et al.* [15] found that models underestimate the carbon uptake during the growing season in boreal forest ecosystems due to tardiness in the LAI peak.

One of the main reasons for the lack of comparison between model outputs and satellite observations is data limitation. While satellites have been recording vegetation growth since the 1980s, the data were difficult to use due to frequent missing values. The first complete satellite global timeseries did not appear until 1991 [16,17]. These products were initially used to validate simple climatic models of vegetation distribution [12], but their usage has increased steadily in a range of applications. For example, they are used to estimate the biomass of grasslands [18], boreal forests [19] and mangroves [20].

During this time, LSMs continued to develop in sophistication and diversity [21]. While the core processes represented in these models remain similar, they vary greatly in their parameterization. This is particularly true in the responses to

temperature and drought. Moreover, refined observational forcing data have become widely available. This allows LSMs to be run offline using observed climatology, as in this paper, or offline with self-generated climatology as part of an Earth-System-Model (ESM) (as in Part II of this study, Anav et al. [22]). Running offline allows the uncertainty corresponding to process representation to be isolated from climate-related uncertainties, which ultimately can be use to improve ESMs and future climatic projections. This evaluation is key in model development.

One important process that remains to be evaluated is the lengthening of the growing season over the Northern Hemisphere. This has been observed by several authors in satellite, modeled and field data [23,24]. Changes in seasonal variation and the mean values of LAI, mostly due to an increase in temperature at the beginning of the growing season, have important implications on the global carbon cycle. However, considerable uncertainty remains with regard to greening trends and the ability of models to reproduce satellite-derived trends.

With new and improved LAI data now available [25–28], a more precise validation of model output is imperative. The objective of this paper is to compare LAI from satellite-derived measurements with modeled output from a set of 8 LSMs over the Northern Hemisphere. We ask three questions to fulfill this objective:

- Do uncoupled (LSMs) models correctly reproduce the spatial variability of LAI shown by satellite data over the Northern Hemisphere?
- How does the length of the growing season in the different models compare with the satellite data? And where are the main discrepancies (onset or dormancy)?
- What are the trends in LAI and the growing season over this period?

2. Materials and Methods

2.1. Model Data

We use monthly LAI output from eight LSMs from the TRENDY compendium [8]. The models differ in the way they simulate and parameterize several processes (Table 1) and in the way they calculate LAI. All of the models were forced using the same observed climatic and CO_2 data (corrected CRU v3.1 merged with NCEP) and simulated two experiments over the last century:

- S1: real CO_2 growth and climate kept constant, recycling the first 10 years of the century.
- S2: real CO_2 and climate. In the present study we use the S2 simulations. All model outputs were regridded to a common 1 × 1 degree grid. Although satellite data are available before 1986, we focus on the last 20 years of the 20th century simulations (1986–2005) to be consistent with the analyses of the coupled models (Anav et al., this issue [22]).

Table 1. Characteristics of the eight dynamic global vegetation models (re-drawn from Sitch *et al.* [8]).

Model Name	Abbreviation	Spatial resolution	Number of PFTs	Vegetation	Fire dynamics	Full Nitrogen Cycle	Reference
Community Land Model 4CN	CLM	0.5° × 0.5°	16	Imposed	Yes	Yes	[29]
Lund-Potsdam-Jena	LPJ	0.5° × 0.5°	11	Dynamic	Yes	No	[6]
LPJ-GUESS	GUESS	0.5° × 0.5°	11	Dynamic	Yes	No	[30]
ORCHIDEE-CN	OCN	3.75° × 2.5°	12	Imposed	Yes	Yes	[31]
ORCHIDEE	ORC	0.5° × 0.5°	12	Imposed	No	No	[32]
Sheffield-DGVM	SDGVM	3.75° × 2.5°	6	Imposed	Yes	No	[33]
TRIFFID	TRI	3.75° × 2.5°	5	Dynamic	No	No	[34]
VEGAS	VEG	0.5° × 0.5°	4	Dynamic	No	No	[35]

2.2. LAI Parameterization and Calculation

Models differ in the way they calculate LAI, but all of them reported 1-sided LAI and use
self-calculated LAI, independent from the satellite measurements. Their main difference is the choice of imposed or dynamic vegetation. The former uses a land-cover map to generate PFT categories, while the latter generates PFT categories based on climatic and competition dynamics.

- CLM4CN. The model has 16 PFTs. In this version the carbon-nitrogen cycling model simulates leaf carbon and specific leaf area to calculate the LAI for each PFT.
- LPJ. The leaf area index is updated daily and depends on temperature, soil water, and plant productivity for each PFT. The models have 3 different phenology types (evergreen, summergreen, raingreen) and 11 PFTs.
- LPJ-GUESS. The leaf area index is updated daily and depends on temperature, soil water, and plant productivity for each PFT. The models have 3 different phenology types (evergreen, summergreen, raingreen) and 11 PFTs.
- ORCHIDEE. LAI is estimated based on temperature. It also uses a maximum LAI threshold after which no more carbon is allocated to the leaves.
- OCN employs an approach based on the pipe-model for allocation, which results in much more rapid leaf development, and does not prescribe a maximum leaf area-rather, the maximal annual LAI is an emergent outcome of the NPP of the vegetation and the costs (roots, shoot) for maintaining the leaf area, which varies as a function of water and nitrogen stress.
- SDGVM. LAI is calculated to optimize stem & root NPP. This is achieved through consideration of the net carbon balance of the bottom layer of the canopy. The fraction of NPP available for leaf production is adjusted each year based on this carbon balance. The rate at which this fraction is adjusted is PFT-dependent.
- TRIFFID. LAI is calculated for each of the 5 PFTs, based on parameters describing the minimum, maximum and balanced LAI if full cover is reached. The actual LAI is then calculated as a function of the balanced LAI and the phonological status of the vegetation, which depends on temperature.
- VEGAS. The model has five PFTs: broadleaf tree, needleleaf tree, C3 grass, C4 grass, and crop. Whether a tree PFT is deciduous or evergreen is dynamically determined, so it has essentially 7 functional types. Phenology is calculated for each PFT as the balance between growth and

respiration. The actual leaf mass is calculated based on photosynthesis allocation, and then converted to leaf area index.

2.3. Satellite Data

The LAI data set used in this study was generated using an Artificial Neural Network (ANN) from the latest version (third generation) of the GIMMS AVHRR NDVI data for the period July 1981 to December 2010 at a 15-day frequency (Zhu *et al.* this issue [36]). The ANN was trained with best-quality Collection 5 MODIS LAI product and corresponding GIMMS NDVI data for an overlapping period of 5 years (2000 to 2004) and then tested for its predictive capability over another five year period (2005–2009). The average uncertainty of the MODIS LAI product is estimated to be 0.66 LAI units [24], though it varies depending on the mean LAI, and the data is for 1-sided LAI; further details are provided in Zhu *et al.* [36]. The 10 years of MODIS LAI/FPAR (2000–2009) was further processed to generate climatology. The ANN was further trained on the climatology fields. The NDVI3g data have now a 30-year history of development. The data was further regridded to the same 1 × 1 grid, using a linear interpolation; all missing values were filtered when average over a coarser resolution.

2.4. Study Region

The main focus of this study is the high northern extra-tropics. This area was chosen due to the fact that satellite data is more reliable over this region than others, because there are fewer clouds. Additionally, we want to study the response of phenology to temperature and there are no clear seasonal changes in vegetation growth over the tropics. Hence our study region comprises all the land areas north of 30°N. All results, with the exception of zonal LAI, are projected over a stereographic projection from the North Pole, with the latitude ranging from 30°N to 90°N.

2.5. Leaf Phenology Analyses

Growing season onset, dormancy and length were calculated based on the seasonal amplitude. LAI has been shown to have a normal distribution over the year in northern latitudes [37], so we consider the start of the growing season to be 20% of the maximum amplitude. This processes has been proven to be more stable for monthly data, compared to an approach based on sudden LAI changes.

In order to analyze changes in the growing season, we mask regions where there are minimal changes in LAI over the year (e.g., evergreen forests and mixed forest with a small deciduous component). These regions were defined as those where the difference between the maximum and minimum LAI amplitude is less than 0.5. We also masked regions where the LAI decreased in the middle of

the summer (drought deciduousness), assuming those months to have constant LAI.

For the gridcells with enough variation, we calculated a critical threshold value (CT) above which we assume the plants to be photosynthetically active (Equation (1))

$$CT^{x,y} = LAI_{min}^{x,y} + 0.2 \times (LAI_{max}^{x,y} - LAI_{min}^{x,y}) \quad (1)$$

where LAI Min and Max represent minimum and maximum gridcell LAI over one year. The length of the growing season for each year was calculated as the number of months with an LAI value above this threshold; the onset is the first of these months and the dormancy is the last. Since part of the growing season occurs after the end of the year [38], we included the first three months of the following year in the calculations. Hence, the growing season offset can occur on the following year, having DOY higher than 365. Even when calculated monthly all results are presented in days (number of days passed until the end of the calculated month). The procedure was repeated for each gridcell, year and dataset. Mean length, onset and dormancy represent the average over the whole time period (Figure 1).

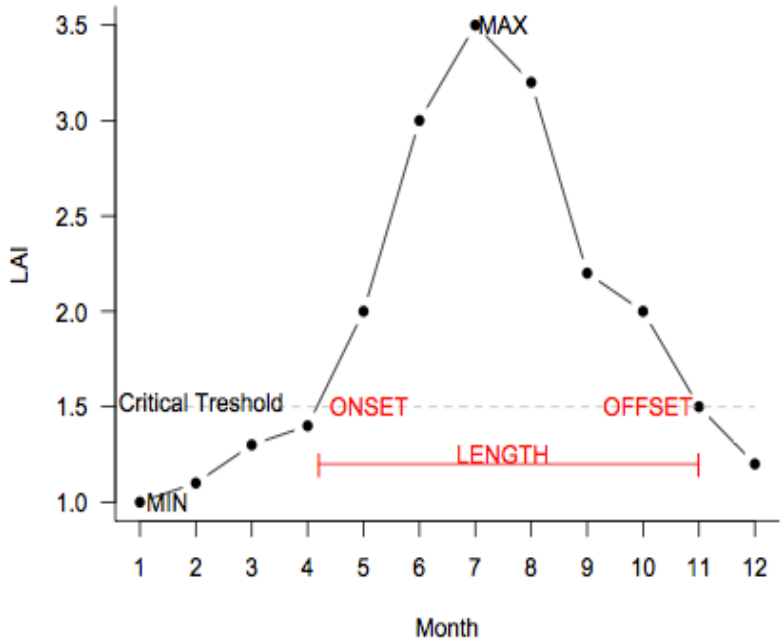

Figure 1. Growing season onset, dormancy (offset) and length calculation based on the seasonal amplitude. A critical threshold value is calculated for each gridcell and each year based on the maximum and minimum Leaf Area Index (LAI).

In order to quantify the differences between the models and data we calculate the root mean square errors (Equation (2)) between each model and the satellite observations for each grid cell and all growing season variables, and the seasonal amplitude.

$$RSME = \sqrt{\sum_{x=1,y=1}^{xy=n} \frac{(Sat^{xy} - Model^{xy})^2}{n}} \quad (2)$$

2.6. Temporal Trends

In order to calculate the temporal changes in annual average LAI and growing season length (GSL), linear trends were calculated for each gridcell for the whole time period. The values are presented as net change in both variables, in m^2 m^{-2} and in days/year respectively. This approach has been used by other authors [34] giving important insights on the drivers of change.

3. Results

3.1. Mean LAI

All of the models overestimate mean LAI, LAI trend and interannual variability (IAV) over the high-latitude Northern Hemisphere compared to the satellite observations (Figure 2). In general, models with the highest average LAI also have strong positive trends. This occurs regardless of whether the models use imposed or dynamic vegetation, or the number of PFTs implemented. Interestingly, models with a trend and average LAI closest to the satellite records, such as ORCHIDEE, OCN and TRIFFID have very different values of IAV, ranging from values similar to the satellite data up to 4 times higher. On the contrary, the most dissimilar models to the observations, such as LPJ and CLM4CN, have larger IAV.

Looking at the spatial distribution of LAI, most of the models simulate the observed spatial distribution pattern (Figure 3). Peaks in LAI are evident over the boreal forest (55°–65°N) and the North American temperate forest (30°–55°N). The lowest values are found over the cold Gobi plateau and the Siberian Tundra. As noted above, there is a general overestimation of mean LAI in the models, relative to observations. LAI values range from 0 to 2.5 in the satellite data, while for the models they are as high as 5. Models and observations agree on values over the deserts and low-LAI regions but the differences are higher (3–4) over the boreal region. As shown by spatial correlations, differences between satellite data and models are higher in VEGAS and TRIFFID, and smaller in LPJ and LPJ-GUESS (Figure 3). It is noteworthy that much of the discrepancies occur over evergreen vegetation, suggesting that the lack of regenerative vegetative states, fire and gap dynamics over this region lead to an overestimation of the number of fully grown trees on models, which ultimately means a much higher LAI than observed. However, satellite signal saturation—this is the inability of the satellite to distinguish between areas with high LAI-

could be leading to an underestimation of LAI in dense forested areas such as the boreal forest, which might also account for the lower LAI over this area.

.

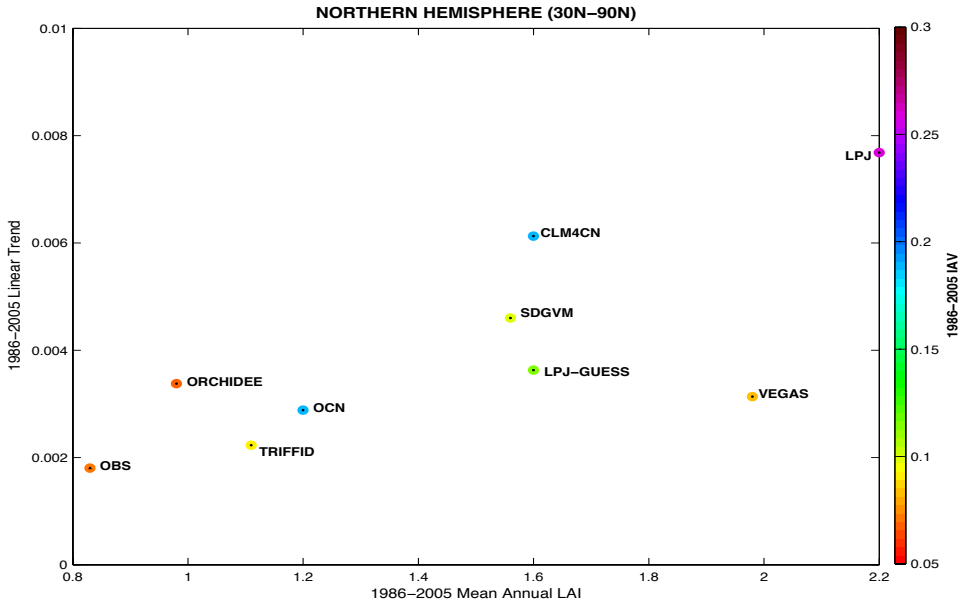

Figure 2. Linear trend against average LAI for each model and satellite observations, with IAV represented as colors. The data represents the whole high-latitude Northern Hemisphere (30°–90°) for the time period 1986–2005

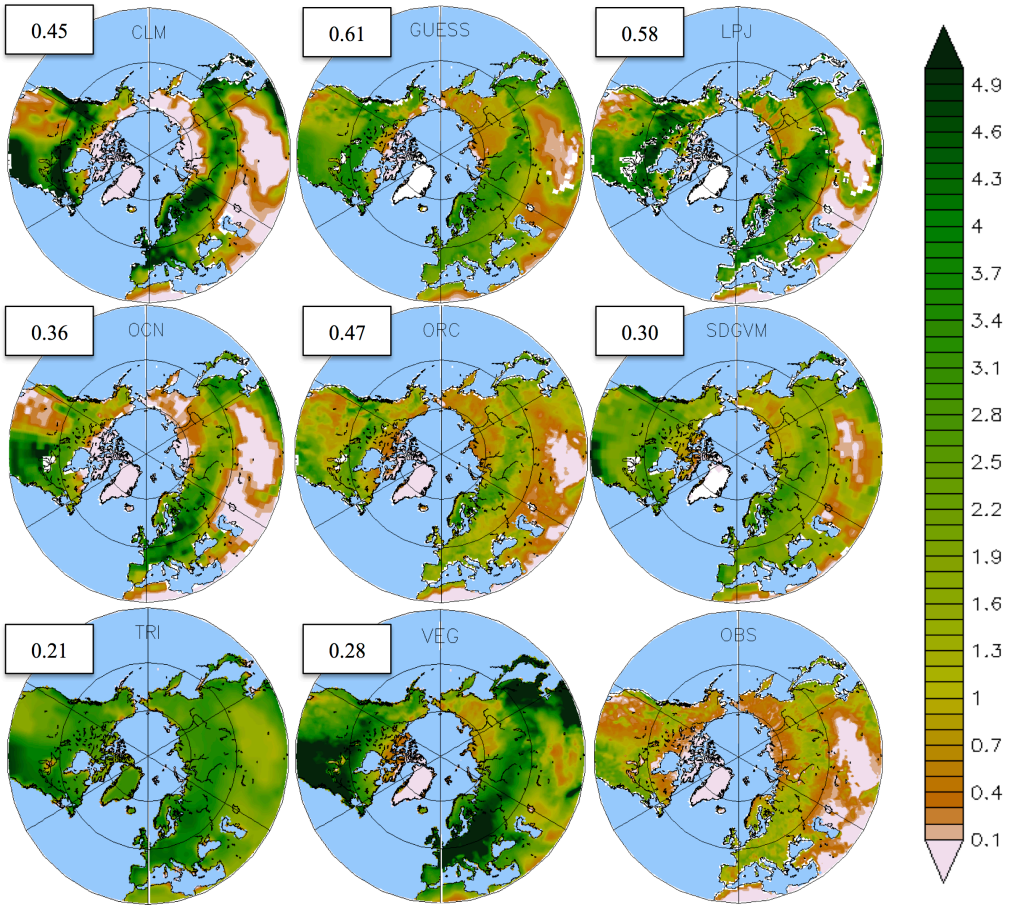

Figure 3. Spatially distributed annual mean LAI for 8 LSMs (1–8) and satellite observations over the Northern Hemisphere (30°–90°N), for the period 1986–2005. Spatial correlations between each model and observations are given in the white boxes.

The seasonal amplitude patterns show large disagreements between the models and the satellite data (Figure 4). Most models overestimate the mean amplitude (RSME = 1.02–2.21), which is particularly evident over Europe and Eastern North America. The exception here is SDGVM, which displays little seasonality and performs better than the rest of the models in reproducing the satellite-derived observations. The RSME show that models using dynamic vegetation are less similar to observations than those using imposed vegetation. Regardless, most models correctly simulate the spatial variability of the seasonal amplitude; this is true for CLM, GUESS, OCN and VEGAS to some extent. TRIFFID shows almost no seasonality over this area, which is mainly driven by the omnipresence of the evergreen PFT over the Northern Hemisphere (not shown) (Figure 4).

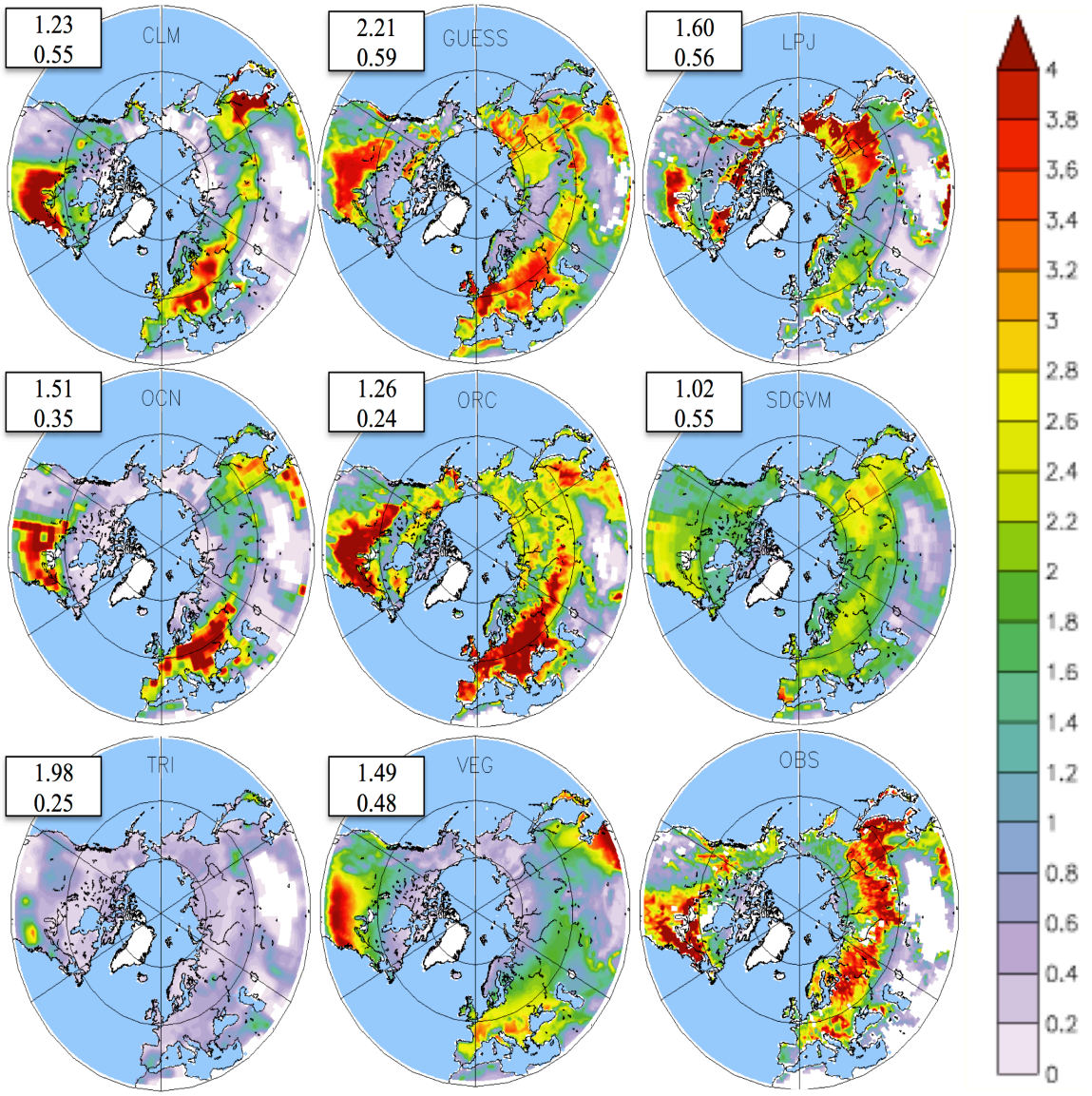

Figure 4. Seasonal Amplitude in LAI for 8 LSMs and satellite observations for the Northern Hemisphere (30°–90°N) for the period 1986–2005. Root mean square errors and spatial correlations between each model and the observations are given in the white boxes.

3.2. Growing Season

The growing season onset derived from LAI is broadly consistent across the models, with high correlations compared to the satellite data (>0.5) (Figure 5). In general the satellite observations show a later onset as latitude increases, remarkably similar to the thermal gradient. CLM, LPJ-GUESS, LPJ, SDGVM and, to a lesser extent, OCN, ORCHIDEE and VEGAS correctly reproduce this spatial pattern, as shown by the RSME and spatial correlations. This is not surprising as those models include a thermal limitation to photosynthesis and a snow scheme. TRIFFID shows no detectable onset above 50°N but has later values compared to the satellite below that threshold, likely due to the distribution of the evergreen PFT over the whole NH. Models that have the highest correlations with the satellite on the SA also show very similar values to the satellite on the onset, as shown by RSME (Figure 5).

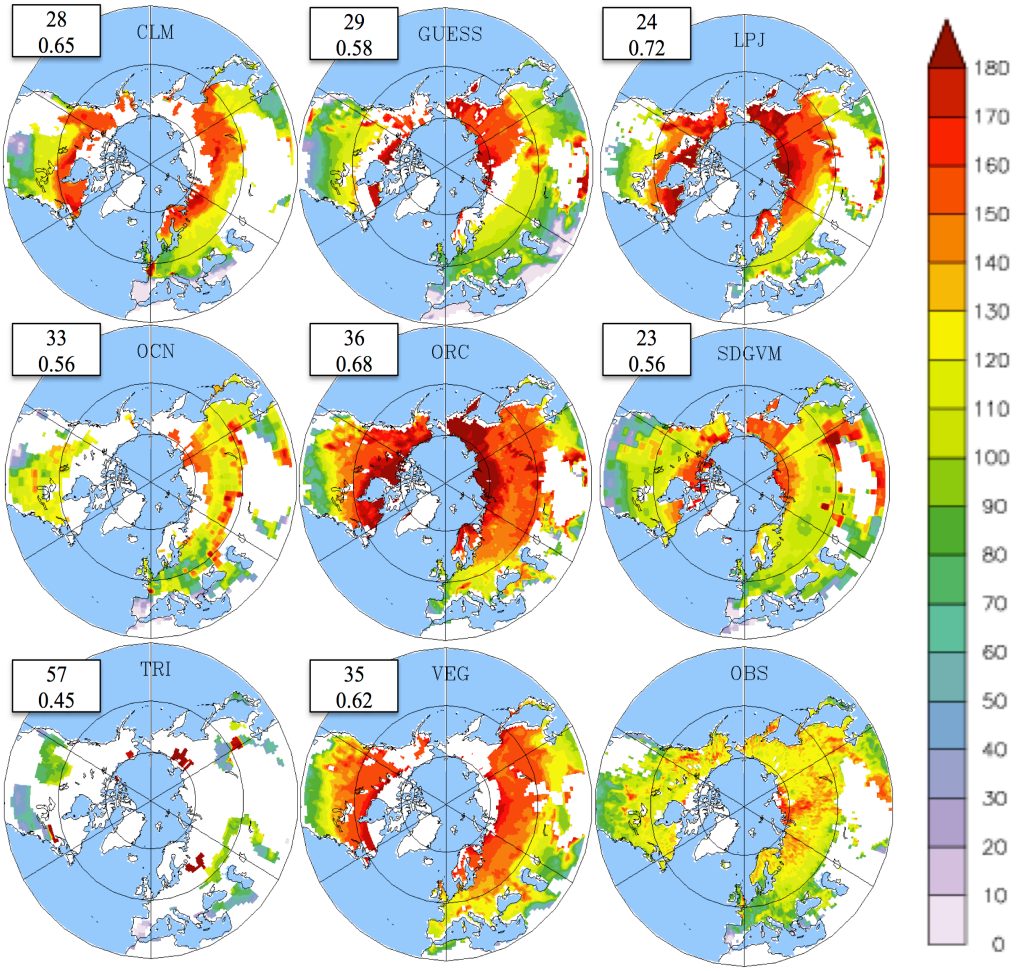

Figure 5. Mean (1986–2005) growing season onset (day) for 8 LSMs and satellite observations over the Northern Hemisphere (30°–90°N). Spatial correlations and root mean square errors between each model and the observations are given in the white boxes.

The discrepancies between the models and satellite observations are larger when considering the end of the growing season or dormancy (Figure 6). While the satellite data shows a latitudinal gradient, with the dormancy occurring earlier at higher latitudes, most models overestimate the dormancy day (RSME = 31–63). Out of the eight models, LPJ-GUESS, LPJ, ORCHIDEE and VEGAS have a similar dormancy distribution with minor discrepancies over the taiga and boreal forest, as shown by the spatial correlations. CLM, OCN and TRIFFID have patchy areas of agreement, while SDGVM has a much later dormancy than the satellite data. In some regions, particularly boreal deciduous forest, modeled dormancy can happen after the end of the year (DOY higher than 365). However, over these months the snow corrupts the satellite signal, leading to an underestimation of LAI. This partially explains why the dormancy date errors are larger than those of the onset.

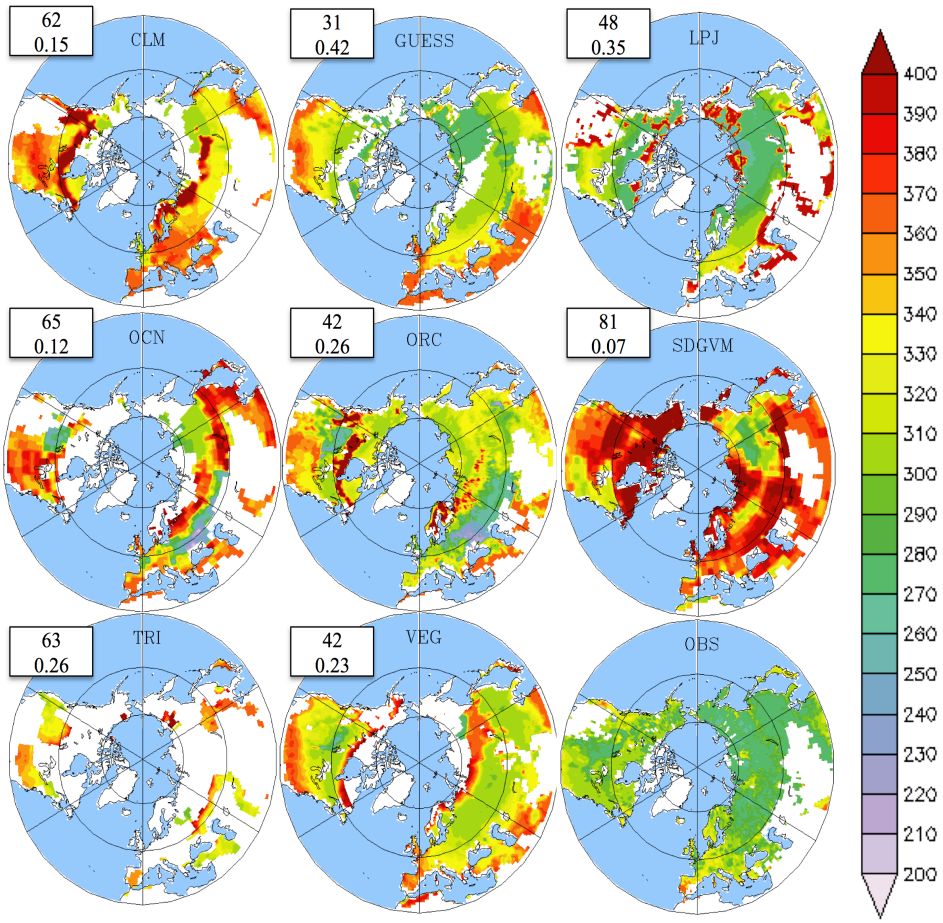

Figure 6. Mean (1986–2005) growing season dormancy (day) for 8 LSMs and satellite observations over the Northern Hemisphere (30°–90°N). Spatial correlations and root mean square errors between each model and the observations are given in the white boxes. DOYs above 365 represent DOYs of the following year.

All of the models predict a later dormancy date (day), particularly over the northern temperate region (30°–50°N) (Figure 6). This means that leaves in the models remain for longer than they should. However, the late dormancy is not in line with the vegetation photosynthetic activity. When the same methodology used to calculate the LAI-growing period was applied to gross primary productivity (GPP), we found that the dormancy began at 277 ± 7 days in the models, which is remarkably earlier than previously predicted by LAI (315 ± 10 days), even on the low-north latitudes (287 ± 18). It is evident that all of the models keep inactive leaves for longer than they should, which does not have an impact on the C cycle but could potentially modify radiation and turbulent fluxes, therefore affecting planetary boundary layer dynamics.

There is a higher level of agreement in growing season length between the satellite data and the models than for dormancy dates (Figure 7). Surprisingly, the satellite observations display a very homogeneous length over regions > 50°N, with values between 120–150 days. Similar to the previous patterns, LPJ, LPJ-GUESS, CLM, ORCHIDEE and VEGAS have the highest agreement with the satellite data, as shown by the RSME and spatial correlations. Interestingly, the disagreement between models and observations occurs mostly over the lower latitudes of the Northern Hemisphere. OCN displays the same patchy agreement that shows on the onset and SDGVM displays the least agreement with an opposite GSL distribution. The length of the growing season has the highest error compared to the satellite data, where 6 out of 8 models display longer GSL, mostly driven by a late leaf shedding (Table 2).

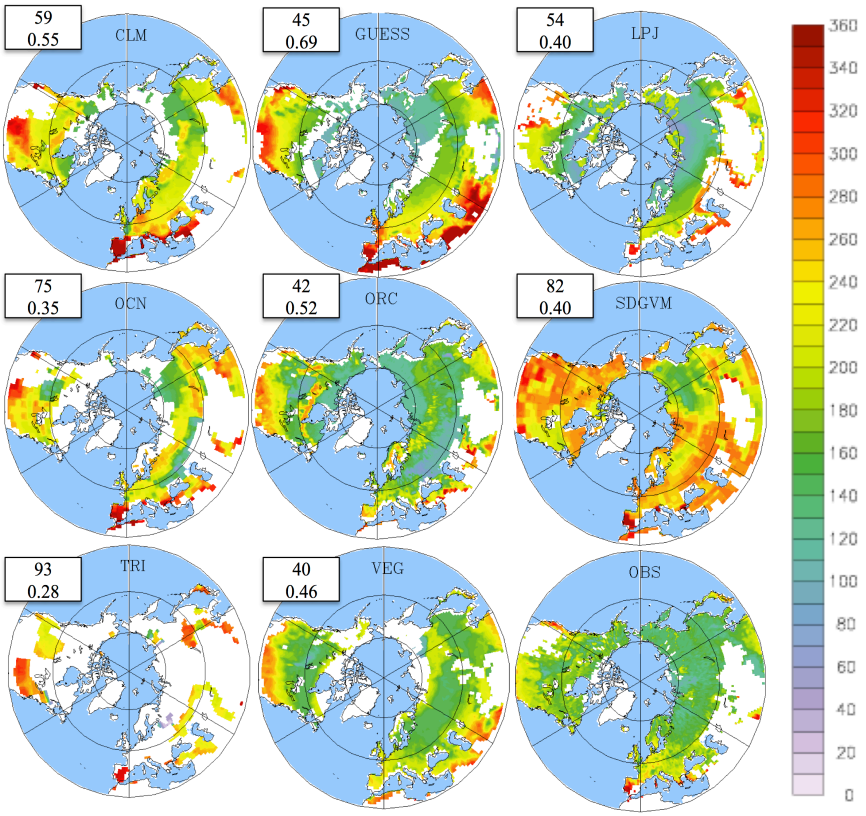

Figure 7. Mean growing season length (1986–2005) in days for 8 LSMs and satellite observations over the Northern Hemisphere (30°–90°N). Spatial correlations and root mean square errors between each model and the observations are given in the white boxes.

When looking at the hemispheric mean values it is clear that all of the models overestimate the LAI, dormancy and length of the growing season (Table 2). Satellite LAI average for the Northern Hemisphere was 0.83, while LAI from the models varies between 0.98–2.16. Both growing season onset and dormancy were later in all of the models, in some cases by more than a month. The effect of the late offset translates as an increased GSL, with values 9 to 180 days higher than the satellite data (Table 2). However, when the dormancy period is calculated based on GPP the modeled values become much closer to the observations, with an average GSL of 144 ± 15 days, compared to 184 days in the satellite data. This again suggests a decoupling between the active period of photosynthesis and leaves in the models.

Table 2. Average LAI, growing season onset, dormancy and length for the Northern Hemisphere for each model and the satellite observations. The values for dormancy and length based on GPP are presented in brackets.

Model	LAI	Onset (day)	Dormancy (day)	Length (days)
CLM	1.6	131	351 (288)	220 (164)
LPJ_GUESS	1.6	125	314 (285)	189 (151)
LPJ	2.2	130	319 (278)	189 (134)
OCN	1.2	121	342 (268)	221 (142)
ORCHIDEE	0.98	151	323 (268)	172 (134)
SDGVM	1.56	122	374 (275)	252(145)
TRIFFID	1.11	133	355 (274)	222(125)
VEGAS	1.98	136	336 (277)	200 (139)
LAI3g	0.83	111	295	184

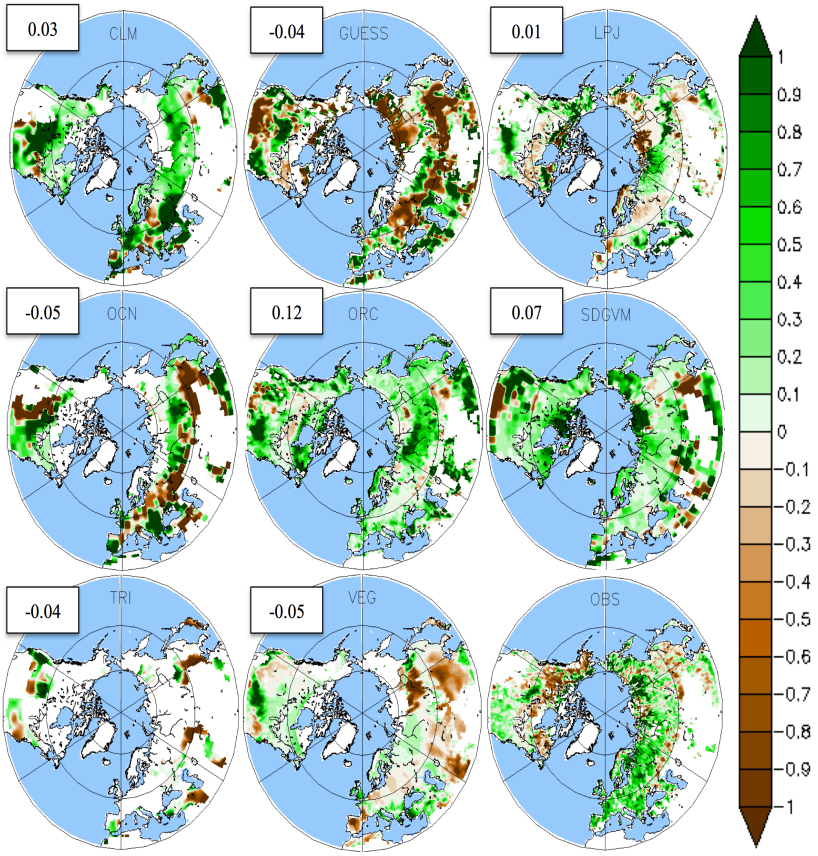

Figure 8. LAI linear trends over the period 1986–2005 for 8 LSMs and the satellite observations. Spatial correlations between each model and the observations are given in the white boxes.

3.3. Temporal Trends

All models show a positive LAI trend in most of the Northern Hemisphere, which is consistent with the satellite observations (Figure 8). Nevertheless, there is little agreement on the spatial distribution of this phenomenon, with spatial correlation values between −0.05 and 0.12. In the satellite observation most of the greening occurs over 55°–90°N in Eurasia, while in models it is homogeneously distributed. More puzzling is the reduction of LAI in LPJ-GUESS, OCN and VEGAS, which could be explained by a decrease in precipitation over this region (not shown). As all models are forced using the same climate, consistent regional patterns must be driven by temperature or precipitation. The greening over the high latitudes occurs in all models and is driven by an increased temperature.

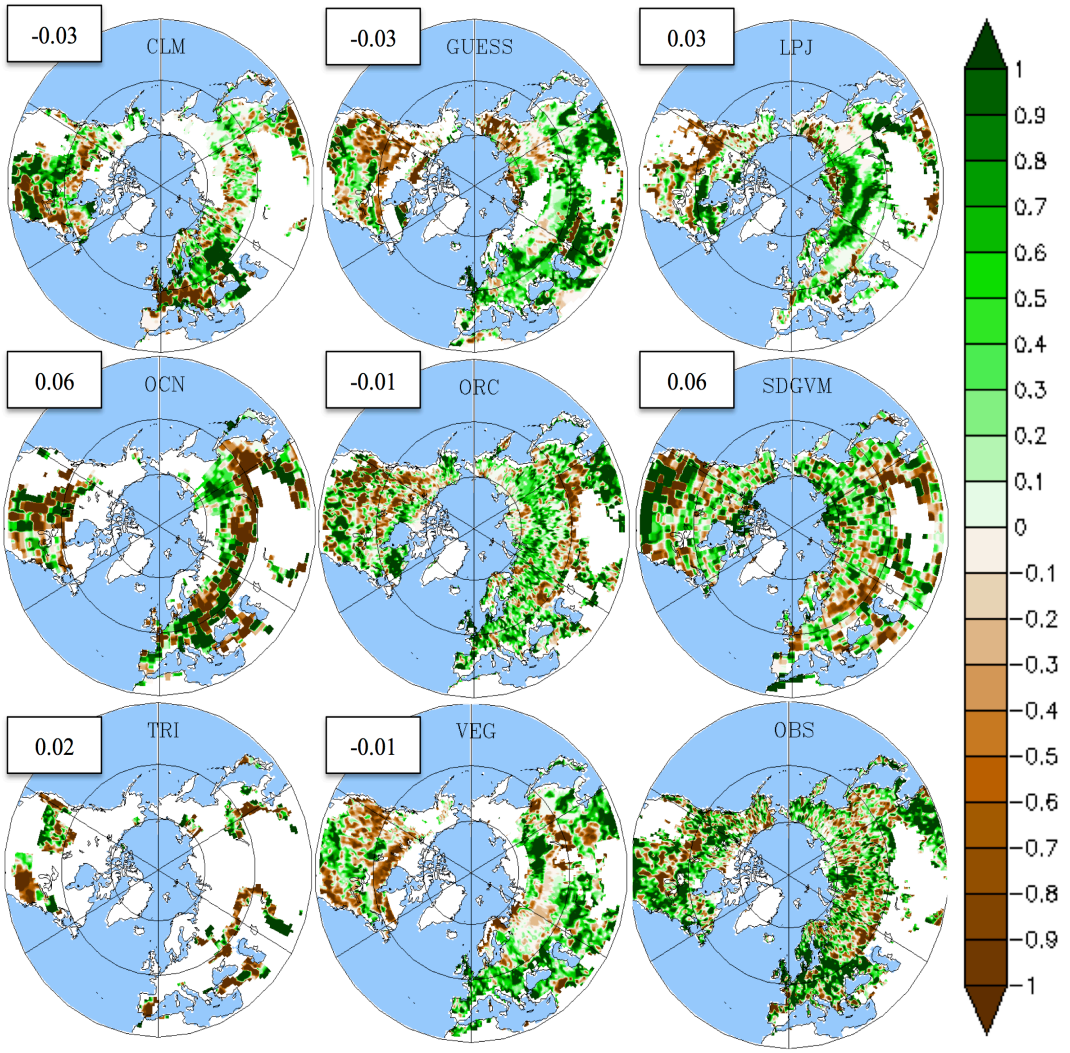

Figure 9. Growing season length trends over the period 1986–2005 for 8 LSMs and the satellite observations. Brown indicates an increase in the length of the growing season and green a decrease (days/year). In the white boxes, the values of the spatial correlation between each model and the satellite observations are given.

The models also show a general increase in the GSL albeit with a few areas where it decreases (Figure 9). However, similar to previous trends, there is little agreement over the spatial distribution. Clearly, models that perform better at calculating the GSL (both on the onset and dormancy) and average LAI more accurately reproduce observed linear trends (Figure 9). In most models, changes in the GSL match those of LAI. This is the case for CLM, OCN, ORCHIDEE, SDGVM and the satellite data, all of which use prescribed vegetation. LPJ, GUESS and VEGAS show an increased length over Eurasia and a decrease over North America, and their patterns resemble the precipitation trends for this period (not shown). This discrepancy between LAI and GSL changes is difficult to explain but could be driven by vegetation shifts from deciduous to evergreen forests. Changes in the GSL in TRIFFID, while only occurring over a small area, match the observations.

4. Discussion

The first important point to address is the validity of the satellite data. Satellite data does not represent true observations per se, but rather a model in itself. However, it is the closest product to observations, and available globally. It has been widely validated, but nevertheless there are some important issues that need to be considered. The satellite LAI product may have some problems detecting LAI in wintertime, since there is little sunlight in high latitudes. Sun angles are low and the satellite signals are heavily corrupted. Additionally snow cover affects reflection in winter and early spring. Hence, in the processing of any satellite data, there is a sun-angle cut-off. In these regions in the winter period there is little or no data. This partially explains the difference with modeled dormancy dates. However, this does not matter since the soil during this time is frozen and the plants are not photosynthesizing, hence there are no changes in LAI. The methods used to detect the growing season will also ignore this period, since we are only interested in LAI when it starts to change, during the spring. In the region occupied by boreal forests, the same applies. The majority of the Boreal forests are photosynthetically inactive since they are covered in snow. They do however have green needles. These will begin to appear in late winter and early spring as radiation increases. The sun angles in some regions are above the processing cut-off limits and the satellite sensor will begin to register NDVI values. However the ground is still frozen and therefore there is no photosynthetic activity even if the air temperatures begin to rise above freezing during some hours of the day [36].

Over the boreal forest region (55°–65°N), all models exhibit an overestimation in LAI of 2–3 units compared to the satellite but also when compared with literature estimates [39]. We know that the satellite has an error

precision of 20% at a pixel scale [40,41], field measurements have reported values around 2.7 ± 1.18 for the evergreen boreal forest [41] and 2.3 ± 0.6 for the deciduous forest [42]. The annual average over this region is around 1–2, which is inline with the satellite observations plus error. The average model values in this region are around 4, more similar to the expected maximum [39], than the expected mean (2.6–2.7). It seems that modeled LAI is higher all year round. These values are similar to the temperate forests, which suggests that having only one PFT for broadleaf forest might not be sufficient as is the case for TRIFFID, SDGVM and VEGAS. Moreover, models that include a wider range of PFTs, such as ORCHIDEE and LPJ-GUESS, are more similar to the satellite observations. Another possible explanation lies in the fact that models based on observed vegetation perform better than dynamic models. The lack of important ecosystem processes such as gap dynamics and fire, could be leading to the simulation of a mature forest state, which ultimately increases the PFT LAI.

There is great discrepancy in the calculation of the GSL with values that differ for more than a month, due to differences in the phenology module of each model. CLM4CN is one of the models that best predicts the GSL, since its LAI is derived from simulated leaf carbon and balanced with nitrogen [29]. More interestingly, models that use a thermal gradient to determine LAI (e.g., LPJ and LPJ-GUESS) [6,30] more accurately simulate the GSL than models with a more complex phenology, such as models where LAI is calculated from the leaf biomass (e.g., OCN [31], ORCHIDEE [32] and VEGAS [35]) or those that use a hydrological budget (e.g., SDGVM [32]). The exception is TRIFFID: while the model uses a thermal gradient for LAI [34], the introduction of a “chilling” phenology (leave shedding due to freezing) seems to overestimate the evergreen component in the Northern Hemisphere.

In spite of the differences in the phenology modules of the models, all predict an onset 15–20 days later than the satellite. Work by Jeong *et al.* [43] suggests that most models fail to calculate an adequate budburst due to the usage of mean air temperature threshold instead of accumulated heat variable, which generates better results. The authors also argue that the effect could come from the lack of representation of PFTs, which is consistent with our results–a higher number of PFTs leads to a better LAI and GSL representation. Another possible explanation is the overestimation of the effect of frozen soil thaw in the models.

All models predict a later dormancy, which occurs a month later than the satellite data. This happens due to all models having a constant leaf shedding over time once the temperature has reached a minimum certain threshold. While this might be true for the evergreen component, it creates a longer GSL for the deciduous forest [44-46]. Moreover, the difference in the dormancy date between GPP and LAI clearly points out that models need to improve their LAI dormancy. While this might not have an impact on the C cycle, it could potentially alter the radiation and turbulent fluxes.

A longer growing season allows for a longer time of leaf growth, which explains the increasing LAI trend in the models, with the whole process being driven by temperature [47–49]. In most cases LAI plateaus at the maximum value, so if the growing season is longer, there are more days with maximum leaf area, which leads to a higher average value. This seems to be true for models with prescribed vegetation, although models that simulate dynamic vegetation follow the precipitation pattern more closely.

5. Conclusion

We compare LAI from eight different uncoupled LSMs against satellite data over the Northern Hemisphere, during the 1986–2005 period. This was achieved by calculating the mean LAI, seasonal amplitude and growing season variables (onset, dormancy an length). Our results show that all models overestimate LAI by 2–3 units, particularly over the boreal forest, relative to the satellite data and literature estimates. Models that include a high number of plant functional types (10–16) compare more favorably to the satellite data than those that only have a few (4–5). Models that calculate their phenology based on temperature perform better than those with complex photosynthetic modules. Likewise, models with prescribed vegetation more closely match observations than those that simulate it dynamically. Finally, all models overestimate the length of the by 4–40 days based on LAI compared with the observations, largely due to the dormancy date occurring 20–60 days later. This is inconsistent with the photosynthetic active period calculated by GPP, which was on average 3 months smaller. This highlights the need to improve the deciduous phenology in all models, particularly leaf shedding.

While vegetation models have developed a great deal, there is still a need for improvement. LAI is a key variable in all models and its correct representation, both temporarily and spatially, is key to predicting correct carbon fluxes. As the literature suggests, any overestimate in the length of the growing season and its trend is likely to affect albedo and have important effects on the radiation budget of the area. The satellite data represents a unique opportunity to test models against observational data and to determine where improvements can be made. Moreover, additional variables can be validated, allowing the identification of possible problems within the models.

Acknowledgments

We acknowledge the TRENDY-DGVM project that is responsible for all the data on DGVMs used in this work. We also thank Ranga Myneni for his valuable contribution and comments on the development of the paper and Xuhui Wang for is help on the methodology. The corresponding author also thanks the CONACYT-CECTI and the University of Exeter for their funding during the PhD studies.

Conflicts of Interest

The authors declare no conflict of interest.

References

1. Gomez-Peralta, D.; Oberbauer, S.F.; McClain, M.E.; Philippi, T.E. Rainfall and cloud-water interception in tropical montane forests in the eastern Andes of Central Peru. For. Ecol. Manag. **2008**, *255*, 1315–1325.
2. Running, S.W.; Coughlan, J.C. A general model of forest ecosystem processes for regional applications I. Hydrologic balance, canopy gas exchange and primary production processes. Ecol. Model. **1988**, *42*, 125–154.
3. Bréda, N.J.J. Ground-based measurements of leaf area index: A review of methods, instruments and current controversies. J. Exp. Bot. **2003**, *54*, 2403–2417.
4. Knyazikhin, Y.; Martonchik, J.V.; Diner, D.J.; Myneni, R.B.; Verstraete, M.; Pinty, B.; Gobron, N. Estimation of vegetation canopy leaf area index and fraction of absorbed photosynthetically active radiation from atmosphere-corrected MISR data. J. Geophys. Res. **1998**, *103*, 32239–32256.
5. Landsberg, J.J.; Waring, R.H. A generalised model of forest productivity using simplified concepts of radiation-use efficiency, carbon balance and partitioning. For. Ecol. Manag. **1997**, *95*, 209–228.
6. Sitch, S.; Smith, B.; Prentice, I.C.; Arneth, A.; Bondeau, A.; Cramer, W.; Kaplan, J.O.; Levis, S.; Lucht, W.; Sykes, M.T.; *et al*. Evaluation of ecosystem dynamics, plant geography and terrestrial carbon cycling in the LPJ dynamic global vegetation model. Glob. Change Biol. **2003**, *9*, 161–185.
7. Sitch, S.; Huntingford, C.; Gedney, N.; Levy, P.E.; Lomas, M.; Piao, S.L.; Betts, R.; Ciais, P.; Cox, P.; Friedlingstein, P.; *et al.* Evaluation of the terrestrial carbon cycle, future plant geography and climate-carbon cycle feedbacks using five Dynamic Global Vegetation Models (DGVMs). Glob. Change Biol. **2008**, *14*, 2015–2039.
8. Sitch, S.; Friedlingstein, P.; Gruber, N.; Jones, S.; Murray-Tortarolo, G.; Ahlstrom, A.; Doney, S.C.; Graven, H.; Heinze, C.; Huntingford, C.; *et al*. Trends and drivers of the regional-scale sources and sinks of carbon dioxide over the past two decades Biogeosciences Discussions (in press).
9. Diaz, S.; Cabido, M. Plant functional types and ecosystem function in relation to global change. J. Veg. Sci. **1997**, *8*, 463–474.
10. Diaz, S.; Cabido, M.; Casanoves, F. Plant functional traits and environmental filters at a regional scale. J. Veg. Sci. **1998**, *9*, 113–122.
11. Badeck, F.-W.; Bondeau, A.; Böttcher, K.; Doktor, D.; Lucht, W.; Schaber, J.; Sitch, S. Responses of spring phenology to climate change. New Phytol. **2004**, *162*, 295–309.

12. Buermann, W.; Dong, J.; Zeng, X.; Myneni, R.B.; Dickinson, R.E. Evaluation of the utility of satellite-based vegetation leaf area index data for climate simulations. J. Clim. **2001**, *14*, 3536–3550.
13. Maignan, F.; Bréon, F.-M.; Chevallier, F.; Viovy, N.; Ciais, P.; Garrec, C.; Trules, J.; Mancip, M. Evaluation of a global vegetation model using time series of satellite vegetation indices. Geosci. Model Dev. **2011**, *4*, 1103–1114.
14. Richardson, A.D.; Anderson, R.S.; Arain, M.A.; Barr, A.G.; Bohrer, G.; Chen, G.; Chen, J.M.; Ciais, P.; Davis, K.J.; Desai, A.R.; *et al*. Terrestrial biosphere models need better representation of vegetation phenology: Results from the North American carbon program site synthesis. Glob. Change Biol. **2011**, *18*, 566–584.
15. Randerson, J.T.; Hoffman, F.M.; Thornton, P.E.; Mahowald, N.M.; Lindsay, K.; Lee, Y.-H.; Nevison, C.D.; Doney, S.C.; Bonan, G.; Stöckli, R.; *et al.* Systematic assessment of terrestrial biogeochemistry in coupled climate–carbon models. Glob. Chang. Biol. **2009**, *15*, 2462–2484.
16. Prince, S.D. A model of regional primary production for use with coarse resolution satellite data. Int. J. Remote Sens. **1991**, *12*, 1313–1330.
17. Myneni, R.B.; Ramakrishna, R.; Nemani, R.; Running, S.W. Estimation of global leaf area index and absorbed par using radiative transfer models. IEEE Trans. Geosci. Remote Sens. **1997**, *35*, 1380–1393.
18. Friedl, M.A.; Schimel, D.S.; Michaelsen, J.; Davis, F.W.; Walker, H. Estimating grassland biomass and leaf area index using ground and satellite data. Int. J. Remote Sens. **1994**, *15*, 1401–1420.
19. Chen, J.M.; Cihlar, J. Retrieving leaf area index of boreal conifer forests using Landsat TM images. Remote Sens. Environ. **1996**, *55*, 153–162.
20. Green, E.P.; Mumby, P.J.; Edwards, A.J.; Clark, C.D.; Ellis, A.C. Estimating leaf area index of mangroves from satellite data. Aquat. Bot. **1997**, *58*, 11–19.
21. Prentice, I.C.; Bondeau, A.; Cramer, W.; Harrison, S.P.; Hickler, T.; Lucht, W.; Sitch, S.; Smith, B.; Sykes, M.T. Dynamic Global Vegetation Modeling: Quantifying Terrestrial Ecosystem Responses to Large-Scale Environmental Change. In Terrestrial Ecosystems in a Changing World; Canadell, J.G., Pataki, D.E., Pitelka, L.F., Eds.; Springer: New York City, NY, USA, 2007;
pp. 175–192.
22. Anav, A.; Murray-Tortarolo, G.; Friedlingstein, P.; Sitch, S.; Piao, S.; Zhu, Z. Evaluation of land surface models in reproducing satellite Derived leaf area index over the high-latitude northern hemisphere. Part II: Earth system models. *Remote Sens.* **2013**, *5*, 3637–3661.
23. Xu, L.; Myneni, R.B.; Chapin, F.S. III; Callaghan, T.V.; Pinzon, J.E.; Tucker, C.J.; Zhu, Z.; Bi, J.; Ciais, P.; Tømmervik, H.; *et al.* Temperature and

vegetation seasonality diminishment over northern lands. *Nat. Clim. Change* **2013**, doi: 10.1038/nclimate1836.
24. Anav, A.; Menut, L.; Khvorostyanov, D.; Viovy, N. Impact of tropospheric ozone on the Euro-Mediterranean vegetation. Glob. Chang. Biol. **2011**, *17*, 2342–2359.
25. Yang, W.; Tan, B.; Huang, D.; Rautiainen, M.; Shabanov, N.V.; Wang, Y.; Privette, J.L.; Huemmrich, K.F.; Fensholt, R.; Sandholt, I.; *et al.* MODIS leaf area index products: From validation to algorithm improvement. IEEE Trans. Geosci. Remote Sens. **2006**, *44*, 1885–1898.
26. Gao, F.; Morisette, J.T.; Wolfe, R.E.; Ederer, G.; Pedelty, J.; Masuoka, E.; Myneni, R.; Tan, B.; Nightingale, J. An algorithm to produce temporally and spatially continuous MODIS-LAI time series. IEEE Geosci. Remote Sens. Lett. **2008**, *5*, 60–64.
27. Ganguly, S.; Schull, M.A.; Samanta, A.; Shabanov, N.V.; Milesi, C.; Nemani, R.R.; Knyazikhin, Y.; Myneni, R.B. Generating vegetation leaf area index earth system data record from multiple sensors. Part 1: Theory. *Remote Sens. Environ*. **2008**, 112, 4333–4343.
28. Ganguly, S.; Nemani, R.R.; Zhang, G.; Hashimoto, H.; Milesi, C.; Michaelis, A.; Wang, W.; Votava, P.; Samanta, A.; Melton, F.; *et al.* Generating global Leaf Area Index from Landsat: Algorithm formulation and demonstration. Remote Sens. Environ. **2012**, *122*, 185–202.
29. Oleson, K.W.; Lawrence, G.B.; Flanner, M.G.; Kluzek, E.; Levis, P.J.S.; Swenson, S.C.; Thornton, E.; Feddema, J.; Heald, C.L.; Lamarque, J.; *et al.* Technical Description of Version 4.0 of the Community Land Model (CLM); NCAR: Boulder, Colorado, USA, 2010.
30. Smith, B.; Prentice, I.C.; Sykes, M.T. Representation of vegetation dynamics in the modelling of terrestrial ecosystems: Comparing two contrasting approaches within European climate space. Glob. Ecol. Biogeogr. **2001**, *10*, 621–637.
31. Zaehle, S.; Friend, A.D. Carbon and nitrogen cycle dynamics in the O-CN land surface model: 1. Model description, site-scale evaluation, and sensitivity to parameter estimates. Glob. Biogeochem. Cycles **2010**, *24*, doi: 10.1029/2009GB003521
32. Krinner, G.; Viovy, N.; de Noblet-Ducoudré, N.; Ogée, J.; Polcher, J.; Friedlingstein, P.; Ciais, P.; Sitch, S.; Prentice, I.C. A dynamic global vegetation model for studies of the coupled atmosphere-biosphere system. Glob. Biogeochem. Cycles **2005**, *19*, doi: 10.1029/2003GB002199.
33. Woodward, F.I. Vegetation-climate feedbacks in a greenhouse world. Philos. Trans. R. Soc. Lond. B Biol. Sci. **1998**, *353*, 29–39.
34. Cox, P. Description of the TRIFFID dynamic global vegetation model. *Techinal Note 24, Met Office.* **2001**. URL: http://www.metoffice.gov.uk/research/hadleycentre/pubs/HCTN/index.html.

35. Zeng, N.; Qian, H.; Roedenbeck, C.; Heimann, M. Impact of 1998–2002 midlatitude drought and warming on terrestrial ecosystem and the global carbon cycle. Geophys. Res. Lett. **2005**, *32*, doi: 10.1029/2005GL024607.
36. Zhu, Z.; Bi, J.; Pan, Y.; Ganguly, S.; Anav, A.; Xu, L.; Samanta, A.; Piao, S.; Nemani, R.R.; Myneni, R. B. Global data sets of vegetation Leaf Area Index (LAI)3g and fraction of Photosynthetically Active Radiation (FPAR)3g derived from Global Inventory Modeling and Mapping Studies (GIMMS) Normalized Difference Vegetation Index (NDVI3g) for the period 1981 to 2011. *Remote Sens.* **2013**, *5*, 927–948.
37. Piao, S.; Friedlingstein, P.; Ciais, P.; Viovy, N.; Demarty, J. Growing season extension and its impact on terrestrial carbon cycle in the Northern Hemisphere over the past 2 decades. Glob. Biogeochem. Cycles **2007**, *21*, doi: 10.1029/2006GB002888.
38. Zhang, P.; Anderson, B.; Barlow, M.; Tan, B.; Myneni, R.B. Climate-related vegetation characteristics derived from Moderate Resolution Imaging Spectroradiometer (MODIS) leaf area index and normalized difference vegetation index. J. Geophys. Resea. Atmos. **2004**, *109*, doi: 10.1029/2004JD004720.
39. Asner, G.P.; Scurlock, J.M.O.; Hicke, J.A. Global synthesis of leaf area index observations: Implications for ecological and remote sensing studies. Glob. Ecol. Biogeogr. **2003**, *12*, 191–205.
40. Berterretche, M.; Hudak, A.T.; Cohen, W.B.; Maiersperger, T.K.; Gower, S.T.; Dungan, J. Comparison of regression and geostatistical methods for mapping Leaf Area Index (LAI) with Landsat ETM+ data over a boreal forest. Remote Sens. Environ. **2005**, *96*, 49–61.
41. Wang, Y.; Woodcock, C.E.; Buermann, W.; Stenberg, P.; Voipio, P.; Smolander, H.; Häme, T.; Tian, Y.; Hu, J.; Knyazikhin, Y.; *et al.* Evaluation of the MODIS LAI algorithm at a coniferous forest site in Finland. *Remote Sens. Environ.* **2004**, *91*, 114–127.
42. Bonan, G.B. Importance of Leaf Area Index and forest type when estimating photosynthesis in boreal forests. Remote Sens. Environ. **1993**, *43*, 303–314
43. Jeong, S.-J.; Ho, C.-H.; Gim, H.-J.; Brown, M.E. Phenology shifts at start *vs.* end of growing season in temperate vegetation over the Northern Hemisphere for the period 1982–2008. Glob. Change Biol. **2011**, *17*, 2385–2399.
44. Hickler, T.; Smith, B.; Prentice, I.C.; Mjöfors, K.; Miller, P.; Arneth, A.; Sykes, M.T. CO_2 fertilization in temperate FACE experiments not representative of boreal and tropical forests. Glob. Change Biol. **2008**, *14*, 1531–1542.

45. Norby, R.J.; Sholtis, J.D.; Gunderson, C.A.; Jawdy, S.S. Leaf dynamics of a deciduous forest canopy: No response to elevated CO_2. Oecologia **2003**, *136*, 574–584.
46. Iivonen, S.; Kaakinen, S.; Jolkkonen, A.; Vapaavuori, E.; Linder, S. Influence of long-term nutrient optimization on biomass, carbon, and nitrogen acquisition and allocation in Norway spruce. Can. J. For. Res. **2006**, *36*, 1563–1571.
47. Lucht, W.; Prentice, I.C.; Myneni, R.B.; Sitch, S.; Friedlingstein, P.; Cramer, W.; Bousquet, P.; Buermann, W.; Smith, B. Climatic control of the high-latitude vegetation greening trend and pinatubo effect. Science **2002**, *296*, 1687–1689.
48. De Jong, R.; Verbesselt, J.; Zeileis, A.; Schaepman, M. Shifts in global vegetation activity trends. *Remote Sens.* **2013**, *5*, 1117–1133.
49. Mao, J.; Shi, X.; Thornton, P.; Hoffman, F.; Zhu, Z.; Myneni, R. Global latitudinal-asymmetric vegetation growth trends and their driving mechanisms: 1982–2009. *Remote Sens.* **2013**, *5*, 1484–1497.

Remote Sens. **2013**, *5*, 1-x manuscripts; doi:10.3390/rs50x000x

OPEN ACCESS
Remote Sensing
ISSN 2072-4292
www.mdpi.com/journal/remotesensing
Article

Evaluation of Land Surface Models in Reproducing Satellite Derived LAI over the High-Latitude Northern Hemisphere. Part II: Earth System Models

Alessandro Anav [1*], Guillermo Murray-Tortarolo [2], Pierre Friedlingstein [3], Stephen Sitch [4], Shilong Piao [5], Zaichun Zhu [6]

1 College of Engineering, Mathematics & Physical Sciences, Harrison Building, North Park Road, Exeter EX4 4QF, UK; E-Mail: A.Anav@exeter.ac.uk
2 College of Engineering, Mathematics & Physical Sciences, Harrison Building, North Park Road, Exeter EX4 4QF, UK; E-Mail: gnm202@exeter.ac.uk
3 College of Engineering, Mathematics & Physical Sciences, Harrison Building, North Park Road, Exeter EX4 4QF, UK; E-Mail: P.Friedlingstein@exeter.ac.uk
4 College of Engineering, Mathematics & Physical Sciences, Harrison Building, North Park Road, Exeter EX4 4QF, UK; E-Mail: S.A.Sitch@exeter.ac.uk
5 Department of Ecology, Peking University, Beijing 100871, China and Institute of Tibetan Plateau Research, Chinese Academy of Sciences, Beijing 100085, China; E-Mail: slpiao@pku.edu.cn
6 Department of Earth and Environment, Boston University, 675 Commonwealth Avenue, Boston, MA 02215, USA; E-Mail: zhu.zaichun@gmail.com

* Author to whom correspondence should be addressed; E-Mails: A.Anav@exeter.ac.uk;
Received: / Accepted: / Published: 12 August 2013

Abstract: Leaf Area Index (LAI) is a key parameter in the Earth System Models (ESMs) since it strongly affects land-surface boundary conditions and the exchange of matter and energy with the atmosphere. Observations and data products derived from satellite remote sensing are important for the validation and evaluation of ESMs, from regional to global scales. Several decades' worth of satellite data products are now available at global scale, which represents a unique opportunity to contrast observations against model results. The objective of this study is to assess whether ESMs

correctly reproduce the spatial variability of LAI when compared with satellite data, and to compare the length of the growing season in the different models with the satellite data. To achieve this goal, we analyse outputs from 11 coupled carbon-climate models that are based on the set of new global model simulations planned in support of the IPCC Fifth Assessment Report. We focus on the average LAI and the length of the growing season on Northern Hemisphere over the period 1986-2005. Additionally we compare the results with previous analyses (Part I) of uncoupled land surface models (LSMs) to assess the relative contribution of vegetation and climatic drivers on the correct representation of LAI. Our results show that models tend to overestimate the average values of LAI and have a longer growing season. The similarities with the uncoupled models suggest that representing the correct vegetation fraction in each grid cell is more important in controlling the distribution and value of LAI than the climatic variables. We conclude that validating LAI in each model against satellite observations should be a fundamental step for all modelling groups, and this process is more central than the correct LAI parameterization against climate.???

Keywords: LAI; CMIP5; Earth System Models; Leaf Phenology; Remote Sensing of Vegetation;

---

1. Introduction

The Leaf Area Index (LAI) is defined as one-sided green leaf area per unit ground area in broadleaf canopies, and as the projected needle leaf area in coniferous canopies [1]. LAI is a key parameter in most ecosystem productivity models and global (or regional) models of climate, hydrology, biogeochemistry and ecology [2].

Usually defined as the time evolution of the LAI, leaf phenology depends primarily on the climatic conditions for a given biome [3]. It strongly affects land-surface boundary conditions and the exchange of matter and energy with the atmosphere, influencing the surface albedo, roughness, and dynamics of the terrestrial water cycle [4,5]. Changes in the phase of LAI may therefore have impacts on climate [6,7], on the terrestrial carbon cycle [8], and on the atmospheric chemistry through the emission and deposition of several compounds [9-12]. Therefore, accurate estimates of canopy phenology are critical to quantifying carbon and water exchange between forests and the atmosphere and its response to climate change [8].

Phenology studies based on field observations [13,14], remote-sensing data [15-19], atmospheric CO_2 observations [20], and biogeochemical models [21] indicate that the vegetation growing season length (GSL) has significantly increased over the past decades [8]. Specifically, in the temperate and boreal regions of the Northern Hemisphere, the growing season begins in spring with increasing temperatures and solar radiation, the melting of snow, eventual thawing of the soil organic horizons, and the start of photosynthesis [22]. It terminates in autumn as temperatures and solar radiation decrease, soils refreeze, and photosynthesis ceases [23,24]. Therefore, temperature anomalies in spring and autumn affect the timing and duration of the growing season [8,25], which in turn control the seasonal onset and ending of the ecosystem carbon uptake period in these regions [8,26,27]. Rising temperatures during recent decades have resulted in a widely reported pattern of earlier and longer-lasting growing seasons from local to continental scales [27-33]. The greater rate of change observed in the beginning of the growing season is thought to be a response to rapid spring warming, and earlier snowmelt and soil thaw [29,34], while the smaller change in termination date is likely connected with lower rates of autumn warming [35] and the influence of other environmental effects on autumn phenology and growth cessation [36-38].

The importance of land surface processes in the climate system has mostly been supported by modelling studies on climate sensitivity to albedo [39-41], soil moisture [42-44], surface roughness [45], and leaf area index [6, 46-51].

In the first versions of general circulation models (GCMs) and regional climate models (RCMs) the soil-vegetation-atmosphere transfer (SVAT) schemes [52] were originally designed to simulate exchanges of matter and energy between the land surface and the atmosphere, with vegetation leaf area index as a forcing variable, rather than a prognostic state [6, 49, 53-57].

In order to improve the representation of the dynamical behaviour of the vegetation, a number of models have recently evolved to include biogeochemical processes [58-66].

In the last few years a new generation of general circulation models has become available to the scientific community. In comparison to the former model generation, these Earth System Models incorporate additional components describing the atmosphere's interaction with land-use and vegetation, as well as explicitly taking into account atmospheric chemistry, aerosols and the carbon cycle [67].

The inclusion of Earth system components in a climate model has a two-fold benefit. Firstly, it allows a consistent calculation of the impacts of climate change on atmospheric composition or ecosystems [68]. Secondly, it allows the incorporation of biogeochemical feedbacks, which can be negative, dampening the sensitivity of the climate to external forcing [69], or positive, amplifying the sensitivity [70]. However, adding Earth systems components and processes

increases the complexity of the model system, thus a consistent validation of the variables simulated by these models is needed.

The assessment of vegetation phenology using remotely sensed data has a long history [71,72] with more recent studies making use of satellite data to examine the potential effects of climate change on phenology [15, 73-77]. In fact, remote sensing has been widely recognised as a valuable tool for the detection and analyses of simulated data, both spatially and temporally. The past decade has seen a particularly rapid increase in the number of launched satellites, as well as an improvement in both spatial and spectral resolution of data they produce. Therefore, the ability to rapidly assess LAI using vegetation indices from remotely sensed imagery provides a means to rapidly assess ESMs' skills at simulating vegetation greenness over a wide geographic area.

The existence of vegetation models that use prescribed climate represents a unique opportunity to compare and contrast the effect of inner climatic variation on ESMs against the effect of differences in the vegetation modules. In other words, comparing different LSMs allows the detection of flaws in the vegetation dynamics, while comparing ESMs allows the identification of climate effect on vegetation processes, and the comparison of the two leads to the weighing of both effects.

In this context, we check the ability of different ESMs to reproduce the spatial and temporal variability of the satellite observed LAI. Specifically, the objective of this study is to assess whether ESMs correctly reproduce the spatial variability of LAI when compared with satellite data, and asses how long the growing season is in the different models compared with the satellite data over the Northern Hemisphere. In fact, as described above, over this area several authors have observed an increase in the growing season length. These changes in LAI, mostly due to an increase in temperature at the beginning of the growing season, have important implications on the global carbon cycle [8] and on atmospheric chemistry [9-12] simulated by the ESMs. Therefore, obtaining an accurate prediction of the temporal evolution of LAI is imperative not only in predicting the correct LAI seasonal changes, but also because of the feedbacks of LAI with the atmosphere.

In addition, we compare results from uncoupled models from part I [78] with the ESMs to elucidate the weighed role of vegetation and climate on the spatial and temporal evolution of LAI.

2. Material and methods

2.1. CMIP5 Simulations

We analyze output from 11 CMIP5 coupled carbon-climate models that, at the time of our analysis, had been submitted to the Program for Climate Model Diagnosis and Inter-comparison (PCMDI) Earth System Grid (ESG) [79].

The land components of these ESMs differ in their representations of vegetation types, soil properties, human disturbances, carbon and nitrogen pools, as well as in their horizontal resolutions. The models used in this study, along with the main features controlling their terrestrial carbon cycle, are listed in **Table 1**.

Our analysis focuses on the historical period (20^{th} century simulations; CO_2 concentration driven), which was forced by a variety of externally imposed changes such as increasing greenhouse gas and sulphate aerosol concentrations, change in solar radiation, and forcing by volcanic eruptions [91]. Considering the historical experiments, in general for most of the CMIP5 models the simulation starts in the year 1850 and ends in 2005. Within this period, we focus only on the last 20 years of the 20^{th} century simulation (1986–2005); in fact, although satellite data are available before 1986, we decided to use the same reference period used by [92] in order to be consistent with their analysis and results.

Besides, it is noteworthy that some models have only one realisation, but other models have many runs; these realisations represent climate simulations with different initial conditions. In the next section, we present results only from the first realization for each individual model.

For comparisons and evaluations, we re-grid all model outputs to a common 1°×1° grid using a bilinear interpolation method. This resolution was chosen to be consistent with the resolution of uncoupled models [78]. Although the CMIP5 archive includes daily means for a few variables, to be consistent with uncoupled models analysis [78] we focus here only on the monthly mean model output.

Table 1. CMIP5 Earth System Models used in this study with the associated land models and main features controlling the terrestrial carbon cycle.

MODELS	SOURCE	LAND MODELS	DYNAMIC VEGETATION	#PFTs	N CYCLE	RESOLUTION (Lon x Lat)	REFERENCE
BCC-CSM1	Beijing Climate Center, China	BCC_AVIM1.0	N	15	N	2.8125°x~2.8125°	[80]
BNU-ESM	Beijing Normal University, China	CoLM	Y	n/a	Y	2.8125°x~2.8125°	[81]
CanESM2	Canadian Centre for Climate Modelling and Analysis, Canada	CLASS2.7 + CTEM1	N	9	N	2.8125°x~2.8125°	[82]
CESM1-BGC	National Center for Atmospheric Research, United States	CLM4	N	15	Y	0.9°x1.25°	[83]
GFDL-ESM2G	Geophysical Fluid Dynamics Laboratory, United States	LM3	Y	5	N	2.5°x2°	[84]
HadGEM2-CC	Met Office Hadley Centre, UK	JULES + TRIFFID	Y	5	N	1.875°x1.25°	[85]
INMCM4	Institute for Numerical Mathematics, Russia	Simple model	N	n/a	N	2°x1.5°	[86]
IPSL-CM5A-MR	Institut Pierre Simon Laplace, France	ORCHIDEE	N	13	N	2.5°x1.25°	[87]
MIROC-ESM	Japan Agency for Marine-Earth Science and Technology, Japan;	MATSIRO + SEIB-DGVM	Y	13	N	2.8125°x~2.8125°	[88]

	Environmental Studies, Japan						
MPI-ESM-MR	Max Planck Institute for Meteorology, Germany	JSBACH + BETHY	Y	12	N	1.875°x1.875°	[89]
NorESM1-ME	Norwegian Climate Centre, Norway	CLM4	N	16	Y	2.5°x1.9°	[90]

2.2. Satellite data

The LAI data set used in this study (LAI3g) was generated using an Artificial Neural Network (ANN) from the latest version (third generation) of GIMMS AVHRR NDVI data for the period July 1981 to December 2010 at 15-day frequency. The ANN was trained with best-quality Collection 5 MODIS LAI product and corresponding GIMMS NDVI data for an overlapping period of 5 years (2000 to 2004) and then tested for its predictive capability over another five year period (2005 to 2009). The accuracy of the MODIS LAI product is estimated to be 0.66 LAI units [93] and the data is for 1-sided LAI. Further details on the LAI3g and the comparison with other satellite products are provided in [93, 94].

2.3. Leaf Phenology Analysis

Growing season onset, dormancy and length were all calculated based on the LAI seasonal amplitude. In fact, LAI has been shown to have a normal distribution over the year in northern latitudes [95], so we consider the start of the growing season to be 20% of the maximum amplitude. The values of 20% was defined after different tests were conducted using different thresholds; we found that this value provided the best results.

Overall, this method has being proven to be more stable for monthly data, compared to an approach based on sudden LAI changes [8]. It also should be noted that due to the lack of daily data for the LAI we were unable to use other methods used in previous studies based on the daily LAI variability [8].

In order to analyze changes in the growing season, we mask out regions where there are small changes in LAI over the year (e.g. evergreen forests and mixed forest with a small deciduous component). All grid points where the difference between the maximum and minimum LAI amplitude is less than 0.5 are ignored in this analysis.

Considering every grid cell (x,y) where the seasonal amplitude is greater than 0.5, we calculated a critical threshold value ($CT^{x,y}$) above which we assume the plants to be photosynthetically active**:**

$$\mathrm{CT}^{x,y} = LAI_{\min}^{x,y} + 0.2 * \left(LAI_{\max}^{x,y} - LAI_{\min}^{x,y} \right) \qquad (1)$$

where $LAI_{\min}^{x,y}$ and $LAI_{\max}^{x,y}$ represent the minimum and maximum LAI over one year for the grid cell (x,y). This procedure was repeated on each grid cell and for each year for any given CMIP5 model. The length of the growing

season was then calculated as the number of months with a value above this threshold; the onset is the first month above that value and the dormancy is the last. Finally, mean length, onset and dormancy were calculated as the average over the whole time period. It should be noted that, even when calculated monthly, all results are presented as days; we retrieved the daily values from the monthly data by multiplying all monthly results by 30.

The temporal changes in the mean annual LAI and GSL were estimated by the linear trend value obtained from a least squares fit line computed in period 1986–2005 of satellite and model data.

For all the variables, in order to quantify the mismatch between models and data, we calculate the root mean square errors (RMSE) and the spatial correlation coefficient between each model and the satellite observations.

3. Results

3.1 Mean LAI

In **Figure 1** we present the mean annual LAI (upper panel), the mean annual land precipitation (middle panel), and the mean annual surface temperature (bottom panel) for each model for the period 1986–2005, with the corresponding interannual variability and trends. Considering the temperature x-axis, models falling at the left (right) of observations (CRU, [96]) indicate a cold (warm) bias, while on the y axis models above (below) the observations have a stronger (lower) trend than observations. The same consideration is also valid for the precipitation, namely models falling at the left (right) of observations (CRU) indicate a dry (wet) bias, while on the y axis models above (below) the observations have a stronger (lower) trend than observations. It should also be noted that, to be consistent with LAI, we show the precipitation and temperature only over the land points of the Northern Hemisphere.

The evaluation of the simulated precipitation and temperature is needed to assess whether any bias in the simulated LAI can be related to poor performance of the ESMs at reproducing physical variables, or is mainly due to the poor representation of some biogeochemical processes in the land surface models of ESMs.

Looking at the LAI (**Figure 1**), in general, except CanESM2 and INMCM4, all the models overestimate the mean annual LAI over the Northern Hemisphere. The poorest performance has been found in GFDL-EMS2G, which shows a mean value of 2.7, much larger than the reference value (0.83); all the other models show a mean annual LAI ranging from 1.2 and 1.7. Conversely, the trends are well captured by quite a few models; specifically, many models are

clustered around the reference value, and, according to the observations, all the models show a greening in the last 20 years. The only far outlier is BNU-ESM, having a positive trend 6 times larger than the observed value. The interannual variability is in general well captured by most of the models, although a general overestimation of the year-to-year variability is found for a few models; the exceptions are CanESM2 and MPI-ESM-MR, which show an interannual variability slightly lower than LAI3g. Also, in this case, BNU-ESM is the only outlier in reproducing the IAV, having a year-to-year variability much larger than the reference value.

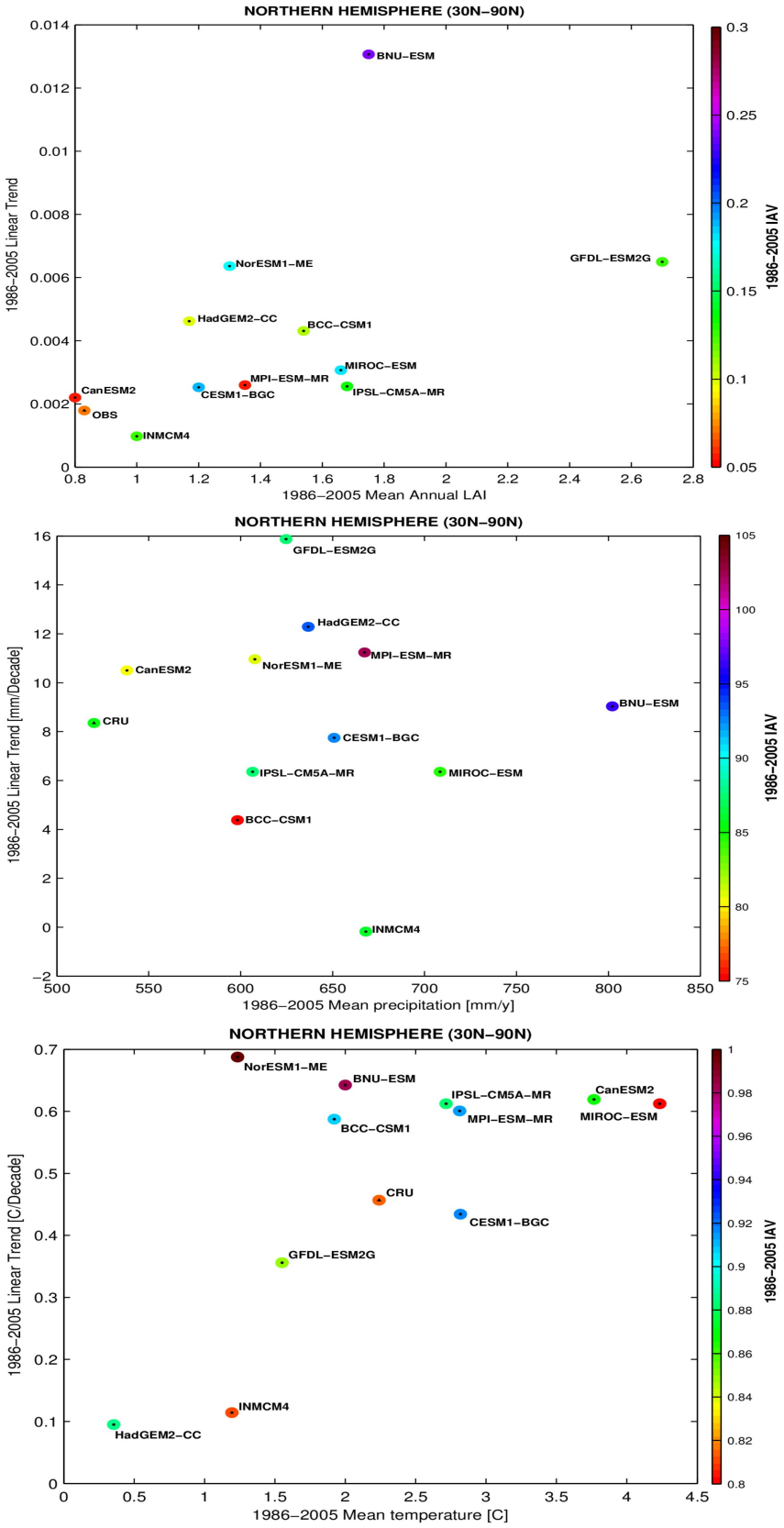

Figure 1. The x-axis shows the observed and simulated mean annual LAI (top), annual land precipitation (middle), and mean annual surface temperature over land (bottom). The y-axis shows the temporal trend, while the colorbar reports the interannual variability as computed from the annual standard deviation.

The large bias found in BNU-ESM could be related in some way to the strong wet bias that this model has in reproducing the observed precipitation. Specifically, whilst the mean annual precipitation as reported by CRU data is 520 mm/y, BNU-ESM shows a mean value of 802 mm/y. However, it should also be noted that, except CanESM2, all the other models also have a wet bias.

The wet bias found in all the CMIP5 ESM could explain the LAI overestimation: in fact the best agreement between observed and simulated LAI is found for CanEMS2, this being the only model without a wet bias. Although in the boreal and arctic region the temperature is the main limiting factor for the carbon assimilation, at mid-latitudes the precipitation plays a pivotal role through its control on the soil moisture [97,98].

The precipitation trends in general are well reproduced by the models, being all scattered around the reference data and all showing a wettening over the last 20 years. The exceptions are INMCM4, which does not show any trend in the land precipitation and GFDL-ESM2G, which has a wet bias two times larger than CRU. The interannual variability of the reference data is about 85 mm/y and only INMCM4, IPSL-CM5A-MR, GFDL-ESM2G and MIROC-ESM well reproduce this value, while CanESM2 (~80 mm/y), NorESM1-ME (~80 mm/y) and BCC-CSM1 (75 mm/y) have a slightly lower IAV and the remaining models show a larger IAV. It is noteworthy that MPI-ESM-MR has a IAV two times larger than the reference data.

Looking at the temperature, all the models are clustered around the reference data and only HadGEM2-CC (cold bias) and MIROC-ESM (warm bias) show a bias greater than 1.5 °C. In addition, all the models predict a warming in the Northern Hemisphere during the last 20 years; the weaker trends have been found in HadGEM2-CC and INMCM4 being about 4 times smaller than the one reported by CRU. The observed temperature interannual variability is about 0.8 °C and only INMCM4 and MIROC-ESM have a similar IAV; all the other models show a larger IAV than CRU with NorESM1-ME having an IAV of about 1 °C.

Although models in general show good skills in reproducing the observed climate, we would highlight that this agreement in the mean values over a large region could arise from a compensation between overestimation in some points of the domain and underestimation in other points [92]. This suggests that to perform an exhaustive model validation we should look at the spatial patterns (e.g. maps).

Figure 2 displays the spatial distribution of the mean annual LAI in the Northern Hemisphere as calculated from the CMIP5 ESMs and observed by satellite over the period 1986–2005. Results are projected over a stereographic projection from the North Pole, with the latitude ranging from 30°N to 90°N.

The observed spatial pattern of LAI is characterized by a wide maximum over Northern America and by a negative gradient extending from central Europe to

Northern-Eastern Asia, with a broad minimum in the Tibetan plateau due to the sparse vegetation. Although there is an overall overestimation by most of the CMIP5 models, quite a few models correctly reproduce this pattern: in particular CESM1-BGC, IPSL-CM5A-MR, and NorESM1-ME show a very good agreement with observations in terms of locations of the maximum and minimum values, as well as fairly simulating the gradient over the Eurasian region. This is confirmed by the relatively high value (> 0.6) of the spatial correlation computed between the models and the reference data. Conversely GFDL-ESM2G is not able to reproduce this spatial pattern, and LAI values above 5 are simulated over the whole North America and Asia; for this reason this model exhibits the lowest spatial correlation (0.21)

.

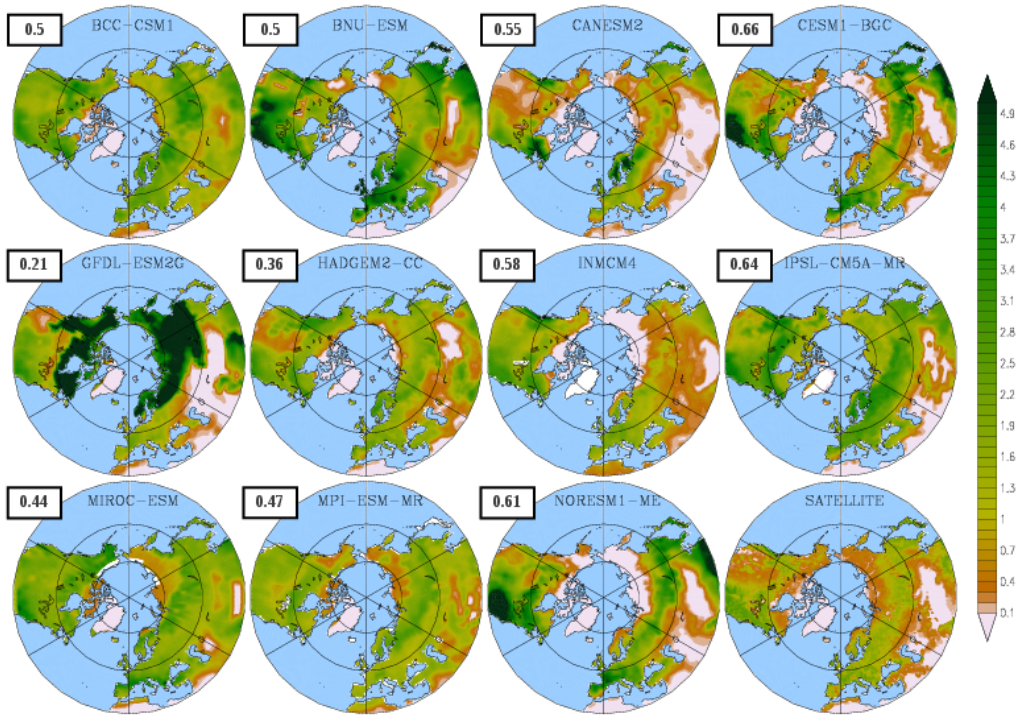

Figure 2. Spatial distribution of mean annual LAI as simulated by 11 CMIP5 ESMs and observed by satellite over the period 1986-2005 in the Northern Hemisphere (30-90ºN). The value in the box represents the spatial correlation between modeled and satellite mean annual values obtained by averaging over all the grid points

The seasonal amplitude patterns show large disagreement between the models and the satellite data (**Figure 3**). Some models (e.g. BNU-ESM and MIROC-ESM) clearly overestimate the mean amplitude, which is particularly evident over the whole North America and Eurasia. Other models (e.g. CESM1-BGC, HadGEM2-CC, MPI-ESM-MR, and NorESM1-ME) show a smaller seasonality than satellite data, while INMCM4, CanESM2 and BCC-CSM1 perform better than the rest of the models in reproducing the satellite-derived observations. The RMSE, indicating the mean error of the models in

reproducing a given variable, suggests that CanESM2 has the lowest error: in fact this model, albeit it slightly underestimates the seasonal amplitude over the Russia, has the correct magnitude for the observed seasonal amplitude. The same considerations are also valid for IPSL-CM5A-MR, INMCM4 and BCC-CSM1 which show a RMSE of 1.1. Conversely, BNU-ESM and MIROC-ESM show a larger seasonal amplitude than the satellite data, therefore they have high RMSE values.

The spatial correlation, indicating how well models reproduce the observed spatial pattern, confirm that CanESM2, INMCM4 overperform the spatial pattern of the seasonal amplitude compared to other models.

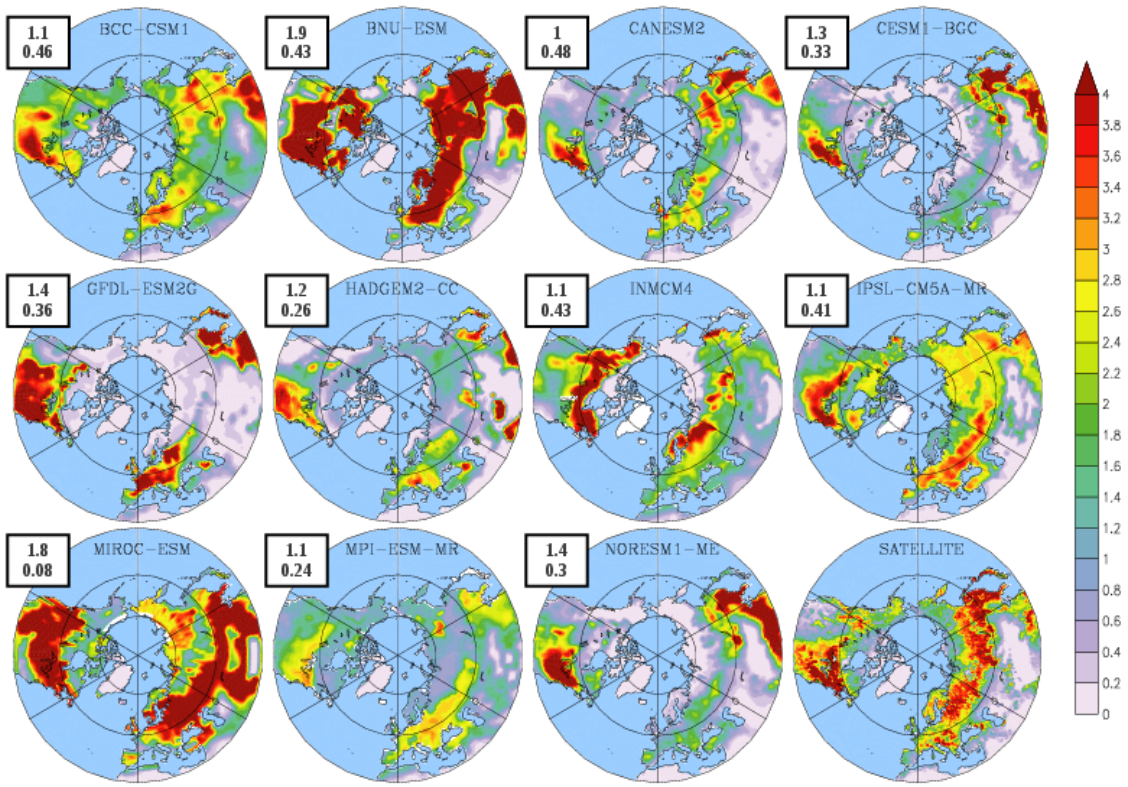

Figure 3. LAI Seasonal amplitude as simulated by 11 ESMs and satellite observations for the Northern Hemisphere (30-90ºN). In the box the value of root mean square error and spatial correlation, as computed from mean annual data and averaged over all the grid points, are presented for each model against the observations.

3.2 Growing Season

Figure 4 displays the spatial distribution of the mean onset dates of green-up as calculated from the CMIP5 ESMs and satellite observation for the period

1986–2005. As expected the satellite data show that the mean green-up date is progressively delayed with increasing latitude and increasing continentally [8]. The latest dates of green-up occur in northern Siberia, northern Canada, and over the Tibetan Plateau, owing to low temperatures. The growing season onset derived from CMIP5 ESMs shows much disagreement between the models. Some models (BNU-ESM, BCC-CSM1) correctly reproduce the observed spatial pattern being the correlation greater than 0.6, other models have some patchy areas of agreement that lead to high correlations, while HadGEM2-CC and IPSL-CM5A-MR do not reproduce the observed spatial distribution, as confirmed by the negative correlations.

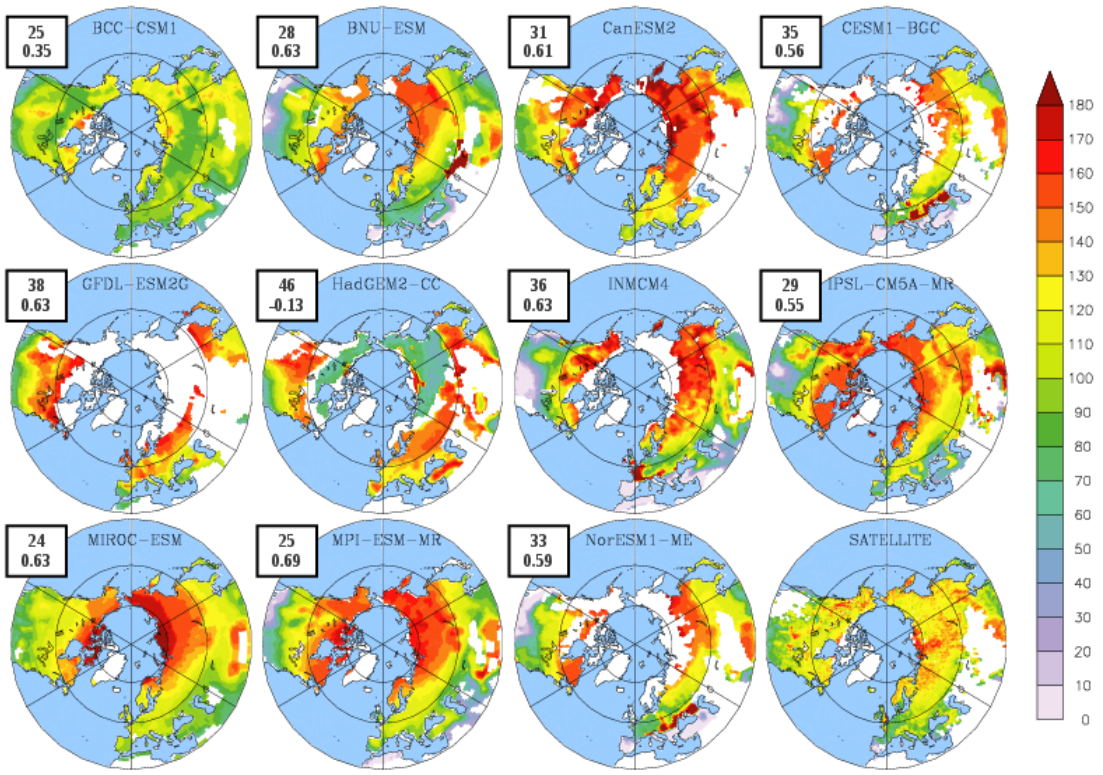

Figure 4. Mean growing season onset (day) as simulated by 11 CMIP5 ESMs and satellite observations over the Northern Hemisphere (30-90 ºN). For each model we masked out all the grid points where the seasonal amplitude is less than 0.5 (see **Figure 3**). In the box the value of root mean square error (in days) and spatial correlation, as computed from mean annual data and averaged over all the grid points, are presented for each model against the observations.

The models that correctly reproduce the green-up spatial pattern show an overestimation of the onset day, namely these models generally predict later onset values, particularly over the boreal forests of Siberia. This leads to the large RMSE values found for the onset in most of the models. The exception is

BCC-CSM1 which predicts slightly earlier onset values over Northern-Eastern Asia compared to satellite observations. It should also be noted that IPSL-CM5A-MR shows a green-up date of about 1 month over the whole Northern-Eastern Eurasia, while satellite data shows that the green-up occurs after 5-6 months, and this explains the large RMSE found for this model.

Considering GFDL-ESM2G, this model shows a larger onset date in the few “non-masked” grid points, while a large area of Eurasia and Northern America shows a seasonal amplitude less than 0.5. This suggests a problem in the initialization of the vegetation during the spin up phase: in fact the GFDL land model only allows coniferous trees to grow in cold climates, i.e. deciduous trees and grass do not grow in these cold regions. As a result, coniferous trees are established in areas where there should be tundra or cold deciduous trees, and therefore the seasonal amplitude is lower than expected.

Satellite data shows that the dates of vegetation senescence (**Figure 5)** occur in reverse order of the green-up onset, namely the green-up wave progresses northwards and dormancy wave progresses southwards. The discrepancies between models and satellite observations are even higher on the growing season dormancy, with most of the models failing to reproduce this pattern. Considering all the 11 ESMs only BNU-ESM, INMCM4, and CanESM2 have a dormancy distribution similar to the observed pattern, the spatial correlation being larger than 0.4. However, BNU-ESM and INMCM4 overestimate the offset date, and it explains the large RMSE error found for these 2 models. Contrarily, HadGEM2-CC, IPSL-CM5A-MR and MPI-ESM-MR show a slight negative spatial correlation, the latter 2 also having a large RMSE.

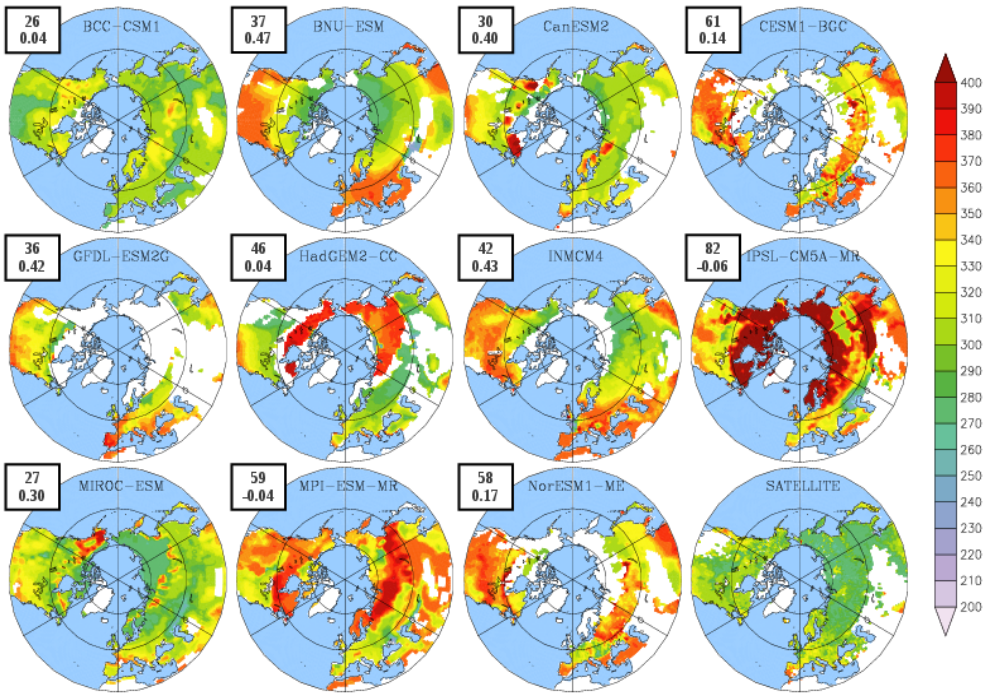

Figure 5. Mean growing season dormancy (day) as simulated by 11 CMIP5 ESMs and satellite observations over the Northern Hemisphere (30-90 ºN). For each model we masked out all the grid points where the seasonal amplitude is less than 0.5 (see **Figure 3**). In the box the value of root mean square error (in days) and spatial correlation, as computed from mean annual data and averaged over all the grid points, are presented for each model against the observations.

Compared to other CMIP5 models, GFDL-ESM2G has a smaller RMSE than the average. However it should be noted that it has been computed considering only a few grid points, due to the incorrect representation of the seasonal amplitude.

Looking at the satellite data, the growing season length is found to increase dramatically with decreasing latitude (**Figure 6**). It is the shortest in central and eastern Siberia along the Arctic coast, with a duration of only 3 months. In contrast, most of Europe, Eastern China and Southern North America have long growing seasons. The growing season length shows better agreement between satellite data and models, although individual models still exhibit large errors in reproducing the observed the spatial pattern. In spite of the high variability in onset and dormancy, the individual model performance somehow improves on the growing season length. This could be related to a compensation of the errors of models in simulating the onset and offset dates.

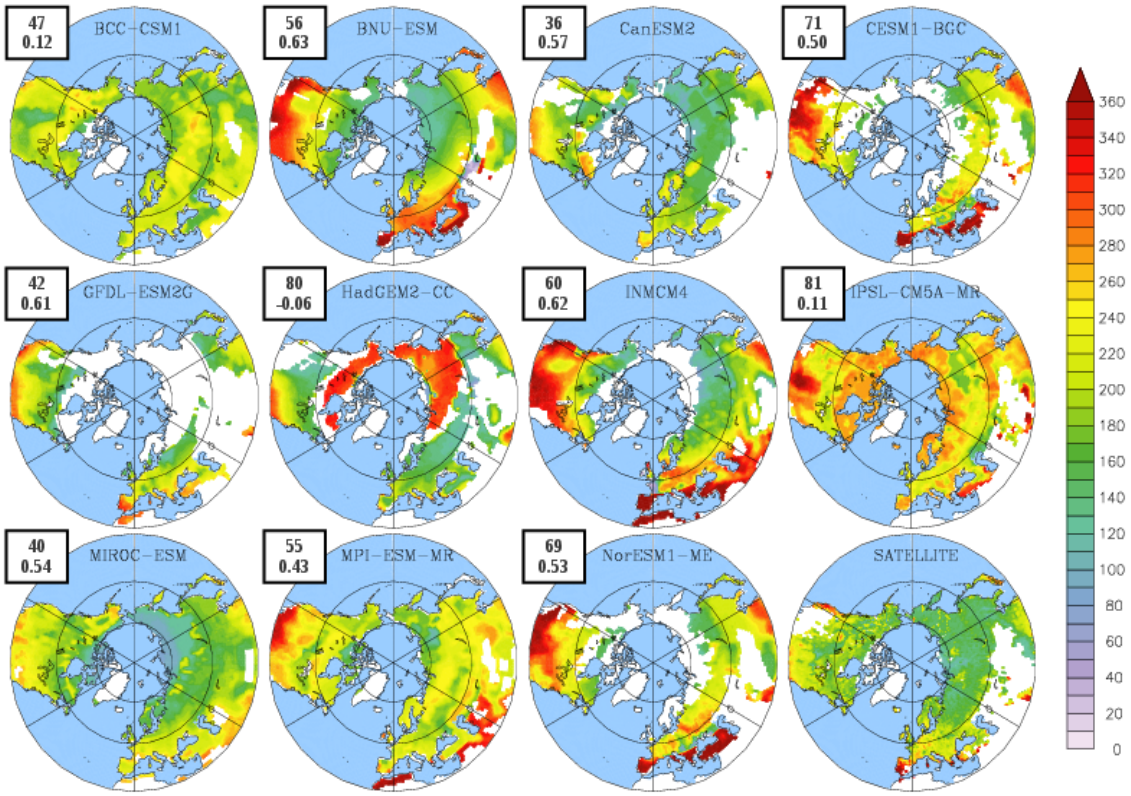

Figure 6. Mean growing season length (days) for 11 CMIP5 ESMs and satellite observations over the Northern Hemisphere (30-90 ºN). For each model we masked out all the grid points where the seasonal amplitude is less than 0.5 (see **Figure 3**). In the box the value of root mean square error (in days) and spatial correlation, as computed from mean annual data and averaged over all the grid points, are presented for each model against the observations.

Looking at the spatial pattern, the best results are found in BNU-ESM, INMCM4, CESM1-BGC, NorEMS1-ME, MIROC-ESM and CanESM2, being the correlation systematically greater than 0.5. Besides, in the few grid points covered by deciduous forests GFDL-ESM2G shows a good agreement with satellite GSL and this explains the relative high correlation and low RMSE compared to other ESMs. Consistent with previous results, HadGEM2-CC and IPSL-CM5A-MR show a negative correlation, indicating the inability of these models to reproduce the observed spatial variability. In addition HadGEM2-CC and IPSL-CM5A-MR also show the highest RMSE for the GSL, the IPSL-CM5A-MR error being almost 3 times larger than the lowest RMSE found in CanESM2.

3.3 Temporal Trends

Quite a few models predict an overall increase of LAI with time in most of the Northern Hemisphere, which is consistent with the satellite observations (**Figure 7**) which show a greening over the whole Eurasia and almost no

negative trend over the Northern Hemisphere, with a small exception over western North America and few locations in the Eurasian boreal forest.

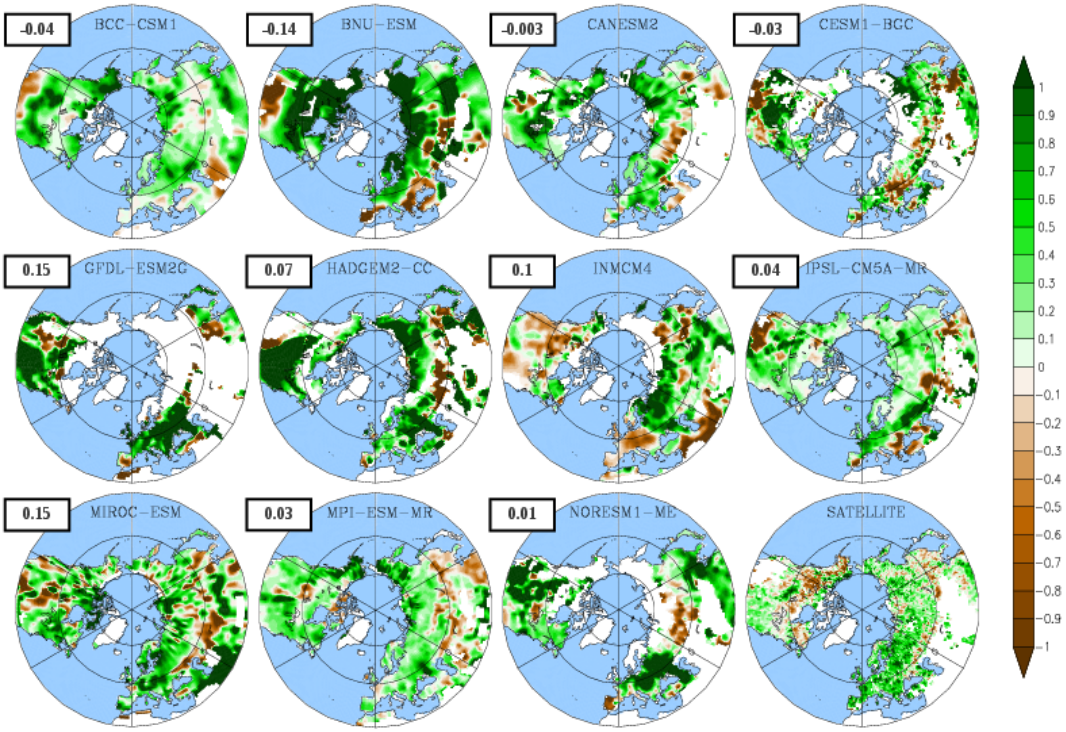

Figure 7. Observed and simulated LAI trends (%) computed over the period 1986-2005 for 11 CMIP5 ESMs and satellite observations over the Northern Hemisphere (30-90 ºN). For each model we masked out all the grid points where the seasonal amplitude is less than 0.5 (see **Figure 3**). The value in the box represents the spatial correlation between modeled and satellite mean annual values obtained by averaging over all the grid points.

From the whole compendium, BNU-ESM, GFDL-ESM2G, HadGEM2-CC and NorESM1-ME display the highest increase in LAI (see also **Figure 1**), mostly over the eastern coast of North America, Europe and the boreal forest of Asia. IPSL-CM5A-MR, MIROC-ESM, BCC-CSM1 and INMCM4 have an intermediate signal with the increase shown over the same regions, and some patchy areas where LAI decreased. We found that none of the models were able to reproduce the correct spatial pattern, the spatial correlation being close to 0 for almost all the models, except MIROC-ESM, which shows a positive correlation of 0.15.

The models also show a general increase in the growing season length, with patchy areas where it decreases (**Figures 8**). It is clear that from the 11 ESMs, those that perform better at calculating the growing season (both on the onset and dormancy) and LAI also do better for the trends, despite there being no spatial correlation between CMIP5 models and satellite data.

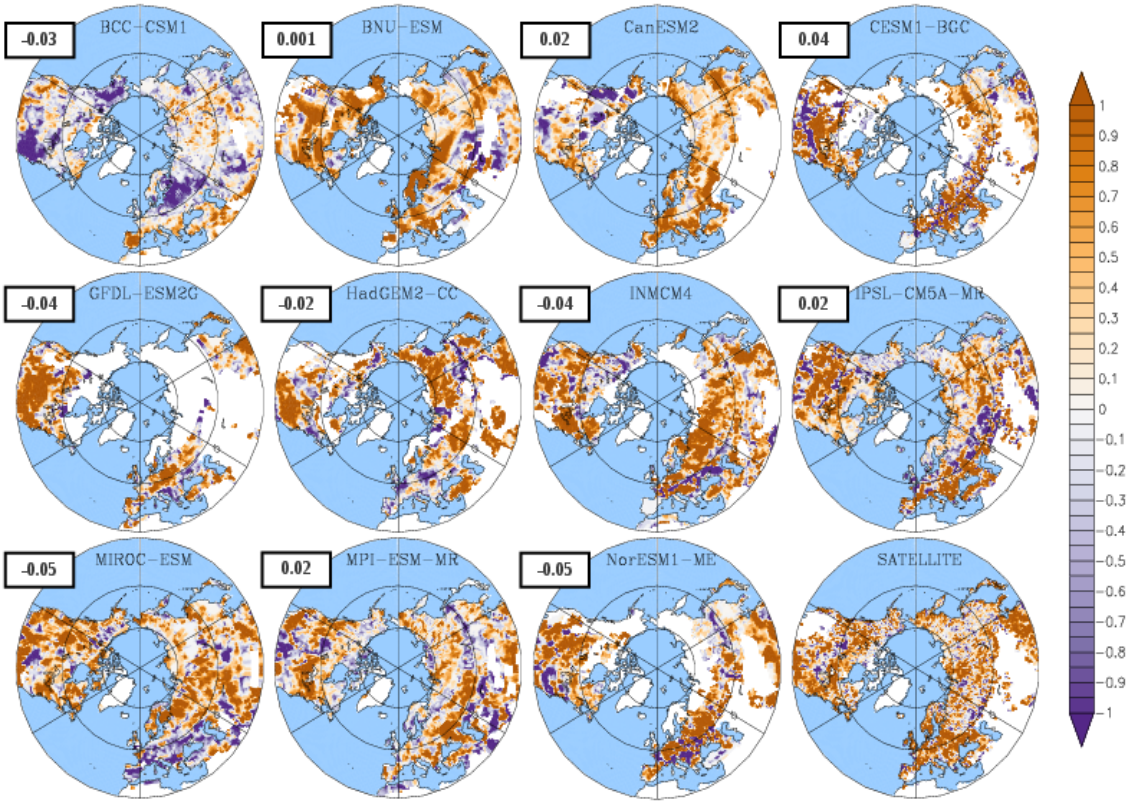

Figure 8. Observed and simulated GSL trends (days/year) computed over the period 1986-2005 for 11 CMIP5 ESMs and satellite observations over the Northern Hemisphere (30-90 ºN). For each model we masked out all the grid points where the seasonal amplitude is less than 0.5 (see **Figure 3**). The value in the box represents the spatial correlation between modeled and satellite mean annual values obtained by averaging over all the grid points.

4. Discussion

Results show that all coupled models correctly reproduce the spatial pattern of LAI (**Figure 2**), although an overall overestimation is found (**Figure 1**). GFDL-ESM2G clearly shows a strong overestimation over the Northern Hemisphere. Such overestimation in boreal forest is related to the substitution of tundra with coniferous forests; this result is supported by the low seasonal amplitude found over the whole Northern region of Eurasia.

Table 2 reports the comparison of simulated LAI and the leaf phenology, averaged over the whole domain of interest, against satellite observations.

Table 2. Average LAI, onset, dormancy and growing season length average for the Northern Hemisphere for each model and satellite observations. The values for dormancy and length based on GPP are presented in brackets.

Model	LAI	Onset	Dormancy	Length
BCC-CSM1	1.54	126	300 (274)	174 (146)
BNU-ESM	1.75	132	320 (280)	188 (148)
CanESM2	0.8	163	312 (295)	149 (149)
CESM1-BGC	1.2	117	340 (305)	223 (190)
GFDL-ESM2G	2.7	156	325 (304)	169 (152)
HadGEM2-CC	1.17	132	317 (279)	185 (132)
INMCM4	1.0	125	325 (289)	200 (164)
IPSL-CM5A-MR	1.68	77	340 (276)	263 (131)
MIROC-ESM	1.66	151	301 (276)	150 (130)
MPI-ESM-MR	1.35	134	333 (274)	199 (147)
NorESM1-ME	1.3	120	339 (303)	219 (186)
LAI3g	**0.83**	**138**	**289**	**151**

Looking at **Table 2**, it is clear that all the models overestimate not only the average LAI, but also the mean dormancy and length of the growing season, while the onset shows much agreement between model means and observations (**Table 2**). Satellite LAI average for the Northern Hemisphere is 0.83 while LAI from the models varies between 0.8 to 2.7. Growing season onset was earlier in 8 of the 11 models, while dormancy came between 11 to 51 days later in the models.

However, when the GSL period is calculated based on the gross primary production (GPP) the modeled values become much closer to the satellite values, with an average growing season length of 152±20 days, very similar to the 151 days from the satellite data. The same consideration is also valid for the growing season dormancy: in particular, looking at the spatial pattern, when the offset is computed using the GPP instead of the LAI, all the models show a geographical distribution very similar to the observations (**Figure 9**). This is confirmed by a relevant decrease in the RMSE values and an increase in the spatial correlations compared to results of **Figure 5**. These results suggest that the leaves in the models remain for longer than they should (discussed later).

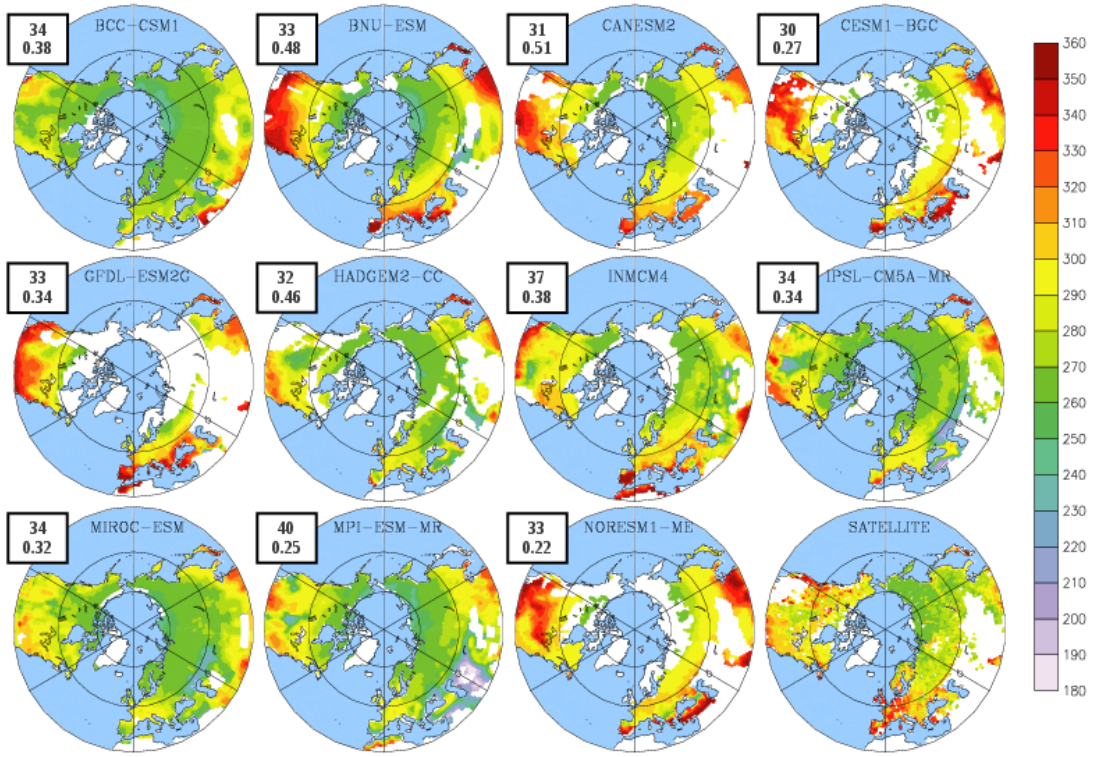

Figure 9. Mean growing season dormancy (day) as simulated by 11 CMIP5 ESMs and satellite observations over the Northern Hemisphere (30-90 ºN) computed using the GPP. For each model we masked out all the grid points where the LAI seasonal amplitude is less than 0.5 (see **Figure 3**). In the box the value of root mean square error (in days) and spatial correlation, as computed from mean annual data and averaged over all the grid points, are presented for each model against the observations.

Although the wet bias found in most of the analyzed CMIP5 models could explain the positive bias in LAI, this overestimation of the mean LAI is consistent with results from the uncoupled models (**Table 3**), suggesting that it is unlikely that differences in climate in the coupled models are solely responsible for this positive bias. This general overestimation could also be explained by a combination of underestimation of observed LAI, likely due to a saturation of satellite instrumentation, particularly on areas with dense vegetation, and by missing parameterizations of disturbances in the models (e.g. pollution, insect attack, nutrient limitation, grazing, fire dynamics), which leads to a larger amount of carbon stored in the biomass, which, in turn, leads to a larger LAI. The combination of these two effects explains why we found a relevant overestimation of simulated LAI in both coupled and uncoupled models.

The geographical pattern of average LAI is also similar between coupled and uncoupled models [78]. The overestimation of LAI is found consistently over the boreal forest (55ºN) when compared to the satellite observations, with better agreement over areas with scarce vegetation. When comparing models with the

same vegetation model (TRIFFID vs HADGEM2-CC, ORCHIDEE vs IPSL-CM5A-MR and CLM vs NorESM1 or CESM1-BGC) there are little differences in the distribution of LAI, suggesting that climatic variations in the coupled models are less important in controlling the distribution of LAI than having the correct vegetation distribution.

The onset patterns are similar among all coupled and uncoupled models, with the latest onset occurring over the boreal region. The similarities are even stronger over the dormancy where all models display a general overestimation over the boreal region, possibly explained by the late leaf shed in all models [99].

These results suggest that both coupled and uncoupled models predict a later dormancy (day) and a longer growing season length in comparison to satellite observation (**Table 3**). It seems that leaves in the models remain for longer than they should. However the late dormancy is not in line with the vegetation photosynthetic activity: in fact, when the same methodology to calculate the end of the photosynthetic active period was applied to the gross primary productivity (GPP), we found that the dormancy began at 277±7 days in the uncoupled models and 287±13 days in case of CMIP5 models, which is remarkably earlier than previously predicted by LAI, and much closer to the observed value of 289 days. It is evident that all models are keeping inactive leaves for longer than they should, which does not have any impact on the carbon cycle but could potentially modify surface radiation budget and turbulent fluxes, affecting therefore the PBL dynamics, which in turn could lead to potential bias in lower atmospheric dynamics simulated by ESMs. In addition to those ESMs having an interactive tropospheric chemistry component, the presence of inactive leaves could modify the deposition fluxes that strongly depend on the area of the canopy [11]. Conversely, the longer offset simulated by offline models does not affect simulation results since the climate is provided as input data and the feedbacks between the land surface and the atmosphere are not taken into account.

Table 3. Comparison of coupled and uncoupled ensemble means of LAI and phenology averaged over the Northern Hemisphere (30-90 ºN).

	LAI	**Onset**	**Dormancy**	**Length**
Uncoupled	1.55 ± 0.45	119 ± 36	324 ± 16 (277±7)	205 ± 49 (137±20)
Coupled	1.47 ± 0.51	130 ± 23	323 ± 15 (287±13)	193 ± 34 (152±20)
LAI3g	**0.83**	**138**	**289**	**151**

Looking at the LAI trends, all the coupled models show a clear greening over the whole Northern America and Eurasia, consistent with satellite data, while not all the offline models show the same pattern over the high latitudes of the Northern Hemisphere. Considering all the ESMs, the greening of the high latitudes is likely driven by positive temperature trend (**Figure 1**) but in some of the offline models we observe a browning over the same region, suggesting that offline modelled LAI is also sensitive to moisture changes, as most of the browning occurs over areas where precipitation shows a decrease (not shown).

The previous similarities between coupled and uncoupled models, similar geographical distribution of LAI with higher values than the satellite data, and an extended growing season mostly driven by a later dormancy all suggests that the correct initialization and distribution of vegetation in the models is the most important feature in the correct representation of LAI. Nevertheless climatic variables, temperature in particular, have proven to be the main drivers of changes over time [100].

5. Concluding Remarks

We compared LAI from 11 Earth-System Models from CMIP5 against satellite data and uncoupled models from part I, for the Northern Hemisphere during the 1986-2005 period. We compared the mean annual LAI, the spatial pattern of LAI and the onset, dormancy and length of the growing season. Our results show that models consistently overestimate the mean value of LAI, and also have an increased growing season, mostly due to a later dormancy. This is consistent with the finding on the uncoupled models.

We conclude that validating LAI in each model against satellite observations should be a fundamental step for all modelling groups, and this process is more central than the correct LAI parameterization against climate. This is essential since changes in LAI have been used to show the existence of an increased growing season over the last decades, and since LAI is a fundamental parameter in all models, required to correctly calculate the hydrological, energetic and carbon fluxes.

Acknowledgments

We acknowledge the World Climate Research Programme's Working Group on Coupled Modelling, which is responsible for CMIP, and we thank the climate modeling groups (listed in Table 1 of this paper) for producing and making available their model output. For CMIP the U.S. Department of Energy's Program for Climate Model Diagnosis and Intercomparison provides coordinating support and led development of software infrastructure in partnership with the Global Organization for Earth System Science Portals. We also thank Ranga Myneni for his valuable contribution and comments on the

development of the paper, Xuhui Wang for his help on the methodology, and the three anonymous reviewers who helped to improve the paper.

References and Notes

1. Myneni, R.B.; Hoffman, S.; Knyazikhin, Y.; Privette, J. L.; Glassy, J.; Tian, Y.; Wang, Y.; Song, X.; Zhang, Y.; Smith, G.; *et al.* Global products of vegetation leaf area and fraction absorbed PAR from year one of MODIS data. *Remote Sens. Environ*. **2002**, *83*, 214–231.
2. Sellers, P.J.; Randall, D.A.; Betts, A.K.; Hall, F.G.; Berry, J.A.; Collatz, G.J.; Denning, A.S.; Mooney, H.A.; Nobre, C.A.; Sato, N.; *et al.* Modeling the exchanges of energy, water, and carbon between continents and the atmosphere. *Science* **1997**, *275*, 502–509.
3. Botta, A.; Viovy, N.; Ciais, P.; Friedlingstein, P. A global prognostic scheme of leaf onset using satellite data. *Global Change Biol.* **2000**, *6*, 709–726.
4. Pielke, R.A.; Avissar, R.; Raupach, M.; Dolman, A.J.; Zeng, X.; Denning, A.S. Interactions between the atmosphere and terrestrial ecosystems: influence on weather and climate. *Global Change Biol.* **1998**, *4*, 461–475.
5. Brovkin, V. Climate-vegetation interaction. *J. Phys.* **2002**, *4*, 57–72.
6. Chase, T.N.; Pielke, R.; Kittel, T.; Nemani, R.; Running, S. Sensitivity of a general circulation model to global changes in leaf area index. *J. Geophys. Res.* **1996**, *101*, 7393–7408.
7. Betts, R.A.; Cox, P.M.; Lee, S.E.; Woodward, F.I. Contrasting physiological and structural vegetation feedback in climate change simulations. *Nature* **1997**, *387*, 796-799.
8. Piao, S.; Friedlingstein, P.; Ciais, P.; Viovy, N.; Demarty, J. Growing season extension and its impact on terrestrial carbon cycle in the Northern Hemisphere over the past 2 decades. *Global Biogeochem. Cy.* **2007**, *21*, GB3018, doi:10.1029/2006GB002888.
9. Guenther, A.; Karl, T.; Harley, P.; Wiedinmyer, C.; Palmer, P. I.; Geron, C. Estimates of global terrestrial isoprene emissions using MEGAN (Model of Emissions of Gases and Aerosols from Nature). *Atmos. Chem. Phys.* **2006**, *6*, 3181–3210.
10. Lathière, J.; Hauglustaine, D.A.; Friend, A.D.; De Noblet-Ducoudré, N.; Viovy, N.; Folberth, G.A. Impact of climate variability and land use changes on global biogenic volatile organic compound emissions. *Atmos. Chem. Phys.* **2006**, *6*, 2129-2146.
11. Petroff, A.; Mailliat, A.; Amielh, M.; Anselmet, F. Aerosol dry deposition on vegetative canopies. Part 1: Review of present knowledge. *Atmos. Environ.* **2008**, *42*, 3625–3653.
12. Anav, A.; Menut, L.; Khvorostyanov, D.; Viovy, N. A comparison of two canopy conductance parameterizations to quantify the interactions between

surface ozone and vegetation over Europe. *J. Geophys. Res.* **2012**, *117*, G03027.
13. Menzel, A.; Fabian, P. Growing season extended in Europe. *Nature* **1999**, *397*, 659.
14. Ahas, R.; Jaagus, J.; Aasa, A. The phenological calendar of Estonia and its correlation with mean air temperature. *Int. J. Biometeorol.* **2000**, *44*, 159–166.
15. Myneni, R.B.; Keeling, C. D.; Tucker, C.J.; Asrar, G.; Nemani, R.R. Increased plant growth in the northern latitudes from 1981–1991. *Nature* **1997**, *386*, 698–702.
16. Zhou, L.; Tucker, C.J.; Kaufmann, R.K.; Slayback, D.; Shabanov, N.V.; Myneni, R.B. Variations in northern vegetation activity inferred from satellite data of vegetation index during 1981 to 1999. *J. Geophys. Res.* **2001**, *106*, 20069–20083.
17. Tucker, C.J.; Slayback, D.; Pinzon, J.E.; Los, S.O.; Myneni, R.B.; Taylor, M.G. Higher northern latitude normalized difference vegetation index and growing season trends from 1982 to 1999. *Int. J. Biometeorol.* **2001**, *45*, 184–190.
18. Suzuki, R.; Nomaki, T.; Yasunari, T. West-east contrast of phenology and climate in northern Asia revealed using a remotely sensed vegetation index. *Int. J. Remote Sens.* **2003**, *47*, 126–138.
19. Stöckli, R.; Vidale, P.L. European plant phenology and climate as seen in a 20-year AVHRR land-surface parameter dataset. *Int. J. Remote Sens.* **2004**, *25*, 3303–3330.
20. Keeling, C.D.; Chin, J.F.S.; Whorf, T.P. Increased activity of northern vegetation in inferred from atmospheric CO_2 measurements. *Nature* **1996**, *382*, 146–149.
21. Lucht, W.; Prentice, I.C.; Myneni, R.B.; Sitch, S.; Friedlingstein, P.; Cramer, W.; Bousquet, P.; Buermann, W.; Smith, B. Climatic control of the high-latitude vegetation greening trend and Pinatubo effect. *Science* **2002**, *296*, 1687–1689.
22. Barichivich, J.; Briffa, K.R.; Osborn, T.J.; Melvin, T.M.; Caesar, J. Thermal growing season and timing of biospheric carbon uptake across the Northern Hemisphere. *Global Biogeochem. Cy.* **2012**, *26*.
23. Kimball, J.; McDonald, K.; Running, S.; Frolking S. Satellite radar remote sensing of seasonal growing seasons for boreal and subalpine evergreen forests. *Remote Sens. Environ*. **2004**, *90*, 243–258.
24. Euskirchen, E.S.; McGuire, A.D.; Kicklighter, D.W.; Zhuang, Q.; Clein, J.S.; Dargaville, R.J.; Dye, D.G.; Kimball, J.S.; McDonald, K.C.; Melillo, J.M.; Romanovsky, V.E.; Smith, N.V. Importance of recent shifts in soil thermal dynamics on growing season length, productivity, and carbon sequestration

in terrestrial high-latitude ecosystems. *Global Change Biol.* **2006**, *12*, 731–750.
25. Linderholm, H. Growing season changes in the last century. *Agr. Forest Meteorol.* **2006**, *137*, 1–14.
26. Churkina, G.; Schimel, D.; Braswell, B.; Xiao, X. Spatial analysis of growing season length control over net ecosystem exchange. *Global Change Biol.* **2005**, *11*, 1777–1787.
27. Richardson, A.D.; Black, T.A.; Ciais, P.; Delbart, N.; Friedl, M.A.; Gobron, N.; Hollinger, D.Y.; Kutsch, W.L.; Longdoz, B.; Luyssaert, S.; *et al.* Influence of spring and autumn phenological transitions on forest ecosystem productivity. *Philos. T. R. Soc. B.* **2010**, *365*, 3227–3246.
28. Keeling, C.; Chin, J.; Whorf, T. Increased activity of northern vegetation inferred from atmospheric CO2 measurements. *Nature* **1996**, *382*, 146–149.
29. Myneni, R.; Keeling, C.; Tucker, C.; Asrar, G.; Nemani, R. Increased plant growth in the northern high latitudes from 1981 to 1991. **Nature 1997**, *386*, 698–702.
30. Menzel, A.; Fabian, P. Growing season extended in Europe. *Nature* **1999**, *397*, 659.
31. Zhou, L.; Tucker, C.J.; Kaufmann, R.K.; Slayback, D.; Shabanov, N.V.; Myneni, R.B. Variations in northern vegetation activity inferred from satellite data of vegetation index during 1981 to 1999. *J. Geophys. Res.* **2001**, *106*, 20069–20083.
32. Mao, J; Shi, X.; Thornton, P.E.; Piao, S.; Wnag, X. Causes of spring vegetation growth trends in the northern mid–high latitudes from 1982 to 2004. *Environ. Res. Lett.* **2012**, *7*, 014010 doi:10.1088/1748-9326/7/1/014010.
33. Mao, J.; Shi, X.; Thornton, P.E.; Hoffman, F.M.; Zhu, Z.; Myneni, R.B. Global Latitudinal-Asymmetric Vegetation Growth Trends and Their Driving Mechanisms: 1982–2009. *Remote Sens.* **2013**, *5*, 1484-1497.
34. Smith, N.V.; Saatchi, S. S.; Randerson, J.T. Trends in high northern latitude soil freeze and thaw cycles from 1988 to 2002. *J. Geophys. Res.* **2004**, *109*.
35. Christidis, N.; Stott, P.; Brown, S.; Karoly, D.; Caesar J. Human contribution to the lengthening of the growing season during 1950–99. *J. Clim.* **2007**, *20*, 5441–5454.
36. Suni, T.; Berninger, F.; Markkanen, T.; Keronen, P.; Rannik, Ü.; Vesala T. Interannual variability and timing of growing-season CO2 exchange in a boreal forest. *J. Geophys. Res*. **2003**, *108*.
37. Kimball, J.; McDonald, K.; Running, S.; Frolking, S. Satellite radar remote sensing of seasonal growing seasons for boreal and subalpine evergreen forests. *Remote Sens. Environ* **2004**, *90*, 243–258.

38. Hänninen, H.; Tanino, K. Tree seasonality in a warming climate. *Trends Plant Sci.* **2011**, *16*, 412–416.
39. Charney, J.; Quirk, W.J.; Chow, S.-H.; Kornfield, J. A comparative study of the effects of albedo change on drought in semi-arid regions. *J. Atmos. Sci.* **1977**, *34*, 1366–1385.
40. Sud, Y.C.; Fennessy, M.J. A study of the influence of surface albedo on July circulation in semi-arid regions using the GLAS GCM. *J. Climatol.* **1982**, *2*, 105–125.
41. Dirmeyer, P.A., Shukla, J. Albedo as a modulator of climate response to tropical deforestation. *J. Geophys. Res.* **1994**, *99*, 20863–20877.
42. Shukla, J.; Mintz, Y. Influence of land-surface evapotranspiration on the Earth's climate. *Science* **1982**, *215*, 1498–1501.
43. Douville, H.; Chauvin, F.; Broqua, H. Influence of soil moisture on the Asian and African monsoons. Part I: Mean monsoon and daily precipitation. *J. Climate* **2001**, *14*, 2381–2403.
44. Zampieri, M.; D'Andrea, F.; Vautard, R.; Ciais, P.; de Noblet-Ducoudré, N.; Yiou, P. Hot European Summers and the Role of Soil Moisture in the Propagation of Mediterranean Drought. *J. Climate* **2009**, *22*, 4747–4758.
45. Sud, Y.C.; Shukla, J.; Mintz, Y. Influence of land surface roughness on atmospheric circulation and precipitation: A sensitivity study with a general circulation model. *J. Appl. Meteor.* **1988**, *27*, 1036–1054.
46. Bounoua, L.; Collatz, G.J.; Los, S.O.;. Sellers, P.J; Dazlich, D.A.; Tucker, C.J.; Randall, D.A. Sensitivity of climate to changes in NDVI. *J. Climate* **2000**, *13*, 2277–2292.
47. Oleson, K.W.; Bonan, G.B. The effects of remotely sensed plant functional type and leaf area index in simulations of boreal forest surface fluxes by the NCAR land surface model. *J. Hydrometeor.* **2000**, *1*, 431–446.
48. Buermann, W.; Dong, J.; Zeng, X.; Myneni, R.B.; Dickinson, R.E. Evaluation of the utility of satellite-based leaf area index data for climate simulation. *J. Climate* **2001**, *14*, 3536–3550.
49. Van den Hurk, B.J.J.M.; Viterbo, P.; Los, S.O. Impact of leaf area index seasonality on the annual land surface evaporation in a global circulation model. *J. Geophys. Res.* **2003**, *108*, 4191, doi:10.1029/2002JD002846.
50. Tian, Y.; Dickinson, R.E.; Zhou, L.; Myneni, R.B.; Friedl, M.; Chaaf, C.B.; Carroll, M.; Gao, F. Land boundary conditions from MODIS data and consequences for the albedo of a climate model. *Geophys. Res. Lett.* **2004**, *31*, L05504.
51. Kang, H.-S.; Xue, Y.; Collatz, G.J. Impact assessment of satellite-derived leaf area index datasets using a general circulation model: Seasonal variability. *J. Climate* **2007**, *20*, 993–1015.
52. Dickinson, R.E.; Henderson-Sellers, A; Kennedy, P.J. Biosphere-Atmosphere Transfer Scheme (BATS) Version 1e as coupled to the NCAR

community climate model. NCAR Technical Note, NCAR/TN-387+ STR, 1993, National Center for Atmospheric Research, Boulder, CO.
53. Giorgi, F.; Marinucci M.R.; Bates, G.T. Development of a second generation regional climate model (RegCM2). I. Boundary-layer and radiative transfer processes. *Mon Weather Rev* **1993**, *121*, 2794–2813
54. Schulz, J.-P.; Dümenil, L.; Polcher, J.; Schlosser, C.A.; Xue, Y. Land surface energy and moisture fluxes: Comparing three models. *J. Appl. Meteor.* **1998**, *37*, 288–307.
55. Lawrence, D.M.; Slingo, J.M. An annual cycle of vegetation in a GCM. Part II: Global impacts on climate and hydrology. *Clim. Dynam.* **2004**, *22*, 107–122.
56. Stier, P.; Feichter, J.; Kinne, S.; Kloster, S.; Vignati, E.; Wilson, J.; Ganzeveld, L.; Tegen, I.; Werner, M.; Balkanski, Y.; *et al.* The aerosol-climate model ECHAM5-HAM. *Atmos. Chem. Phys.* **2005**, *5*, 1125-1156.
57. Hourdin, F.; Musat, I.; Bony, S.; Braconnot, P.; Codron, F.; Dufresne, J.-L.; Fairhead, L.; Filiberti, M. A.; Friedlingstein, P.; Grandpeix, J.-Y.; *et al.* The LMDZ4 general circulation model: climate performance and sensitivity to parametrized physics with emphasis on tropical convection. *Clim. Dynam.* **2006**, *19*, 3445–3482.
58. Foley, J.A.; Prentice, I.C.; Ramankutty, N.; Levis, S.; Pollard, D.; Sitch, S.; Haxeltine, A. An integrated biosphere model of land surface processes, terrestrial carbon balance, and vegetation dynamics. *Global Biogeochem. Cy.* **1996**, *10*, 603-628.
59. Sellers, P.J.; Randall, D.A.; Collatz, G.J.; Berry, J.A.; Field, C.B.; Dazlich, D.A.; Zhang, C.; Collelo, G.D.; Bounoua, L. A revised land surface parameterization (SiB2) for atmospheric GCMs, Part I : Model Formulation. *J. Climate* **1996**, *9*, 676–705.
60. Foley, J.A.; Levis, S.; Prentice, I.C.; Pollard, D.; Thompson, S.L. Coupling dynamic models of climate and vegetation. *Global Change Biol.* **1998**, *4*, 561-579.
61. Foley, J.A.; Levis, S.; Costa, M.H.; Cramer, W.; Pollard, D. Incorporating dynamic vegetation cover within global climate models. *Ecol. Appl.* **2000**, *10*, 1620-1632.
62. Bonan, G.; Levis, S.; Sitch, S.; Vertenstein, M.; Oleson, K.W. A dynamic global vegetation model for use with climate models: concepts and description of simulated vegetation dynamics. *Global Change Biol.* **2003**, *9*, 1543–1566.
63. Pitman, A.J. The evolution of, and revolution in, land surface schemes designed for climate models. *Int. J. Climatol.* **2003**, *23*, 479–510.
64. Sitch, S.; Smith, B.; Prentice, I.C.; Arneth, A.; Bondeau, A.; Cramer, W.; Kaplan, J.O.; Levis, S.; Lucht, W.; Sykes, M.T.; *et al*. Evaluation of ecosystem dynamics, plant geography and terrestrial carbon cycling in the

LPJ dynamic global vegetation model. *Global Change Biol.* **2003**, 9, 161–185.

65. Krinner, G.; Viovy, N.; de Noblet-Ducoudré, N.; Ogée, J.; Polcher, J.; Friedlingstein, P.; Ciais, P.; Sitch, S.; Prentice, I.C. A dynamic global vegetation model for studies of the coupled atmosphere-biosphere system. *Global Biogeochem. Cy.* **2005**, *19*, GB1015.
66. Alessandri, A.; Gualdi, S.; Polcher, J.; Navarra, A. Effects of Land Surface-Vegetation on the Boreal Summer Surface Climate of a GCM. *J. Climate* **2007**, 20, 225–278.
67. Taylor, K.; Stouffer, R.; Meehl, G. An overview of CMIP5 and the experiment design. *B. Am. Meteorol. Soc.* **2012**, *93,* 485–498.
68. Collins, W.J.; Bellouin, N.; Doutriaux-Boucher, M.; Gedney, N.; Halloran, P.; Hinton, T.; Hughes, J.; Jones, C.D.; Joshi, M.; Liddicoat, S.; *et al.* Development and evaluation of an Earth-System model – HadGEM2. *Geosci. Model Dev.* **2011**, 4, 1051-1075.
69. Charlson, R.J.; Lovelock, J.E.; Andreae, M.O.; Warren, S.G. Oceanic phytoplankton, atmospheric sulphur, cloud albedo and climate. *Nature* **1987**, *326*, 655–661.
70. Cox, P.M.; Betts, R.A.; Jones, C.D.; Spall, S.A.; Totterdell, I.J. Acceleration of global warming due to carbon-cycle feedbacks in a coupled climate model. *Nature* 2000, *408*, 184–187.
71. Rea, J.; Ashley, M. Phenological evaluations using Landsat-1 sensors. *Int. J. Biometeorol* **1976**, *20*, 240–248
72. Girard, C.M. (1982). Estimation of phenological stages and physiological states of grasslands from remote-sensing data. *Vegetatio* **1982**, *48*, 219–226.
73. White, M.A.; Thornton, P.E.; Running, S.W. (1997). A continental phenology model for monitoring vegetation responses to interannual climatic variability. *Global Biogeochem. Cy.* **1997**, *11*, 217–234.
74. Zhang, X.; Friedl, M.A.; Schaaf, C.B.; Strahler, A.H.; Hodges, J.C.F.; Gao, F.; Reed, B.C.; Huete A. Monitoring vegetation phenology using MODIS. *Remote Sens. Environ.* **2003**, *84*, 471–475.
75. Zhou, L.; Kaufmann, R.K.; Tian, Y.; Myneni, R.B.; Tucker, C.J. Relation between interannual variations in satellite measures of northern forest greeness and climate between 1982 and 1999. *J. Geophys. Res.* **2003**, *108*, 4004, doi:10.1029/2002JD002510.
76. Zhang, P.; Anderson, B.; Barlow, M.; Tan, B.; Myneni R.B. Climate-related vegetation characteristics derived from Moderate Resolution Imaging Spectroradiometer (MODIS) leaf area index and normalized difference vegetation index. *J. Geophys. Res.* **2004**, *109*, D20105.

77. Ahl, D.E.; Gower, S.T.; Burrows, S.N.; Shabanov, N.V.; Myneni, R.B.; Knyazikhin, Y. Monitoring spring canopy phenology of a deciduous broadleaf forest using MODIS. *Remote Sens. Environ.* **2006**, *104*, 88–95.
78. Murray-Tortarolo, G.; Anav, A.; Friedlingstein, P.; Sitch, S.; Piao, S.; Zhu, Z. Evaluation of DGVMs in reproducing satellite derived LAI over the Northern Hemisphere. Part I: Uncoupled DGVMs. *Remote Sensing* **2013**, Submitted.
79. http://pcmdi3.llnl.gov/esgcet/
80. Wu, T.; Li, W.; Ji, J.; Xin, X.; Li, L.; Wang, Z.; Zhang, Y.; Li, J.; Zhang, F.; Wei, M.; Shi, X.; *et al.* Global carbon budgets simulated by the Beijing Climate Center Climate System Model for the last century. *J. Geophys. Res.* **2013**, *118*, doi:10.1002/jgrd.50320
81. http://esg.bnu.edu.cn/BNU_ESM_webs/htmls/index.html
82. Arora, V.K.; Scinocca, J.F.; Boer, G.J.; Christian, J.R.; Denman, K.L.; Flato, G.M.; Kharin, V.V.; Lee, W.G.; Merryfield, W.J. Carbon emission limits required to satisfy future representative concentration pathways of greenhouse gases. *Geophys. Res. Lett.* **2011**, *38*,.
83. Lindsay, K.; Bonan, G.B.; Doney, S.C.; Hoffman, F.M.; Lawrence, D.M.; Long, M.C.; Mahowald, N.M.; Moore, J.K.; Randerston, J.T.; Thornton, P.E. Preindustrial Control and 20th Century Carbon Cycle Experiments with the Earth System Model CESM1-(BGC). Submitted to *J. Climate*, **2013**.
84. Dunne, J.P.; John, J.G.; Shevliakova, E.; Stouffer, R.J.; Krasting, J.P.; Malyshev, S.L.; Milly, P.C.D.; Sentman, L.T.; Adcroft, A.J. Cooke, W.; Dunne, K.A.; *et al.* GFDL's ESM2 global coupled climate-carbon Earth System Models. Part II: Carbon system formation and baseline simulation characteristics. *J Climate* **2013,** *26*, 2247–2267.
85. Collins, W.J.; Bellouin, N.; Doutriaux-Boucher, M.; Gedney, N.; Halloran, P.; Hinton, T.; Hughes, J.; Jones, C.D.; Joshi, M.; Liddicoat, S.; Martin, G.; O'Connor, F.; Rae, J.; Senior, C.; Sitch, S.; Totterdell, I.; Wiltshire, A.; Woodward, S. Development and evaluation of an Earth-system model–HadGEM2. *Geosci. Model Dev.* **2011**, *4*, 1051-1075.
86. Volodin, E.M.; Dianskii, N.A.; Gusev, A.V. Simulating present day climate with the INMCM4.0 coupled model of the atmospheric and oceanic general circulations. *Izv. Ocean. Atmos. Phys.* **2010**, *46*, 414–431.
87. Dufresne, J.-L.; Foujols, M.-A.; Denvil, S.; Caubel, A.; Marti, O.; Aumont, O.; Balkanski, Y.; Bekki, S.; Bellenger, H.; Benshila, R.; Bony, S.; Bopp, L. Climate change projections using the IPSL-CM5 Earth System Model: from CMIP3 to CMIP5. *Clim. Dynam.* **2013**, *40*, 2123-2165
88. Watanabe, S.; Hajima, T.; Sudo, K.; Nagashima, T.; Takemura, T.; Okajima, H.; Nozawa, T.; Kawase, H.; Abe, M.; Yokohata, T.; Ise, T.; Sato, H.; Kato, E.; Takata, K.; Emori, S.; Kawamiya, M. MIROC-ESM 2010: model description and basic results of CMIP5-20c3m experiments. *Geosci. Model Dev.* **2011**, *4*, 845-872.

89. Raddatz, T.; Reick, C.H.; Knorr, W.; Kattge, J.; Roeckner, E. Schnur, R.; Schnitzler, K.-G.; Wetzel, P.; Jungclaus, J. Will the tropical land biosphere dominate the climate-carbon cycle feedback during the twenty-first century? *Clim. Dynam.*, **2007**, *29*, 565-574.
90. Bentsen, M.; Bethke, I.; Debernard, J.B.; Iversen, T.; Kirkevåg, A.; Seland, Ø.; Drange, H.; Roelandt, C.; Seierstad, I.A.; Hoose, C.; Kristjánsson, J.E. The Norwegian Earth System Model, NorESM1-M – Part 1: Description and basic evaluation. *Geosci. Model Dev. Discuss.* **2012**, 5, 2843-2931,
91. Taylor, K. E., R. J. Stouffer, and G. A. Meehl, 2012: AN OVERVIEW OF CMIP5 AND THE EXPERIMENT DESIGN. Bull. Amer. Meteorol. Soc., 93, 485-498.
92. Anav, A.; , Friedlingstein, P.; Kidston, M.; Bopp, L.; Ciais, P.; Cox, P.M.; Jones, C.D.; Jung, M.; Myneni, R.B.; Zhu, Z. Evaluating the land and ocean components of the global carbon cycle in the CMIP5 Earth System Models. *J Climate* **2013**, In Press.
93. Zhu, Z.; Bi, J.; Pan, Y.; Ganguly, S.; Anav, A.; Xu, L.; Samanta, A.; Piao, S.; Nemani, R.R.; Myneni, R.B. Global Data Sets of Vegetation Leaf Area Index (LAI)3g and Fraction of Photosynthetically Active Radiation (FPAR)3g Derived from Global Inventory Modeling and Mapping Studies (GIMMS) Normalized Difference Vegetation Index (NDVI3g) for the Period 1981 to 2011. Remote Sens. 2013, 5, 927-948.
94. Fang, H.; Jiang, C.; Li, W.; Wei, S.; Baret, F.; Chen, J.M.; Haro, J.G.; Liang, S.; Liu, R.; Myneni, R.B.; Pinty, B.; Xiao, Z.; Zhu Z. Characterization and intercomparison of global moderate resolution leaf area index (LAI) products: Analysis of climatologies and theoretical uncertainties. *J. Geophys. Res.* **2013**, 118.
95. Zhang, P.; Anderson, B.; Barlow, M.; Tan, B.; Myneni, R.B. Climate-related vegetation characteristics derived from Moderate Resolution Imaging Spectroradiometer (MODIS) leaf area index and normalized difference vegetation index. *J. Geophys. Res.* **2004**, *109*.
96. Mitchell, T.D.; Jones, P.D. An improved method of constructing a database of monthly climate observations and associated high-resolution grids. *Int. J. Climatol.* **2005** *25*, 693–712.
97. Nemani, R.R.; Keeling, C.D.; Hashimoto, H.; Jolly, W.M.; Piper, S.C.; Tucker, C.J.; Myneni, R.B.; Running, S.W. Climate-driven increases in global terrestrial net primary production from 1982 to 1999. *Science*, **2003**, *300*, 1560–1563.
98. Piao, S.; Ciais, P.; Friedlingstein, P.; de Noblet-Ducoudre, N.; Cadule, P.; Viovy, N.; Wang, T. Spatiotemporal patterns of terrestrial carbon cycle during the 20th century. *Global Biogeochem. Cy.* **2009**, *23*, GB4026, doi:10.1029/ 2008GB003339.

99. Richardson, A.D.; Anderson, R.S.; Arain, M.A.; Barr, A.G.; Bohrer, G.; Chen, G.; Chen, J.M.; Ciais, P.; Davis, K.J.; Desai, A.R.; *et al.* Terrestrial biosphere models need better representation of vegetation phenology: results from the North American Carbon Program Site Synthesis. *Global Change Biol.* ***2011***, *18*, 566–584.
100. Jeong, S.-J.; Ho, C.-H.; Gim, H.J.; Brown, M.E. Phenology shifts at start vs. end of growing season in temperate vegetation over the Northern Hemisphere for the period 1982–2008. *Global Change Biol.* **2011**, *17*, 2385–2399.

Chapter 3. Comparing model results against observations at multiple scales in the tropics.

3.1 Summary

One of the most challenging tasks to model the land C cycle is the evaluation of the results over the tropics. This is due to fewer observations being available (e.g. Fluxnet sites over the tropics represent about a quarter of the total, and most of them started over the last 10 years), the signal from satellite products usually becomes saturated over dense forest and because our understanding of the underlying driving processes (i.e. soil moisture storage) is also limited (Poulter et al. 2009). Additionally, LUC and biomass burning also play a pivotal role in regulating C emissions and uptake over the tropics, representing up to 29% of the total human C emissions to the atmosphere (Fearnside, 2000).

This means that evaluating the modelled results against available observations over the tropics is a key step in order to improve our representation of the land C cycle in all DGVMs. The discrepancy between observations and model results may shed a light onto missing or misrepresented processes and will help to reduce uncertainty in future predictions.

This chapter is comprised by two parts, each of them evaluating the C cycle at a different scale over the tropics. The first scale is the African continent and it is the result of my collaboration on the paper by Valentini et al. (2013). The paper compiles information about the C cycle from a vast number of sources, I was responsible for the analysis of the output from the TRENDY DGVMs. Here I present a similar analysis to those results, where I compared the NEP flux from the models against atmospheric CO_2 inversions, but for a longer time period (1990-2009) than the original analysis (2000-2009) and present a brief discussion expanding on the main paper by Valentini et al. (2013) results.

The second part of the chapter is the evaluation of the observed C stocks (vegetation and soil) for the country-scale case study of Mexico. These results are part of a submitted paper (Murray-Tortarolo et al. in progress) where I evaluated the present C stocks and calculated the predicted change in past and future stored C. This is a fundamental missing piece of information for policy-makers in the country, as no previous study has investigated the land-C

cycle of the country using a processed based approach. The paper is included fully as part of this chapter.

3.2 Africa: continent level estimates

3.2.1 Introduction

Africa plays an important role in the global C budget. For example 17% of global carbon emissions from land-use change, over half of the global gross fire emissions and about half of the interannual variability of the global carbon balance have been attributed to Africa (Williams et al., 2007; Canadell et al., 2009b; van der Werf et al., 2010). About a third of the tropical biomass carbon sink (or 16% of the total terrestrial carbon sink) over the period 2000-2005 is thought to be due to the African tropical forests (Lewis et al., 2009, Malhi and Grace, 2000).

In spite of the importance of this continent to the global C cycle, estimates of NEP and NBP for the African forests remains insufficient for accurate estimation and in comparison to other world regions (Ciais et al., 2009). The same is true for other important land cover classes in Africa, such as savannahs, shrublands, crops and wetlands.

However new products that account for the C exchange between the land and the atmosphere became available in recent years. One of these products is the atmospheric inversion of CO_2. These consist of an inversion of an atmospheric transport to predict the exchange of CO_2 between the land and the atmosphere and can account for the flux coming from different sources (e.g. human, natural). Results from five early inversions (done in the 1990's) suggest that Africa was CO_2 neutral (Williams et al. 2007), however these products has been deeply refined in recent decades and several more have became available.

On the other hand, few DGVM studies have explored the African carbon cycle and its response to climate, CO_2 and land use change drivers. For example, applying the model ORCHIDEE with dynamic vegetation disabled, Ciais et al. (2009) simulated a source-sink shift in the continental C balance from +0.14 PgC y^{-1} in the 1980s to -0.13 PgC y^{-1} in the 1990s. Nevertheless, new results from the TRENDY model compendium are available, which also cover the African region (Sitch et al. 2015).

The objective of this chapter is to compare modelled NEP results with atmospheric inversions for Africa over the period 1990-2005 and to evaluate the results from the TRENDY DGVMs.

These results extend on my collaboration to the paper by Valentini et al. (2013) and a comparison between the two is included in the discussion. Here one important caveat must be mentioned, in order to be consistent with the procedure of Valentini et al. (20130), I used NEP from the TRENDY runs V1, which are the same than the paper. Nonetheless, these runs do not include LUC, which is needed in order to compare NEP with the atmospheric inversions. I derived a LUC mean value for Africa based on the main paper. However, the new runs (V2 and V3) include a representation of LUC and would be a better fit for comparison, but are not presented here to maintain consistentcy.

3.2.1 Methods

Datasets

DGVMs: I used data from 9 DGVMs from the TRENDY compendium (Sitch et al. 2015) for the S2 simulation, which is forced by climate and atmospheric CO_2. I used NEP for the period 1990-2005. I calculated the model ensemble as the mean of all models and the uncertainty as the standard deviation. I also plotted the individual model NEP for the same time period. To compare NEP with the atmospheric inversions I derived a mean value for LUC from Valentini et al., (2013).

Inversions: I used the mean annual CO_2 posterior flux from atmospheric CO_2 inversion from 10 different products from Peylin et al. (2013) for the period 1990-2005. The uncertainty was calculated as the standard deviation across products. The data was corrected by the land/sea fraction and regridded to a common 1x1 grid (TRENDY grid) for easier comparison.

Data analysis

I calculated the mean and gridded-mean NEP flux for the period 1990-2009. The long-term gridded trend was computed as the linear trend of NEP against time in each pixel, while the continental-level long-term trend was computed from the yearly means. I also computed the spatial correlation (area weighted) between the annual means, and the long-term trend across products.

3.2.2 Results

Both the inversions and the models represent Africa as a sink of C, however I found an estimate for the land C flux much larger for the models than the inversions (0.4 ± 0.3 vs. 0.06 ± 1.3 $PgCyr^{-1}$, respectively). This is primarily due to the fact that the inversion estimate does include land use changes C fluxes while the DGVM estimates used here do not account for LUC. Including the LUC central estimate (0.32 ± 0.05 $PgC\ yr^{-1}$) reduces the discrepancy between top-doan and bottom-up models to almost the same value.

I also analysed the variables spatially and temporarily. Spatially I found a similar sink (~50 gCm^2yr^{-1}) for most of the continent with marked regional discrepancies: inversions showed a sink of C for central and east Africa, but a source of C over the Sahel region and the Congo basin (Figure 3.1 a, d). The model ensemble displays a sink of C almost everywhere, with the greatest values in central Africa. The clear differences in the uptake lead to a small spatial correlation between products (r=0.23).

There are also great discrepancies in the spatial trend over these 20 years. The inversions display higher C-fluxes to the atmosphere for most of the continent, particularly over the source regions. On the contrary the models predicted an increasing sink almost everywhere, with the exception of the Sahel (Figure 3.1 b, e). In term of the IAV, both products predict opposite patterns. The inversions showed a change of phase from being a source in 1991-2000, to a sink in 2001-2009, while the models simulated a sink of C for every year (Figure 3.1. c, f)

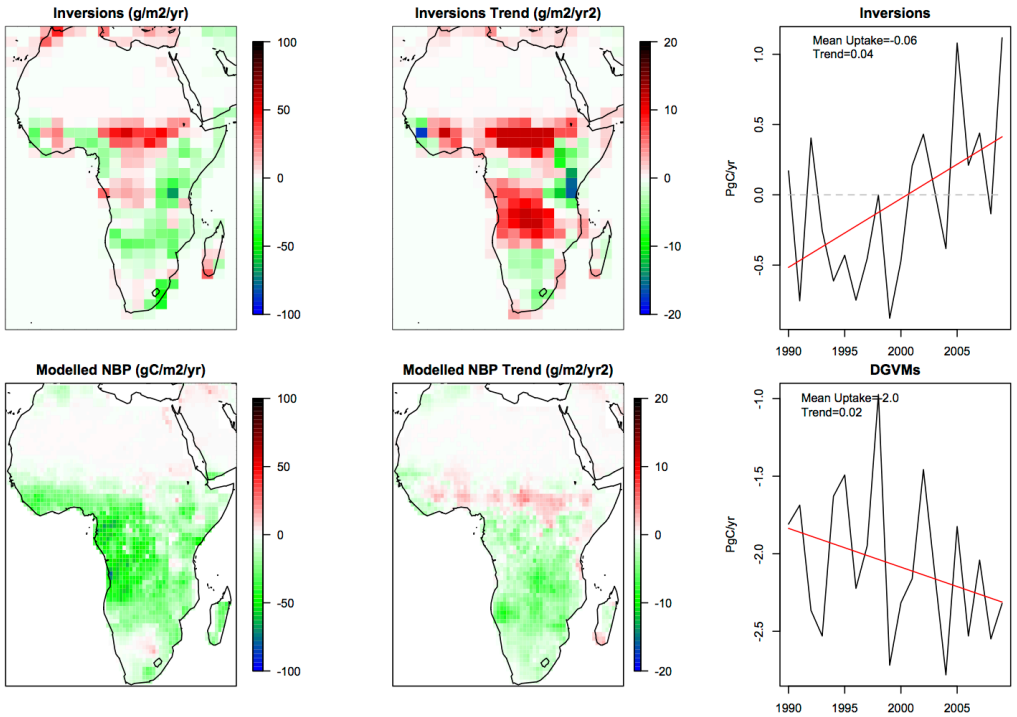

Figure 3.1. Land C flux (left), trend (middle) and annual mean (right) for atmospheric CO_2 inversions (top) and modelled NBP (bottom). For all cases a negative value represents a sink of C by the land.

3.2.3 Discussion

Both the DGVMs and the inversion indicate that Africa as a continent was a sink of C over this 20 year period, as reported in Valentini et al. (2013). However my results also show that there is great discrepancy between the values and the long-term trend, likely coming from the uncertainty in each product. For the particular case of the atmospheric inversions, the lack of CO_2 measuring stations (only 7 in the whole continent) and the challenging modelling of the ITCZ leads to large errors (SD of all inversions) of ±1.3PgC. For the case of the models, the estimates were more constrained, with 8 out of 9 predicting a sink of C and while the error is smaller (± 0.3 PgC) there are clear differences among models, particularly for the Sahel, where some models display the region as a source of C, much like the inversions (Figure 3.2). In addition, the S2 run -used here in the DGVMs- does not include LUC, which could explain why the continent-level estimates are higher than the inversions.

The major source of discrepancy comes from two regions: the Sahel and the Congo Basin. I compared the results against local field-sample studies. The Sahel has been experiencing an increase in drought and longer dry season lengths over recent years (1960-2010), which in turn has led to a decrease in species richness and biomass (Gonzales et al. 2012). While both modelled

ensemble and inversions predict a decreasing land-C flux trend, the individual models differ in their response. Human induced climate change has been attributed to be the main driver of this change since 1990s (Epule et al. 2013), but the effect of changing rainfall over vegetation processes on the area is not linear (Hein and De Ridder 2006).

The second region of discrepancy is the Congo Basin. This region has the highest C density of Africa and recent studies found a decrease in photosynthetic activity due to moisture limitations over the past 10 years (2000-2010) (Zhou et al. 2014). This pattern was better represented in the atmospheric inversions (a positive trend) than in the individual models, which all calculated a sink. A deeper model analysis is needed to understand why models fail to reproduce this decline, but is likely that the models misrepresent the effect of drought over the tropical wet forest (Sitch et al. 2008).

My results build up on Valentini et al. (2013) and suggest the need to re-asses the C cycle over Africa with DGVMs that include LUC and are better parametrized for their drought response.

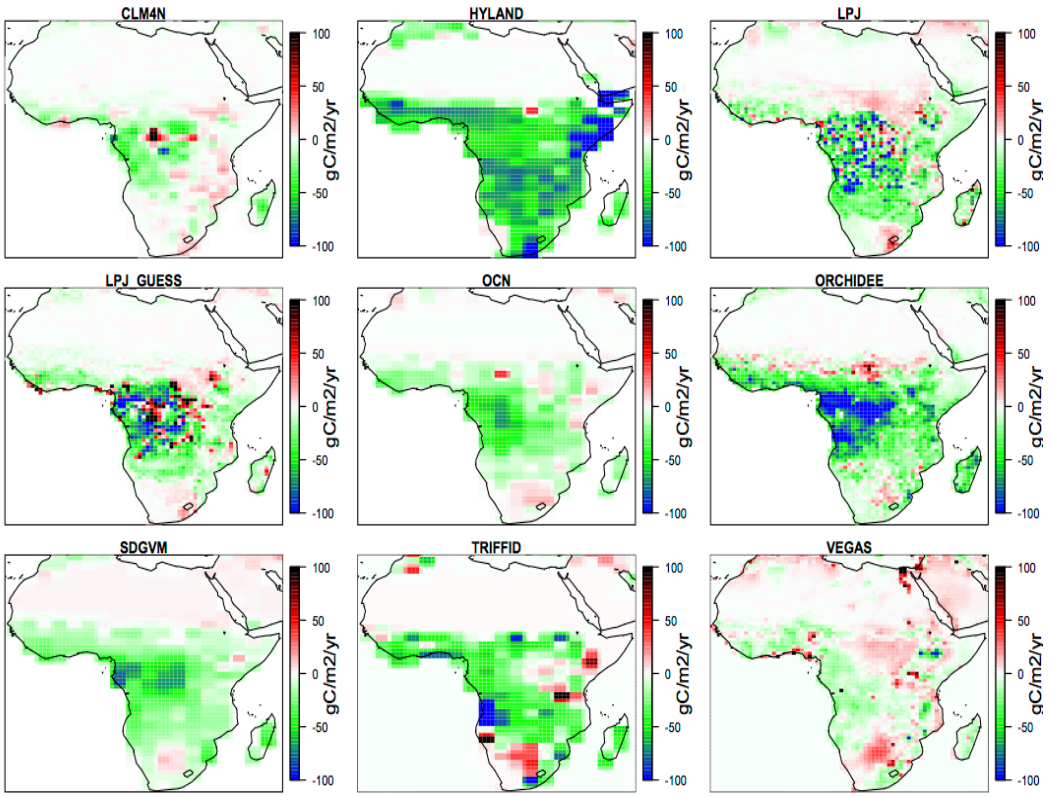

Figure 3.2. Africa gridded NBP for each individual model for 1990-2009. For all cases a positive value indicates a source of C into the atmosphere.

The Carbon Cycle in Mexico: past, present and future of C stocks and fluxes.

Guillermo Murray-Tortarolo[1], Pierre Friedlingstein[1], Stephen Sitch[1], Víctor J. Jaramillo[2], Fabiola Murguía-Flores[3], Alessandro Anav[1], Yi Liu[4], Almut Arneth[5], Athanasios Arvanitis[5], Anna Harper[1], Atul Jain[6], Etsushi Kato[7], Charlie Koven[8], Benjamin Poulter[9], Benjamin D. Stocker[10], Andy Wiltshire[11], Sonke Zaehle[12] and Ning Zeng[13].

1) University of Exeter, UK.
2) Instituto de Investigaciones en Ecosistemas y Sustentabilidad, Universidad Nacional Autónoma de México, México.
3) University of Bristol, UK
4) University of New South Wales, Australia.
5) Karlsruhe Institute of Technology, Germany
6) University of Illinois, USA.
7) The Institute of Applied Energy, Japan.
8) Lawrence Berkeley National Laboratory, USA.
9) University of Montana, USA
10) Imperial College, UK
11) Met Office, UK.
12) Max Planck Institute for Biogeochemistry, Germany
13) University of Maryland, USA

Abstract

We modelled the carbon (C) cycle in Mexico with a process-based approach. We used different available products (satellite data, field measurements, models and flux towers) to estimate C stocks and fluxes in the country at three different time frames: present (defined as the period 2000-2005), the past century (1901-2000) and the remainder of this century (2010-2100). Our estimate of the gross primary productivity (GPP) for the country was 2137 ± 1023 TgC yr^{-1} and a total C stock of 34,506 ± 7483 TgC, with 20,347 ± 4622 PgC in vegetation and 14,159 ± 3861 in the top 20 cm of soil.

Contrary to other current estimates for recent decades, our results showed that Mexico was a C sink over the period 1990-2009 (+31 TgC yr^{-1})

and that C accumulation over the last century amounted to 1210 ±1040 TgC. We attributed this sink to the CO_2 fertilization effect on GPP, which led to an increase of 3408 ± 1060 TgC, while both climate and land use reduced the country C stocks by -458 ± 1001 and -1740 ± 878 TgC, respectively. Under different future scenarios the C sink was likely to continue over 21st century, with decreasing C uptake as the climate forcing became more extreme. Our work provides valuable insights on relevant driving processes of the C-cycle such as the role of drought in marginal lands (e.g. grasslands and shrublands) and the impact of climate change on the mean residence time of C in tropical ecosystems.

1 Introduction

The global carbon (C) cycle has been altered by anthropogenic activity with the release of CO_2 into the atmosphere through fossil fuel burning and land use and land cover changes since the industrial revolution (Keeling et al., 1995). As a consequence C stocks have increased in the atmosphere, land and oceans. About 50% of the annual anthropogenic emissions are sequestered in the marine and terrestrial ecosystems (Le Quéré et al., 2014). In the latter, the atmospheric CO_2 increase has led to greater gross primary productivity (GPP), as a result of the fertilization effect on the plants' photosynthetic machinery, hence leading to higher C storage (Norby et al., 2005). However GPP and the net biome productivity (NBP) display high interannual variability due to the effect of climate variability on vegetation processes (e.g. plant production and water use, growing season extension, fire, drought induced mortality) (Sitch et al., 2015).

The interaction among climatic forcing, atmospheric CO_2 and terrestrial C remains one of the main uncertainties in our understanding of the global C cycle and in our ability to model it, particularly concerning future projections. Different authors have documented contrasting qualitative and quantitative results regarding the future evolution of the land C cycle. These range from a strong future C sink due to a longer growing season in the Northern Hemisphere and the CO_2 fertilization effect, to C sources from drought-induced tropical forest dieback and temperature-induced enhancements in mid-latitude soil respiration (Friedlingstein et al., 2006; Cox et al., 2000; Friedlingstein et al., 2013).

These differences in the future of land C arise from two sources: the strength of the carbon cycle feedbacks (driven by the sensitivity of land C to atmospheric CO_2 increase and climate change) and the poor representation of smaller-scale processes (e.g. disturbance) in the models (Ciais et al., 2013). Thus, regional studies are growing in importance to close the gap in our knowledge. These use finer resolution climate information and other data sources from the field (e.g. site-level carbon stocks), from satellites, and ecosystem-level information for particular regions. An example is the Regional Carbon Cycle Assessment and Processes (RECCAP) initiative, which has promoted studies on drivers of the land C cycle in different regions worldwide (e.g. Dolman et al., 2012; Gloor et al., 2012; King et al., 2015; Piao et al., 2012; Valentini et al., 2014), but further work is needed at finer scales (e.g. country level) (Enting et al., 2012).

In this context, we centred our investigation on Mexico's C cycle. Until now, studies on the C stocks or fluxes at the country level have been estimated from changes in vegetation C due to land use change (Masera et al. 1997; Cairns et al. 2003) and less frequently soil C has been incorporated in the calculations (de Jong et al. 2010). While these studies provide important insights on the processes driving the C-cycle (e.g. LUC), they place Mexico as a source of C (Pacala et al. 2007), which may be a biased conclusion derived from estimating C fluxes from biomass change only (Table 1). This approach results in that important ecological processes are not taken into account, such as the effect of CO_2 fertilization on GPP or the impacts of climate change. In contrast, results from global models and atmospheric CO_2 inversions place the country as a sink of C (Hayes et al., 2012; King et al., 2012), but they lack an understanding of the driving mechanisms of change. Hence, a more comprehensive understanding of the C balance in Mexico is needed, to aid in policy formulation and to identify regions that may provide important ecosystem services like C sequestration.

Table 1: Different estimates for the land C-flux of the country. A negative sign indicates a source to the atmosphere and a positive a sink.

Land C Flux estimates			
Author(s)	**Years**	**Method**	**Estimate (total) TgC yr^{-1}**
Masera et al. 1997	1985-1987	Changes in vegetation cover	-52.6
Cairns et al. 2000	1977-1992	Changes in vegetation cover*	-18.6
De Jong et al. 2010	1993-2002	Inventory-based	-18.4
Haynes et al. 2011	1993-2002	Inventory-based	-18.4
Haynes et al. 2011	2000-2006	Forward models	29.0
Haynes et al. 2011	2000-2006	Inverse models	8.7
This work	1990-2009	DGVMs Atmospheric Inversions LUC-only	31.4 21.4 -19.5
This work	1901-2009	DGVMs	12.1

*This estimate only accounts for part of the South of Mexico

In this study, we provide a country level perspective of the C cycle in Mexico and use different products and complementary approaches to estimate C stocks and fluxes over three different time frames: the present (2005-2009), the last century (1901-2000) and the remainder of this century (2010-2100). The country represents a unique opportunity to compare the different approaches, due to the high variety of climates and vegetation (Challenger, 1998), which includes a wide range of land cover types (Figure 1). Thus, in addition to the country level analysis, we can compare estimates and products by land cover type. Additionally, the high environmental heterogeneity allows that multiple processes that drive the C cycle globally can be found at a smaller spatial scale (e.g. fire, drought, tropical deforestation); thus, providing insights on the global drivers of the land C.

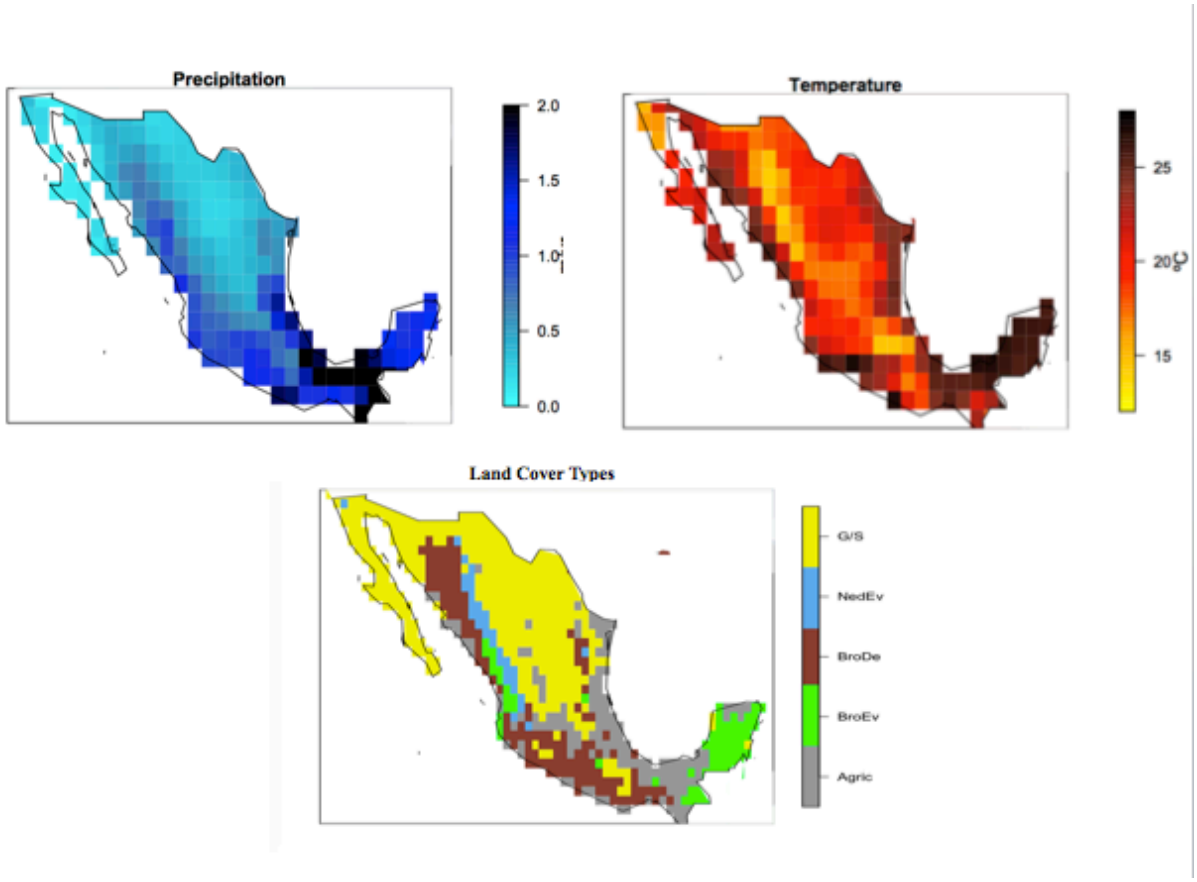

Figure 1. Observed Precipitation ($mmyr^{-1}$), Temperature (ºC), and Land Cover Types for Mexico (mean of 2000-2005). Agric: Croplands, BroEv: Broadleaf Evergreen Forest, BroDe: Broadleaf Deciduous Forest, NedEv: Needleleaf Evergreen Forest, G/S: Grassland/Shrubland.

We address the following research questions for the different time periods under consideration:

1. Present-day: What are the magnitudes of C stocks and fluxes at the country level? How do they vary geographically and by land cover type? How do the estimates with the different approaches compare?
2. Past: How have C stocks and fluxes changed over the last century? How do these relate to changes in atmospheric CO_2, precipitation, temperature and land use?
3. Future: How are C stocks and fluxes projected to change over the 21st century under different climate-change scenarios?

2 Methods

2.1 Datasets

Climate: We used observed temperature and precipitation data from CRU v3.1 (Harris et al., 2013). We expressed the change over time as the total for

the last century. These data were also used to force the Dynamic Global Vegetation Models (DGVMs) (Figure 1).

Land cover: we used the observed vegetation dataset by Ramankutty and Foley (1999). This was derived from satellite data and contains 18 different categories (Figure 1). Ten categories were present in Mexico (Sup. 1). In order to simplify the analysis, we aggregated the vegetation into five broad categories: broadleaf evergreen forest, broadleaf deciduous forest, needleleaf evergreen forest, grassland/shrubland and croplands (Figure 1d).

DGVMs: We used vegetation C, soil C, heterotrophic respiration (Rh), GPP and the net biome productivity (NBP) from an ensemble of 9 DGVMs (Sup. 2) from the TRENDY v2 project (Le Quéré et al., 2014; Sitch et al., 2015). All models were forced using the same input data and spin-up protocol. To attribute the relevant driver (CO_2 fertilization, climate or LUC) of past change a set of factorial experiments was conducted over the period 1901-2012 where the effect of individual drivers and their combinations were analysed. The runs were: S1- CO_2 effect only; S2-S1- climate effect only; S3-S2- the LULCC effect only, and S3 the combined effect of all drivers and their interactions. A full description of the experiment can be found in Sitch et al. 2015.

Earth System Models (ESMs): We used NBP, precipitation and temperature for four IPCC Representative Concentration Pathways or RCPs (2.6, 4.5, 6.0 and 8.5) based on an ensemble of 9 CMIP5 models common to all RCPs (Sup. 2) (Taylor et al., 2011). A full description of the models can be found in (Anav et al., 2013).

Model Tree Ensemble (MTE): This is a data-driven model of gross primary productivity (GPP) based on flux tower observations, the satellite fraction of the active photosynthetic active radiation (fAPAR) and climate fields. It uses a Model Tree Ensemble (MTE) which is a machine learning system based on the data structure (Jung et al., 2011, 2009).

Satellite: To estimate aboveground biomass we used annual passive microwave satellite-based vegetation optical depth (VOD). VOD is an indicator of vegetation water content of aboveground biomass and can be approximated to mean biomass (Liu et al., 2011, 2013). We approximated the vegetation C from VOD using a linear coefficient for each cover type, derived from the best fit to the modeled aboveground biomass. To estimate GPP we used data derived from MODIS v17 f. The MODIS GPP algorithm is described in Running et al.

(2004). A simple light use efficiency model (MOD17) is at the core of the GPP algorithm and it requires daily inputs of incoming photosynthetically active radiation (PAR) and climatic variables.

Field data: To estimate vegetation C we used the data from the REDD-Mexico initiative, which contains extensive field measurements from the National Forestry Commission (Alianza MREDD+, 2013), for the year 2004 (Sup. 3). For soil C, we used the topsoil C concentrations (0-20 cm depth) from 4000 sampling sites (SEMARNAT, 2002) covering most of the country; soil sampling was conducted between 2000 and 2006. An alternative source for soil C was the harmonized soil database from FAO v1.2 (FAO/IIASA/ISRIC/ISSCAS/JRC, 2012). We multiplied C concentrations by the reference bulk density and the soil depth from the same database to estimate soil C stocks.

Land Use Change (LUC): We used data for the agricultural fraction from Hurtt et al. (2011). LUC emissions were obtained from the DGVMs.

Atmospheric inversions: for the analysis on the land C flux for the present-day we used the mean annual CO_2 posterior flux from atmospheric CO_2 inversion from 10 different products from Peylin et al. (2013) for the period 1990-2005. The uncertainty was calculated as the standard deviation across products. Due to the broad scale of the product (5x5 degrees) we only presented the national average and not the gridded means.

All datasets were re-gridded to a common 1°x1° grid.

2.2 Data Analysis

For the present-day analysis we first we computed the gridded mean GPP (satellite, MTE and DGVMs), soil C (field data, DGVMS and FAO) and aboveground vegetation C (field data, satellite and DGVMS). Then, we calculated those values for each land cover type and the total for the country for the period 2000-2005 which was common to all datasets. We also computed the mean NBP from all DGVMs, but for an extended time period (1990-2009), as this flux is strongly affected by the interanual variability of the Earth system. Our ‘best estimate’ for each C pool or flux was the mean across all products (i.e. the contribution of each product was equally weighted). The error was computed as the standard deviation for all years for all products pooled together. We also computed a spatially weighted correlation across products.

For the analysis on past changes, we calculated cumulative NBP from the DGVMs ensemble for the period 1901-2000 (100 years) for the three different runs. We then attributed to environmental drivers (change in NBP for the run S1:CO_2, S2-S1: climate and S3-S2: LULCC). We calculated the gridded linear change for each run and each driving factor (i.e. change in stored C by climate vs. precipitation and temperature trend). The mean residence time of C in the soil (MRT) was calculated by dividing the linear change of soil C by change in soil heterotrophic respiration (Rh).

For the analysis on future scenarios, we calculated the change in cumulative NBP for each RCP from the ensemble of ESMs for the 21st century (2010-2100). We did this by grid, by land cover type, and for the whole country. For the gridded plots we stippled the areas where at least 66% (6) of the models agreed on the sign of change in total stored C.

3 **Results**

3.1 Present

Total GPP for the country was 2137 ± 1023 TgCyr^{-1} (Table 2). In terms of the distribution by land cover type, the forest areas represented 56% of the total GPP and the croplands and grasslands/shrublands most of the rest (44%). The highest GPP per unit area occurred in the broadleaf evergreen forests (2.2 ± 0.2 kgC m^{-2} yr^{-1}) and the lowest in the grasslands and shrublands (0.6 ± 0.1 kgC m^{-2} yr^{-1}; Table 2).

Table 2: Mean GPP, Total Area and Total GPP by Land Cover Type for the period 2000-2005.

Gross Primary Productivity for Mexico (2000-2005)			
Land Cover type	Mean kgC m^{-2} yr^{-1}	Area 10^9 m^2	Total TgC yr^{-1}
Broadleaf evergreen forest	2.2 ± 0.23	257	553 ± 264
Broadleaf deciduous forest	1.2 ± 0.16	438	519 ± 356
Needleleaf evergreen forest	1.4 ± 0.31	92	134 ± 34
Grassland/Shrubland	0.6 ± 0.12	747	420 ± 260
Croplands	1.2 ± 0.09	423	508 ± 210
TOTAL		1957	**2137 ± 1023**

In terms of the country's geography, we found the highest GPP in the South and Southeast with a steep decrease to the North; the lowest GPP occurred in north-central region (Figure 2a). The three different products (i.e. satellite, flux towers (MTE) and DVGMs) displayed similar GPP distributions (Figure 2b, c, d), with DVGMs estimating higher values over the mountainous ranges in the East and the West of the country and part of the central plateau. The spatial correlations between products were very high: satellite-MTE=0.97, satellite-DGVMs=0.92, and MTE-DGVMs=0.91 (see also Sup. 4).

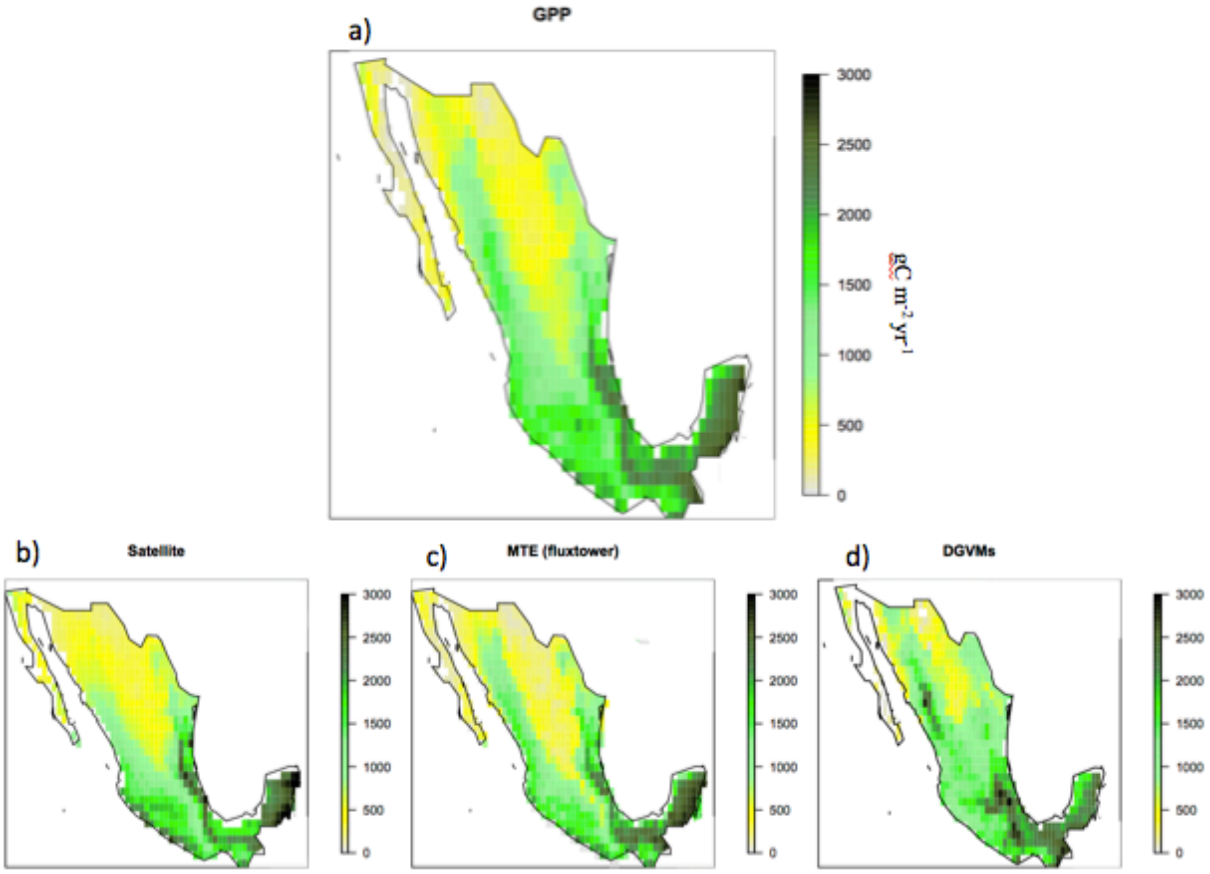

Figure 2: Mean GPP ($gCm^{-2}yr^{-1}$) for a) ensemble of the three products, b-d) individual products (Satellite, MTE and DGVMs). All maps correspond to the period 2000-2005.

Our estimate for the total C stock in Mexico was 34,506 ± 7843 TgC (Table 3), of which 20,347 ± 4,622 TgC (59%) was stored in the vegetation and 14,159 ± 3,861 TgC (41%) was stored in the soil (Table 3).

Table 3: Mean (kgC m^{-2}) and total (TgC) carbon stored in the vegetation and soil in each land cover type for the period 2000-2005.

TOTAL STORED C	**Vegetation C**		**Soil C**		**Total**	
Land Cover Type	Mean kgC m^{-2}	Sum TgC	Mean kgC m^{-2}	Sum TgC	Mean kgC m^{-2}	Sum TgC
Broadleaf evergreen forest	22.9 ± 0.9	5884 ±1220	12.1 ± 0.4	3100 ± 1167	35.0 ± 1.3	8984 ± 2387
Broadleaf deciduous forest	12.4 ± 0.5	5431 ± 1319	8.9 ± 0.6	3880 ± 1235	21.3 ± 1.1	9311 ± 2554
Needleleaf evergreen forest	15.1 ± 0.9	1385 ± 575	10.9 ± 0.4	1336 ± 586	26.0 ± 1.3	2721 ± 1161
Grassland/Shrubland	6.0 ± 0.7	4482 ± 1556	4.7 ± 0.7	3535 ± 1208	10.7 ± 1.4	8017 ± 2764
Cropland	7.5± 0.3	3158 ± 1190	6.2 ± 0.5	2635 ± 790	13.7 ± 0l8	5793 ± 1980
TOTAL		20,347 ± 4622		14,159 ± 3861		34,506 ± 7483

Similar to GPP, the forested areas accounted for 60% of the total stored C, with 40% in grasslands/shrublands and croplands. The broadleaf evergreen forest showed the highest C stock per unit area in the vegetation (22.9 kgC m^{-2}) and soil (12.1 kgC m^{-2}), whereas the grassland/shrubland the smallest (6.0 and 4.7 kgC m^{-2}, respectively) (Table 3, Figure 3, Sup. 5).

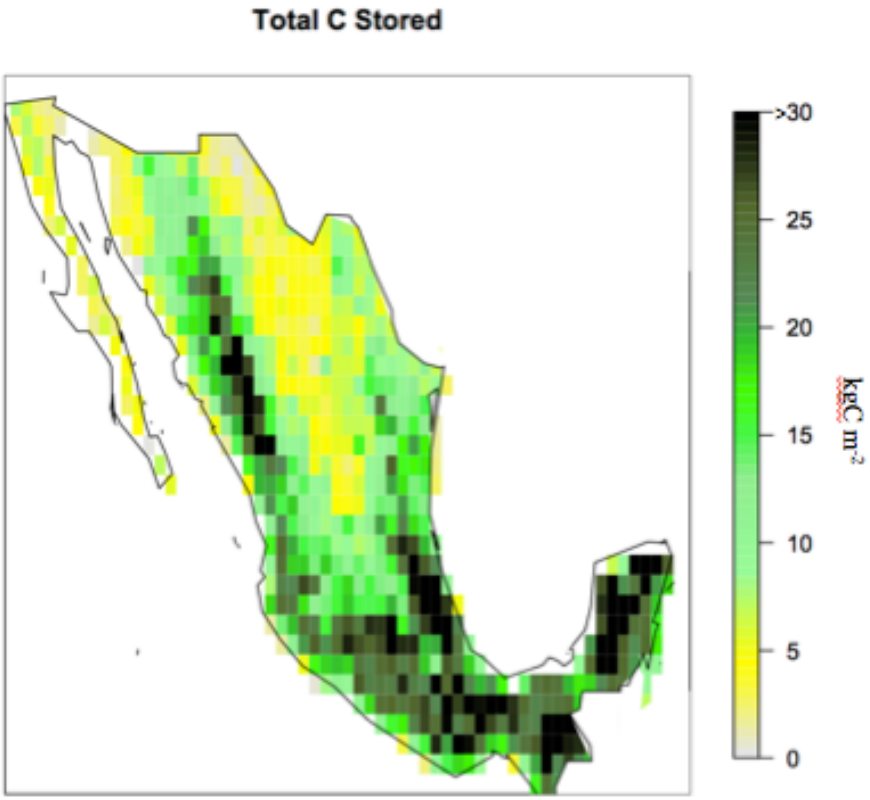

Figure 3: Total stored C in soil and vegetation (kgC m^{-2}), ensemble from all products (6) for the period 2000-2005.

Vegetation C estimates from the three products (DGVMs, satellite and field data) were in broad agreement at the country level and by land-cover type (Figure 4; Sup. 5). The largest differences among products were evident in the grassland/shrubland, with both DGVMs and satellite-based estimates 15-24% higher than those obtained from field measurements, which was evident in the geographical distribution of C stocks (Figure 4a, b, c; Sup. 5). The spatial correlations between products were lower than for GPP: field-DGVMs=0.79, field-satellite=0.84, and DGVMs-satellite=0.74.

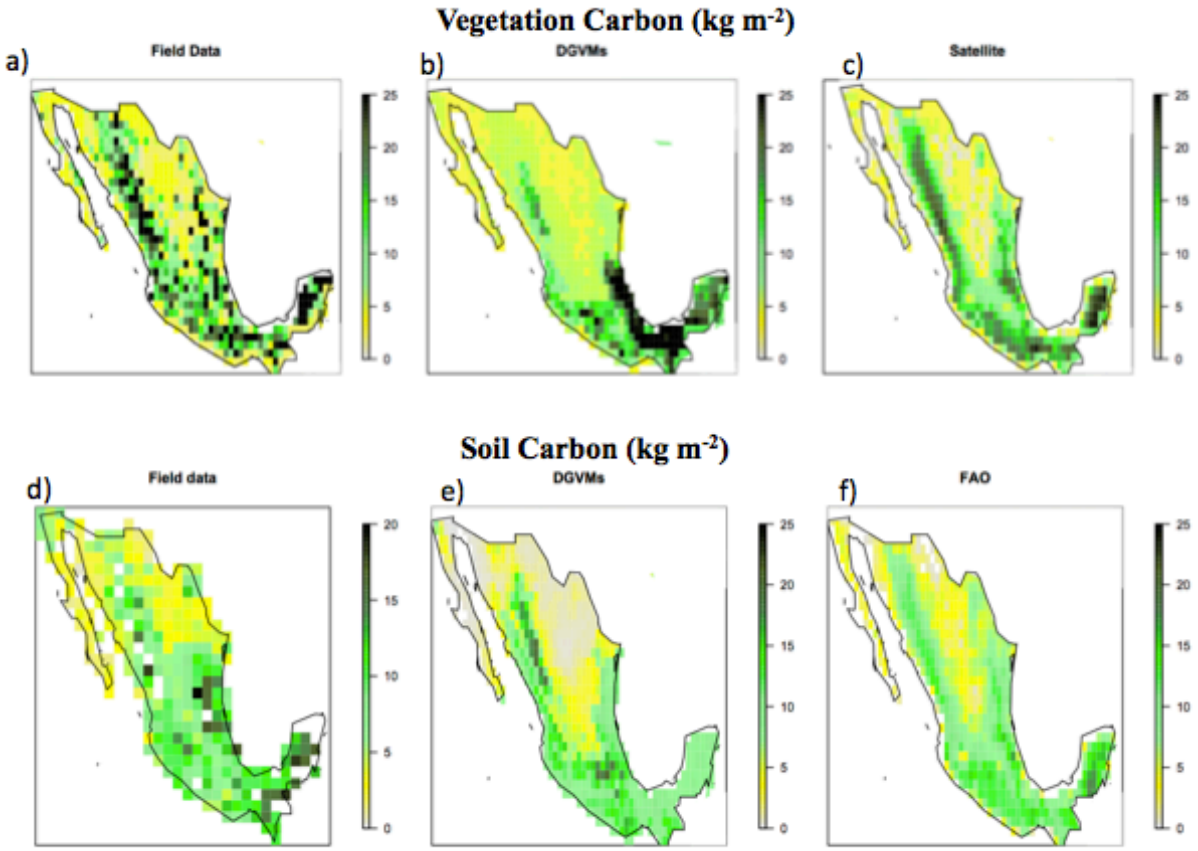

Figure 4: Top) Vegetation stored carbon for three products: field data, DGVMs and satellite (kgCm^{-2}). Bottom) Soil stored carbon for three products: field data, DGVMs and FAO estimates based on multiple datasets (kgC m^{-2}). Mean for the time-period 2000-2005.

The differences among products were greater for soil C. The field data estimates were on average 15% higher than with the other two products. In particular, the DGVMs and the FAO database appeared to underestimate soil C in the grasslands and shrublands in Northern Mexico, with a value 27% lower than the field data (Figure 4d, e, f; Sup. 5). Nonetheless, there were similarities in the geographical patterns across products, which depicted generally higher soil C towards the South and lower towards the North, particularly in the central region. The spatial correlations between products were generally lower than for vegetation C stocks: field-DGVMs=0.68, field-FAO=0.69, and DGVMs-FAO=0.92.

Our results showed that Mexico was a sink of C over recent decades (1990-2009), gaining 31.4 ± 18.6 TgC yr^{-1} (Table 4).

Table 4: Land C-flux to the atmosphere (NBP) for the period 1990-2009 by land cover type. For all cases a positive value indicates a sink and vice versa.

Land-C Flux for Mexico (1990-2009)		
Land Cover type	Mean gC m^{-2} yr^{-1}	Total TgC yr^{-1}
Broadleaf evergreen forest	100.8	20.6
Broadleaf deciduous forest	-42.1	-8.9
Needleleaf evergreen forest	22.2	1.5
Grassland/Shrubland	55.2	21.3
Croplands	-52.2	-3.1
TOTAL		**31.4 ± 18.6**

However, the sink was not equally distributed across land covers, with the broadleaf evergreen forest, the needleleaf evergreen forest and the grasslands gaining C, but the broadleaf deciduous forest and the croplands losing C. In terms of the geographical distribution of NBP, most of the country displayed positive values, except in areas of the Northwest and the central East of the country, which lost C (Figure 5). The atmospheric inversions also displayed a positive value for the country with a value of 21.4 ± 12.7 TgC yr^{-1} (Table 1).

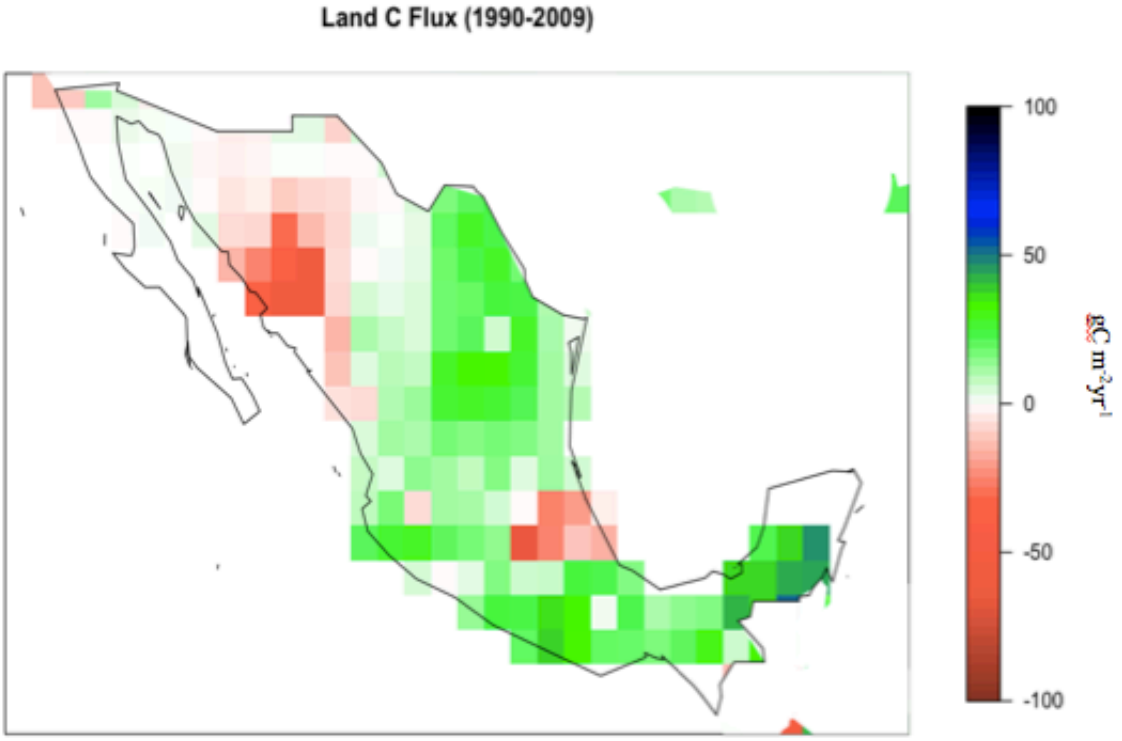

Figure 5: Land-C Flux (NBP) to the atmosphere for the period 1990-2009 ($gCm^{-2}yr^{-1}$). A positive value indicates a sink of C and vice versa.

3.2 Past

The model results with the DGVMs showed that over the last century Mexico has been a C sink, during which there was an overall gain of 1210 ± 1040 TgC. Geographically, NBP was not homogeneously distributed. The South and central regions of the country lost C, while brad regions towards the North and the Yucatan Peninsula represented a C sink (Figure 6).

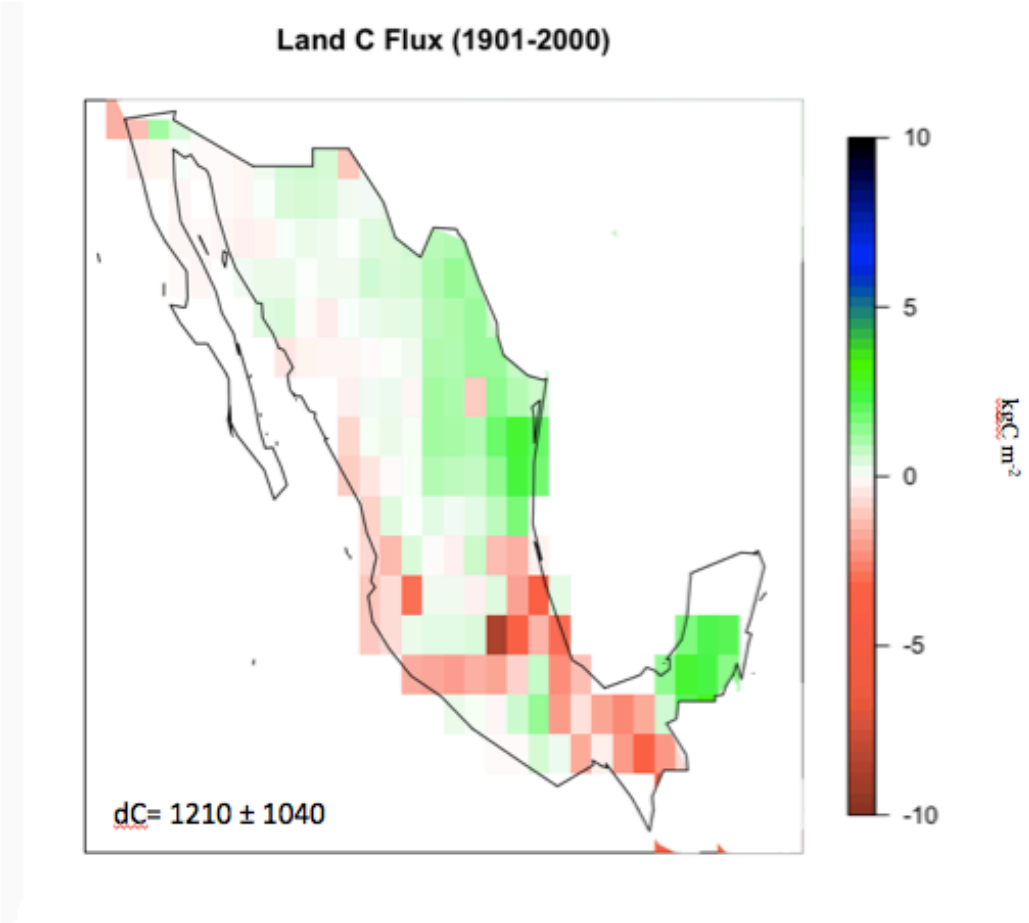

Figure 6: Total change in land C during 1901-2000 ($kgCm^{-2}$). A positive sign indicates C gain. dC= total change in stored C (TgC).

Three drivers of these regional trends could be identified at this scale with the processes included in the DGVMs: a) the rise in atmospheric CO_2, b) long-term climate variability and change, and c) land use change (LUC). a) The effect of elevated CO_2 led to enhanced C storage across the whole of Mexico (3408 ±1060 TgC), with the highest C gain occurring over the forested regions (Figure 7).

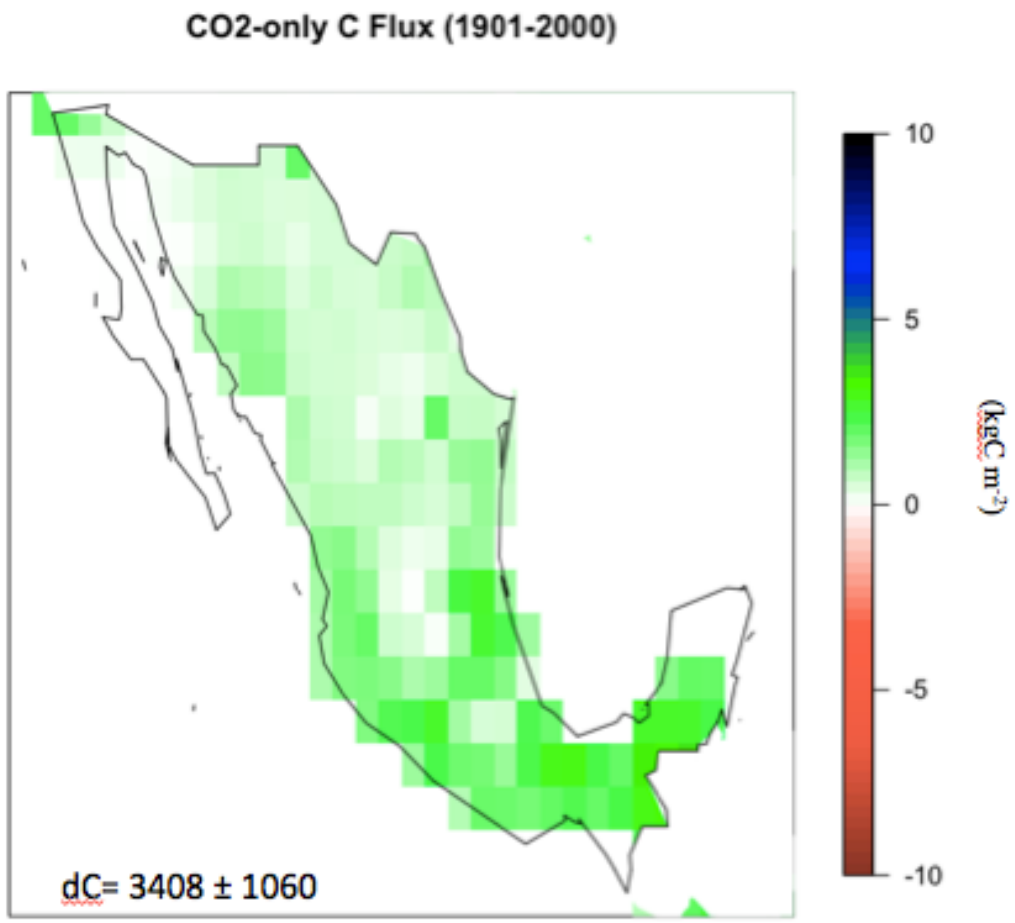

Figure 7: Change in total stored C by the effect of CO2-only over the period 1901-2000 ($kgCm^{-2}$). A positive sign indicates C gain. dC= total change in stored C (TgC).

b) Climate impacts were highly contrasting across the country. Thus, when accounted nationwide, the positive and negative effects almost counteracted each other, although the negative effect dominated the flux with emissions of -458 ± 1001 TgC. Climate led to a decrease in C storage over most areas of the country, with the exception of the Northeast and the Yucatan Peninsula (Figure 8a). Over the last 100 years, both precipitation and temperature showed an increase in most of the country, except for decreases in precipitation especially in the Baja California Peninsula in the the northwest (Figure 8c). The loss of C over most of the country in spite of generally positive climate trends was driven by a faster increase of heterotrophic respiration (Rh) than GPP, thus leading to a decrease in the mean residence time of soil C (Suppl. 8).

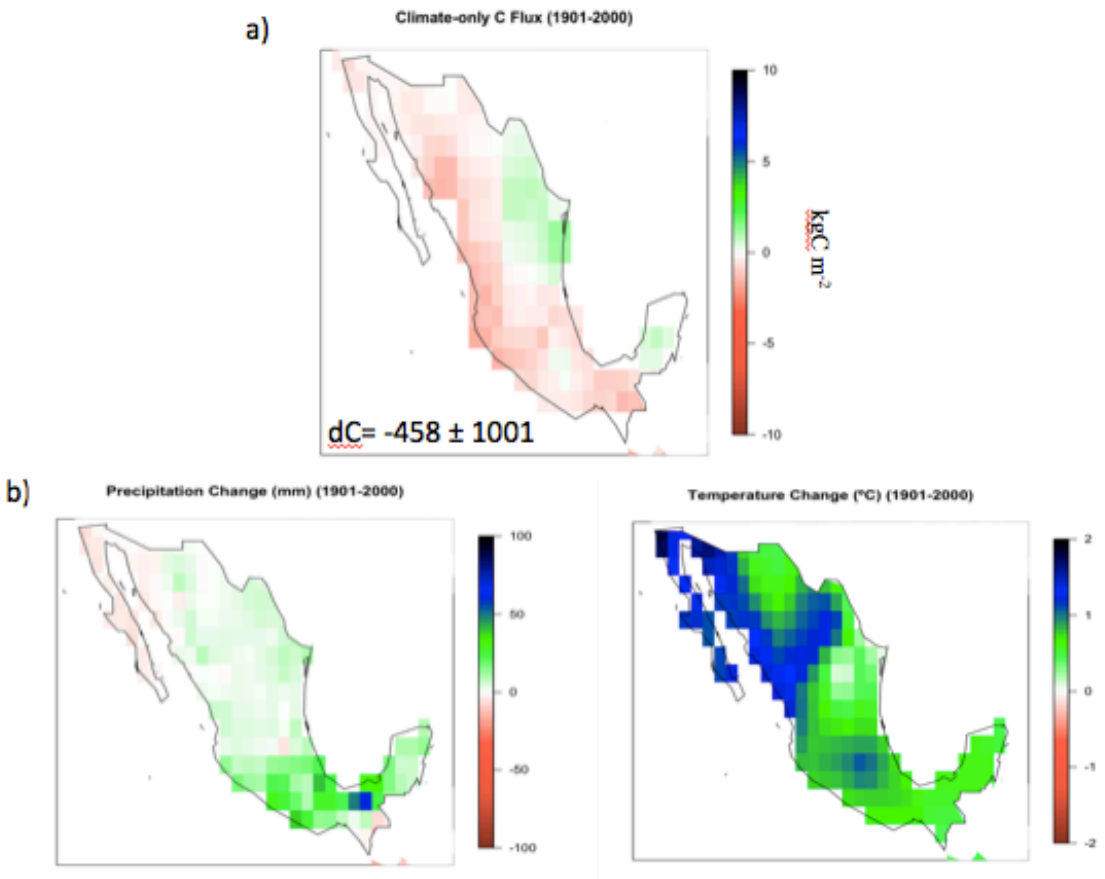

Figure 8: top) Change in stored C by the effect of climate-only for the period 1901-2000 ($kgCm^{-2}$). A positive sign indicates C gain. dC= total change in stored C (TgC). Bottom) change in climate (precipitation and temperature) for the same time-period.

c) The negative effect of LUC on total stored C (-1740 ± 878 TgC) occurred mostly over the South of the country and along the Gulf of Mexico and Pacific coasts (Figure 9a). Carbon emissions from LUC were apparently related to the distribution of changes in the agricultural fraction over the same time period (Figure 9b).

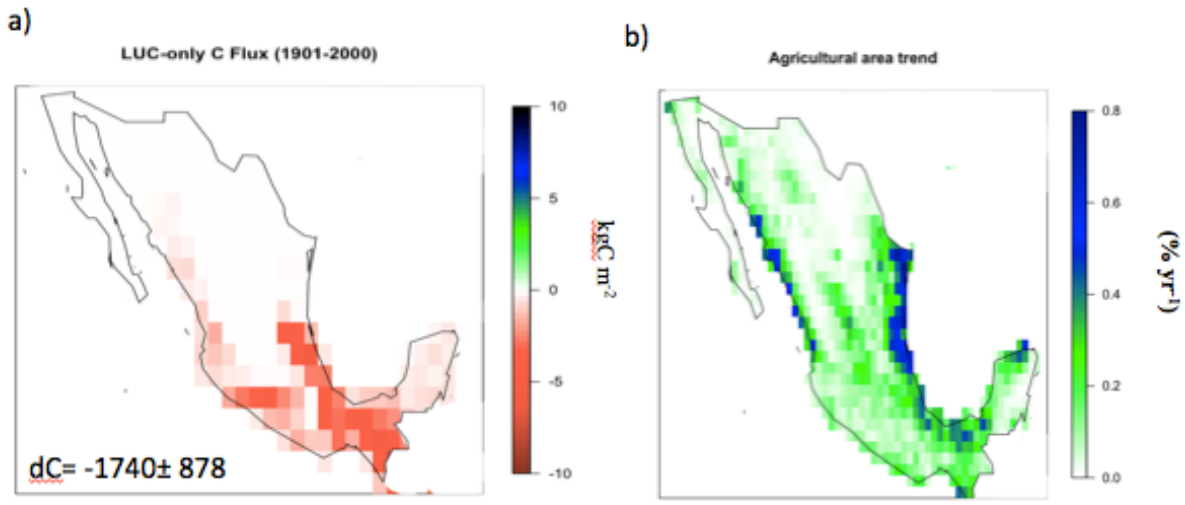

Figure 9: a) Change in stored C by the effect of LUC-only for the period 1901-2000 (kgC m^{-2}). A positive sign indicates C gain. dC= total change in stored C (TgC). b) Agricultural area change for the same time period.

Thus, when the three drivers were considered simultaneously, we found that the fertilization effect of CO_2 on GPP during those 100 years was greater than the climate and LUC negative effects, resulting in a positive net C storage at the scale of the country.

3.3 Future

In three out of four RCPs scenarios, the Earth System Models predicted Mexico to remain a C sink up to 2100; only in the most extreme scenario (RCP8.5), the country would become a C source. The total amount of stored C decreased as the radiative forcing increased, from 3.0 PgC in RCP2.6, to 2.1 PgC in RCP4.5, to 1.5 PgC in RCP6.0 and -0.7 PgC in RCP8.5.

Geographically, Northern Mexico was generally a C source in all RCPs and at least two thirds of the models agreed on this trend (Figure 10). As the radiative force increased, most of the country turned into a C source and model agreement also increased. However, there was a significant uncertainty in the magnitude and even sign of the changes in other parts of the country, especially over the Yucatan Peninsula (Figure 10).

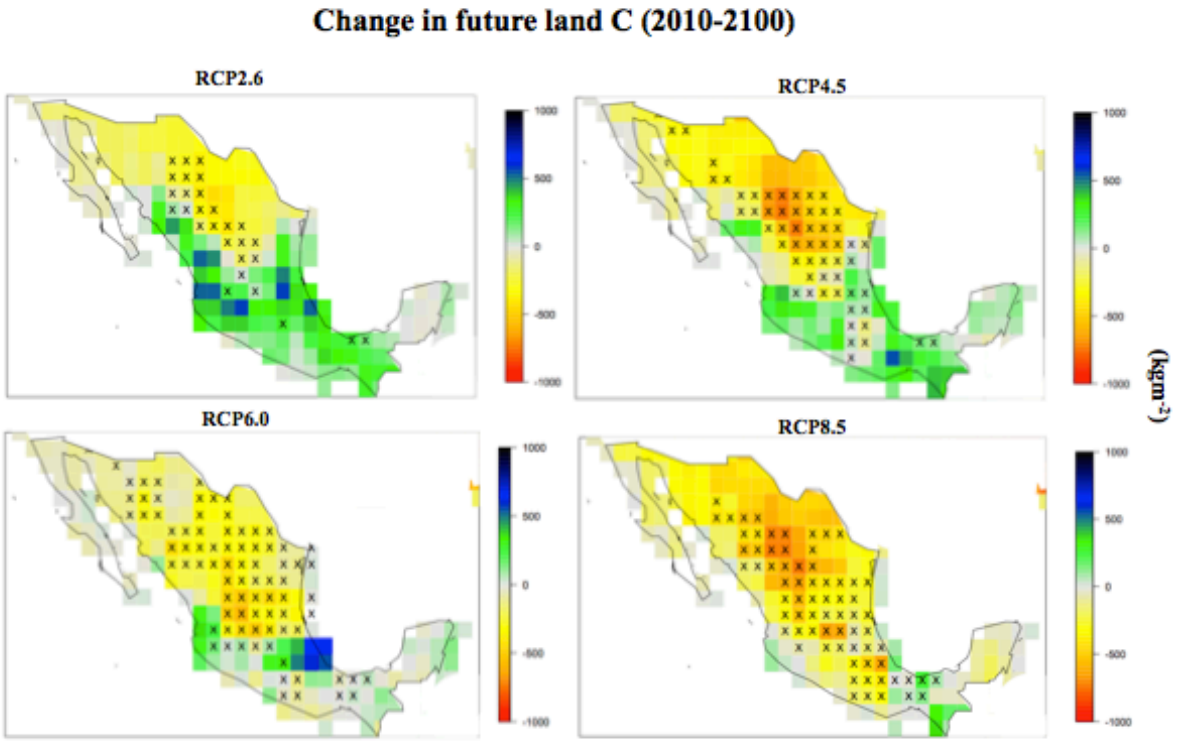

Figure 10: Gridded future change in total stored C for four RCPs for the period 2010-2100 (kgCm^{-2}). The stippling represents areas where >66% of the models agree on the sign of the flux.

Under all RCPs, precipitation decreased (Sup 7) and temperature increased over the 21st century in the whole country (Sup 6), with the larger changes occurring with increasing radiative forcing. Under these scenarios, very likely Mexico would face drier conditions, with the North of the country drying faster than the South.

4 Discussion

4.1 Present

The GPP (2137 TgC yr^{-1}) estimated in our study for Mexico corresponds to 2% of the global values (Ciais et al. 2013), similar to the fraction of the land area the country represents. As far as we know, this is the first estimate of gross primary productivity at the country level combining different products. Although there are no site-level GPP data, there are a few site estimates of net primary productivity (NPP) in Mexican ecosystems and we can compare them by assuming NPP to be 0.5 of GPP (Farquar and Sharkey, 1982). Among those, Martínez-Yrízar et al. (1996) estimated an aboveground NPP of 0.6-0.8 kgC m^{-2}

yr^{-1} in the tropical dry forest of Chamela, Mexico, similar to our findings of 0.6 ± 0.2 kgC m^{-2} yr^{-1} for broadleaf deciduous forests. García-Moya and Montanés-Castro (1992) estimated NPP in a semiarid grassland in central Mexico between 0.3 and 0.6 kgC m^{-2} yr^{-1}, similar to our finding of 0.3 ± 0.2 kgC$m^{-2}yr^{-1}$ for grasslands/shrublands. Such overall agreement provides elements to constrain C fluxes, although more field measurements are needed to provide better comparisons at the country scale.

The total C stock (vegetation and soil) for the country of 34,506 ± 7483 TgC, estimated with different products (field data, DGVMS and satellite), differs from the 24000 TgC estimated by Masera et al. (2001) with a C accounting model. More recent and comprehensive estimates put the total C stock for Mexico at around 33000 TgC (Pacala et al., 2007), which is similar to our value. Interestingly, the baseline estimate of 19,000 TgC for the total C stock in forests by Masera et al. (2001) compares to our 20,347 TgC for forest vegetation. This means that the highest source of discrepancy across estimates concerns soil C, with our estimate of 14,159 TgC almost three times higher than Masera et al. (2001) of 5,000 TgC.

Total aboveground biomass C for Mexico represents ~4% of the global biomass stocks (Ciais et al., 2013). Our estimates for land cover types are difficult to compare to field-based studies because of the coarse scale of resolution used in our study, which provides large-scale averages and does not capture the heterogeneity of land cover at the local scale. Also, difficulties arise when comparing with other modelling approaches because of differences in criteria to establish land cover classes and in the methods for calculation. Nevertheless, it is interesting that our mean estimate of 22.9 ± 0.9 kgC m^{-2} in the broadleaf evergreen forest is similar to the mean value of 20.5 kgC m^{-2} from Masera et al. (2001) for the same land cover, with a different modelling approach, and even to the 19.5 kgC m^{-2} reported for the Los Tuxtlas region from field measurements (Hughes et al., 1999). Also, our estimate for the needleaf evergreen forest of 15.1 ± 0.9 kgC m^{-2} compares to the mean temperate forest C stock of 12.6 kgCm^{-2} of Masera et al. (2001). However, it is important to note that field measurements by Jasso (2014) showed a range from 2.1 to 20.8 kgC m^{-2} for pine and fir dominated forests depending on altitude, which indicates the high degree of variability for this land cover type. Important discrepancies were found over the grasslands/shrublands for which

we estimated a mean vegetation C of 6.1 ± 0.7 kgC m^{-2}, while field studies (e.g. Búrquez et al., 2010; Navar et al., 2014) estimated 1.6-4.4 $kgCm^{-2}$ in the deserts over the North of the country.

Total soil C storage in the country is ~0.6% of the global stock (Ciais et al., 2013). This represents a smaller percentage than the other stocks and fluxes, because the FAO and field data used in this study included only the top 20 cm of soil; thus, the size of the soil C stock is underestimated. Batjes (1996) showed that, on average, topsoil (20 cm) represents a third of the global soil C stock. A field study in the dry tropics of Mexico (Jaramillo et al., 2003) showed that 37-59% of the soil C stock was in the top 20 cm of soil in land covers which comprised dry and floodplain forest and pasture. In the tropical evergreen forest of Los Tuxtlas (Hughes et al., 2000), soil C in the top 30 cm of soil represented 46% of the soil C stock to a 1 m depth. Thus, the amount of C stored in soil at the country scale is likely to be at least twice as high as estimated here and further work is needed to better constrain this calculation.

If we compare the estimates among products and consider the high correlations, it seems that the C stocks in the vegetation and the GPP fluxes are remarkably well constrained and compare favourably against field data and findings by other authors (Pacala et al. 2007). However, model development and improvement, particularly over non-forested areas, is needed, where the DGVM estimates showed the highest differences compared to field values.

Our results also showed that Mexico was a C sink over recent decades (1990-2009), gaining 31.4 ± 18.6 TgC yr^{-1}. This is similar to recent calculations by Hayes et al. (2013) using inverse (+8.7 TgC yr^{-1}) and forward models (29.0 TgC yr^{-1}) and to the result from atmospheric CO_2 inversions (21.4 TgC yr^{-1}). However, it is in disagreement with all inventory based calculations (Masera et al., 1997; Cairns et al., 2000; de Jong et al., 2010) that place Mexico as source of C (Table 1). The discrepancy may arise because the latter estimates are only based on changes in vegetation stocks, which does not take into account important ecosystem processes such as the effect of CO_2 fertilization and the impacts of climate change. In other words, those estimates are closer to the LUC C-flux than to NBP (see Table 1). Based on our estimates and the recent literature, we argue that it is likely that Mexico is currently a sink and not a source of C, if we disregard emissions from fossil fuels.

4.2 Past

Similar to the present-day, our results indicated that the terrestrial ecosystems in the country were a C-sink over the last 100 years, gaining 1,210 ± 1040 TgC in total. Such increment was driven by the CO_2 fertilization effect on vegetation (3408 ± 1060 $TgCyr^{-1}$), which enhanced GPP and subsequently biomass and possibly soil C to different degrees. Both the climate (-458 ± 1001 $TgCyr^{-1}$) and the land use (-1740 ± 878 $TgCyr^{-1}$) drivers showed a generalized negative effect on C storage. Our estimates are highly consistent with those derived from global models for Latin America, which show these land ecosystems as C sinks (Pan et al. 2011). However, during the period 1901-2000 the country's emissions from fossil fuels amounted to about 10,600 TgC (Le Quéré et al., 2014). This suggests that only 11% of the emissions from fossil fuels were actually captured back into the land and emphasizes the need for more efficient fossil-fuel and LUC policies.

The lost of C over the NE of Mexico is likely driven by climate. A long-term drought identified over the NE of Mexico and Southeast USA (Cayan et al., 2010), has led to a reduction in grassland productivity (Grover and Musick, 1990) and the subsequent loss of stored C due to increased dry season intensity and length (Murray-Tortarolo et al., Submitted). However, the overall negative effect of climate on C storage in other regions is likely linked to its impact on C mean residence time (MRT; Sup. 8). The increase in temperature leads to a higher respiration rate and soil C loss. As the MRT decreases, it results in certain regions becoming a C source to the atmosphere. This source, nevertheless, is apparently overridden by the impact of higher precipitation on plant productivity in many regions of Mexico. In this sense, MRT is one of the main sources of uncertainty for the future of global soil C (Carvalhais et al., 2014; Friend et al., 2014) and a more comprehensive analysis over the country, based on observed data, is lacking.

Other regions which experienced C loss are linked to the impact of LUC. LUC accounted for a loss of 1740 TgC over this period, with most of the emissions (60%) occurring in forested regions and 32% in the broadleaf forests over the South. Interestingly, about a third of the emissions (34%) were accounted for in croplands. Country-level estimates by Masera et al. (1997) calculated the flux at 61 $TgC\ yr^{-1}$ based on changes only in vegetation stocks for their baseline year in the 1980s. More comprehensive analyses including C

emissions from the soil C, estimated net emissions from LUC in forests of Mexico for the period 1993-2002 at 23.7 TgC yr^{-1} (de Jong et al., 2010; Hayes et al. 2012). Despite the different methodologies, all approaches establish that the highest LUC emissions fluxes have occurred mostly over the South of Mexico.

When the effects of all drivers were considered, the models showed that changes in climatic variables had a smaller impact on stored C than LUC during the period 1901-2009. This was due to the fact that the impacts of LUC were consistently negative on all land cover types, whereas climatic variables showed a heterogeneous effect (i.e., positive and negative) on the land cover types, which are differentially distributed over the country. Notably, climate trends alone have promoted C capture in broadleaf forests during the past 100 years, but this was overridden by LUC. However, there is no evidence from field measurements to support or disprove this claim. While there are studies on the consequences of LUC on C pools at the site and regional levels (Hughes et al. 2000; Jaramillo et al. 2003; de Jong et al. 2010), there is very little work on the effect of climate change on NBP over Mexico (e.g. Dai et al., 2014), making this a fundamental missing piece in our understanding of C cycle at local to regional scales. This is particularly important because the DGVMs used here are poorly constrained for their drought response (Morales et al., 2007; Sitch et al., 2003), a key process for the C balance over the arid regions of Mexico (grasslands/shrublands), which cover about 40% of the land area.

4.2 Future

In three out of four scenarios, Mexico represents a potential C sink in the remaining of this century. It is only in the scenario with the highest temperature and lowest precipitation (RCP8.5) that the country actually turns into a C source. While the CO_2 fertilization dominates the magnitude of the sink across all RCPs, the effect of climate becomes more negative and predominant as the RCP becomes more extreme (Table 5). Similar modelling results have been found at the global scale, with an increasing climate-carbon feedback as the future scenario becomes more extreme (Cox et al., 2000; Friedlingstein et al., 2006).

Table 5: Sensitivity of carbon to climate in four RCPs for the whole country. dC: change in total stored C, dT change in temperature, **γ:** Change in the Land-C flux relative to the change in temperature, **γo** land carbon sensitivity to climate in the past. A negative **γ-γo** implicates a less positive or negative effect of climate in the land-C-flux in the future compared to the present.

Period/RCP	**dC**	**dT**	**γ**	**γo-γ**
	PgC	ºK	PgC/ºK	PgC/ºK
1901-2000	1.2	0.88	1.36*	
RCP2.6	3.0	2.4	1.25	-0.11
RCP4.5	2.1	3.6	0.58	-0.78
RCP6.0	1.5	4.5	0.33	-1.03
RCP8.5	-0.7	6.1	-0.21	-1.57

Important considerations should be taken into account. The CO_2 fertilization effect is likely limited not only by climate, but also by the effect of limiting nutrients on C uptake –a process that is not considered in many Earth-System-Models (ESMs) (Reich et al., 2014, 2006) or by more severe fires as a result of more intense and recurrent ENSO (Yocom et al., 2010). Additionally, as shown by the past trends, a decrease in the MRT of soil C can change an ecosystem from a C-sink into a source. There is a lack of field information to estimate MRT and its response to temperature and soil moisture to fully understand the implications for the future of stored C, especially in tropical and sub-tropical ecosystems.

5 Final considerations

We quantify different aspects of the C cycle for Mexico (GPP and the total land C flux, as well as vegetation and soil C stocks) using different products over three time periods. As far as we know, this is the first time these pools and fluxes have been quantified for the whole country with a process-based approach. It takes into account different drivers (e.g. CO_2, climate and LUC) and provides a more realistic estimate of the C cycle for the country.

Additionally, we quantify fluxes (e.g. GPP and NBP), not previously estimated at the country scale.

Contrary to other inventory-based estimates (de Jong et al. 2010; Pacala et al. 2007; Hayes et al. 2012), our analysis shows that over the last 100 years and recent decades the country was a C sink. Our results suggest this is mainly due to the positive effect of CO_2 fertilization and to precipitation and temperature changes in some regions. This pattern is likely to persist, although with a diminishing trend, over the remaining part of the century. Such a sink however only accounts for 11% of C emissions from fossil fuels during the period, which clearly points towards the need of more fuel-efficient policies and emissions controls.

Our work also identifies the need to study the role of drought in marginal lands (e.g. grasslands and shrublands) and to determine soil carbon MRT in tropical ecosystems. Finally, as we used data coming from global sources (e.g. DGVMs, ESMs, satellite), the methodology proposed here can be used to analyse the full-C cycle of regions elsewhere.

Authors Contributions

GMT, PF, SS and VJJ designed, executed and wrote the paper. FMF, AA and YL provided and analized data. The rest of the authors provided the DGVMs data and helped writting the paper.

Aknoledgements

The lead author (GMT) thanks CONACYT-CECTI, the University of Exeter and Secretaria de Educacion Publica (SEP) for their funding for this project. The authors extend their thanks to Dr. Carlos Ortiz Solorio and to the Colegio de Posgraduados for the field soil data and to the Alianza Redd+ Mexico for the field biomass data. This project would not have been possible withouth the valuable data from the CMIP5 models

References

Alianza MREDD+, 2013. Mapa y base de datos sobre la distribución de la biomasa aérea de la vegetación leñosa en México.Woods Hole Research Center, USAID, CONAFOR, CONABIO, Proyecto México Noruega. México.

Anav, A., Friedlingstein, P., Kidston, M., Bopp, L., Ciais, P., Cox, P., Jones, C., Jung, M., Myneni, R., Zhu, Z., 2013. Evaluating the Land and Ocean Components of the Global Carbon Cycle in the CMIP5 Earth System Models. J. Clim. 26, 6801–6843. doi:10.1175/JCLI-D-12-00417.1

Batjes, N. h., 1996. Total carbon and nitrogen in the soils of the world. Eur. J. Soil Sci. 47, 151–163. doi:10.1111/j.1365-2389.1996.tb01386.x

Búrquez, A., Martínez-Yrízar, A., Núñez, S., Quintero, T., Aparicio, A., 2010. Aboveground biomass in three Sonoran Desert communities: Variability within and among sites using replicated plot harvesting. J. Arid Environ. 74, 1240–1247. doi:10.1016/j.jaridenv.2010.04.004

Cairns, M.A., Olmsted, I., Granados, J., Argaez, J., 2003. Composition and aboveground tree biomass of a dry semi-evergreen forest on Mexico's Yucatan Peninsula. For. Ecol. Manag. 186, 125–132. doi:10.1016/S0378-1127(03)00229-9

Carvalhais, N., Forkel, M., Khomik, M., Bellarby, J., Jung, M., Migliavacca, M., Mu, M., Saatchi, S., Santoro, M., Thurner, M., Weber, U., Ahrens, B., Beer, C., Cescatti, A., Randerson, J.T., Reichstein, M., 2014. Global covariation of carbon turnover times with climate in terrestrial ecosystems. Nature 514, 213–217. doi:10.1038/nature13731

Cayan, D.R., Das, T., Pierce, D.W., Barnett, T.P., Tyree, M., Gershunov, A., 2010. Future dryness in the southwest US and the hydrology of the early 21st century drought. Proc. Natl. Acad. Sci. 107, 21271–21276. doi:10.1073/pnas.0912391107

Challenger, A., 1998. Utilización y conservación de los ecosistemas terrestres de México. Pasado, presente y futuro. Conabio, IBUNAM y Agrupación Sierra Madre, México.

Ciais, P., C. Sabine, G. Bala, L. Bopp, V. Brovkin, J. Canadell, A. Chhabra, R. DeFries, J. Galloway, M. Heimann, C. Jones, C. Le Quéré, R.B. Myneni, S. Piao and P. Thornton, 2013: Carbon and Other Biogeochemical Cycles. In: *Cli- mate Change 2013: The Physical Science Basis. Contribution of Working Group I to the Fifth Assessment Report of the Intergovernmental Panel on Climate Change* [Stocker, T.F., D. Qin, G.-K. Plattner, M. Tignor, S.K. Allen, J. Boschung, A. Nauels, Y. Xia, V. Bex and P.M. Midgley (eds.)]. Cambridge University Press, Cambridge, United Kingdom and New York, NY, USA.

Cox, P.M., Betts, R.A., Jones, C.D., Spall, S.A., Totterdell, I.J., 2000. Acceleration of global warming due to carbon-cycle feedbacks in a coupled climate model. Nature 408, 184–187. doi:10.1038/35041539

Dai, Z., Birdsey, R.A., Johnson, K.D., Dupuy, J.M., Hernandez-Stefanoni, J.L., Richardson, K., 2014. Modeling carbon stocks in a secondary tropical dry forest in the Yucatan Peninsula, Mexico. Water. Air. Soil Pollut. 225, 1–15. doi:10.1007/s11270-014-1925-x

De Jong, B., Anaya, C., Masera, O., Olguín, M., Paz, F., Etchevers, J., Martínez, R.D., Guerrero, G., Balbontín, C., 2010. Greenhouse gas emissions between 1993 and 2002 from land-use change and forestry in Mexico. For. Ecol. Manag. 260, 1689–1701. doi:10.1016/j.foreco.2010.08.011

Dolman, A.J., Shvidenko, A., Schepaschenko, D., Ciais, P., Tchebakova, N., Chen, T., van der Molen, M.K., Belelli Marchesini, L., Maximov, T.C., Maksyutov, S., Schulze, E.-D., 2012. An estimate of the terrestrial carbon budget of Russia using inventory-based, eddy covariance and inversion methods. Biogeosciences 9, 5323–5340. doi:10.5194/bg-9-5323-2012

Enting, I.G., Rayner, P.J., Ciais, P., 2012. Carbon Cycle Uncertainty in REgional Carbon Cycle Assessment and Processes (RECCAP). Biogeosciences 9, 2889–2904. doi:10.5194/bg-9-2889-2012

FAO/IIASA/ISRIC/ISSCAS/JRC, 2012. Harmonized World Soil Database (version 1.2).

Friedlingstein, P., Cox, P., Betts, R., Bopp, L., von Bloh, W., Brovkin, V., Cadule, P., Doney, S., Eby, M., Fung, I., Bala, G., John, J., Jones, C., Joos, F., Kato, T., Kawamiya, M., Knorr, W., Lindsay, K., Matthews, H.D., Raddatz, T., Rayner, P., Reick, C., Roeckner, E., Schnitzler, K.-G., Schnur, R., Strassmann, K., Weaver, A.J., Yoshikawa, C., Zeng, N., 2006. Climate–Carbon Cycle Feedback Analysis: Results from the C4MIP Model Intercomparison. J. Clim. 19, 3337–3353. doi:10.1175/JCLI3800.1

Friedlingstein, P., Meinshausen, M., Arora, V.K., Jones, C.D., Anav, A., Liddicoat, S.K., Knutti, R., 2013. Uncertainties in CMIP5 Climate Projections due to Carbon Cycle Feedbacks. J. Clim. 27, 511–526. doi:10.1175/JCLI-D-12-00579.1

Friend, A.D., Lucht, W., Rademacher, T.T., Keribin, R., Betts, R., Cadule, P., Ciais, P., Clark, D.B., Dankers, R., Falloon, P.D., Ito, A., Kahana, R., Kleidon, A., Lomas, M.R., Nishina, K., Ostberg, S., Pavlick, R., Peylin, P., Schaphoff, S., Vuichard, N., Warszawski, L., Wiltshire, A., Woodward, F.I., 2014. Carbon residence time dominates uncertainty in terrestrial vegetation responses to future climate and atmospheric CO2. Proc. Natl. Acad. Sci. 111, 3280–3285. doi:10.1073/pnas.1222477110

Garcia-Moya, Montanes-Castro, 1992. Saline grassland near Mexico City. C, in: Primary Productivity of Grass Ecosystems of the Tropics and Sub-Tropics. Chapman and Hall, London., pp. 70–99.

Gloor, M., Gatti, L., Brienen, R., Feldpausch, T.R., Phillips, O.L., Miller, J., Ometto, J.P., Rocha, H., Baker, T., de Jong, B., Houghton, R.A., Malhi, Y., Aragão, L.E.O.C., Guyot, J.-L., Zhao, K., Jackson, R., Peylin, P., Sitch, S., Poulter, B., Lomas, M., Zaehle, S., Huntingford, C., Levy, P., Lloyd, J., 2012. The carbon balance of South America: a review of the status, decadal trends and main determinants. Biogeosciences 9, 5407–5430. doi:10.5194/bg-9-5407-2012

Grover, H.D., Musick, H.B., 1990. Shrubland encroachment in southern New Mexico, U.S.A.: An analysis of desertification processes in the American southwest. Clim. Change 17, 305–330. doi:10.1007/BF00138373

Harris, I., Jones, P. d., Osborn, T. j., Lister, D. h., 2013. Updated high-resolution grids of monthly climatic observations – the CRU TS3.10 Dataset. Int. J. Climatol. n/a–n/a. doi:10.1002/joc.3711

Hayes, D.J., Turner, D.P., Stinson, G., McGuire, A.D., Wei, Y., West, T.O., Heath, L.S., de Jong, B., McConkey, B.G., Birdsey, R.A., Kurz, W.A., Jacobson, A.R., Huntzinger, D.N., Pan, Y., Post, W.M., Cook, R.B., 2012. Reconciling estimates of the contemporary North American carbon balance among terrestrial biosphere models, atmospheric inversions, and a new approach for estimating net ecosystem exchange from inventory-based data. Glob. Change Biol. 18, 1282–1299. doi:10.1111/j.1365-2486.2011.02627.x

Hughes, R.F., Kauffman, J.B., Jaramillo, V.J., 1999. Biomass, carbon, and nutrient dynamics of secondary forests in a humid tropical region of méxico. Ecology 80, 1892–1907. doi:10.1890/0012-9658(1999)080[1892:BCANDO]2.0.CO;2

Hurtt, G., Chini, L., Frolking, S., Betts, R., Feddema, J., Fischer, G., Fisk, J., Hibbard, K., Houghton, R., Janetos, A., Jones, C., Kindermann, G., Kinoshita, T., Klein Goldewijk, K., Riahi, K., Shevliakova, E., Smith, S., Stehfest, E., Thomson, A., Thornton, P., van Vuuren, D., Wang, Y., 2011. Harmonization of land-use scenarios for the period 1500–2100: 600 years of global gridded annual land-use transitions, wood harvest, and resulting secondary lands. Clim. Change 109, 117–161. doi:10.1007/s10584-011-0153-2

Jasso, R., 2014. Crecimiento, biomasa y carbono arbóreo en un gradiente altitudinal en bosques templados. Tesis de Maestría, Posgrado en Ciencias Biológicas, UNAM.

Jung, M., Reichstein, M., Bondeau, A., 2009. Towards global empirical upscaling of FLUXNET eddy covariance observations: validation of a model tree ensemble approach using a biosphere model. Biogeosciences 6, 2001–2013. doi:10.5194/bg-6-2001-2009

Jung, M., Reichstein, M., Margolis, H.A., Cescatti, A., Richardson, A.D., Arain, M.A., Arneth, A., Bernhofer, C., Bonal, D., Chen, J., Gianelle, D., Gobron, N., Kiely, G., Kutsch, W., Lasslop, G., Law, B.E., Lindroth, A., Merbold, L., Montagnani, L., Moors, E.J., Papale, D., Sottocornola, M., Vaccari, F., Williams, C., 2011. Global patterns of land-atmosphere fluxes of carbon dioxide, latent heat, and sensible heat derived from eddy covariance, satellite, and meteorological observations. J. Geophys. Res. Biogeosciences 116, G00J07. doi:10.1029/2010JG001566

Keeling, C.D., Whorf, T.P., Wahlen, M., Van Der Plicht, J., 1995. Interannual extremes in the rate of rise of atmospheric carbon dioxide since 1980. Nature 375, 666–670.

King, A.W., Andres, R.J., Davis, K.J., Hafer, M., Hayes, D.J., Huntzinger, D.N., de Jong, B., Kurz, W.A., McGuire, A.D., Vargas, R., Wei, Y., West, T.O., Woodall, C.W., 2015. North America's net terrestrial CO2 exchange with the atmosphere 1990–2009. Biogeosciences 12, 399–414. doi:10.5194/bg-12-399-2015

King, A.W., Hayes, D.J., Huntzinger, D.N., West, T.O., Post, W.M., 2012. North American carbon dioxide sources and sinks: magnitude, attribution, and uncertainty. Front. Ecol. Environ. 10, 512–519. doi:10.1890/120066

Le Quéré, C., Moriarty, R., Andrew, R.M., Peters, G.P., Ciais, P., Friedlingstein, P., Jones, S.D., Sitch, S., Tans, P., Arneth, A., Boden, T.A., Bopp, L., Bozec, Y., Canadell, J.G., Chevallier, F., Cosca, C.E., Harris, I., Hoppema, M., Houghton, R.A., House, J.I., Jain, A., Johannessen, T., Kato, E., Keeling, R.F., Kitidis, V., Klein Goldewijk, K., Koven, C., Landa, C.S., Landschützer, P., Lenton, A., Lima, I.D., Marland, G., Mathis, J.T., Metzl, N., Nojiri, Y., Olsen, A., Ono, T., Peters, W., Pfeil, B., Poulter, B., Raupach, M.R., Regnier, P., Rödenbeck, C., Saito, S., Salisbury, J.E., Schuster, U., Schwinger, J., Séférian, R., Segschneider, J., Steinhoff, T., Stocker, B.D., Sutton, A.J., Takahashi, T., Tilbrook, B., van der Werf, G.R., Viovy, N., Wang, Y.-P., Wanninkhof, R., Wiltshire, A., Zeng, N., 2014. Global carbon budget 2014. Earth Syst. Sci. Data Discuss. 7, 521–610. doi:10.5194/essdd-7-521-2014

Le Quéré, C.L., Raupach, M.R., Canadell, J.G., Al, G.M. et, Al, C.L.Q. et, Al, C.L.Q. et, Raupach, M.R., Canadell, J.G., Marland, G., Bopp, L., Ciais, P., Conway, T.J., Doney, S.C., Feely, R.A., Foster, P., Friedlingstein, P., Gurney, K., Houghton, R.A., House, J.I., Huntingford, C., Levy, P.E., Lomas, M.R., Majkut, J., Metzl, N., Ometto, J.P., Peters, G.P., Prentice, I.C., Randerson, J.T., Running, S.W., Sarmiento, J.L., Schuster, U., Sitch, S., Takahashi, T., Viovy, N., Werf, G.R. van der, Woodward, F.I., Al, C.L.Q. et, Al, C.L.Q. et, Raupach, M.R., Canadell, J.G., Marland, G., Bopp, L., Ciais, P., Conway, T.J., Doney, S.C., Feely, R.A., Foster, P., Friedlingstein, P., Gurney, K., Houghton, R.A., House, J.I., Huntingford, C., Levy, P.E., Lomas, M.R., Majkut, J., Metzl, N., Ometto, J.P., Peters, G.P., Prentice, I.C., Randerson, J.T., Running, S.W., Sarmiento, J.L., Schuster, U., Sitch, S., Takahashi, T., Viovy, N., Werf, G.R. van der, Woodward, F.I., 2009. Trends in the sources and sinks of carbon dioxide. Nat. Geosci. 2, 831–836. doi:10.1038/ngeo689

Liu, Y.Y., Evans, J.P., McCabe, M.F., de Jeu, R.A.M., van Dijk, A.I.J.M., Dolman, A.J., Saizen, I., 2013. Changing Climate and Overgrazing Are Decimating Mongolian Steppes. PLoS ONE 8, e57599. doi:10.1371/journal.pone.0057599

Liu, Y.Y., Parinussa, R.M., Dorigo, W.A., De Jeu, R.A.M., Wagner, W., van Dijk, A.I.J.M., McCabe, M.F., Evans, J.P., 2011. Developing an improved soil moisture dataset by blending passive and active microwave satellite-

based retrievals. Hydrol Earth Syst Sci 15, 425–436. doi:10.5194/hess-15-425-2011

Martinez-Yrizar, A., Maass, J.M., Perez-Jimenez, L.A., Sarukhan, J., 1996. Net primary productivity of a tropical deciduous forest ecosystem in western Mexico. J. Trop. Ecol. 12, 169–175. doi:10.1017/S026646740000938X

Masera, O.R., Cerón, A.D., Ordóñez, A., 2001. Forestry Mitigation Options for Mexico: Finding Synergies between National Sustainable Development Priorities and Global Concerns. Mitig. Adapt. Strateg. Glob. Change 6, 291–312. doi:10.1023/A:1013327019175

Morales, P., Hickler, T., Rowell, D.P., Smith, B., Sykes, M.T., 2007. Changes in European ecosystem productivity and carbon balance driven by regional climate model output. Glob. Change Biol. 13, 108–122. doi:10.1111/j.1365-2486.2006.01289.x

Murray-Tortarolo, G., et al., Submitted. Changes in the dry season intensity are a key driver of trends in NPP. Nature Geosci.

Navar, J., Rodriguez-Flores, F. de J., Dominguez-Calleros, P.A., Perez-Verdin, G., 2014. Diversity-Productivity Relationship in the Northeastern Tamaulipan Thornscrub Forest of Mexico. Int. J. Ecol. 2014, e196073. doi:10.1155/2014/196073

Norby, R.J., DeLucia, E.H., Gielen, B., Calfapietra, C., Giardina, C.P., King, J.S., Ledford, J., McCarthy, H.R., Moore, D.J.P., Ceulemans, R., De Angelis, P., Finzi, A.C., Karnosky, D.F., Kubiske, M.E., Lukac, M., Pregitzer, K.S., Scarascia-Mugnozza, G.E., Schlesinger, W.H., Oren, R., 2005. Forest response to elevated CO2 is conserved across a broad range of productivity. Proc. Natl. Acad. Sci. U. S. A. 102, 18052–18056. doi:10.1073/pnas.0509478102

Pacala, S., Birdsey, R., Bridgham, S., Conant, R., Davis, K., Houghton, R., Jenkins, J., Johnston, M., Marland, G., Paustian, K., 2007. The North American Carbon Budget Past and Present, in: The First State of the Carbon Cycle Report (SOCCR): The North American Carbon Budget and Implications for the Global Carbon Cycle. A Report by the U.S. Climate Change Science Program and the Subcommittee on Global Change Research. National Oceanic and Atmospheric Administration, National Climatic Data Center, Asheville, NC, USA, pp. 29–36.

Pappas, C., Fatichi, S., Leuzinger, S., Wolf, A., Burlando, P., 2013. Sensitivity analysis of a process-based ecosystem model: Pinpointing parameterization and structural issues. J. Geophys. Res. Biogeosciences 118, 505–528. doi:10.1002/jgrg.20035

Piao, S.L., Ito, A., Li, S.G., Huang, Y., Ciais, P., Wang, X.H., Peng, S.S., Nan, H.J., Zhao, C., Ahlström, A., Andres, R.J., Chevallier, F., Fang, J.Y., Hartmann, J., Huntingford, C., Jeong, S., Levis, S., Levy, P.E., Li, J.S., Lomas, M.R., Mao, J.F., Mayorga, E., Mohammat, A., Muraoka, H., Peng, C.H., Peylin, P., Poulter, B., Shen, Z.H., Shi, X., Sitch, S., Tao, S., Tian, H.Q., Wu, X.P., Xu, M., Yu, G.R., Viovy, N., Zaehle, S., Zeng, N., Zhu, B., 2012. The carbon budget of terrestrial ecosystems in East Asia over the last two decades. Biogeosciences 9, 3571–3586. doi:10.5194/bg-9-3571-2012

Prentice, I.C., Farquhar, G.D., Fasham, M.J.., Heimann, M., Jaramillo, V., Kheshi, H.S., Le Quéré, C.L., Scholes, R.J., Wallace, D.W.., 2001. IPCC TAR.

Ramankutty, N., Foley, J.A., 1999. Estimating historical changes in global land cover: Croplands from 1700 to 1992. Glob. Biogeochem. Cycles 13, 997–1027. doi:10.1029/1999GB900046

Reich, P.B., Hobbie, S.E., Lee, T., Ellsworth, D.S., West, J.B., Tilman, D., Knops, J.M.H., Naeem, S., Trost, J., 2006. Nitrogen limitation constrains sustainability of ecosystem response to CO2. Nature 440, 922–925. doi:10.1038/nature04486

Reich, P.B., Hobbie, S.E., Lee, T.D., 2014. Plant growth enhancement by elevated CO2 eliminated by joint water and nitrogen limitation. Nat. Geosci. 7, 920–924. doi:10.1038/ngeo2284

Running, S.W., Nemani, R.R., Heinsch, F.A., Zhao, M., Reeves, M., Hashimoto, H., 2004. A Continuous Satellite-Derived Measure of Global Terrestrial Primary Production. BioScience 54, 547–560. doi:10.1641/0006-3568(2004)054[0547:ACSMOG]2.0.CO;2

SEMARNAT, 2002. Evaluacion de la degradacion de suelo causada por el hombre en la Republica Mexicana.

Sitch, S., Friedlingstein, P., Gruber, N., Jones, S.D., Murray-Tortarolo, G., Ahlström, A., Doney, S.C., Graven, H., Heinze, C., Huntingford, C., Levis, S., Levy, P.E., Lomas, M., Poulter, B., Viovy, N., Zaehle, S., Zeng,

N., Arneth, A., Bonan, G., Bopp, L., Canadell, J.G., Chevallier, F., Ciais, P., Ellis, R., Gloor, M., Peylin, P., Piao, S.L., Le Quéré, C., Smith, B., Zhu, Z., Myneni, R., 2015. Recent trends and drivers of regional sources and sinks of carbon dioxide. Biogeosciences 12, 653–679. doi:10.5194/bg-12-653-2015

Sitch, S., Smith, B., Prentice, I.C., Arneth, A., Bondeau, A., Cramer, W., Kaplan, J.O., Levis, S., Lucht, W., Sykes, M.T., Thonicke, K., Venevsky, S., 2003. Evaluation of ecosystem dynamics, plant geography and terrestrial carbon cycling in the LPJ dynamic global vegetation model. Glob. Change Biol. 9, 161–185. doi:10.1046/j.1365-2486.2003.00569.x

Taylor, K.E., Stouffer, R.J., Meehl, G.A., 2011. An Overview of CMIP5 and the Experiment Design. Bull. Am. Meteorol. Soc. 93, 485–498. doi:10.1175/BAMS-D-11-00094.1

Valentini, R., Arneth, A., Bombelli, A., Castaldi, S., Cazzolla Gatti, R., Chevallier, F., Ciais, P., Grieco, E., Hartmann, J., Henry, M., Houghton, R.A., Jung, M., Kutsch, W.L., Malhi, Y., Mayorga, E., Merbold, L., Murray-Tortarolo, G., Papale, D., Peylin, P., Poulter, B., Raymond, P.A., Santini, M., Sitch, S., Vaglio Laurin, G., van der Werf, G.R., Williams, C.A., Scholes, R.J., 2014. A full greenhouse gases budget of Africa: synthesis, uncertainties, and vulnerabilities. Biogeosciences 11, 381–407. doi:10.5194/bg-11-381-2014

Yocom, L.L., Fulé, P.Z., Brown, P.M., Cerano, J., Villanueva-Díaz, J., Falk, D.A., Cornejo-Oviedo, E., 2010. El Niño–Southern Oscillation effect on a fire regime in northeastern Mexico has changed over time. Ecology 91, 1660–1671. doi:10.1890/09-0845.1

PART 2: PROCESS ANALYSIS

Chapter 4. Recent Trends in the Land Carbon Cycle

Chapter 3. Changes in dry season intensity is a key driver of regional NPP trends

The third part of the thesis is guided by the analysis of processes that drive global NBP and NPP. As shown in chapter 1 (introduction), several different drivers can alter the rate at which C is exchange between the biosphere and the atmosphere. They have been studied at great detail at multiple scales, however large uncertainty remains on the relative contribution of each driver to the total change in NBP at regional scales. Moreover some of the relationships (i.e. precipitation and NPP) are non linear and a more in depth study is needed to fully understand how they interact and the implications this can have for the future.

Two chapters comprise the second part. Chapter 4 focuses on the regional trends in NBP driven by changes atmospheric CO_2 and climate acting concurrently. We found that the land has been a C sink over the last 20 years (1990-2009) with increasing NBP trends as NPP grew faster than RH. However the trends were not distributed homogeneously across the land and several regions show a decline in NBP driven by declining precipitation. This was the end of this study, but a more in-depth relationship between drought and negative NBP trends was missing.

Chapter 5 fills this gap, analysing the relationship between vegetation productivity and changes in the dry season intensity and length. We found that small changes in the water fluxes during the dry season have a large effect on annual NPP and biomass and act as a key driver of regional differences in productivity. Moreover, increasing dryness over arid ecosystems reduced NPP globally; an effect that we predicted will continue into the future and could reduce global NPP by up to 10%.

Chapter 4: Recent Trends in the Land Carbon Cycle

4.1 Summary

4.1.1 introduction

Land ecosystems are responsible for the uptake of 28% of the anthropogenic CO_2 emissions (Le Quéré et al. 2013). Models suggest this is driven primarily driven by the CO_2 fertilization effect on photosynthesis and subsequent increment in total stored C on land (McGuire et al., 2001). However this effect is not distributed homogeneously across the planet (Pan et al. 2011).

Additionally, effect of climate on the land C varies across the planet, leading to regional differences in the magnitude and direction of the land-C flux (Sarmiento et al. 2010). This is particularly important as extreme climate events occurred during the 1990–2009 period across many regions of the world, including North America (south-western USA, 2000–2002), Europe (2003), Amazonia (2005), and eastern Australia (2001–2008), raising considerable attention in the ecological community regarding the consequences of recent climate variability on ecosystem structure and function (Allen et al., 2010) and the carbon cycle (Ciais et al., 2005; Van der Molen et al., 2011; Reichstein et al., 2013).

While there is growing literature on regional carbon budgets (e.g. RECCAP: Valentini et al. 2014; McGuire et al, 2012; Luyssaert et al. 2012; Piao et al. 2009), no consistent attribution (i.e. over the same time period, using the same models and the same forcing datasets) has been conducted.

The objective of this chapter is to calculate the recent changes in the land C uptake (1990-2009), to attribute these trends to the underlying processes, and to go beyond the global scale and analyse regional changes in the carbon cycle and their environmental drivers. This chapter is the result of my collaboration in the paper:

> Sitch, S., Friedlingstein, P., Gruber, N., Jones, S. D., Murray-Tortarolo, G., Ahlström, A., Doney, S. C., Graven, H., Heinze, C., Huntingford, C., Levis, S., Levy, P. E., Lomas, M., Poulter, B., Viovy, N., Zaehle, S., Zeng, N., Arneth, A., Bonan, G., Bopp, L., Canadell, J. G., Chevallier, F., Ciais, P., Ellis, R., Gloor, M., Peylin, P., Piao, S., Le Quéré, C., Smith, B., Zhu, Z., and Myneni, R. 2015. **Trends and drivers of regional sources and**

sinks of carbon dioxide over the past two decades, *Biogeosciences.* doi:10.5194/bg-12-653-2015

4.1.2 Methodology

We used the output from 9 DGVMs forced with the same climatic data and similar spin-up protocol, for the period 1990-2009. Two simulations were conducted: S1=CO_2 only and S2= CO_2 + Climate for the full century. All modelled output was regridded to a similar grid and weighted by the land/sea fraction.

4.1.3 Summary of results

Globally land ecosystems were a sink of C of 2.4 ± 0.7 $PgCyr^{-1,}$ with an increasing trend of 0.055 ± 0.030 $PgCyr^{-2}$ as a result of NPP increasing faster then Rh. However important regional differences occurred, driven mainly by climate variability and change.

Over the Northern Hemisphere (NH), in response to warming, models simulate an earlier onset (ensemble mean model trend = −0.078 ± 0.131 days yr^{-1}) and delayed termination of the growing season (0.217 ± 0.097 days yr^{-1}) based on LAI, and thus a trend towards a longer growing season in the northern extratropics (0.295 ± 0.228 days yr^{-1}). This, in addition to the CO_2 fertilization effect, led to an increase in NPP of 0.63 ± 0.02 PgC yr^{-2}. However at the same time, the warming in boreal regions led to increased microbial decomposition, reducing the mean residence time of carbon in soils. Additionally, widespread drought over the Mongolian Plateau and southern USA led to a decreasing NBP. So while the NH remained a sink of C (with a magnitude of.3 ± 0.3 PgC yr^{-2}) because of increased CO_2, the long-term trend was close to zero as the change in RH balanced the increase in NPP.

Over the tropics NBP increased steadily due to CO_2 fertilization in all DGVMs, with a magnitude of 0.96 ± 0.43 PgC yr^{-1} and an increasing trend of 0.04 ±0.01 PgC yr^{-2}. However important regional differences occur, with decreasing NBP trends over the Amazon basin, Northern Africa and Australia, clearly linked to decreased precipitation. Rh trend was also positive and slightly smaller than NPP, possibly also stimulated by the increase of CO_2 via increases in litter input into soils.

The regional findings can be summarized briefly as (1) the land CO_2 sink has increased over the study period, almost entirely through increases in tropical and southern regions with negligible increase in northern regions; (2) globally and in most regions, the land sinks are not increasing as fast as the growth rate of excess atmospheric CO_2 above preindustrial and (3) precipitation, particularly when decreasing, plays a fundamental role in determining regional decreases in NBP.

4.1.4 My contribution to the paper

This chapter is the result of my collaboration on the paper of Sitch et al. (2015) and my involvement in the TRENDY modelling group activities (http://dgvm.ceh.ac.uk/node/9). I led the DGVM comparison against remote sensing data, and was responsible for analysing part the post-processed data (i.e. I provided some calculations for the tables and main text), and produced the main figures for the paper. I was actively involved in all the scientific discussions and contributed to the analyses and interpretation of results.

I include this study in my thesis because 1) I did most of this during my first year of PhD studies. It was an opportune way to develop coding, analysis skills, and better familiarize myself with dynamic global vegetation models (DGVMs) and global modelling studies in general. I gained valuable skills comparing different models, manipulating large databases, analysing different spatial and temporal scales and plotting advanced figures, which I applied in all other chapters, and 2) it was the background for the rest of my thesis, as I derived the rest of the analysis from this study.

Biogeosciences, 12, 653–679, 2015
www.biogeosciences.net/12/653/2015/
doi:10.5194/bg-12-653-2015

Biogeosciences Open Access

Recent trends and drivers of regional sources and sinks of carbon dioxide

S. Sitch[1], P. Friedlingstein[1], N. Gruber[2], S. D. Jones[3], G. Murray-Tortarolo[1], A. Ahlström[4], S. C. Doney[5], H. Graven[6], C. Heinze[7,8,9], C. Huntingford[10], S. Levis[11], P. E. Levy[12], M. Lomas[13], B. Poulter[14], N. Viovy[15], S. Zaehle[16], N. Zeng[17], A. Arneth[18], G. Bonan[11], L. Bopp[15], J. G. Canadell[19], F. Chevallier[15], P. Ciais[15], R. Ellis[10], M. Gloor[20], P. Peylin[15], S. L. Piao[21], C. Le Quéré[3], B. Smith[4], Z. Zhu[22,23], and R. Myneni[24]

[1]University of Exeter, Exeter EX4 4QF, UK
[2]Institute of Biogeochemistry and Pollutant Dynamics, ETH Zurich, Zurich, Switzerland
[3]Tyndall Centre for Climate Change Research, University of East Anglia, Norwich NR4 7TJ, UK
[4]Lund University, Department of Physical Geography and Ecosystem Science, Sölvegatan 12, 223 62 Lund, Sweden
[5]Marine Chemistry and Geochemistry Department, Woods Hole Oceanographic Institution, 266 Woods Hole Road, Woods Hole, MA 02543, USA
[6]Department of Physics and Grantham Institute for Climate Change, Imperial College London, London SW7 2AZ, UK
[7]Geophysical Institute, University of Bergen, Bergen, Norway
[8]Bjerknes Centre for Climate Research, Bergen, Norway
[9]Uni Climate, Uni Research AS, Bergen, Norway
[10]Centre for Ecology and Hydrology, Benson Lane, Wallingford OX10 8BB, UK
[11]National Center for Atmospheric Research, Boulder, Colorado, USA
[12]Centre for Ecology and Hydrology, Bush Estate, Penicuik, Midlothian EH26 0QB, UK
[13]Department of Animal & Plant Sciences, University of Sheffield, Sheffield S10 2TN, UK
[14]Institute on Ecosystems and Department of Ecology, Montana State University, Bozeman, MT 59717, USA
[15]Laboratoire des Sciences du Climat et de l'Environnement, CEA CNRS UVSQ, 91191 Gif-sur-Yvette, France
[16]Biogeochemical Integration Department, Max Planck Institute for Biogeochemistry, P.O. Box 10 01 64, 07701 Jena, Germany
[17]Department of Atmospheric and Oceanic Science, University of Maryland, College Park, MD 20740, USA
[18]Karlsruhe Institute of Technology, Garmisch-Partenkirchen, Germany
[19]Global Carbon Project, CSIRO Oceans and Atmosphere Flagship, Canberra, Australia
[20]University of Leeds, School of Geography, Woodhouse Lane, Leeds LS9 2JT, UK
[21]College of Urban and Environmental Sciences, Peking University, Beijing 100871, China
[22]State Key Laboratory of Remote Sensing Science, Institute of Remote Sensing and Digital Earth, Chinese Academy of Sciences, Beijing 100101, China
[23]Center for Applications of Spatial Information Technologies in Public Health, Beijing 100101, China
[24]Department of Geography and Environment, Boston University, 675 Commonwealth Avenue, Boston, MA 02215, USA

Correspondence to: S. Sitch (s.a.sitch@exeter.ac.uk)

Received: 21 November 2013 – Published in Biogeosciences Discuss.: 23 December 2013
Revised: 30 November 2014 – Accepted: 19 December 2014 – Published: 2 February 2015

Published by Copernicus Publications on behalf of the European Geosciences Union.

Abstract. The land and ocean absorb on average just over half of the anthropogenic emissions of carbon dioxide (CO_2) every year. These CO_2 "sinks" are modulated by climate change and variability. Here we use a suite of nine dynamic global vegetation models (DGVMs) and four ocean biogeochemical general circulation models (OBGCMs) to estimate trends driven by global and regional climate and atmospheric CO_2 in land and oceanic CO_2 exchanges with the atmosphere over the period 1990–2009, to attribute these trends to underlying processes in the models, and to quantify the uncertainty and level of inter-model agreement. The models were forced with reconstructed climate fields and observed global atmospheric CO_2; land use and land cover changes are not included for the DGVMs. Over the period 1990–2009, the DGVMs simulate a mean global land carbon sink of $-2.4 \pm 0.7\,\mathrm{Pg\,C\,yr^{-1}}$ with a small significant trend of $-0.06 \pm 0.03\,\mathrm{Pg\,C\,yr^{-2}}$ (increasing sink). Over the more limited period 1990–2004, the ocean models simulate a mean ocean sink of $-2.2 \pm 0.2\,\mathrm{Pg\,C\,yr^{-1}}$ with a trend in the net C uptake that is indistinguishable from zero ($-0.01 \pm 0.02\,\mathrm{Pg\,C\,yr^{-2}}$). The two ocean models that extended the simulations until 2009 suggest a slightly stronger, but still small, trend of $-0.02 \pm 0.01\,\mathrm{Pg\,C\,yr^{-2}}$. Trends from land and ocean models compare favourably to the land greenness trends from remote sensing, atmospheric inversion results, and the residual land sink required to close the global carbon budget. Trends in the land sink are driven by increasing net primary production (NPP), whose statistically significant trend of $0.22 \pm 0.08\,\mathrm{Pg\,C\,yr^{-2}}$ exceeds a significant trend in heterotrophic respiration of $0.16 \pm 0.05\,\mathrm{Pg\,C\,yr^{-2}}$ – primarily as a consequence of widespread CO_2 fertilisation of plant production. Most of the land-based trend in simulated net carbon uptake originates from natural ecosystems in the tropics ($-0.04 \pm 0.01\,\mathrm{Pg\,C\,yr^{-2}}$), with almost no trend over the northern land region, where recent warming and reduced rainfall offsets the positive impact of elevated atmospheric CO_2 and changes in growing season length on carbon storage. The small uptake trend in the ocean models emerges because climate variability and change, and in particular increasing sea surface temperatures, tend to counteract the trend in ocean uptake driven by the increase in atmospheric CO_2. Large uncertainty remains in the magnitude and sign of modelled carbon trends in several regions, as well as regarding the influence of land use and land cover changes on regional trends.

1 Introduction

Soon after the first high-precision measurements of atmospheric CO_2 started in the late 1950s, it became clear that the global-mean CO_2 growth rate is substantially lower than expected if all anthropogenic CO_2 emissions remained in the atmosphere (e.g. Keeling et al., 1976). The search for this "missing" carbon and the identification of the processes driving carbon sinks has been one of the dominating questions for carbon cycle research in the past decades (e.g. Tans et al., 1990; Sarmiento and Gruber, 2002; and others). While much progress has been achieved (e.g. Prentice et al., 2001; Sabine et al., 2004; Denman et al., 2007; Le Quéré et al., 2009), and estimates have converged considerably (Sweeney et al., 2007; Khatiwala et al., 2013; Wanninkhof et al., 2013), the spatial attribution of recent sink rates for the ocean and land, and particularly their changes through time, remain uncertain. To balance the global carbon budget, the combined sinks by land and ocean must have increased over recent decades (Keeling et al., 1995; Canadell et al., 2007; Raupach et al., 2008; Sarmiento et al., 2010; Gloor et al., 2010; Ballantyne et al., 2012). Sarmiento et al. (2010) showed that some of the increasing sinks are driven by the ocean, but also identified an even more substantial increase in the net uptake by the land biosphere between the 1980s and the 1990s. This increase in the global land and ocean sink has been sustained to date (Ballantyne et al., 2012).

There are several studies on the trends in carbon exchanges at the regional level based on atmospheric CO_2 observations (top-down approach) (Angert et al., 2005; Buermann et al., 2007; Chevallier et al., 2010; Sarmiento et al., 2010) and changes in high-latitude greenness on land (Nemani et al., 2003; Myneni et al., 1997) and changes in sea surface temperature in the ocean (Park et al., 2010). Atmospheric CO_2-based top-down approaches provide large-scale constraints on the land and ocean surface processes, but they cannot unambiguously identify the underlying processes or the regions driving these changes. Bottom-up studies using dynamic global vegetation models (DGVMs) or ocean biogeochemical general circulation models (OBGCMs) mechanistically represent many of the key land (Prentice et al., 2007) and ocean processes (Le Quéré et al., 2005), and offer the opportunity to investigate how changes in the structure and functioning of land ecosystems and the ocean in response to changing environmental conditions affect biogeochemical cycles. Therefore DGVMs and OBGCMs potentially allow for a more comprehensive analysis of surface carbon trends and provide insight into possible mechanisms behind regional trends in the carbon cycle.

There is a growing literature on regional carbon budgets for different parts of the world (Ciais et al., 1995; Phillips et al., 1998; Fan et al., 1998; Pacala et al., 2001; Janssens et al., 2003; Stephens et al., 2007; Piao et al., 2009; Lewis et al., 2009a; Ciais et al., 2010; Pan et al., 2011; Tjiputra et al., 2010; Roy et al., 2011; Schuster et al., 2013; Lenton et al., 2013), using bottom-up (inventory, carbon cycle models) and top-down methodologies, although they typically cover different time intervals. To date, no globally consistent attribution has been attempted for regional sources and sinks of atmospheric CO_2. This paper attempts to fill this gap by combining top-down and bottom-up approaches discussed in the regional syntheses of the REgional

Carbon Cycle Assessment and Processes project (RECCAP; Canadell et al., 2013) and by using factorial simulations to elucidate the processes that drive trends in the sources and sinks of atmospheric CO_2.

This study has two major aims. The first of these is to estimate the regional trends in the carbon exchange over the period 1990–2009, associated with changes in climate and atmospheric CO_2 concentration, for three land regions (northern land, tropical land, and southern land) and seven ocean regions (North Pacific, equatorial Pacific, South Pacific, North Atlantic, equatorial/South Atlantic, Indian Ocean, and Southern Ocean) (Fig. 1). The second aim is to determine which factors and processes among those included in the models are driving the modelled/observed trends in the regional land/ocean to atmosphere net CO_2 fluxes. For the land models, those factors and processes included are the CO_2 fertilisation effect on productivity and storage, as well as climate effects on productivity, respiration, and climate-caused natural disturbances (see Table S1 in the Supplement for details represented in individual models). A particular focus is on the impacts of climate variation and change on land ecosystems at the regional scale, as extreme climate events occurred during the period of 1990–2009 across many regions of the world, including North America (southwestern USA, 2000–2002), Europe (2003), Amazonia (2005), and eastern Australia (2001–2008), raising considerable attention in the ecological community regarding the consequences of recent climate variability on ecosystem structure and function (Allen et al., 2010) and the carbon cycle (Ciais et al., 2005; Van der Molen et al., 2011; Reichstein et al., 2013).

This study addresses the changes in the magnitude of the global carbon sink but does not discuss the efficiency of the sinks, which is widely discussed elsewhere (Raupach et al., 2014; Gloor et al., 2010; Ciais et al., 2013). These DGVMs have been extensively evaluated against observation-based gross primary production (GPP), land to atmosphere net CO_2 flux, and CO_2 sensitivity of net primary production (NPP) compared to results from free-air CO_2 enrichment (FACE) experiments (Piao et al., 2013).

Consideration of land use and land cover change (LULCC) on regional trends is beyond the scope of the present study, and therefore models assume a fixed present-day land use throughout the simulation period. Thus our results presented should be interpreted with this caveat in mind. There are large uncertainties in the global LULCC flux and its change through time, with an estimated decrease from 1.6 ± 0.5 Pg C yr^{-1} (1990–1999) to 1.0 ± 0.5 Pg C yr^{-1} (2000–2009) (LeQuéré et al., 2013). In addition, the net land use (LU) flux for the period 1990–2009 will be influenced by earlier LULCC (i.e. legacy fluxes), confounding the analysis. The response of the large fluxes associated with net primary productivity and heterotrophic respiration to climate variability and CO_2 are the focus of this study. Other companion papers investigate ecosystem response to interannual and seasonal timescales (Piao et al., 2013), and the carbon balance

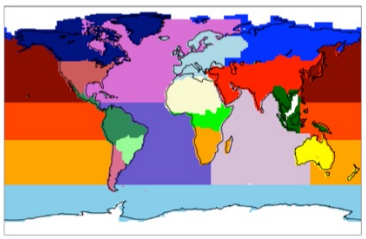

Figure 1. Land and ocean regions. The three land regions: northern land, tropical land, and southern land. Northern land comprises boreal North America (navy blue), Europe (light blue), boreal Asia (blue), temperate North America (pale red), and temperate Asia (red). Tropical land comprises tropical South American forests (sea green), northern Africa (sand), equatorial Africa (green), and tropical Asia (dark green). Southern land comprises South American savanna (pale green), temperate South America (violet), southern Africa (orange), and Australia and New Zealand (yellow). Ocean regions comprise North Pacific (dark red), equatorial Pacific (orange-red), South Pacific (orange), North Atlantic (orchid), equatorial/South Atlantic (slate blue), Indian Ocean (thistle), Southern Ocean (sky blue), and Arctic Ocean and Antarctica (white).

for individual land and ocean regions over the period 1990–2009 (see RECCAP special issue; Canadell et al., 2013, http://www.biogeosciences.net/special_issue107.html).

Trends and variability in the air–sea CO_2 fluxes simulated by the employed OBGCMs are driven by the increase in atmospheric CO_2 and by variability and change in ocean temperature, circulation, winds, and biology largely governed by climate variability. The air–sea CO_2 flux arising from the increase in atmospheric CO_2 is often referred to as the flux of anthropogenic CO_2, while the remainder, induced by changes in the natural cycling of carbon in the ocean–atmosphere system, is called the "natural" CO_2 component (e.g. Gruber et al., 2009). Although this conceptual separation has its limits (McNeill and Matear, 2013), it provides for a powerful way to understand how different forcings affect the net ocean sink.

DGVM results are compared with estimates of the residual land sink (RLS) and remote sensing products indicating trends of greening and browning in the northern region. Regional sources and sink trends are attributed to processes based on factorial simulations.

2 Methods

2.1 Dynamic global vegetation models

Following the studies of Le Quéré et al. (2009) and Sitch et al. (2008), a consortium of DGVM groups set up a project

to investigate further the spatial trends in land–atmosphere flux and agreed to perform a factorial set of DGVM simulations over the historical period, 1901–2009. These simulations have contributed to the RECCAP activity (Canadell et al., 2011, 2013). There are now a variety of DGVMs with origins in different research communities that typically contain alternative parameterisations and a diverse inclusion of processes (Prentice et al., 2007; Piao et al., 2013). DGVMs have emerged from the land surface modelling (LSM), forest ecology, global biogeography, and global biogeochemical modelling communities. Representative of these research strands are the following nine DGVMs, which are applied here: Hyland (Levy et al., 2004), JULES (Cox, 2001; Clark et al., 2011), LPJ (Sitch et al., 2003), LPJ-GUESS (Smith et al., 2001), NCAR-CLM4 (Thornton et al., 2007, 2009; Bonan and Levis, 2010; Lawrence et al., 2011), ORCHIDEE (Krinner et al., 2005), OCN (Zaehle and Friend, 2010), SDGVM (Woodward et al., 1995; Woodward and Lomas, 2004), and VEGAS (Zeng, 2003; Zeng et al., 2005). In this study we focus on two aspects of land surface modelling: the carbon and the hydrological cycles. In the case of land surface models coupled to GCMs, energy exchange between the land surface and atmosphere is also simulated.

2.2 Ocean biogeochemical general circulation models

A total of four different groups have conducted the factorial simulations over the analysis period with three-dimensional OBGCMs and submitted their results to the RECCAP archive. These are MICOM-HAMOCCv1 (BER) (Assmann et al., 2010), CCSM-WHOI using CCSM3.1 (BEC) (Doney et al., 2009a, b), CCSM-ETH using CCSM3.0 (ETH) (Graven et al., 2012), and NEMO-PlankTOM5 (UEA) (Buitenhuis et al., 2010). Details of the models are given in the respective publications cited and in Table 2. Not all model simulations are independent of each other, as several of them share components. BEC and ETH employ the same OBGCM, but differ in their spin-up and surface forcing. The employed models have relatively similar horizontal resolution of the order of 1 to 3° in longitude and latitude, i.e. none of them is eddy-permitting or eddy-resolving. The four ecosystem/biogeochemical models are also of comparable complexity, i.e. including explicit descriptions of at least one phytoplankton and zooplankton group, with some models considering up to three explicitly modelled groups for phytoplankton and two for zooplankton. All models use the same gas exchange parameterisation of Wanninkhof (1992), although with different parameters. In particular, the ETH model used a lower value for the gas exchange coefficient than originally used in the CCSM standard configuration, yielding a global-mean gas transfer velocity that is more than 25 % lower than those of the other models (Graven et al., 2012). This reduction reflects the mounting evidence based on radiocarbon analyses that the original global-mean gas transfer velocity of Broecker et al. (1985) was too high (Peacock, 2004; Sweeney et al., 2007; Müller et al., 2008).

2.3 Data sets

2.3.1 Land

Climate forcing is based on a merged product of Climate Research Unit (CRU) observed monthly 0.5° climatology (v3.0, 1901–2009; New et al., 2000) and the high-temporal-resolution NCEP reanalysis. The merged product has a 0.5° spatial and 6 h temporal resolution. A coarse-resolution 3.75° × 2.5° version at monthly timescales was also produced (see Table 1 for spatial resolution of individual DGVMs). Global atmospheric CO_2 was derived from ice core and NOAA monitoring station data, and provided at annual resolution over the period 1860–2009. As land use and land cover change was not simulated in these model experiments, models assume a constant land use (invariant agricultural coverage) throughout the simulation period. Atmospheric nitrogen deposition data for CLM4CN and OCN were sourced from Jean-Francois Lamarque (personal communication, 2012) and Dentener et al. (2006), respectively.

Gridded fields of leaf area index (LAI) are used in the evaluation of DGVM northern greening trends. These LAI data sets were based on remote sensing data and were generated from the AVHRR GIMMS NDVI3g product using an artificial neural network (ANN)-derived model (Zhu et al., 2013). The data set has a temporal resolution of 15 days over the period 1981–2011, and a spatial resolution of 1/12°.

2.3.2 Ocean

Unlike how the land models simulations were set up, no common climatic forcing data set was used for the ocean model simulations. In fact, some models provided several simulation results obtained with different climatic forcings. Models were forced by the NCEP climatic data (Kalnay et al., 1996) in their original form, or in the modified CORE (Common Ocean-ice Reference Experiments – Corrected Normal Year Forcing (CORE-CNYF; Large and Yeager, 2004)) form (Table 2).

2.3.3 Atmospheric inversion

Simulated trends in land to atmospheric net CO_2 flux are compared with those from version 11.2 of the CO_2 inversion product from the Monitoring Atmospheric Composition and Climate – Interim Implementation (MACC-II) service (http://copernicus-atmosphere.eu/). The horizontal resolution of the inversion is 3.75 × 2.5 square degrees (longitude × latitude), and weekly temporal resolution, with nighttime and daytime separated. The accuracy varies with the period and the location over the globe, depending on the density and the information content of the assimilated data, and usually decreases with increasing the resolution. Uncertainty

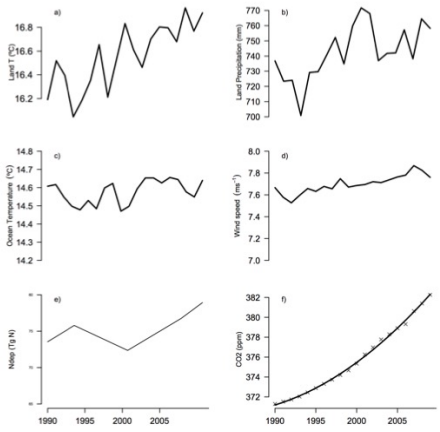

Figure 2. Global trends in environmental driving variables: **(a)** land temperature, **(b)** land precipitation, **(c)** ocean temperature, **(d)** wind speed, **(e)** N deposition, and **(f)** atmospheric [CO_2].

numbers at various scales can be found in Table 2 of Peylin et al. (2013). The inversion covers years 1979–2011, and a previous release has been documented by Chevallier et al. (2010). It uses a climatological prior without interannual variability, except for fossil fuel CO_2 emissions.

2.4 Experimental design

2.4.1 Land

Model spin-up consisted of recycling climate mean and variability from the early decades of the 20th century (1901–1920) with 1860 atmospheric CO_2 concentration of 287.14 ppm until carbon pools and fluxes were in steady state (zero mean annual land to atmospheric net CO_2 flux). The land models were then forced over the 1861–1900 transient simulation using varying CO_2 and continued recycling of climate as in the spin-up. The land models were then forced over the 1901–2009 period with changing CO_2, climate, and fixed present-day land use according to the following simulations:

- S_L1: changing CO_2 only (i.e. time-invariant present-day land use mask, fixed pre-industrial climate);
- S_L2: changing CO_2 and climate (i.e. time-invariant present-day land use mask).

For DGVMs including the N cycle, N deposition was a time-variant forcing in both simulations, such that the difference between S_L2 and S_L1 includes the synergistic effects of N deposition on CO_2 fertilisation (Zaehle et al., 2010).

Figure 2 shows the historical changes in climate, atmospheric CO_2 concentration, and nitrogen deposition over the period 1990–2009 used to force the DGVMs. A summary of DGVM characteristics is given in Table 1. A more detailed description of DGVM process representations is given in Table S1.

2.4.2 Ocean

The ocean models employed two different approaches for creating the initial conditions for the experiments. The first approach, followed by CCSM-ETH, CCSM-WHOI, and BER, involved first a multiple-century-long spin-up with climatological forcing and with atmospheric CO_2 held constant at its pre-industrial value, bringing these models very close to a climatological steady state for pre-industrial conditions (in some models $\sim$1750; in others $\sim$1850). In the second step, the models were then integrated forward in time through the historical period until 1948, with atmospheric CO_2 prescribed to follow the observed trend and a climatological forcing. The length of the spin-up varies from a few hundred years to several thousand years, resulting in differing global integrated drift fluxes, although their magnitudes are substantially smaller than 0.05 Pg C yr^{-1} with essentially no rate of change. The second approach, followed by NEMO-PlankTOM5 (UEA), was to initialise the model with reconstructed initial conditions in 1920, and then also run it forward in time until 1948 with prescribed atmospheric CO_2, repeating the daily forcing conditions of a single year (1980). The modelled export production was tuned to obtain an ocean CO_2 sink of 2.2 Pg C yr^{-1} in the 1990s. This second method offers the advantage that the model's carbon fields remain closer to the observations compared to the long spin-up approach, but it comes at the cost of generating a drift that affects the mean conditions and to a lesser extent the trend. Tests with the model runs of Le Quéré et al. (2010) suggest the drift in the mean CO_2 sink is about 0.5 Pg C yr^{-1} and the drift in the trend is about 0.005 Pg C yr^{-2} globally, and is largest in the Southern Ocean.

From $\sim$ 1950 onward, the models performed two separate simulations:

- S_O1: CO_2 only, i.e. atmospheric CO_2 increases, but models are forced with climatological atmospheric boundary conditions (referred to as ACO2 in the RECCAP archive);
- S_O2: CO_2 and climate, i.e. as S_O1, but models are forced with "realistic" year-to-year variability in atmospheric boundary conditions (ANTH).

In these runs, both S_O1 and S_O2 are affected by the same drift, and their differences thus remove the drift. The CCSM-based models performed an additional experiment to better separate between the fluxes of natural and anthropogenic CO_2:

Table 1. Characteristics of the nine dynamic global vegetation models.

Model name	Abbreviation	Spatial resolution	Land surface model	Full nitrogen cycle	River export flux	Fire simulation	Harvest/grazing flux	Source
Community Land Model 4CN	CLM4CN	$0.5^\circ \times 0.5^\circ$	Yes	Yes	No	Yes	No	Oleson et al. (2010); Lawrence et al. (2011)
Hyland	HYL	$3.75^\circ \times 2.5^\circ$	No	No	No	No	Yes	Friend et al. (1997); Levy et al. (2004)
Lund–Potsdam–Jena	LPJ	$0.5^\circ \times 0.5^\circ$	No	No	No	Yes	Yes	Sitch et al. (2003)
LPJ-GUESS	LPJ-GUESS	$0.5^\circ \times 0.5^\circ$	No	No	No	Yes	No	Smith et al. (2001)
ORCHIDEE-CN	OCN	$3.75^\circ \times 2.5^\circ$	Yes	Yes	No	No	Yes	Zaehle and Friend (2010); Zaehle et al. (2010)
ORCHIDEE	ORC	$0.5^\circ \times 0.5^\circ$	Yes	No	No	No	No	Krinner et al. (2005)
Sheffield-DGVM	SDGVM	$3.75^\circ \times 2.5^\circ$	No	No	Yes	Yes	No	Woodward et al. (1995)
TRIFFID	TRI	$3.75^\circ \times 2.5^\circ$	Yes	No	No	No	No	Cox (2001)
VEGAS	VEGAS	$0.5^\circ \times 0.5^\circ$	Yes	No	Yes	Yes	Yes	Zeng et al. (2005)

Table 2. Characteristics of the four ocean biogeochemical general circulation models (OBGCMs). All include NPZD-type ecosystem models and N, P, Si, and Fe nutrient components.

Model name	Abbreviation	Spatial resolution	Meteorological forcing	Gas transfer formulation	Years used	Source
MICOM-HAMOCCv1	BER	$2.4^\circ \times 0.8-2.4^\circ$	NCEP	Wanninkhof (1992)	1990 to 2009	Assmann et al. (2010)
CCSM-WHOI	BEC	$3.6^\circ \times 0.8-1.8^\circ$	NCEP	Wanninkhof (1992)	1990 to 2009	Doney et al. (2009a, b)
CCSM-ETH	ETH	$3.6^\circ \times 0.9 \times 1.9^\circ$	CORE	Wanninkhof (1992)	1990 to 2007	Graven et al. (2012)
NEMO-PlankTOM5	UEA	$2^\circ \times 0.5-2^\circ$	NCEP	Wanninkhof (1992)	1990 to 2009	Buitenhuis et al. (2010)

– S_O3: pre-industrial CO_2 and climate, i.e. atmospheric CO_2 is fixed at its pre-industrial level, but atmospheric boundary conditions vary as in S_O2 (PIND).

From these simulations, only the results from 1990 through to 2009 were analysed. Only the UEA and CCSM-WHOI models made results available for the S_O1 and S_O2 simulations for the entire analysis time. The results for the BER model for 2009 are incomplete, and the CCSM-ETH simulations extend only to 2007. In order to maintain a sufficiently large set of models, we decided to focus our analysis primarily on the 1990–2004 period, but occasionally also include the results through to 2009, with the important caveat that the latter are based only on two models.

2.5 Output variables

2.5.1 Land

In this study we focus primarily on the simulated carbon cycle variables, net NPP, RH (heterotrophic respiration), and LAI, a measure of vegetation greenness. The land to atmosphere net CO_2 flux is

$$\text{land to atmosphere net}\,CO_2\,\text{flux} = -\text{NBP}$$
$$= \text{RH} + \text{wildfire flux riverine C flux} + \text{harvest} - \text{NPP},$$

where we have adopted the atmospheric perspective with regard to the sign of the fluxes, i.e. negative numbers indicate a sink for atmospheric CO_2 and a negative trend indicates an increasing sink or a decreasing source.

DGVMs typically do not represent all these processes; a list for each individual DGVM is given in Table 1. DGVM results for simulation S_L2 are compared against the global RLS, calculated as the annual anthropogenic CO_2 emissions (fossil fuel, cement manufacture, and land use C flux) minus the annual CO_2 growth rate and model mean ocean C sink as given by Friedlingstein et al. (2010). The ocean uptake is from the same OGGCMs as the ones used here, and the land use C flux is based on a book-keeping approach from Houghton (2010). Note the RLS depends on a LULCC model of emissions (the one of Houghton). Strictly speaking, comparison of model land to atmosphere net CO_2 flux with RLS is therefore inconsistent because these models treat areas affected by LUC as pristine ecosystems, and these areas are generally associated with a high land carbon sinks. Simulated net carbon flux from S2 is therefore likely to overestimate the RLS sink, by construction.

The regional analysis will focus on three large land regions (Fig. 1), and within these regions, trends at a finer spatial resolution, from multi-grid-cell to the sub-region, are analysed.

The comparison of DGVM simulated trends in the northern growing season against satellite-derived NDVI (normalised difference vegetation index) observations was based on eight models (JULES, LPJ, LPJ-GUESS, NCAR-CLM4, ORCHIDEE, OCN, SDGVM, VEGAS), which provided LAI outputs. The means and trends in the onset, end, and length of growing season were computed. Growing season variables were calculated using the methodology of Murray-Tortarolo et al. (2013). Leaf onset is defined as the day when LAI begins to increase above a critical threshold (CT), defined as

$$\text{CT} = \text{LAI}_{\text{min}} + 0.2 \cdot (\text{LAI}_{\text{max}} - \text{LAI}_{\text{min}}),$$

where LAI_{min} and LAI_{max} represent the minimum and maximum LAI over the annual cycle. Similarly, leaf senescence, or offset, or end of growing season, is defined as the day when LAI decreases below the CT. The length of the growing season in days is calculated as the end minus the onset. This calculation was made for each grid cell above 30° N (i.e. northern extratropics) from the models and the satellite data. In addition, any grid cell where LAI varied by less than 0.5 over the annual cycle from the satellite data was considered to be predominantly evergreen (e.g. boreal forest), and thus excluded from the analysis. We also masked out regions where LAI decreases in the summer (drought deciduous vegetation). In addition, when the growing season spans over the end of year (e.g. Mediterranean and some pixels particularly on the southern margin of the domain), we include the first 3 months of the second year in our analysis. Means and trends were calculated using a linear model over the period 1990–2009.

2.5.2 Ocean

The modelling groups provided output on a monthly basis for the years 1990 through to 2004 and 2009 at two levels of priority. Tier-one data included the surface ocean fields of the air–sea CO_2 flux, oceanic pCO_2, dissolved inorganic carbon (DIC), alkalinity (Alk), temperature (T), salinity (S), and mixed layer depth. The second-tier data included the biological export at 100 m, the vertically integrated net primary production, and the surface chlorophyll a concentration. Some models also supplied three-dimensional climatological fields of DIC, Alk, T, and S.

To determine the different factors contributing to the modelled trends and variations, we undertook two (linear) separations:

- The contribution of climate variability and change on the ocean carbon cycle: $X\_\mathrm{var} = X(\mathrm{S\_O2}) - X(\mathrm{S\_O1})$, X is any variable or flux, where the expression in parentheses represents the results of the corresponding simulation, and X_var represents the impact of climate change and variability on the ocean carbon cycle.
- The contribution of anthropogenic CO_2: $X\_\mathrm{ant} = X(\mathrm{S\_O2}) - X(\mathrm{S\_O3})$.

For each of the integrations, but particularly for the changing CO_2 and climate simulation S_O2, we analysed the factors contributing to the temporal change in the air–sea CO_2 flux F by a linear Taylor expansion (see e.g. Lovenduski et al., 2007 and Doney et al., 2009a):

$$\Delta F = \partial F/\partial \mathrm{ws} \cdot \Delta \mathrm{ws} + \partial F/\partial T \cdot \Delta T + \partial F/\partial \mathrm{ice} \cdot \Delta \mathrm{ice} + \partial F/\partial \mathrm{sDIC} \cdot \Delta \mathrm{sDIC} + \partial F/\partial \mathrm{sAlk} \cdot \Delta \mathrm{sAlk} + \partial F/\partial \mathrm{FS} \cdot \Delta S,$$

where ws is the wind speed, ice is the sea-ice fraction, sDIC and sAlk are the salinity normalised DIC and Alk concentrations, and $\partial F/\partial \mathrm{FS}$ is the change in the air–sea CO_2 flux in response to freshwater fluxes. This latter term includes not only the sensitivity of oceanic pCO_2 to changes in salinity but also the dilution effects of freshwater on DIC and Alk (see Doney et al., 2009a, for details). The partial derivatives were computed directly from the model equations for the mean conditions in each region. The changes in the driving components were derived from the trend computed via a linear regression of the model results and then multiplied by the length of the time series.

3 Results

3.1 Global Trends

3.1.1 Land

The ensemble mean global land to atmosphere net carbon dioxide flux from S_L2 is $-2.38 \pm 0.72\,\mathrm{Pg\,C\,yr^{-1}}$ over the period 1990–2009 ($P = 0.04$, where P is the probability of a trend statistically indistinguishable from zero; a significance level of 0.05 is selected) (Fig. 3, Fig. S1 in the Supplement, Table 3). The numbers behind ± signs are the 1 standard deviation of 20-year means for nine DGVMs. This compares to the global RLS of $-2.45 \pm 1.17\,\mathrm{Pg\,C\,yr^{-1}}$, inferred from the global carbon budget by Friedlingstein et al. (2010) over the same period. All DGVMs agree on an increasing land sink with a net flux trend over this period ranging between -0.02 and $-0.11\,\mathrm{Pg\,C\,yr^{-2}}$, corresponding to the OCN and Hyland DGVMs, respectively (Table 3). DGVMs simulate an increase in the land C sink with an ensemble mean trend of $-0.06 \pm 0.03\,\mathrm{Pg\,C\,yr^{-2}}$ ($P < 0.05$) over the period 1990–2009 (Table 3) in response to changes in climate and atmospheric CO_2 content. The two DGVMs with a fully coupled carbon and nitrogen cycle (CN) also simulate an increase in the land sink, at -0.02 ($P = 0.6$) for OCN and $-0.05\,\mathrm{Pg\,C\,yr^{-2}}$ ($P = 0.06$) for CLM4CN. DGVMs suggest the increase in global land sink between 1990 and 2009 is driven by increases in simulated global NPP (Fig. 3).

DGVMs simulate an ensemble mean global NPP of $62.9 \pm 8.73\,\mathrm{Pg\,C\,yr^{-1}}$ over the period 1990–2009 (Table 3). All DGVMs simulate an increase in NPP over this period, with an ensemble mean DGVM trend in NPP of $0.22 \pm 0.08\,\mathrm{Pg\,C\,yr^{-2}}$ ($P = 0.00$) (Table 3). Models with a higher NPP trend also produce a higher land to atmosphere net CO_2 flux trend (Fig. S2 in the Supplement). The ensemble mean NPP trend of $0.22 \pm 0.08\,\mathrm{Pg\,C\,yr^{-2}}$ ($P < 0.01$) from simulation S_L2 (CO_2 and climate forcing) contrasts with an ensemble trend of $0.19 \pm 0.08\,\mathrm{Pg\,C\,yr^{-2}}$ ($P < 0.01$) and $0.03 \pm 0.05\,\mathrm{Pg\,C\,yr^{-2}}$ ($P = 0.24$) over the same period for the S_L1 (CO_2 only) and S_L2–S_L1 (the climate effect), respectively (Tables S2, S3 in the Supplement). These results suggest that the simulated increase in global NPP is mainly in response to increasing atmospheric CO_2 (direct

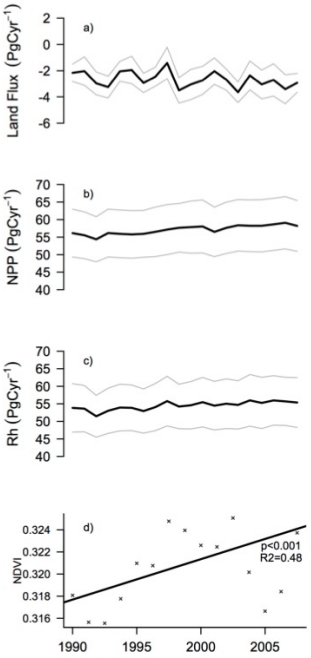

Figure 3. Global trends in ensemble land model responses. **(a)** DGVM mean model land to atmosphere net CO_2 flux and standard deviation (grey lines); (**b**) component fluxes, NPP; and (**c**) RH (= RH + wildfire + riverine C flux); and (**d**) remotely sensed trends in annual mean NDVI (crosses), a measure of vegetation greenness, and a linear regression through the data points (bold line).

CO_2 fertilisation of photosynthesis, in addition to the indirect benefits from an improved water balance in water-limited ecosystems due to the physiological effects of CO_2 on water use efficiency). VEGAS, CLM4CN, and OCN simulate the smallest positive trends in NPP among the DGVMs in response to elevated CO_2 forcing (Table S2). This suggests that the potential CO_2 fertilisation effect may be already strongly limited by present-day nitrogen availability in some ecosystems (Vitousek and Howarth, 1991). There is more uncertainty among models on the impact of climate changes on global NPP, with only two models simulating a significant positive trend (Table S3).

DGVMs simulate an ensemble mean global RH of $57.5 \pm 9.8\,\mathrm{Pg\,C\,yr^{-1}}$ over the period 1990–2009 (Table 3). All DGVMs simulate an increase in RH for S_L2 (CO_2 and climate), with an ensemble mean trend of

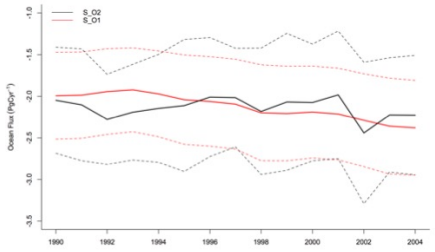

Figure 4. Global trends in ensemble ocean model fluxes. Black line: results from simulation S_O2 with variable "climate" and increasing CO_2. Red line: results from simulation S_O1 with constant "climate" and increasing CO_2. The dashed grey and dashed red lines indicate the ± uncertainty bands given by the four models that contribute to the ensemble mean.

$0.16 \pm 0.05\,\mathrm{Pg\,C\,yr^{-2}}$ ($P < 0.01$) over the period 1990–2009 (Table 3). This is lower than the trend in global NPP, resulting in a trend towards increasing net land carbon uptake. This is unsurprising as there is a lagged response in increases in RH relative to NPP, reflecting the turnover time of the newly incorporated plant material. The ensemble mean trend in RH is $0.12 \pm 0.06\,\mathrm{Pg\,C\,yr^{-2}}$ ($P < 0.01$) and $0.04 \pm 0.02\,\mathrm{Pg\,C\,yr^{-2}}$ ($P = 0.09$) over the same period for the S_L1 (CO_2 only) and S_L2–S_L1 (the climate effect), respectively (Tables S2, S3). This implies the dominant effect on RH is increased substrate for microbial respiration, with the additional litter input into soils, as a consequence of enhanced NPP, rather than enhanced rates of microbial decomposition with rising temperatures. Nevertheless, the simulated mean residence time (MRT = soil carbon / RH) of soil organic matter decreases, in response to warming, which is especially pronounced in high-latitude regions (Fig. S3 in the Supplement). The difference in land–atmosphere flux trend between the CN models OCN ($-0.02\,\mathrm{Pg\,C\,yr^{-2}}$) and CLM4CN ($-0.05\,\mathrm{Pg\,C\,yr^{-2}}$) is largely due their difference in RH trends at 0.14 and $0.11\,\mathrm{Pg\,C\,yr^{-2}}$, respectively, rather than differential responses of simulated NPP to elevated CO_2 (Table 3).

Only four DGVMs simulated wildfire fluxes (CLM4CN, LPJ, LPJ-GUESS, SDGVM). No significant trends in the global wildfire flux were reported by any of the DGVMs.

3.1.2 Ocean

The global ocean is simulated to have acted as a very substantial sink for atmospheric CO_2 but one that has increased only slightly over the last two decades (see also discussion in Wanninkhof et al., 2013). The mean ocean sink in the four models (CCSM-ETH, CCSM-WHOI, UEA, and BER) increased from $\sim -2.0\,\mathrm{Pg\,C\,yr^{-1}}$ in the early 1990s to

$\sim -2.1\,\mathrm{Pg\,C\,yr^{-1}}$ during the first 5 years of the 21st century (Fig. 4).

We separate the mean and variable components by using our factorial experiments, i.e. by using S_O1 results to identify the ocean uptake in the absence of climate variability and change, and the difference between S_O2 and S_O1 as measure of the impact of climate change. This separation reveals that, in the absence of climate variability and change, the global ocean uptake would have increased from about $-1.98 \pm 0.04\,\mathrm{Pg\,C\,yr^{-1}}$ for the 1990–1994 period to $-2.3 \pm 0.09\,\mathrm{Pg\,C\,yr^{-1}}$ for 2000–2004 (for the two models that provided S_O1 results up to 2009 (CCSM-WHOI and UEA), the uptake flux would have increased from -1.99 to $-2.56\,\mathrm{Pg\,C\,yr^{-1}}$ for 2005–2009). This global net uptake flux and its substantial trend in time ($-0.03\,\mathrm{Pg\,C\,yr^{-2}}$ for 1990–2004, and $-0.04\,\mathrm{Pg\,C\,yr^{-2}}$ for 1990–2010) is entirely driven by the increase in atmospheric CO_2 and is – integrated globally – numerically equivalent to the ocean uptake flux of anthropogenic CO_2. Climate variability and change modified these fluxes, and particularly the trend in these models. The four models suggest an enhancement of the uptake in the early 1990s (1990–1994) of about $-0.2\,\mathrm{Pg\,C\,yr^{-1}}$, turning into a reduction of the uptake in the subsequent period (1995–1999), followed by a further reduction in the 2000–2004 period of $\sim +0.1\,\mathrm{Pg\,C\,yr^{-1}}$. This trend toward reduced uptake in response to climate variability and change of $+0.03\,\mathrm{Pg\,C\,yr^{-2}}$ nearly completely compensates for the anthropogenic CO_2 driven increase in uptake, causing the overall uptake of CO_2 to have a nearly flat trend over the 1990–2004 period of $<0.01\,\mathrm{Pg\,C\,yr^{-2}}$ The same tendencies are found for the two models that extend over the entire 1990–2009 period: in these models, climate change and variability reduces the CO_2-driven trend of $-0.04\,\mathrm{Pg\,C\,yr^{-2}}$ by more than $+0.02\,\mathrm{Pg\,C\,yr^{-2}}$, to around $-0.02\,\mathrm{Pg\,C\,yr^{-2}}$.

With consideration of the different factors affecting the ocean carbon sink following our Taylor expansion, we find increasing sea surface temperature to be a globally important driver for the positive trends (reduced sinks) induced by climate change and variability. Over the 1990–2004 period, the surface ocean warmed, on average, by $0.004\,^{\circ}\mathrm{C\,yr^{-1}}$ ($0.005\,^{\circ}\mathrm{C\,yr^{-1}}$ from 1990 through to 2009). Isochemically, this leads to an increase in the oceanic pCO_2 of $\sim 0.06\,\mu\mathrm{atm\,yr^{-1}}$, which appears small. However, it needs to be compared with the trend in the global-mean air–sea pCO_2 difference of about $\sim 0.1\,\mu\mathrm{atm\,yr^{-1}}$ that is required in order to generate a trend in the ocean uptake of $-0.03\,\mathrm{Pg\,C\,yr^{-2}}$ (see e.g. Matsumoto and Gruber, 2005; Sarmiento and Gruber, 2006). The overall sink is therefore largely a consequence of the increase in atmospheric CO_2 (i.e. it mostly corresponds to the uptake flux of anthropogenic CO_2), but it includes a substantial perturbation flux stemming from the impact of climate variability and change on the ocean carbon cycle.

3.2 Regional trends

3.2.1 Land

Northern land

All DGVMs agree on a land C sink over the northern land region, with a mean land–atmosphere flux of $-1.03 \pm 0.30\,\mathrm{Pg\,C\,yr^{-1}}$ over the period 1990–2009 (Fig. S4 in the Supplement, Table 3). The ensemble mean land–atmosphere flux trend is near zero for this region between 1990 and 2009 (Fig. S5 in the Supplement). Of particular interest are sub-regions with a simulated positive land–atmosphere flux trend (Fig. 5), implying a diminishing sink of atmospheric CO_2 or an increasing source of CO_2 to the atmosphere. At least six models out of nine agree on a decreasing regional land sink across some areas in temperate North America, eastern Europe, northeastern China, and Mongolia (Fig. 5). These largely correspond to regions with negative trends in precipitation (Fig. 6).

Over the northern region, which covers almost 50 % of the land surface, DGVMs simulate an ensemble mean NPP of $24.1 \pm 4.48\,\mathrm{Pg\,C\,yr^{-1}}$, which represents almost 40 % of the global total (Table 3). All DGVMs simulate an increase in northern NPP over this period, with a trend in NPP of $0.06 \pm 0.02\,\mathrm{Pg\,C\,yr^{-2}}$ ($P < 0.01$) (Table 3). However, enhanced productivity in the northern land region accounts for only around 29 % of the simulated global trend in NPP. The ensemble mean NPP trend of $0.06 \pm 0.02\,\mathrm{Pg\,C\,yr^{-2}}$ ($P < 0.01$) from simulation S2 (CO_2 and climate forcing) compares to a trend of $0.07 \pm 0.03\,\mathrm{Pg\,C\,yr^{-2}}$ ($P < 0.01$) and $-0.00 \pm 0.04\,\mathrm{Pg\,C\,yr^{-2}}$ ($P = 0.85$) for the S_L1 (CO_2 only) and S_L2–S_L1 (the climate effect), respectively (Tables S2, S3). All DGVMs simulate a positive trend in NPP in response to elevated CO_2 across the northern land region, and trends are all significant at the 95 % confidence level with the exception of CLM4CN ($P = 0.21$).

Large areas in temperate North America and Asia experienced warming combined with reductions in precipitation over the period 1990–2009 (Fig. 5). Indeed, although DGVMs simulate larger mean NPP in temperate compared to boreal regions (Table S5 in the Supplement), they simulate significant positive trends in boreal North America and boreal Asia, whereas trends in both temperate North America and Asia are smaller and not significant at the 95 % confidence level (Table S5).

In response to warming, models simulate an earlier onset (ensemble mean model trend $= -0.078 \pm 0.131\,\mathrm{days\,yr^{-1}}$) and delayed termination of the growing season ($0.217 \pm 0.097\,\mathrm{days\,yr^{-1}}$) based on LAI, and thus a trend towards a longer growing season in the northern extratropics ($0.295 \pm 0.228\,\mathrm{days\,yr^{-1}}$) (Fig. 7). This is in broad agreement with observed greening trends (Zhu et al., 2013; Murray-Tortarolo et al., 2013): onset $= -0.11\,\mathrm{days\,yr^{-1}}$, offset $= 0.252\,\mathrm{days\,yr^{-1}}$, and

Table 3. Mean and trends in NPP, RH, and land–atmosphere flux as simulated by individual DGVMs and the ensemble mean.

MODEL	NPP ($Pg\,C\,yr^{-1}$)	Trend ($Pg\,C\,yr^{-2}$)	P value	RH ($Pg\,C\,yr^{-1}$)	Trend ($Pg\,C\,yr^{-2}$)	P value	Land–atm CO_2 flux ($Pg\,C\,yr^{-1}$)	Trend ($Pg\,C\,yr^{-1}$)	P value
Global_Land									
CLM4CN	51.508	0.148	0.000	47.668	0.106	0.000	−1.459	−0.052	0.059
HYLAND	73.422	0.319	0.000	68.835	0.203	0.000	−3.466	−0.109	0.000
LPJ	59.306	0.216	0.000	47.612	0.117	0.000	−2.251	−0.068	0.061
LPJ-GUESS	62.506	0.174	0.000	55.448	0.145	0.000	−1.802	−0.043	0.346
OCN	53.941	0.155	0.000	50.611	0.135	0.000	−2.272	−0.015	0.568
ORCHIDEE	75.516	0.293	0.000	72.037	0.208	0.000	−3.479	−0.086	0.046
SDGVM	60.965	0.240	0.000	53.778	0.190	0.000	−2.127	−0.044	0.170
TRIFFID	71.929	0.305	0.000	69.167	0.244	0.000	−2.762	−0.061	0.265
VEGAS	57.308	0.113	0.006	51.930	0.092	0.000	−1.783	−0.018	0.551
Ensemble	**62.934**	**0.218**	**0.000**	**57.454**	**0.160**	**0.000**	**−2.378**	**−0.055**	**0.048**
SD	**8.729**	**0.076**		**9.791**	**0.053**		**0.721**	**0.030**	
Northern_Land									
CLM4CN	17.523	0.043	0.003	16.215	0.036	0.000	−0.670	−0.007	0.612
HYLAND	19.139	0.098	0.000	17.591	0.080	0.000	−0.876	−0.014	0.311
LPJ	24.566	0.079	0.001	19.578	0.062	0.006	−1.168	−0.006	0.735
LPJ-GUESS	28.484	0.039	0.085	25.883	0.067	0.009	−0.634	0.023	0.521
OCN	21.008	0.044	0.035	19.264	0.047	0.008	−1.117	0.007	0.632
ORCHIDEE	30.337	0.070	0.007	29.112	0.063	0.000	−1.226	−0.006	0.740
SDGVM	25.144	0.063	0.006	22.598	0.065	0.006	−0.828	0.004	0.762
TRIFFID	28.476	0.088	0.009	27.006	0.103	0.001	−1.470	0.016	0.455
VEGAS	21.895	0.048	0.012	18.914	0.043	0.001	−1.322	−0.000	0.968
Ensemble	**24.064**	**0.063**	**0.001**	**21.796**	**0.063**	**0.001**	**−1.034**	**0.002**	**0.865**
SD	**4.484**	**0.022**		**4.562**	**0.020**		**0.295**	**0.012**	
Tropical_Land									
CLM4CN	26.400	0.090	0.000	24.464	0.058	0.000	−0.692	−0.039	0.110
HYLAND	34.489	0.112	0.000	32.695	0.067	0.000	−1.560	−0.044	0.001
LPJ	25.830	0.100	0.001	21.224	0.035	0.001	−0.817	−0.049	0.031
LPJ-GUESS	21.922	0.078	0.000	19.332	0.051	0.000	−0.785	−0.036	0.038
OCN	22.750	0.084	0.000	21.476	0.065	0.000	−0.982	−0.017	
ORCHIDEE	31.313	0.151	0.000	29.640	0.108	0.000	−1.673	−0.043	0.084
SDGVM	23.505	0.118	0.000	20.677	0.075	0.000	−0.984	−0.038	0.030
TRIFFID	29.801	0.141	0.000	28.925	0.096	0.000	−0.876	−0.045	0.218
VEGAS	23.472	0.041	0.061	21.994	0.033	0.004	−0.278	−0.010	0.527
Ensemble	**26.609**	**0.102**	**0.000**	**24.492**	**0.065**	**0.000**	**−0.961**	**−0.036**	**0.045**
SD	**4.350**	**0.034**		**4.752**	**0.025**		**0.428**	**0.013**	
Southern_Land									
CLM4CN	7.617	0.014	0.187	7.017	0.011	0.036	−0.098	−0.005	0.719
HYLAND	19.875	0.109	0.000	18.623	0.056	0.000	−1.035	−0.051	0.000
LPJ	8.940	0.037	0.074	6.833	0.021	0.004	−0.267	−0.013	0.355
LPJ-GUESS	12.124	0.058	0.003	10.255	0.026	0.001	−0.385	−0.031	0.192
OCN	10.222	0.027	0.165	9.909	0.023	0.053	−0.174	−0.004	0.744
ORCHIDEE	13.884	0.073	0.002	13.304	0.037	0.000	−0.581	−0.036	0.027
SDGVM	12.358	0.059	0.034	10.539	0.050	0.000	−0.317	−0.010	0.701
TRIFFID	13.707	0.077	0.020	13.290	0.045	0.000	−0.417	−0.032	0.269
VEGAS	11.971	0.024	0.382	11.049	0.016	0.140	−0.182	−0.009	0.656
Ensemble	**12.300**	**0.053**	**0.011**	**11.202**	**0.032**	**0.000**	**−0.384**	**−0.021**	**0.196**
SD	**3.528**	**0.031**		**3.597**	**0.016**		**0.285**	**0.017**	

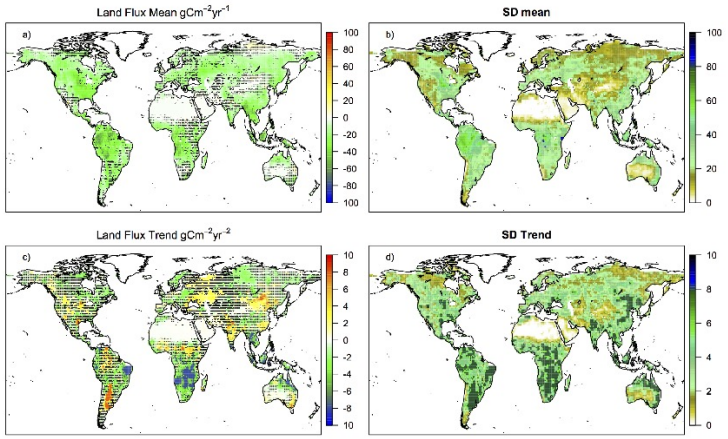

Figure 5. **(a)** Average land to atmosphere net CO_2 flux over the period 1990–2009 for the ensemble mean and model disagreement, with stippling representing agreement for < 66 % of DGVMs , and **(b)** standard deviation across DGVMs. **(c)** The trend in land to atmosphere net CO_2 flux across the ensemble, and model disagreement, with stippling representing agreement of < 66 % of the DGVMs , and **(d)** the standard deviation of the trend.

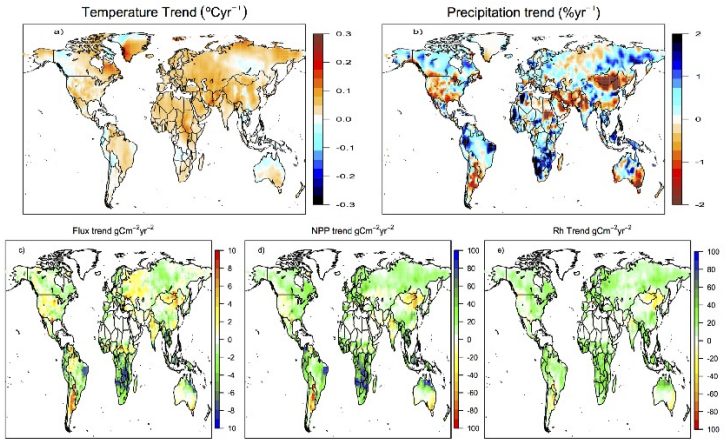

Figure 6. Trends in land climate drivers and process responses. **(a)** Trend in temperature ($^{\circ}C\,yr^{-1}$), **(b)** trend in precipitation (% yr^{-1}), **(c)** trend in land to atmosphere net CO_2 flux ($gC\,m^{-2}\,yr^{-2}$), **(d)** trend in NPP ($gC\,m^{-2}\,yr^{-2}$), and **(e)** trend in RH (= RH + wildfire + Riverine C flux) ($gC\,m^{-2}\,yr^{-2}$).

growing season length $= 0.361$ days yr^{-1}. There is less agreement among models on reproducing the observed browning trends in some regions of the boreal forest.

DGVMs simulate an ensemble mean RH of 21.8 ± 4.6 Pg C yr^{-1} across the northern land region (Table 3). All DGVMs simulate an increase in northern RH over the period 1990–2009, with a significant trend in RH of 0.063 ± 0.02 Pg C yr^{-1} ($P < 0.01$) (Table 3). DGVMs simulate larger mean RH in temperate compared to boreal regions, yet smaller positive trends for Asia (Table S6 in the Supplement). This is because of relatively smaller increases in substrate (i.e. NPP) in temperate regions and greater warming in boreal regions stimulating microbial decomposition, reducing mean residence time of carbon in soils (MRT = soil carbon / RH; see Fig. S3).

No significant trends in the wildfire flux were reported by any of the DGVMs for the northern land region. However, DGVMs agree on simulating a small negative trend in wildfire flux across boreal North America and tundra.

Tropical land

All DGVMs simulate an increasing land C sink over recent decades, in response to changes in climate and atmospheric CO_2 concentration over the tropical land region, with an ensemble mean land–atmosphere flux of -0.96 ± 0.43 Pg C yr^{-1} (Table 3, Fig. S4) and trend of -0.04 ± 0.01 Pg C yr^{-2} ($P = 0.05$), or -0.88 ± 0.33 g C m^{-2} yr^{-2} on an area basis (Table 3, Table S4 in the Supplement Fig. S5). This represents 65 % of the increase in global land sink over the last two decades across the tropical land, which covers 27 % of the land surface (Table S4). DGVMs simulate significant negative trends (i.e. increasing sinks) across tropical Asia and equatorial Africa (Table S4).

DGVMs simulate an ensemble mean NPP of 26.6 ± 4.35 Pg C yr^{-1} averaged over the tropical region, representing 42 % of the global total (Table 3). All DGVMs simulate a significant increase in tropical NPP over this period, with an ensemble mean trend in NPP of 0.10 ± 0.03 Pg C yr^{-2} ($P = 0.00$) for S_L2 (Table 3). This compares to a trend of 0.09 ± 0.03 Pg C yr^{-2} ($P < 0.01$) and 0.02 ± 0.02 Pg C yr^{-2} ($P = 0.33$) over the same period for the S_L1 (CO_2 only) and S_L2–S_L1 (the climate effect), respectively (Tables S2, S3). Again, the simulated trend in NPP is dominated by the simulated response of ecosystems to elevated atmospheric CO_2 content. DGVMs simulate positive NPP trends across tropical South American forests, tropical Asia, equatorial Africa, and North African savanna (Table S5). Nevertheless there are some areas within tropical South America and North African savanna regions with negative trends in NPP (Fig. 6).

All DGVMs simulate an increase in RH over the period 1990–2009, with an ensemble mean RH of 24.49 ± 4.75 Pg C yr^{-1} (Table 3) and trend of 0.065 ± 0.025 Pg C yr^{-2} ($P < 0.01$). This can be largely attributed to the response of ecosystems to elevated CO_2 (Table S2).

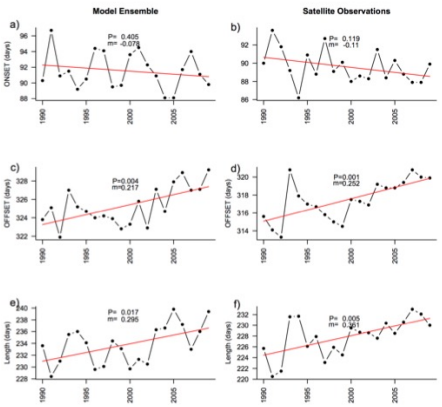

Figure 7. Ensemble-mean trends in the onset **(a, b)**, offset **(c, d)**, and length of growing season in days **(e, f)** for the ensemble mean (left) compared with satellite-derived estimates (right).

No significant trends in the wildfire flux were reported by any of the DGVMs for the tropical land region. However, DGVMs agree on simulating a negative trend in wildfire flux across equatorial Africa and tropical Asia.

Southern land

All DGVMs agree on a net land sink over the southern land during the last two decades, with an ensemble mean land–atmosphere flux of -0.38 ± 0.29 Pg C yr^{-1} (Table 3, Fig. S4). Although all DGVMs simulate an increase in the land sink over the southern extratropics, with an ensemble mean land–atmosphere trend of -0.02 ± 0.02 Pg C yr^{-2} ($P = 0.20$) (Fig. S5) or -0.58 ± 0.45 g C m^{-2} yr^{-2} on an area basis, only trends for HYL and ORC are significant at the 95 % confidence level (Table 3). Ensemble mean trends are significant for temperate South American and southern African regions at 0.005 ± 0.005 Pg C yr^{-2} ($P = 0.05$) and -0.022 ± 0.011 Pg C yr^{-2} ($P = 0.01$), respectively (Table S4). For southern Africa, all DGVMs simulate an increase in the land sink in response to climate variability and change over this period (five out of nine are significant at the 90 % confidence level) (Table S7 in the Supplement, Fig. 6). In contrast, the simulated decrease in land sink for temperate South America is associated with a decrease in precipitation over 1990–2009 (Table S8 in the Supplement).

DGVMs simulate an ensemble mean NPP of 12.3 ± 3.53 Pg C yr^{-1} over the southern extratropics,

which represents ∼20 % of the global total (Table 3) across 24 % of the land surface. All DGVMs simulate an increase in NPP over this period, with a significant ensemble mean trend of $0.05 \pm 0.03\,\mathrm{Pg\,C\,yr^{-2}}$ ($P = 0.01$), i.e. the southern land region accounts for around 25 % of the simulated global trend in NPP. Southern Africa is the only southern sub-region with a significant trend in NPP of $0.041 \pm 0.018\,\mathrm{Pg\,C\,yr^{-2}}$ ($P < 0.01$) (Table S5), due to a positive response of plant production to both CO_2 and climate, and is likely in response to increases in precipitation over the last two decades (Table S7, Fig. 5).

DGVMs simulate an ensemble mean RH of $11.20 \pm 3.60\,\mathrm{Pg\,C\,yr^{-1}}$ over the southern land region (Table 3). All DGVMs simulate an increase in RH over the period 1990–2009, with a significant trend in the ensemble mean RH of $0.03 \pm 0.02\,\mathrm{Pg\,C\,yr^{-2}}$ ($P < 0.01$). This is only partly explained by the response of ecosystems to elevated CO_2; over southern Africa the ensemble mean trend in RH from S_L1 is $0.01 \pm 0.01\,\mathrm{Pg\,C\,yr^{-2}}$ ($P < 0.01$), and a climate-induced positive trend in RH of $0.01 \pm 0.00\,\mathrm{Pg\,C\,yr^{-1}}$ ($P < 0.01$) (Table S2, S7).

No significant trends in the wildfire flux were reported by any of the DGVMs for the southern land region. However DGVMs agree on simulating a negative trend in wildfire flux across southern Africa.

In summary, the globally increasing trend in land carbon sink is about two-thirds due to tropical ecosystems and one-third due to the southern land region, with zero contribution from northern land. This partitioning in trend is quite different from the mean carbon sink fluxes themselves, which is more like 43 : 41 : 16 (northern : tropical : southern).

Qualitative change in processes

A qualitative assessment of the differential responses of the underlying land processes to changes in environmental conditions, and their contribution to the sink–source land–atmosphere flux trends is shown in Fig. 8. Many regions are simulated to have a negative land–atmosphere flux trend, with increases in NPP leading increases in RH. However there are locations with positive trends over the period 1990–2009, i.e. red colours in Fig. 8. In some regions models simulate a positive trend in NPP but an even larger positive trend in RH (eastern Europe, southeastern USA, Amazonia, southern China, North America tundra). Warming is likely to enhance both NPP and RH in high-latitude ecosystems, but primarily RH in low latitudes. Reduced precipitation may partially or fully offset the benefits of elevated atmospheric CO_2 abundance on NPP, and the response of RH to changes in precipitation is not obvious, as this is influenced by the initial soil moisture status. This is because microbial activity increases with increasing soil moisture at low moisture levels, before reaching a maximum activity, and then begins to decline as water completely fills the soil pore spaces and oxygen becomes more limiting to respiration. Locations in the western USA, southern Asia, northern boreal China, southeastern South America, and western and southern Australia are simulated to have negative NPP trends over the last two decades, as a result of reduced rainfall, and there is a less negative trend in RH, possibly due to a reduction in microbial respiration rates with increased soil dryness. The warming and drying in central Asia (northeastern China and Mongolia) and southern Australia is simulated to reduce the rate of microbial decomposition in these regions (Fig. S3), which partly opposes the NPP-driven lagged decrease in RH. The source trend in eastern Europe is simulated as a combination of a negative trend in NPP, as a result of a combination of elevated temperatures and reduced precipitation (i.e. soil drying), and a positive trend in RH driven by increasing temperature, despite reduced plant litter input.

.2 Ocean

Regional fluxes

The large-scale distribution of the modelled mean surface fluxes consists of strong outgassing in the tropical regions, especially in the Pacific, and broad regions of uptake in the mid-latitudes, with a few regions in the high latitudes of particularly high uptake, such as the North Atlantic (Fig. 9). This pattern is largely the result of the exchange flux of natural CO_2 that balances globally to a near-zero flux, but exhibits regionally strong variations (Gruber et al., 2009). Superimposed on this natural CO_2 flux pattern is the uptake of anthropogenic CO_2, which is taken up everywhere, but with substantial regional variation. Large anthropogenic CO_2 uptake fluxes occur in the regions of surface ocean divergence, such as the equatorial Pacific and particularly the Southern Ocean (Sarmiento et al., 1992; Gloor et al., 2003; Mikaloff Fletcher et al., 2006). This is a result of the divergence causing waters to upwell to the surface which have not been exposed to the atmosphere for a while, thereby permitting them to take up a substantial amount of anthropogenic CO_2. This reduces the outgassing that typically characterises these regions as a result of these upwelling waters also bringing with them high carbon loads from the remineralisation of organic matter.

Over the analysis period, the air–sea CO_2 fluxes exhibit only a remarkably small trend in most places, with some regions increasing in uptake, while others show a positive flux anomaly, i.e. lesser uptake. Thus the small global trend in ocean uptake over the 1990–2004 analysis period is a result of also the individual regions having relatively modest trends.

Process analysis

The regional flux trends are, however, much smaller than expected from an ocean with constant circulation that is only responding to increasing atmospheric CO_2, and hence would tend to increase its uptake of anthropogenic CO_2 through

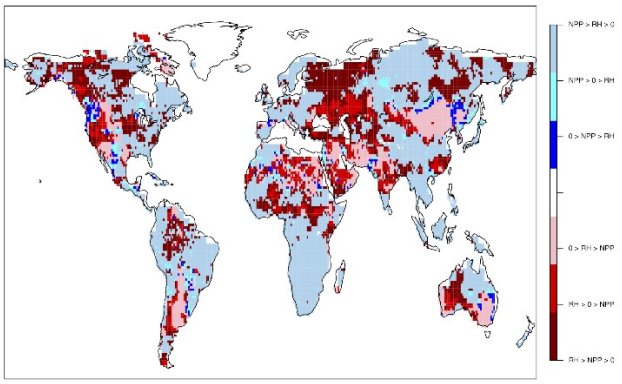

Figure 8. Qualitative change in processes over the period 1990–2009. Negative trend in land–atmosphere net CO_2 flux: enhanced NPP > enhanced RH (= RH + wildfire + riverine C flux) (pale blue); enhanced NPP, reduced RH (turquoise); and reduced NPP < reduced RH (dark blue). Positive trend in land–atmosphere net CO_2 flux: enhanced NPP < enhanced RH (dark red); reduced NPP, enhanced RH (red); and reduced NPP > reduced RH (pink).

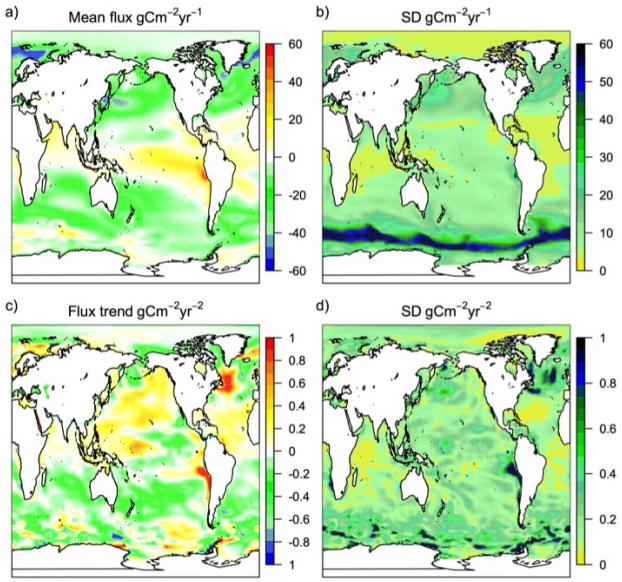

Figure 9. Gridded maps of the ensemble mean sea–air CO_2 flux over the period 1990–2004 **(a)**, standard deviation of the mean flux across the four OBGCMs **(b)**, the trend in the net flux across the ensemble **(c)**, and the standard deviation of the trend **(d)**.

time (Fig. 10). In the absence of climate variability and change, all regions would have flux density trends of more than $-0.05\,\mathrm{g\,C\,m^{-2}\,yr^{-2}}$, with some regions, such as the Southern Ocean, exceeding $-0.15\,\mathrm{g\,C\,m^{-2}\,yr^{-2}}$. However climate variability and change compensate for these negative trends in every single region by increasing them by $+0.04\,\mathrm{g\,C\,m^{-2}\,yr^{-2}}$ or more (with the exception of the South Pacific), such that the overall trends fluctuate from region to region around zero (Fig. 10). The largest reductions in trends are simulated to occur in the North and equatorial Pacific and in the North Atlantic, where they even cause a change in the sign of the overall trend. A similar, although slightly more moderate, pattern is seen if the analysis is undertaken for the entire 1990–2009 period with two models only. The most important difference is found in the North Atlantic, where the climate variability impact is substantially smaller, and not offsetting the anthropogenic CO_2 trend when analysed for 1990–2009.

The mechanisms driving the oceanic flux trends differ between the analysed regions. Attribution of regional trends to specific processes or changes in specific state variables in the different models is a work in progress, and is difficult to achieve with high confidence as yet. This is due to the antagonistic effect of ocean warming on CO_2 solubility and on dissociation of carbonic acid into bicarbonate and carbonate, as well as to the complex changes in ocean circulation and mixing, which themselves influence the biological carbon pumps of the ocean.

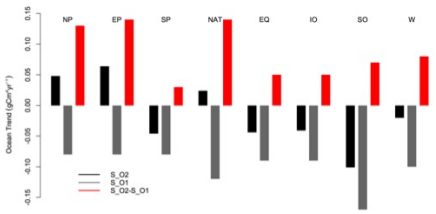

Figure 10. Regional ocean flux trends from 1990 through to 2004 for the standard case, i.e. variable climate and increasing CO_2 (simulation S_O2), and for the constant climate case (simulation S_O1), and their difference (S_O2–S_O1). Ocean regions comprise North Pacific (NP), equatorial Pacific (EP), South Pacific (SP), North Atlantic (NAT), equatorial/South Atlantic (EQ), Indian Ocean (IO), and Southern Ocean (SO), and world oceans (W).

4 Discussion

4.1 Land

The DGVMs used in this study simulate an increase in land carbon uptake over the period 1990–2009. The result is consistent with the earlier findings of Sarmiento et al. (2010), who suggested a large increase in the RLS between 1960 and 1988 and between 1989 and 2009 (Table S9 in the Supplement). The ensemble mean land–atmosphere flux increased by $-1.11\,\mathrm{Pg\,C\,yr^{-1}}$ for the same period, compared to the estimated RLS increase of $-0.88\,\mathrm{Pg\,C\,yr^{-1}}$ from Sarmiento et al. (2010). The DGVM ensemble trends in land uptake for the globe, northern, tropical, and southern land regions of -0.06 ± 0.03, 0.00 ± 0.01, -0.04 ± 0.01, and $-0.02 \pm 0.02\,\mathrm{Pg\,C\,yr^{-2}}$, respectively, compare favourably with the inversion estimates of -0.06 ± 0.04, -0.01 ± 0.01, -0.04 ± 0.02, and $-0.01 \pm 0.01\,\mathrm{Pg\,C\,yr^{-2}}$ over the period 1990–2009. Although encouraging, these results should be interpreted with caution because the inversion accounts for any trend in the land use change flux over this period, whereas DGVMs had fixed land use.

There is empirical evidence of a large increase in biomass in intact forest in tropical South America and Africa (Pan et al., 2011; Baker et al., 2004; Lewis et al., 2009a, b), which is consistent with the DGVM projections presented here. Lewis et al. (2009b) found broad agreement between biomass trends from observations and from a suite of carbon cycle models applied with 20th century forcing of climate and atmospheric CO_2 content, using a similar protocol to the current analysis. DGVMs suggest a large component of the uptake trend is associated with a positive NPP response to elevated CO_2, which is broadly consistent with the enhancement of forest production due to CO_2 observed in FACE experiments (Norby et al., 2005), although they are largely located in temperate forest ecosystems. However, recent studies have highlighted the role of nitrogen in limiting the long-term CO_2 response (Canadell et al., 2007; Norby et al., 2010) in these ecosystems. The long-term plant response to elevated CO_2 is likely affected by nutrients and its impact on plant C allocation (Zaehle et al., 2014), however only two out of the nine models used here (CLM4CN and OCN) include interactive nutrient cycling (see DGVM characteristics, Table S1).

In contrast to the large trend in net C uptake across the tropics, DGVMs simulate no statistically significant trend over the northern land region. In particular, trends in NPP over temperate regions are smaller than those in boreal regions, and are also not significant. Many temperate areas experienced a decrease in rainfall between 1990 and 2009, and suffered periods of prolonged and severe drought. Examples include the drought in the western USA of 2000–2004 (McDowell et al., 2008; Anderreg et al., 2012) and the 2003 summer heatwave in Europe (Ciais et al., 2005). Zscheischler et al. (2014) suggest that negative productivity extremes dominated interannual variability in productivity during the period 1982–2011; these extremes are evident particularly over temperate latitudes.

Satellite observations suggest a general greening trend in high latitudes, with an earlier onset and longer growing season in high-latitude ecosystems, which is reproduced by the DGVMs. Observations suggest a greening tundra and a

slower greening and possible browning in some regions of the boreal forest (Tucker et al., 2001; Bhatt et al., 2010), especially in North America (Beck and Goetz, 2011). In tundra ecosystems, an earlier onset is attributed to warming and earlier snowmelt. In these ecosystems, the start of the growing season corresponds to near peak in radiation. Thus any temperature-induced earlier snowmelt (McDonald et al., 2004; Sitch et al., 2007a) is likely to enhance plant production. Warming may not have such a great effect on the end of the growing season in Arctic tundra ecosystems, as this may be driven primarily by radiation. DGVMs simulate a significant positive trend in NPP in boreal North America and boreal Asia and the circumpolar tundra. Nitrogen limitation is also likely to constrain the productivity at high latitudes, but it was not possible to quantify N-limitation effects on regional trends in this study.

DGVMs simulate decreasing NPP across northeastern China and Mongolia, contributing to the overall decreasing land uptake trend, in response to recent climate. In a regional study, Poulter et al. (2013) investigated the differential response of cool semi-arid ecosystems to recent warming and drying trends across Mongolia and northern China, using multiple sources of evidence, including the LPJ DGVM, FPAR remotely sensed data (derived from GIMMS NDVI3g), and tree-ring widths. They found coherent patterns of high sensitivity to precipitation across data sources, which showed some areas with warming-induced springtime greening and drought-induced summertime browning, and limitations to NPP explained mainly by soil moisture.

Browning has occurred as a consequence of regional drought, wildfire, and insect outbreak, and their interaction, especially in North America (Beck and Goetz, 2011). Disturbance plays a key role in the ecology of many global ecosystems. For example, wildfire plays a dominant role in the carbon balance of boreal forest in central Canada and other regions (Bond-Lamberty et al., 2007), and insect outbreaks like the mountain pine beetle epidemic between 2000 and 2006 in British Colombia, Canada, resulted in the transition of forests from a small carbon sink to a source (Kurz et al., 2008). In general, disturbance and forest management are inadequately represented by the current generation of DGVMs, even though several models include simple prognostic wildfire schemes (Table S1), while some are starting to include other disturbance types such as insect attacks (Jönsson et al., 2012) and windthrow (Lagergren et al., 2012). The extension of DGVMs to include representations of globally and regionally important disturbance types and their response to changing environmental conditions is a priority.

In Table 4, DGVM results are compared with the REC-CAP synthesis papers documenting carbon sources and sinks for individual regions. Note that DGVMs provided one source of evidence for some regional papers. Over Russia, DGVMs agree on a sink yet underestimate that sink's magnitude, likely related to soil respiration (which is unsurprising, as many DGVMs have a limited representation of permafrost and active layer thickness) (Dolman et al., 2012). In South America, DGVMs agree with inventory-based estimates on a sink in natural forests (Gloor et al., 2012). DGVMs also agree with other data sources on the sign and magnitude of the natural land sink over Australia (Harverd et al., 2013). Over Europe DGVMs simulate a smaller mean land sink than the synthesis study suggests (Luyssaert et al., 2012). However, the regional synthesis was conducted over the shorter time period 2001–2005. For the Arctic, DGVMs tend to simulate a lower sink than regional process-based models (McGuire et al., 2012). However, over the 1990–2006 period, DGVMs are in line with observations and inversions on the magnitude and sign of the natural land sink, and DGVM results also suggest a sink trend in line with observations. DGVMs simulate a land sink over South Asia in agreement with inversions; however there were limited data to compare trends from DGVMs and other products (Patra et al., 2013). For East Asia, DGVM results agree remarkably well with remote sensing model–data fusion and inverse models on the magnitude of the land sink over the period 1990–2009. Finally, for Africa, DGVMs are broadly consistent with inventory- and flux-based estimates in simulating a land sink over Africa, albeit of lower magnitude (Valentini et al., 2014).

4.2 Ocean

The investigated OBGCMs consistently simulate an ocean characterised by a substantial uptake of CO_2 from the atmosphere, but with a global integrated trend in the last two decades ($-0.02 \pm 0.01\,\mathrm{Pg\,C\,yr^{-2}}$) that is substantially smaller than that expected based on the increase in atmospheric CO_2. Results based on the predictions from ocean inversion and ocean Green function methods (Mikaloff Fletcher et al., 2006; Gruber et al., 2009; Khatiwala et al., 2009) suggest an increase in ocean uptake with a trend of the order of $-0.04\,\mathrm{Pg\,C\,yr^{-2}}$ over the analysis period (see also Wanninkhof et al., 2013). These latter methods assume constant circulation, while our simulations here include the impact of climate variability and change.

Our analyses reveal that recent climate variability and change has caused the ocean carbon cycle to take up less CO_2 from the atmosphere than expected on the basis of the increase in atmospheric CO_2, i.e. it reduces the efficiency of the ocean carbon sink. Globally, we find that this efficiency reduction is primarily a result of ocean warming, while, regionally, many more processes (e.g. wind changes, alkalinity/DIC concentration changes) are at play.

Is this reduction in uptake efficiency over the analysis period the first sign of a positive feedback between global warming and the ocean carbon cycle – or, alternatively, could it just reflect natural decadal-scale variability in air–sea CO_2 fluxes? Without a formal attribution study, it is not possible to provide a firm answer. We suspect that the majority of the trend in the efficiency is due to

Table 4. Ensemble DGVM regional NBP mean comparison with RECCAP regional chapter analyses.

Region	DGVM mean NBP (TgC yr^{-1})	Region processed-based models	Inventory-based	Flux-based	Inversion	Best estimate
Russia	−199		−761	−709	−653	
South America (forest)	−472 ± 211		−570 ± 170 (1990–94) −530 ± 140 (1995–99) −450 ± 250 (2000–04) −150 ± 230 (2005–09)			
Africa	−410 ± 310		−740 ± 1190	−1340 ± 1320	50 ± 280 (LULCC 510 ± 280)	
Australia & New Zealand	−70 ± 78	−36 ± 29 (LULCC 18 ± 7)				
Europe	−179 ± 92					−891 ± 155 (2001–05)
Arctic (1990–2006)	−86	−177				−96
South Asia	−210 ± 164				−35.4 (1997–06) −317 to −88.3 (2007–08)	
East Asia	−224 ± 141		−293 ± 33 combined inventory–EO-flux approach			270 ± 507

"natural" decadal-scale variability; however, largely based on the results of McKinley et al. (2011) and Fay and McKinley (2013), who showed that whereas trends in oceanic pCO_2 (and air–sea CO_2 fluxes) are variable on a decadal timescale, they do converge towards atmospheric pCO_2 trends when analysed over a longer 30-year period for most global regions. Nevertheless, they also show that warming (partly driven by anthropogenic climate change) in the permanently stratified subtropical gyre of the North Atlantic has started to reduce ocean uptake in recent years. In the Southern Ocean, where Le Quéré et al. (2007) and Lovenduski et al. (2008) used models to suggest a reduction in ocean carbon uptake efficiency over the past 25 years in response to increasing Southern Ocean winds, Fay and McKinley (2013) concluded that the data are insufficient to draw any conclusions.

We should note that the associated uncertainties remain large. Of particular concern is the moderate success of the models in simulating the time-mean ocean sinks and their long-term seasonal cycle (e.g. McKinley et al., 2006). Furthermore, some of the models underestimate the oceanic uptake of transient tracers such as anthropogenic radiocarbon (see e.g. Graven et al., 2012). Such a reduction in the oceanic uptake efficiency is also not suggested by independent measures of oceanic CO_2 uptake, such as the atmospheric O_2 / N_2 method (Manning and Keeling, 2006; Ishidoya et al., 2012), although the large uncertainties in these estimates make the determination of trends in uptake highly uncertain.

All the models have been tuned to reproduce data synthesis on ocean surface pCO_2 (Pfeil et al., 2013; Takahashi et al., 2009) and deep ocean (Key et al., 2004) reasonably well. Specific systematic data assimilation procedures, however, have not been applied. On decadal timescales, the ocean CO_2 flux feedback to climate change (change in hydrography and circulation) and rising ambient CO_2 (change in CO_2 buffering) reacts only slowly on the global average due to the long timescales of oceanic motion and marine CO_2 equilibration with the atmosphere. Changes in biogeochemical and ecosystem processes, such as locally varying gas exchange velocities, phytoplankton blooms, and associated particle flux pulses, can lead to regional interannual variations in air–sea CO_2 fluxes, but may partially cancel for averages over larger regions. With ocean observations only over about a two-decade time frame, it is difficult to quantify longer-term trends due to other proposed mechanisms: a gradual slowing-down of meridional overturning circulation due to a strengthening of density stratification; redissolution of $CaCO_3$ sediment from the seafloor associated with fossil fuel neutralization; and potential changes in biogenic particle fluxes due to carbon overconsumption and changing ballasting (cf. Keller et al., 2014). Whether more complex models will render better results will depend on how well the additional free parameters in more complex biogeochemical models can be constrained by measurements. So far, more complex – and hence potentially more realistic – models do not necessarily give better results than the present nutrient-phytoplankton-zooplankton-detritus (NPZD)-type models models as applied here (Le Quéré et al., 2005; Kriest et al., 2010).

4.3 Reducing uncertainty in regional sinks

In order to better quantify the regional carbon cycle and its trends, DGVM and ocean carbon cycle models need to improve both process representations and model evaluation and benchmarking (Luo et al., 2012). There is a need for up-to-date global climate and land use and cover change data sets to force the DGVMs, as well as a deeper investigation of the quality and differences between the different reanalysis products used to force ocean carbon cycle models. Also, techniques such as detection and attribution can be applied to elucidate trends in the regional carbon cycle and their drivers.

4.3.1 Model evaluation and benchmarking

Piao et al. (2013) evaluated the DGVM model results for their response to climate variability and to CO_2 trends, and the seasonal cycle of CO_2 fluxes were benchmarked in Peng et al. (2014). Piao et al. (2013) found DGVMs to simulate higher mean and interannual variations (IAVs) in gross primary production than a data-driven model (Jung et al., 2011), particularly in the tropics; however, this is the region where the data-driven model is most uncertain. DGVMs were able to capture the IAVs in RLS, although the simulated land–atmosphere net CO_2 flux appears too sensitive to variations in precipitation in tropical forests and savannas. However, Poulter et al. (2014) found an increase in the sensitivity of the net flux to precipitation over the last three decades across continental Australia. Piao et al. (2013) found that the simulated net CO_2 flux was more sensitive than productivity to temperature variations. When compared to ecosystem warming experiments the DGVMs tend to underpredict the response of NPP to temperature at temperate sites. DGVMs simulated an ensemble mean NPP enhancement comparable to FACE experiment observations (Piao et al., 2013). However, modelling of ecosystem function in water-stressed environments and changes in plant water use with elevated CO_2 remains a challenge for DGVMs (Morales et al., 2005; Keenan et al., 2009; De Kauwe et al., 2013).

There is a critical need for comprehensive model benchmarking, as a first step to attempt to reduce model uncertainty. Several prototype carbon cycle benchmarking schemes have been developed (Randerson et al., 2009; Cadule et al., 2010). A more in-depth evaluation and community benchmarking set needs to be agreed upon and implemented which also evaluates models for their implicit land response timescales (especially relevant in the discussion on future tipping elements and non-linear future responses) and for the simulated carbon, water, and nutrient cycles. New emerging frameworks now exist (Blyth et al., 2011; Abramowitz, 2012; Luo et al., 2012; Dalmonech and Zaehle, 2013; Harverd et al., 2013). One example within RECAPP is a multiple-constraint approach applied to reduce uncertainty in land carbon and water cycles over Australia (Haverd et al., 2013).

4.3.2 Model resolution

Simulated ocean carbon dynamics may be sensitive to horizontal resolution, particularly as model resolution improves sufficiently to adequately capture mesoscale eddies. Mesoscale turbulence influences the ocean carbon cycle in a variety of ways, and the present eddy parameterisations may not adequately capture the full range of effects and the responses to climate variability and change. For example, mesoscale processes are thought to modulate biological productivity by altering the supply of limiting nutrients (Falkowski et al., 1991; McGillicuddy et al., 1998; Gruber et al., 2011). A particularly crucial issue involves the wind-driven overturning circulation in the Southern Ocean, where non-eddy-resolving models indicate a strong sensitivity of the overturning circulation and ocean carbon uptake to surface wind stress (Le Quéré et al., 2007; Lovenduski et al., 2008). Some eddy-resolving models, in contrast, suggest that enhanced wind stress is dissipated by increased eddy activity, leading to only a small increase in overturning (Böning, et al., 2008), although more recent results indicate a larger response (Gent and Danabasoglu, 2011; Matear et al., 2013).

4.3.3 Model structure

There is a need for improved representation of ecological processes in land and ocean models, e.g. nutrient cycling (N, P), demographic dynamics, disturbance (wildfire, windthrow, insects), land use and land cover change in land models, and better representation of the key functional diversity in ocean and land biogeochemical models. DGVMs need to represent land use and land cover changes, forest management, and forest age in order to improve estimates of the regional and global land carbon budget. There have been recent developments to include nutrient dynamics, mostly nitrogen, in global land biosphere models (as reviewed by Zaehle and Dalmonech, 2011). Too few model simulations are available to date to allow for an ensemble model trend assessment. However, a few general trends appear robust: as evident from Table 3, CN models generally show less of a response to increasing atmospheric CO_2 due to nitrogen limitation of plant production. N dynamics further alter the climate–carbon relationship, which tend to reduce the C loss from temperate and boreal terrestrial ecosystems due to warming – but with a considerable degree of uncertainty (Thornton et al., 2009; Sokolov et al., 2008; Zaehle et al., 2010). Changes in the nitrogen cycle due to anthropogenic reactive nitrogen additions (both fertiliser to croplands and N deposition on forests and natural grasslands) further modify the terrestrial net C balance and contribute with -0.2 to $-0.5\,\mathrm{Pg\,C\,yr^{-1}}$ to the current land sink (Zaehle and Dalmonech, 2011). Zaehle et al. (2011), using the OCN model, estimated the 1995–2005 trend in land uptake due to N deposition to be $-1.1 \pm 1.7\,\mathrm{Tg\,C\,yr^{-2}}$, with strong regional differences depending on the regional trends in air pollution and reactive N loading of the atmosphere and the nitrogen status of the ecosystems, which are generally lower in less responsive ecosystems close to nitrogen saturation highly polluted regions. The DGVMs applied here do not consider the P cycle; P limitation on land carbon uptake may be particularly important in tropical forests and savannas (Edwards et al., 2005; Wang et al., 2010; Zhang et al., 2014).

There are several additional land processes that have not been considered in this current multi-model analysis. These include the effects of aerosols and tropospheric ozone on the carbon cycle. Unlike a global forcing agent such as CO_2, the effects of air pollutants (aerosols, NO_x, and O_3), with their shorter atmospheric lifetimes, are at the regional scale.

Aerosol-induced changes in radiation quantity and quality (i.e. the ratio of diffuse to direct) affect plant productivity and the land sink (Mercado et al., 2009). From around 1960 until the 1980s, radiation levels declined across industrialised regions, a phenomenon called "global dimming", followed by a recent brightening in Europe and North America with the adoption of air pollution legislation. Reductions in acid rain have been found to greatly influence trends in riverine DOC, vegetation health, and rates of soil organic matter decomposition. Tropospheric ozone is known to be toxic to plants and lead to reductions in plant productivity, and thus reduce the efficiency of the land carbon sink (Sitch et al., 2007b; Anav et al., 2011). Drivers of the land carbon sink related to air pollution – e.g. N deposition, acid precipitation, diffuse and direct radiation, and surface O_3 – have varied markedly in space and time over recent decades. Although likely important for regional carbon cycle trends, quantifying these effects is beyond the scope of the present study.

The Pinatubo eruption in 1991, at the start of the study period, had a major influence on many carbon cycle processes, leading to an enhanced land sink over the period 1991–1993. This has been attributed to a combination of cooling-induced reductions in high-latitude respiration and enhanced productivity associated with changes in diffuse radiation (Jones and Cox, 2001; Lucht et al., 2002; Peylin et al., 2005; Mercado et al., 2009; Frölicher et al., 2013). The direct effect of aerosols on climate drivers is implicitly included in this study (i.e. responses to high-latitude cooling, tropical drying, reduced net incoming solar radiation); however diffuse radiation effects are not included.

Similar gaps need to be addressed in ocean biogeochemical models. The ecosystem modules in the current generation of OBGCMs lack the ability to assess many of the suggested mechanisms by which climate and ocean acidification could alter marine biogeochemistry and ocean carbon storage. Proposed biological processes that could influence ocean carbon uptake and release involve, for example, decoupling of carbon and macronutrient cycling, changes in micronutrient limitation, variations in elemental stoichiometry in organic matter, and changes in the vertical depth scale for the respiration of sinking organic carbon particles (e.g. Boyd and Doney, 2003; Sarmiento and Gruber, 2006). Some advances have been made with the incorporation of dynamic iron cycling and iron limitation, multiple plankton groups, calcification, and nitrogen fixation (Le Quéré et al., 2005). However, the evaluation of these aspects of the models is currently hindered by both data- and process-level information limitations.

4.3.4 Climate and land use and cover data sets

In addition to model structure, the choice of climate forcing and model initial conditions can also contribute to differences in the simulated terrestrial carbon sink. At regional scales, differences in land cover can introduce $\sim 10\,\%$ uncertainty in simulated regional-scale GPP (Jung et al., 2007; Quaife et al., 2008) and $\sim 3.5\,\%$ uncertainty for global NPP. Climate forcing uncertainty tends to have larger effects on carbon flux uncertainty than land cover (Hicke, 2005; Poulter et al., 2011), with up to 25 % differences in GPP reported over Europe (Jung et al., 2007) and a 10 % difference for global NPP (Poulter et al., 2011). Climate forcing uncertainty and land cover (i.e. PFT distributions) can alter long-term trends in land to atmosphere net CO_2 flux and interannual variability of carbon fluxes to climate (Poulter et al., 2011). The DGVMs applied here did not consider LULCC. This is an active area of research; models need a consistent implementation of LULCC. Uncertainties in the simulated net land use flux are associated with assumptions on the implementation of LULCC gridded maps (e.g. whether conversion to cropland in a grid-cell is taken preferentially from grassland, forest, or both), simulated biomass estimates, and subsequent decomposition rates. However DGVMs offer the exciting prospect of disentangling the component fluxes associated with land use (e.g. direct emissions and legacy fluxes) and separating the environmental and direct human impacts on the net LU flux (Gasser and Ciais, 2013; Pongratz et al., 2014; Stocker et al., 2014).

5 Conclusions

Land models suggest an increase in the global land net C uptake over the period 1990–2009, with increases in tropical and southern regions and negligible increase in northern regions. The increased sink is mainly driven by trends in NPP, in response to increasing atmospheric CO_2 concentration, and modulated by change in climate. Over the same period, ocean models suggest a negligible increase in net ocean C uptake – a result of ocean warming counteracting the expected increase in ocean uptake driven by the increase in atmospheric CO_2. At the sub-regional level, trends vary both in sign and magnitude, particularly over land. Areas in temperate North America, eastern Europe, and northeastern China show a decreasing regional land sink trend, due to regional drying, suggesting a possibility for a transition to a net carbon source in the future if drying continues or droughts become more severe and/or frequent. In the ocean, the trends tend to be more homogeneous, but the underlying dynamics differ greatly, ranging from ocean warming, to winds, and to changes in circulation/mixing and ocean productivity, making simple extrapolations into the future difficult.

Our conclusions need to be viewed with several important caveats: only a few models include a fully coupled carbon–nitrogen cycle, and no model included land use and land cover changes. Ocean models tend to be too coarse in resolution to properly represent important scales of motions and mixing, such as eddies and other mesoscale processes, and coastal boundary processes. Furthermore, their representation of ocean ecosystem processes and their sensitivity to

climate change and other stressors (e.g. ocean acidification, deoxygenation, etc.; Gruber, 2011; Boyd, 2011) is rather simplistic.

There is a need for detailed model evaluation and benchmarking in order to reduce the uncertainty in the sinks in the land and ocean and, particularly, in how these sinks have changed in the past and how they may change in the future. For land ecosystems, a concerted effort is needed in the DGVM community to incorporate nutrient cycling as well as land use and land cover change. For the oceans, models need to improve their representation of unresolved physical transport and mixing processes, and ecosystem models need to evolve to better characterise their response to global change.

The Supplement related to this article is available online at doi:10.5194/bg-12-653-2015-supplement.

Acknowledgements. S. Sitch acknowledges financial support by RCUK through NERC (grant no. NE/J010154/). N. Gruber and C. Heinze acknowledge financial support by the European Commission through the EU FP7 projects CARBOCHANGE (grant no. 264879) and GEOCARBON (grant no. 283080). N. Gruber was additionally supported through ETH Zurich. S. C. Doney acknowledges support from the US National Science Foundation (NSF AGS-1048827). P. Friedlingstein, A. Arneth, and S. Zaehle acknowledge support by the European Commission through the EU FP7 project EMBRACE (grant no. 282672). A. Arneth and S. Sitch acknowledge the support of the European Commission-funded project LUC4C (grant no. 603542). The research leading to these results received funding from the European Community's Seventh Framework Programme (FP7 2007–2013) under grant agreement no. 238366. A. Ahlström and B. Smith acknowledge funding through the Mistra Swedish Research Programme on Climate, Impacts and Adaptation (SWECIA). This study is a contribution to the Lund Centre for Studies of Carbon Cycle and Climate Interactions (LUCCI) and the Strategic Research Area Modelling the Regional and Global Earth System (MERGE). This is a contribution to the Bjerknes Centre for Climate Research (BCCR) and core project BIOFEEDBACK of the Centre for Climate Dynamics (SKD) at BCCR. C. Heinze acknowledges support from NOTUR/NorStore projects NN2980K and NS2980K. The authors wish to thank Jonathan Barichivich for discussions on greening trends.

Edited by: F. Joos

References

Abramowitz, G.: Towards a public, standardized, diagnostic benchmarking system for land surface models, Geosci. Model Dev., 5, 819–827, doi:10.5194/gmd-5-819-2012, 2012.

Allen, C. D., Macalady, A., Chenchouni, H., Bachelet, D., McDowell, N., Vennetier, M., Gonzales, P., Hogg, T., Rigling, A., Breshears, D., Fensham, R., Zhang, Z., Kitzberger, T., Lim, J., Castro, J., Allard, G., Running, S., Semerci, A., and Cobb, N.: A global overview of drought and heat-induced tree mortality reveals emerging climate change risks for forests, Forest Ecol. Manag., 4, 660–684, doi:10.1016/j.foreco.2009.09.001, 2010.

Anav, A., Menut, L., Khvorostyanov, D., and Viovy, N.: Impact of tropospheric ozone on the Euro-Mediterranean vegetation, Glob. Change Biol., 17, 2342–2359, 2011.

Anderegg, W. R. L., Berry J. A., Smith, D. D., Sperry J. S., Anderegg, L. D. L., and Field, C. B.: The roles of hydraulic and carbon stress in a widespread climate-induced forest die-off, P. Natl. Acad. Sci. USA, 109, 233–237, doi:10.1073/pnas.1107891109, 2012.

Angert, A., Biraud, S., Bonfils, C., Henning, C. C., Buermann, W., Pinzon, J., Tucker, C. J., and I. Fung: Drier summers cancel out the CO_2 uptake enhancement induced by warmer springs, P. Natl. Acad. Sci., 102, 10823–10827, 2005.

Assmann, K. M., Bentsen, M., Segschneider, J., and Heinze, C.: An isopycnic ocean carbon cycle model, Geosci. Model Dev., 3, 143–167, doi:10.5194/gmd-3-143-2010, 2010.

Baker, T. R., Phillips, O. L., Malhi, Y., Almeida, S., Arroyo, L., Di Fiore, A., Erwin, T., Higuchi, N., Killeen, T. J., Laurance, S. G., Laurance, W. F., Lewis, S. L., Monteagudo, A., Neill, D. A., Nunez Vargas, P., Pitman, N. C. A., Silva, J. N. M., and Vasquez Martinez, R.: Increasing biomass in Amazonian forest plots, Philos. T. R. Soc. B, 359, 353–365, 2004.

Ballantyne, A. P., Alden, C. B., Miller, J. B., Tans, P. P., and White, J. W. C.: Increase in observed net carbon dioxide uptake by land and oceans during the past 50 years, Nature, 488, 70–72, doi:10.1038/nature11299, 2012.

Beck, S. A. and Goetz, S. J.: Satellite observations of high northern latitude vegetation productivity changes between 1982 and 2008: ecological variability and regional differences, Environ. Res. Lett. 6, 045501, doi:10.1088/1748-9326/6/4/045501, 2011.

Bhatt, U. S., Walker, D. A., Raynolds, M. K., Comiso, J. C., Epstein, H. E., Jia, G., Gens, R., Pinzon, J. E., Tucker, C. J., Tweedie, C. E., and Webber, P. J.: Circumpolar Arctic tundra vegetation change is linked to sea ice decline, Earth Interact., 14, 1–20, 2010.

Blyth, E., Clark, D. B., Ellis, R., Huntingford, C., Los, S., Pryor, M., Best, M., and Sitch, S.: A comprehensive set of benchmark tests for a land surface model of simultaneous fluxes of water and carbon at both the global and seasonal scale, Geosci. Model Dev., 4, 255–269, doi:10.5194/gmd-4-255-2011, 2011.

Bonan, G. B. and Levis, S.: Quantifying carbon-nitrogen feedbacks in the Community Land Model (CLM4), Geophys. Res. Lett., 37, L07401, doi:10.1029/2010GL042430, 2010.

Bond-Lamberty, B., Peckham, S. D., Ahl, D. E., and Gower, S. T.: Fire as the dominant driver of central Canadian boreal forest carbon balance, Nature, 450, 89–92, 2007.

Böning, C. W., Dispert, A., Visbeck, M., Rintoul, S. R., and Schwarzkopf, F. U.: The response of the Antarctic Circumpolar Current to recent climate change, Nat. Geosci., 1, 864–869, 2008.

Boyd, P. and Doney, S. C.: The impact of climate change and feedback process on the ocean carbon cycle, Ocean Biogeochemistry, edited by: Fasham, M., Springer, 157–193, 2003.

Boyd, P. W.: Beyond ocean acidification, Nat. Geosci., 4, 273–274, 2011.

Broecker, W. S., Peng, T.-H., Ostlund, G., and Stuiver, M.: The distribution of bomb radiocarbon in the ocean, J. Geophys. Res., 90, 6953–6970, 1985.

Buermann, W., Lintner, B. R., Koven, C. D., Angert, A., Pinzon, J. E., Tucker, C. J., and Fung, I. Y.: The changing carbon cycle at Mauna Loa observatory, P. Natl. Acad. Sci., 104, 4249–4254, 2007.

Buitenhuis, E. T., Rivkin, R. B., Sailley, S., and Le Quéré, C.: Biogeochemical flues through microzooplankton, Global Biogeochem. Cy., 24, GB4015, doi:10.1029/2009GB003601, 2010.

Cadule, P., Friedlingstein, P., Bopp, L., Sitch, S., Jones, C. D., Ciais, P., Piao, S. L., and Peylin, P.: Benchmarking coupled climate-carbon models against long-term atmospheric CO_2 measurements, Global Biogeochem. Cy., 24, Gb2016, doi:10.1029/2009gb003556, 2010.

Canadell, J. G., Pataki D., Gifford, R., Houghton, R. A., Lou, Y., Raupach, M. R., Smith, P., and Steffen, W.: Saturation of the terrestrial carbon sink, in: Terrestrial Ecosystems in a Changing World, edited by: Canadell, J. G., Pataki, D., and Pitelka, L., 59–78, The IGBP Series, Springer-Verlag, Berlin Heidelberg, 59–78, 2007.

Canadell, J. G., Ciais, P., Gurney, K., Le Quéré, C., Piao, S., Raupach, M. R., and Sabine, C. L.: An international effort to quantify regional carbon fluxes, EOS T. Am. Geophys. Un., 92, 81–82, 2011.

Canadell, J. G., Ciais, P., Sabine, C., and Joos, F. (Eds.): REgional Carbon Cycle Assessment and Processes (RECCAP), Special issue, Biogeosciences, http://www.biogeosciences-discuss.net/special_issue83.html, 2013.

Chevallier, F., Ciais, P., Conway, T. J., Aalto, T., Anderson, B. E., Bousquet, P., Brunke, E. G., Ciattaglia, L., Esaki, Y., Fröhlich, M., Gomez, A., Gomez-Pelaez, A. J., Haszpra, L., Krummel, P. B., Langenfelds, R. L., Leuenberger, M., Machida, T., Maignan, F., Matsueda, H., Morguí, J. A., Mukai, H., Nakazawa, T., Peylin, P., Ramonet, M., Rivier, L., Sawa, Y., Schmidt, M., Steele, L. P., Vay, S. A., Vermeulen, A. T., Wofsy, S., and Worthy, D.: CO_2 surface fluxes at grid point scale estimated from a global 21-year reanalysis of atmospheric measurements, J. Geophys. Res., 115, D21307, doi:10.1029/2010JD013887, 2010.

Ciais, P., Tans, P. P., Trolier, M., White, J. W. C., and Francey, R. J.: A large northern hemisphere terrestrial CO_2 sink indicated by the ^{13}C / ^{12}C ratio of atmospheric CO_2, Science, 269, 1098–1102, doi:10.1126/science.269.5227.1098, 1995.

Ciais, P., Reichstein, M., Viovy, N., Granier, A., Ogee, J., Allard, V., Aubinet, M., Buchmann, N., Bernhofer, C., Carrara, A., Chevallier, F., De Noblet, N., Friend, A. D., Friedlingstein, P., Grunwald, T., Heinesch, B., Keronen, P., Knohl, A., Krinner, G., Loustau, D., Manca, G., Matteucci, G., Miglietta, F., Ourcival, J. M., Papale, D., Pilegaard, K., Rambal, S., Seufert, G., Soussana, J. F., Sanz, M. J., Schulze, E. D., Vesala, T., and Valentini, R.: Europe-wide reduction in primary productivity caused by the heat and drought in 2003, Nature, 437, 529–533, doi:10.1038/nature03972, 2005.

Ciais, P., Canadell, J. G, Luyssaert, S., Chevallier, F., Shvidenko, A., Pousii, Z., Jonas, M., Peylin, P., Wayne King, A., Schulze, E.-D., Piao, S., Roedenbeck, C., Wouters, P., and Breon, F.-M.: Can we reconcile atmospheric estimates of the Northern terrestrial carbon sink with land-based accounting?, Current Opinion in Environmental Sustainability, 2, 225–230, 2010.

Ciais, P., Sabine, C., Bala, G., Bopp, L., Brovkin, V., Canadell, J., Chhabra, A., DeFries, R., Galloway, J., Heimann, M., Jones, C., Le Quéré, C., Myneni, R. B., Piao, S., and Thornton, P.: Carbon and Other Biogeochemical Cycles, in: Climate Change 2013: The Physical Science Basis, Contribution of Working Group I to the Fifth Assessment Report of the Intergovernmental Panel on Climate Change, edited by: Stocker, T. F., Qin, D., Plattner, G.-K., Tignor, M., Allen, S. K., Boschung, J., Nauels, A., Xia, Y., Bex, V., and Midgley, P. M., Cambridge University Press, Cambridge, United Kingdom and New York, NY, USA, 465–570, 2013.

Clark, D. B., Mercado, L. M., Sitch, S., Jones, C. D., Gedney, N., Best, M. J., Pryor, M., Rooney, G. G., Essery, R. L. H., Blyth, E., Boucher, O., Harding, R. J., Huntingford, C., and Cox, P. M.: The Joint UK Land Environment Simulator (JULES), model description – Part 2: Carbon fluxes and vegetation dynamics, Geosci. Model Dev., 4, 701–722, doi:10.5194/gmd-4-701-2011, 2011.

Cox, P. M.: Description of the "TRIFFID" dynamic global vegetation model, Hadley Centre Technical Note, 24, 1–16, 2001.

Dalmonech, D. and Zaehle, S.: Towards a more objective evaluation of modelled land-carbon trends using atmospheric CO_2 and satellite-based vegetation activity observations, Biogeosciences, 10, 4189–4210, doi:10.5194/bg-10-4189-2013, 2013.

De Kauwe, M. G., Medlyn, B. E., Zaehle, S., Walker, A. P., Dietze, M. C., Hickler, T., Jain, A. K., Luo, Y., Parton, W. J., Prentice, C., Smith, B., Thornton, P. E., Wang, S., Wang, Y-P., Wårlind, D., Weng, E. S., Crous, K, Y., Ellsworth, D. S., Hanson, P. J., Seok-Kim, H., Warren, J. M., Oren, R., and Norby, R. J.: Forest water use and water use efficiency at elevated CO_2: a model-data intercomparison at two contrasting temperate forest FACE sites, Glob. Change Biol., 19, 1759–1779, 2013.

Denman, K. L., Brasseur, G., Chidthaisong, A., Ciais, P., Cox, P. M., Dickinson, R. E., Hauglustaine, D., Heinze, C., Holland, E., Jacob, D., Lohmann, U., Ramachandran, S., da Silva Dias, P. L., Wofsy, S. C. , and Zhang, X.: Couplings Between Changes in the Climate System and Biogeochemistry, in: Climate Change 2007: The Physical Science Basis, Contribution of Working Group I to the Fourth Assessment Report of the Intergovernmental Panel on Climate Change, edited by: Solomon, S., Qin, D., Manning, M., Chen, Z., Marquis, M., Averyt, K. B., Tignor, M., and Miller, H. L., Cambridge University Press, Cambridge, United Kingdom and New York, NY, USA, 499–588, 2007.

Dentener, F., Stevenson, D., Ellingsen, K., van Noije, T., Schultz, M., Amann, M., Atherton, C., Bell, N., Bergmann, D., Bey, I., Bouwman, L., Butler, T., Cofala, J., Collins, B., Drevet, J., Doherty, R., Eickhout, B., Eskes, H., Fiore, A., Gauss, M., Hauglustaine, D., Horowitz, L., Isaksen, I. S. A., Josse, B., Lawrence, M., Krol, M., Lamarque, J. F., Montanaro, V., Muller, J. F., Peuch, V. H., Pitari, G., Pyle, J., Rast, S., Rodriguez, J., Sanderson, M., Savage, N. H., Shindell, D., Strahan, S., Szopa, S., Sudo, K., Van Dingenen, R., Wild, O., and Zeng, G.: The global atmospheric environment for the next generation, Environ. Sci. Technol., 40, 3586–3594, doi:10.1021/es0523845, 2006.

Dolman, A. J., Shvidenko, A., Schepaschenko, D., Ciais, P., Tchebakova, N., Chen, T., van der Molen, M. K., Belelli Marchesini, L., Maximov, T. C., Maksyutov, S., and Schulze, E.-D.: An estimate of the terrestrial carbon budget of Russia using inventory-based, eddy covariance and inversion methods, Biogeosciences, 9, 5323–5340, doi:10.5194/bg-9-5323-2012, 2012.

Doney, S. C., Lima, I., Feely, R. A., Glover, D. M., Lindsay, K., Mahowald, N., Moore, J. K., and Wanninkhof, R.: Mechanisms governing interannual variability in upper-ocean inorganic carbon system and air-sea CO_2 fluxes: Physical climate and atmospheric dust, Deep-Sea Res.-Pt. II, 56, 640–655, 2009a.

Doney, S. C., Lima, I., Moore, J. K., Lindsay, K., Behrenfeld, M. J., Westberry, T. K., Mahowald, N., Glover, D. M., and Takahashi, T.: Skill metrics for confronting global upper ocean ecosystem-biogeochemistry models against field and remote sensing data, J. Marine Syst., 76, 95–112, doi:10.1016/j.jmarsys.2008.05.015, 2009b.

Edwards E., S. McCaffery, S., and Evans, J.: Phosphorus status determines biomass response to elevated CO_2 in a legume: C-4 grass community, Glob. Change Biol., 11, 1968–1981, 2005.

Falkowski, P. G., Ziemann, D., Kolber, Z., and Bienfang, P. K.: Role of eddy pumping in enhancing primary production in the ocean, Nature, 352, 55–58, 1991.

Fan, S., Gloor, M., Mahlmam, J., Pacala, S., Sarmiento, J., Takahashi, T., and Tans, P.: A large terrestrial carbon sink in North America implied by atmospheric and oceanic carbon dioxide data and models, Science, 282, 442–446, 1998.

Fay, A. R. and McKinley, G. A.: Global trends in surface ocean *p*CO2 from in situ data, Global Biogeochem. Cy., 27, 541–557, doi:10.1002/gbc.20051, 2013.

Friedlingstein, P., Houghton, R. A., Marland, G., Hackler, J., Boden,T. A., Conway, T. J., Canadell, J. G., Raupach, M. R., Ciais, P., and Le Quéré, C.: Update on CO_2 emissions, Nat. Geosci., 3, 811–812, doi:10.1038/ngeo1022, 2010.

Friend, A. D., Stevens, A. K., Knox, R. G., and Cannell, M. G. R.: A process-based, terrestrial biosphere model of ecosystem dynamics (Hybrid v3.0), Ecol. Model., 95, 249–287, 1997.

Frölicher, T. L., Joos, F., Raible, C. C., and Sarmiento, J. L.: Atmospheric CO_2 response to volcanic eruptions: the role of ENSO, season, and variability, Global Biogeochem. Cy., 27, 239–251, 2013.

Gasser, T. and Ciais, P.: A theoretical framework for the net land-to-atmosphere CO_2 flux and its implications in the definition of "emissions from land-use change", Earth Syst. Dynam., 4, 171–186, doi:10.5194/esd-4-171-2013, 2013.

Gent, P. R. and Danabasoglu, G.: Response to Increasing Southern Hemisphere Winds in CCSM4, J. Climate, 24, 4992–4998, 2011.

Gloor, M., Gruber, N., Sarmiento, J. L., Sabine, C., Feely, D., and Rödenbeck, C.: A first estimate of present and preindustrial air-sea CO_2 flux patterns based on ocean interior carbon measurements and models, Geophys. Res. Lett., 30, 1010, doi:10.1029/2002GL015594, 2003.

Gloor, M., Sarmiento, J. L., and Gruber, N.: What can be learned about carbon cycle climate feedbacks from the CO_2 airborne fraction?, Atmos. Chem. Phys., 10, 7739–7751, doi:10.5194/acp-10-7739-2010, 2010.

Gloor, M., Gatti, L., Brienen, R., Feldpausch, T. R., Phillips, O. L., Miller, J., Ometto, J. P., Rocha, H., Baker, T., de Jong, B., Houghton, R. A., Malhi, Y., Aragão, L. E. O. C., Guyot, J.-L., Zhao, K., Jackson, R., Peylin, P., Sitch, S., Poulter, B., Lomas, M., Zaehle, S., Huntingford, C., Levy, P., and Lloyd, J.: The carbon balance of South America: a review of the status, decadal trends and main determinants, Biogeosciences, 9, 5407–5430, doi:10.5194/bg-9-5407-2012, 2012.

Graven, H. D., Gruber, N., Key, R., Khatiwala, S., and Giraud, X.: Changing controls on oceanic radiocarbon: New insights on shallow-to-deep ocean exchange and anthropogenic CO_2 uptake, J. Geophys. Res., 117, C10005, doi:10.1029/2012JC008074, 2012.

Gruber, N.: Warming up, turning sour, losing breath: Ocean biogeochemistry under global change, Philos. T. R. Soc. A, 369, 1980–1996, doi:10.1098/rsta.2011.0003, 2011.

Gruber, N., Gloor, M., Fletcher, S. E. M., Doney, S. C., Dutkiewicz, S., Follows, M. J., Gerber, M., Jacobson, A. R., Joos, F., Lindsay, K., Menemenlis, D., Mouchet, A., Muller, S. A., Sarmiento, J. L., and Takahashi, T.: Oceanic sources, sinks, and transport of atmospheric CO_2, Global Biogeochem. Cy., 23, GB1005, doi:10.1029/2008GB003349, 2009.

Gruber, N., Lachkar, Z., Frenzel, H., Marchesiello, P., Munnich, M., McWilliams, J., Nagai, T., and Plattner, G.-K.: Eddy-induced reduction of biological production in Eastern Boundary Upwelling Systems, Nat. Geosci., 4, 787–792, doi:10.1038/ngeo1273, 2011.

Haverd, V., Raupach, M. R., Briggs, P. R., J. G. Canadell., Davis, S. J., Law, R. M., Meyer, C. P., Peters, G. P., Pickett-Heaps, C., and Sherman, B.: The Australian terrestrial carbon budget, Biogeosciences, 10, 851–869, doi:10.5194/bg-10-851-2013, 2013.

Hicke, J. A.: NCEP and GISS solar radiation data sets available for ecosystem modeling: Description, differences, and impacts on net primary production, Global Biogeochem. Cy., 19, GB2006, doi:10.1029/2004GB002391, 2005.

Houghton, R. A.: How well do we know the flux of CO_2 from land-use change? Tellus B, 62, 337–351, doi:10.1111/j.1600-0889.2010.00473.x, 2010.

Ishidoya, S., Aoki, S., Goto, D., Nakazawa, T., Taguchi, S., and Patra, P. K.: Time and Space variations of O_2/N_2 ratio in the troposphere over Japan and estimation of the global CO_2 budget for the period 2000–2010, Tellus B, 64, 18964, doi:10.3402/tellusb.v64i0.18964, 2012.

Janssens, I. A., Freibauer, A., Ciais, P., Smith, P., Nabuurs, G.-J., Folberth, G., Schlamadinger, B., Hutjes, R. W. A., Ceulemans, R., Schulze, E.-D., Valentini, R., and Dolman, A. J.: Europe's terrestrial biosphere absorbs 7 to 12 % of European anthropogenic CO_2 emissions, Science 300, 1538–1542, 2003.

Jones, C. D. and Cox, P. M.: Modelling the volcanic signal in the atmospheric CO_2 record, Global Biogeochem. Cy., 15, 453–465, doi:10.1029/2000GB001281, 2001.

Jönsson, A. M., Schröder, M., Lagergren, F., Anderbrandt, O., and Smith, B.: Guess the impact of *Ips typographus* – an ecosystem modelling approach for simulating bark beetle outbreaks, Agr. Forest Meteorol., 166–167, 188–200, 2012.

Jung, M., Vetter, M., Herold, M., Churkina, G., Reichstein, M., Zaehle, S., Cias, P., Viovy, N., Bondeau, A., Chen, Y., Trusilova, K., Feser, F., and Heimann, M.: Uncertainties of modelling GPP over Europe: A systematic study on the effects of using different drivers and terrestrial biosphere models, Global Biogeochem. Cy., 21, GB4021, doi:10.1029/2006GB002915, 2007.

Jung, M., Reichstein, M., Margolis, H. A., Cescatti, A., Richardson A. D., Arain, M. A., Arneth, A., Bernhofer, C., Bonal, D., Chen J., Gianelle, D., Gobron, N., Kiely, G., Kutsch, W., Lasslop, G., Law, B. E., Lindroth, A., Merbold, L., Montagnani, L., Moors, E. J., Papale, D., Sottocornola, M., Vaccari, F., and Williams, C.: Global patterns of land-atmosphere fluxes of carbon dioxide, latent heat, and sensible heat derived from eddy covariance,

satellite, and meteorological observations, J. Geophys. Res., 116, G00J07, doi:10.1029/2010JG001566, 2011.

Kalnay, E., Kanamitsu, M., Kistler, R., Collins, W., Deaven, D., Gandin, L., Iredell, M., Saha, S., Woollen, J., Zhu, Y., Chelliah, M., Ebisuzaki, W., Higgins, W., Janowiak, J., Mo, K. C., Ropelewski, C., Wang, J., Leetmaa, A., Reynolds, R., Jenne, R., and Joseph, D.: The NCEP/NCAR 40-year reanalysis project, B. Am. Meteorol. Soc., 77, 437–471, 1996.

Keeling, C. D., Bacastow, R. B., Bainbridge, A. E., Ekdahl Jr, C. A., Guenther, P. R., Waterman, L. S., and Chinm J. F. S.: Atmospheric carbon dioxide variations at Mauna Loa observatory, Hawaii, Tellus, 28, 538–551, 1976.

Keeling, C. D., Whorf, T. P., Wahlen, M., and van der Plicht, J.: Interannual extremes in the rate of rise of atmospheric carbon dioxide since 1980, Nature, 375, 666–670, 1995.

Keenan, T., García, R., Friend, A. D., Zaehle, S., Gracia, C., and Sabate, S.: Improved understanding of drought controls on seasonal variation in Mediterranean forest canopy CO_2 and water fluxes through combined in situ measurements and ecosystem modelling, Biogeosciences, 6, 1423–1444, doi:10.5194/bg-6-1423-2009, 2009.

Keller, K. M., Joos, F., and Raible, C. C.: Time of emergence of trends in ocean biogeochemistry, Biogeosciences, 11, 3647–3659, doi:10.5194/bg-11-3647-2014, 2014.

Key, R. M., Kozyr, A., Sabine, C. L., Lee, K., Wanninkhof, R., Bullister, J. L., Feely, R. A., Millero, F. J., Mordy, C., and Peng, T.-H.: A global ocean carbon climatology: results from Global Data Analysis Project (GLODAP), Global Biogeochem. Cy., 18, GB4031, doi:10.1029/2004GB002247, 2004.

Khatiwala, S., Primeau, F., and Hall, T.: Reconstruction of the history of anthropogenic CO_2 concentrations in the ocean, Nature, 462, 346–349, doi:10.1038/nature08526, 2009.

Khatiwala, S., Tanhua, T., Mikaloff Fletcher, S., Gerber, M., Doney, S. C., Graven, H. D., Gruber, N., McKinley, G. A., Murata, A., Ríos, A. F., and Sabine, C. L.: Global ocean storage of anthropogenic carbon, Biogeosciences, 10, 2169–2191, doi:10.5194/bg-10-2169-2013, 2013.

Kriest, I., Khatiwala, S., and Oschlies, A.: Towards an assessment of simple global marine biogeochemical models of different complexity, Progr. Oceanogr., 86, 337–360, 2010.

Krinner, G., Viovy, N., de Noblet-Ducoudre, N., Ogee, J., Polcher, J., Friedlingstein, P., Ciais, P., Sitch, S., and Prentice, I. C.: A dynamic global vegetation model for studies of the coupled atmosphere-biosphere system, Global Biogeochem. Cy., 19, Gb1015, doi:10.1029/2003gb002199, 2005.

Kurz, W. A., Dymond, C. C., Stinson, G., Rampley, G. J., Neilson, E. T., Carroll, A. L., Ebata, T., and Safranyik, L.: Mountain pine beetle and forest carbon feedback to climate change, Nature, 452, 987–990, doi:10.1038/nature06777, 2008.

Lagergren, F., Jönsson, A. M., Blennow, K., and Smith, B.: Implementing storm damage in a dynamic vegetation model for regional applications in Sweden, Ecol. Model., 247, 71–82, 2012.

Large, W. G. and Yeager, S.: Diurnal to decadal global forcing for ocean and sea-ice models: The data sets and flux climatologies, NCAR Tech. Rep. TN-460 _STR, 105 pp., 2004.

Lawrence, D. M., Oleson, K. W., Flanner, M. G., Thornton, P. E., Swenson, S. C., Lawrence, P. J., Zeng, X., Yang, Z.-L., Levis, S., Sakaguchi, K., Bonan, G. B., and Slater, A. G.: Parameterization improvements and functional and structural advances in version 4 of the Community Land Model, J. Adv. Model. Earth Syst., 3, M03001, doi:10.1029/2011ms000045, 2011.

Lenton, A., Tilbrook, B., Law, R. M., Bakker, D., Doney, S. C., Gruber, N., Ishii, M., Hoppema, M., Lovenduski, N. S., Matear, R. J., McNeil, B. I., Metzl, N., Mikaloff Fletcher, S. E., Monteiro, P. M. S., Rödenbeck, C., Sweeney, C., and Takahashi, T.: Sea-air CO_2 fluxes in the Southern Ocean for the period 1990–2009, Biogeosciences, 10, 4037–4054, doi:10.5194/bg-10-4037-2013, 2013.

Le Quéré, C. L., Harrison, S. P., Colin Prentice, I. C., Buitenhuis, E. T., Aumont, O., Bopp, L., Claustre, H., Cotrim Da Cunha, L., Geider, R., Giraud, X., Klaas, C., Kohfeld, K. E., Legendre, L., Manizza, M., Platt, T., Rivkin, R. B., Sathyendranath, S., Uitz, J., Watson, A. J., and Wolf-Gladrow, D.: Ecosystem dynamics based on plankton functional types for global ocean biogeochemistry models, Glob. Change Biol., 11, 2016–2040, doi:10.1111/j.1365-2486.2005.1004.x, 2005.

Le Quéré, C, Rödenbeck, C., Buitenhuis, E. T., Conway, T. J., Langenfelds, R., Gomez, A., Labuschagne, C., Ramonet, M., Nakazawa, T., Metzl, N., and Gillett, N.: Saturation of the Southern ocean CO_2 sink due to recent climate change, Science, 316, 1735–1738, doi:10.1126/science.1136188, 2007.

Le Quéré C, Raupach M. R., Canadell, J. G., Marland, G., Bopp, L., Ciais, P., Conway, T. J., Doney, S. C., Feely, R. A., Foster P, Friedlingstein, P., Gurney, K., Houghton, R. A., House, J. I., Huntingford, C., Levy, P. E., Lomas, M. R., Majkut, J., Metzl, N., Ometto, J. P., Peters, G. P., Prentice, I. C., Randerson, J. T., Running, S. W., Sarmiento, J. L., Schuster, U., Sitch, S., Takahashi, T., Viovy, N., van der Werf , G. R., and Woodward, F. I.: Trends in the sources and sinks of carbon dioxide, Nat. Geosci., 2, 831–836, 2009.

Le Quéré, C., Takahashi, T., Buitenhuis, C. E., Rödenbeck, C., and Sutherland, S.: Impact of climate change and variability on the global oceanic sink of CO_2, Global Biogeochem. Cy., 24, GB4007, doi:10.1029/2009GB003599, 2010.

Le Quéré, C., Andres, R. J., Boden, T., Conway, T., Houghton, R. A., House, J. I., Marland, G., Peters, G. P., van der Werf, G. R., Ahlström, A., Andrew, R. M., Bopp, L., Canadell, J. G., Ciais, P., Doney, S. C., Enright, C., Friedlingstein, P., Huntingford, C., Jain, A. K., Jourdain, C., Kato, E., Keeling, R. F., Klein Goldewijk, K., Levis, S., Levy, P., Lomas, M., Poulter, B., Raupach, M. R., Schwinger, J., Sitch, S., Stocker, B. D., Viovy, N., Zaehle, S., and Zeng, N.: The global carbon budget 1959–2011, Earth Syst. Sci. Data, 5, 165–185, doi:10.5194/essd-5-165-2013, 2013.

Levy, P. E., Cannell, M. G. R., and Friend, A. D.: Modelling the impact of future changes in climate, CO_2 concentration and land use on natural ecosystems and the terrestrial carbon sink, Global Environ. Chang., 14, 21–30, 2004.

Lewis, S. L., Lopez-Gonzalez, G., Sonké, B., Affum-Baffoe, K., Baker, T. R., Ojo, L. O., Phillips, O. L., Reitsma, J. M., White, L., James, A., Comiskey, K., Djuikouo, M.-N., Ewango, C. E. N., Feldpausch, T. R., Hamilton, A. C., Gloor, M., Hart, T., Hladik, A., Lloyd, J., Lovett, J. C., Makana, J.-R., Malhi, Y., Mbago, F. M., Ndangalasi, H. J., Peacock, J., Peh, K. S.-H., Sheil, D., Sunderland, T., Swaine, M. D., Taplin, J., Taylor, D., Thomas, S. C., and Wöll, R. V. H.: Increasing carbon storage in intact African tropical forests, Nature, 457, 1003–1006, 2009a.

Lewis, S. L., Lloyd, J., Sitch, S., Mitchard, E. T. A., and Laurance, W. F.: Changing Ecology of Tropical Forests: Evidence and Drivers, Annu. Rev. Ecol. Evol. Syst., 40, 529–49, 2009b.

Lovenduski, N. S., Gruber, N., Doney, S. C., and Lima, I. D.: Enhanced CO_2 outgassing in the Southern Ocean from a positive phase of the Southern Annular Mode, Global Biogeochem. Cy. 21, GB2026, doi:10.1029/2006GB002900, 2007.

Lovenduski, N. S., Gruber, N., and Doney, S. C.: Toward a mechanistic understanding of the decadal trends in the Southern Ocean carbon sink, Global Biogeochem. Cy., 22, 1–9, 2008.

Lucht, W., Prentice, I. C., Myneni, R. B., Sitch, S., Friedlingstein, P., Cramer, W., Bousquet, P., Buermann, W., and Smith, B.: Climate control of the high-latitude vegetation greening trend and Pinatubo effect, Science, 296, 1687–1689, 2002.

Luo, Y. Q., Randerson, J. T., Abramowitz, G., Bacour, C., Blyth, E., Carvalhais, N., Ciais, P., Dalmonech, D., Fisher, J. B., Fisher, R., Friedlingstein, P., Hibbard, K., Hoffman, F., Huntzinger, D., Jones, C. D., Koven, C., Lawrence, D., Li, D. J., Mahecha, M., Niu, S. L., Norby, R., Piao, S. L., Qi, X., Peylin, P., Prentice, I. C., Riley, W., Reichstein, M., Schwalm, C., Wang, Y. P., Xia, J. Y., Zaehle, S., and Zhou, X. H.: A framework for benchmarking land models, Biogeosciences, 9, 3857–3874, doi:10.5194/bg-9-3857-2012, 2012.

Luyssaert, S., Abril, G., Andres, R., Bastviken, D., Bellassen, V., Bergamaschi, P., Bousquet, P., Chevallier, F., Ciais, P., Corazza, M., Dechow, R., Erb, K.-H., Etiope, G., Fortems-Cheiney, A., Grassi, G., Hartmann, J., Jung, M., Lathière, J., Lohila, A., Mayorga, E., Moosdorf, N., Njakou, D. S., Otto, J., Papale, D., Peters, W., Peylin, P., Raymond, P., Rödenbeck, C., Saarnio, S., Schulze, E.-D., Szopa, S., Thompson, R., Verkerk, P. J., Vuichard, N., Wang, R., Wattenbach, M., and Zaehle, S.: The European land and inland water CO_2, CO, CH_4 and N_2O balance between 2001 and 2005, Biogeosciences, 9, 3357–3380, doi:10.5194/bg-9-3357-2012, 2012.

Manning, A. C. and Keeling, R. F.: Global oceanic and land biota sinks from the Scripps atmospheric oxygen flask sampling network, Tellus B, 58B, 95–116, 2006.

Matear, R. J., Chamberlain, M. A., Sun, C. and Feng, M.: Climate change projection of the Tasman Sea from an Eddy-resolving Ocean Model, J. Geophys. Res.-Oceans, 118, 2961–2976, doi:10.1002/jgrc.20202, 2013.

Matsumoto, K. and Gruber, N.: How accurate is the estimation of anthropogenic carbon in the ocean?, An evaluation of the DC* method, Global Biogeochem. Cy., 19, GB3014, doi:10.1029/2004GB002397, 2005.

McDonald, K. C., Kimball, J. S., Njoke, E., Zimmermann, R., and Zhao, M.: Variability in springtime thaw in the terrestrial high latitudes: monitoring a major control on the biospheric assimilation of atmospheric CO_2 with spaceborne microwave remote sensing, Earth Interact., 8, 1–23, 2004.

McDowell, N. G, Pockman, W. T., Allen, C. D., Breshears, D. D., Cobb, N., Kolb, T., Plaut, J., Sperry, J., West, A., Williams, D. G., and Yepez, E. A.: Mechanisms of plant survival and mortality during drought: why do some plants survive while others succumb to drought?. New Phytol., 178, 719–739, 2008.

McGillicuddy Jr, D. J., Robinson, A. R., Siegel, D. A., Jannasch, H. W., Johnson, R., Dickey, T. D., McNeil, J., Michaels, A. F., and Knap, A. H.: Influence of mesoscale eddies on new production in the Sargasso Sea, Nature, 394, 263–266, 1998.

McGuire, A. D., Christensen, T. R., Hayes, D., Heroult, A., Euskirchen, E., Kimball, J. S., Koven, C., Lafleur, P., Miller, P. A., Oechel, W., Peylin, P., Williams, M., and Yi, Y.: An assessment of the carbon balance of Arctic tundra: comparisons among observations, process models, and atmospheric inversions, Biogeosciences, 9, 3185–3204, doi:10.5194/bg-9-3185-2012, 2012.

McKinley, G. A., Takahashi, T., Buitenhuis, E., Chai, F., Christian, J. R., Doney, S. C., Jiang, M.-S., Le Quéré, C., Lima, I., Linday, K., Moore, J. K., Murtugudde, R., Shi, L., and Wetzel, P.: North Pacific carbon cycle response to climate variability on seasonal to decadal timescales. J. Geophys. Res., 111, C07S06, doi:10.1029/2005JC003173, 2006.

McKinley, G. A., Fay, A. R., Takahashi, T., and Metzl, N: Convergence of atmospheric and North Atlantic carbon dioxide trends on multidecadal timescales, Nat. Geosci, 4, 606–610, doi:10.1038/NGEO1193, 2011.

McNeil, B. I. and Matear, R. J.: The non-steady state oceanic CO_2 signal: its importance, magnitude and a novel way to detect it, Biogeosciences, 10, 2219–2228, doi:10.5194/bg-10-2219-2013, 2013.

Mercado, L. M., Bellouin, N., Sitch, S., Boucher, O., Huntingford, C., and Cox, P. M.: Impact of Changes in Diffuse Radiation on the Global Land Carbon Sink, Nature, 458, 1014–1017, 2009.

Mikaloff Fletcher, S. E., Gruber, N., Jacobson, A. R., Doney, S. C., Dutkiewicz, S., Gerber, M., Follows, M., Joos, F., Lindsay, K., Menemenlis, D., Mouchet, A., Müller, S. A., and Sarmiento, J. L.: Inverse estimates of anthropogenic CO_2 uptake, transport, and storage by the oceans, Global Biogeochem. Cy., 20, GB2002, doi:10.1029/2005GB002530, 2006.

Morales, P., Sykes, M. T., Prentice, I. C., Smith, P., Smith, B., Bugmann, H., Zierl, B., Friedlingstein, P., Viovy, N., Sabaté, S., Sánchez, A., Pla, E., Gracia, C. A., Sitch, S., Arneth, A., and Ogee, J.: Comparing and evaluating process-based ecosystem model predictions of carbon and water fluxes in major European forest biomes, Glob. Change Biol., 11, 2211–2233, doi:10.1111/j.1365-2486.2005.01036.x, 2005.

Myneni, R. B., Keeling, C. D., Tucker, C. J., Asrar, G., and Nemani, R. R.: Increased plant growth in the northern high latitudes from 1981 to 1991, Nature, 386, 698–702, doi:10.1038/386698a0, 1997.

Murray-Tortarolo, G., Anav, A., Friedlingstein, P., Sitch, S., Piao, S., Zhu, Z., Poulter, B., Zaehle, S., Ahlstrom, A., Lomas, M., Levis, S., Viovy, N., and Zeng, N.: Evaluation of DGVMs in reproducing satellite derived LAI over the Northern Hemisphere, Part I: Uncoupled DGVMs, Remote Sens., 5, 4819–4838; doi:10.3390/rs5104819, 2013.

Müller, S. A., Joos, F., Plattner, G.-K., Edwards, N. R., and Stocker, T. F.: Modeled natural and excess radiocarbon: Sensitivities to the gas exchange formulation and ocean transport strength, Global Biogeochem. Cy., 22, doi:10.1029/2007GB003065, 2008.

Nemani, R. R., Keeling, C. D., Hashimoto, H., Jolly, W. M., Piper, S. C., Tucker, C. J., Myneni, R. B., and Running, S. W.: Climate-driven increases in global terrestrial net primary production from 1982 to 1999, Science, 300, 1560–1563, 2003.

New, M. G., Hulme, M., and Jones, P. D.: Representing twentieth-century space-climate variability, Part II, Development of 1901–1996 monthly grids of terrestrial surface climate, J. Climate, 13, 2217–2238, 2000.

Norby, R. J., DeLucia, E. H., Gielen, B., Calfapietra, C., Giardina, C. P., King, J. S., Ledford, J., McCarthy, H. R., Moore, D. J. P., Ceulemans, R., De Angelis, P., Finzi, A. C., Karnosky, D. F., Kubiske, M. E., Lukac, M., Pregitzer, K. S., Scarascia-Mugnozza, G. E., Schlesinger, W. H., and Oren, R.: Forest response to elevated CO2 is conserved across a broad range of productivity, P. Natl. Acad. Sci. USA, 102, 18052–18056, 2005.

Norby, R. J., Warren, J. M., Iversen, C. M., Medlyn, B. E., and McMurtrie, R. E.: CO_2 enhancement of forest productivity constrained by limited nitrogen availability, P. Natl. Acad. Sci., 107, 19368–19373, 2010.

Oleson, K. W., Lawrence, D. M., Bonan, G. B., Flanner, M. G., Kluzek, E., Lawrence, P. J., Levis, S., Swenson, S. C., and Thornton, P. E.: Technical description of version 4.0 of the Community Land Model (CLM), NCAR Tech. Note NCAR/TN-478+STR, 257 pp., 2010.

Pacala, S. W., Hurtt, G. C., Baker, D., Peylin, P., Houghton, R. A., Birdsey, R. A., Heath, L., Sundquist, E. T., Stallard, R. F., Ciais, P., Moorcroft, P., Caspersen, J. P., Shevliakova, E., Moore B., Kohlmaier, G., Holland, E., Gloor, M., Harmon, M. E., Fan, S.-M., Sarmiento, J. L., Goodale, C. L., Schimel, D., and Field, C. B.: Consistent land- and atmosphere-based US carbon sink estimates, Science, 292, 2316–2320, 2001.

Pan, Y., Birdsey, R.A., Fang, J., Houghton, R., Kauppi, P. E., Kurz, W. A., Phillips, O. L., Shvidenko, A., Lewis, S. L., Canadell, J. G., Ciais, P., Jackson, R. B., Pacala, S., McGuire, A. D., Piao, S., Rautiainen, A., Sitch, S., Hayes, D., and Watson, C.: A large and persistent carbon sink in the World's forests, 1990–2007, Science, doi:10.1126/science.1201609, 2011.

Park, G.-H., Wanninkhof, R., Doney, S. C., Takahashi, T., Lee, K., Feely, R. A., Sabine, C. L., Triñanes, J., and Lima, I. D.: Variability of global net sea-air CO_2 fluxes over the last three decades using empirical relationships, Tellus B, 62, 352–368, 2010.

Patra, P. K., Canadell, J. G., Houghton, R. A., Piao, S. L., Oh, N.-H., Ciais, P., Manjunath, K. R., Chhabra, A., Wang, T., Bhattacharya, T., Bousquet, P., Hartman, J., Ito, A., Mayorga, E., Niwa, Y., Raymond, P. A., Sarma, V. V. S. S., and Lasco, R.: The carbon budget of South Asia, Biogeosciences, 10, 513–527, doi:10.5194/bg-10-513-2013, 2013.

Peacock, S.: Debate over the ocean bomb radiocarbon sink: Closing the gap, Global Biogeochem. Cy., 18, GB2022, doi:10.1029/2003GB002211, 2004.

Peng S., Ciais, P., Chevallier, F., Peylin, P., Cadule, P., Sitch, S., Piao, S., Ahlström, A., Levy, P., Lomas, M., Poulter, B., Viovy, N., Wang, T., Zaehle, S., Zeng, N., Zhao, F. and Zhao, H.: Benchmarking the seasonal cycle of CO_2 fluxes simulated by terrestrial ecosystem models, Global Biogeochem. Cy., 29, doi:10.1002/2014GB004931, 2014.

Peylin, P., Bousquet, P., Le Quéré, C., Sitch, S., Friedlingstein, P., McKinley, G., Gruber, N., Rayner, P., and Ciais, P.: Multiple constraints on regional CO_2 flux variations over land and oceans, Global Biogeochem. Cy., 19, GB1011, doi:10.1029/2003GB002214, 2005.

Peylin, P., Law, R. M., Gurney, K. R., Chevallier, F., Jacobson, A. R., Maki, T., Niwa, Y., Patra, P. K., Peters, W., Rayner, P. J., Rödenbeck, C., van der Laan-Luijkx, I. T., and Zhang, X.: Global atmospheric carbon budget: results from an ensemble of atmospheric CO_2 inversions, Biogeosciences, 10, 6699–6720, doi:10.5194/bg-10-6699-2013, 2013.

Pfeil, B., Olsen, A., Bakker, D. C. E., Hankin, S., Koyuk, H., Kozyr, A., Malczyk, J., Manke, A., Metzl, N., Sabine, C. L., Akl, J., Alin, S. R., Bates, N., Bellerby, R. G. J., Borges, A., Boutin, J., Brown, P. J., Cai, W.-J., Chavez, F. P., Chen, A., Cosca, C., Fassbender, A. J., Feely, R. A., González-Dávila, M., Goyet, C., Hales, B., Hardman-Mountford, N., Heinze, C., Hood, M., Hoppema, M., Hunt, C. W., Hydes, D., Ishii, M., Johannessen, T., Jones, S. D., Key, R. M., Körtzinger, A., Landschützer, P., Lauvset, S. K., Lefèvre, N., Lenton, A., Lourantou, A., Merlivat, L., Midorikawa, T., Mintrop, L., Miyazaki, C., Murata, A., Nakadate, A., Nakano, Y., Nakaoka, S., Nojiri, Y., Omar, A. M., Padin, X. A., Park, G.-H., Paterson, K., Perez, F. F., Pierrot, D., Poisson, A., Ríos, A. F., Santana-Casiano, J. M., Salisbury, J., Sarma, V. V. S. S., Schlitzer, R., Schneider, B., Schuster, U., Sieger, R., Skjelvan, I., Steinhoff, T., Suzuki, T., Takahashi, T., Tedesco, K., Telszewski, M., Thomas, H., Tilbrook, B., Tjiputra, J., Vandemark, D., Veness, T., Wanninkhof, R., Watson, A. J., Weiss, R., Wong, C. S., and Yoshikawa-Inoue, H.: A uniform, quality controlled Surface Ocean CO_2 Atlas (SOCAT), Earth Syst. Sci. Data, 5, 125–143, doi:10.5194/essd-5-125-2013, 2013.

Phillips, O. L., Malhi, Y., Higuchi, N., Laurance, W. F., Nunez, P. V., Vasquez, R. M., Laurance, S. G., Ferreira, L. V., Stern, M., Brown, S., and Grace, J.: Changes in the carbon balance of tropical forests: Evidence from long-term plots, Science, 282, 439–442, 1998.

Piao, S. L., Fang, J. Y., Ciais, P., Peylin, P., Huang, Y., Sitch, S., and Wang, T: The carbon balance of terrestrial ecosystems in China, Nature, 458, 1009–1014, 2009.

Piao, S. L., Sitch, S., Ciais, P., Friedlingstein, P., Peylin, P., Wang, X. H., Ahlström, A., Anav, A., Canadell, J. G., Huntingford, C., Jung, M., Levis, S., Levy, P. E., Li, J. S., Lin, X., Lomas, M. R., Lu, M ., Luo, Y. Q., Ma, Y. C., Myneni, R. B., Poulter, B., Sun, Z. Z., Wang, T., Viovy, N., Zaehle, S., and Zeng, N.: Evaluation of terrestrial carbon cycle models for their response to climate variability and to CO_2 trends, Glob. Change Biol., 19, 2117–2132, 2013.

Pongratz, J., Reick, C. H., Houghton, R. A., and House, J. I.: Terminology as a key uncertainty in net land use and land cover change carbon flux estimates, Earth Syst. Dynam., 5, 177–195, doi:10.5194/esd-5-177-2014, 2014.

Poulter, B., Frank, D. C., Hodson, E. L., and Zimmermann, N. E.: Impacts of land cover and climate data selection on understanding terrestrial carbon dynamics and the CO_2 airborne fraction, Biogeosciences, 8, 2027–2036, doi:10.5194/bg-8-2027-2011, 2011.

Poulter, B., Pederson, N., Liu, H., Zhu, Z., D'Arrigo, R., Ciais, P., Davi, N., Frank, D., Leland, C., Myneni, R., Piao, S., and Wang, T.: Recent trends in Inner Asian forest dynamics to temperature and precipitation indicate high sensitivity to climate change, Agr. Forest Meteorol., 178–179, 31–45, 2013.

Poulter, B., Frank, D., Ciais, P., Myneni, R., Andela, N., Bi, J., Broquet, G., Canadell, J. G., Chevallier, F., Liu, Y. Y., Running, S. W., Sitch, S. and van der Werf, G. R.: Contribution of semi-arid ecosystems to interannual variability of the global carbon cycle, Nature, doi:10.1038/nature13376, 2014.

Prentice I. C., Farquhar, G. D., Fasham, M. J. R., Goulden, M. L., Heimann, M., Jaramillo, V.J., Kheshgi, H. S., Le Quere, C., Scholes, R. J., Wallace, D. W. R., Contributing Authors Archer, D., Ashmore, M. R., Aumont, O., Baker, D., Battle, M., Bender,

M., Bopp, L. P., Bousquet, P., Caldeira, K., Ciais, P., Cox, P. M., Cramer, W., Dentener, F., Enting, I. G., Field, C. B., Friedlingstein, P., Holland, E. A., Houghton, R. A., House, J. I., Ishida, A., Jain, A. K., Janssens, I. A., Joos, F., Kaminski, T., Keeling, C. D., Keeling, R. F., Kicklighter, D. W., Kohfeld, K. E., Knorr, W., Law, R., Lenton, T. , Lindsay, K., Maier-Reimer, E., Manning, A. C., Matear, R. J., McGuire, A. D., Melillo, J. M., Meyer, R., Mund, M., Orr, J. C., Piper, S., Plattner, K., Rayner, P. J., Sitch, S., Slater, R., Taguchi, S. , Tans, P. P., Tian, H. Q., Weirig, M. F., Whorf, T., and Yool, A.: The carbon cycle and atmospheric carbon dioxide, in. Climate Change 2001: The Scientific Basis edited by: Houghton, J. T., Cambridge Univ. Press, New York, 183–237, 2001.

Prentice, I. C., Bondeau, A., Cramer, W., Harrison, S. P., Hickler, T., Lucht, W., Sitch, S., Smith, B., and Sykes, M. T.: Terrestrial Ecosystems in a changing world, IGBP Book Series, edited by: Canadell. J., Pitelka, L., and Pataki, D., Springer, Heidelberg, Germany, pp. 336, 2007.

Quaife, T., Quegan, S., Disney, M., Lewis, P., Lomas, M. R., and Woodward, F. I.: Impact of land cover uncertainties on estimates of biospheric carbon fluxes, Global Biogeochem. Cy., 22, GB4016, doi:10.1029/2007GB003097, 2008.

Randerson, J. T., Hoffman, F. M., Thornton, P. E., Mahowald, N. M., Lindsay, K., Lee, Y.-H., Nevison, C. D., Doney, S. C., Bonan, G., Stoeckli, R., Covey, C., Running, S. W., and Fung, I. Y.: Systematic assessment of terrestrial biogeochemistry in coupled climate-carbon models, Glob. Change Biol., 15, 2462–2484, 2009.

Raupach, M. R., Canadell, J. G., and Le Quéré, C.: Anthropogenic and biophysical contributions to increasing atmospheric CO2 growth rate and airborne fraction, Biogeosciences, 5, 1601–1613, doi:10.5194/bg-5-1601-2008, 2008.

Raupach, M. R., Gloor, M., Sarmiento, J. L., Canadell, J. G., Frölicher, T. L., Gasser, T., Houghton, R. A., Le Quéré, C., and Trudinger, C. M.: The declining uptake rate of atmospheric CO_2 by land and ocean sinks, Biogeosciences, 11, 3453–3475, doi:10.5194/bg-11-3453-2014, 2014.

Reichstein, M., Bahn, M., Ciais, P., Frank, D., Mahecha, M. D., Seneviratne, S. I., Zscheischler, J., Beer, C., Buchmann, N., Frank, D. C., Papale, D., Rammig, A., Smith, P., Thonicke, K., van der Velde, M., Vicca, S., Walz, A., and Wattenbach, M.: Climate extremes and the carbon cycle, Nature, 500, 287–295, 2013.

Roy, T., Bopp, L., Gehlen, M., Schneider, B., Cadule, P., Frölicher, T. L., Segschneider, J., Tjiputra, J., Heinze, C., and Joos, F.: Regional Impacts of Climate Change and Atmospheric CO_2 on Future Ocean Carbon Uptake: A Multimodel Linear Feedback Analysis, J. Climate, 24, 2300–2318, 2011.

Sabine, C. S., Feely, R. A.., Gruber, N. , Key, R. M., Lee, K., Bullister, J. L., Wanninkhof, R., Wong, C. S., Wallace, D. W. R., Tilbrook, B., Millero, F. J., Peng, T.-H., Kozyr, A., Ono, T., and Rios, A. F.: The oceanic sink for anthropogenic CO_2, Science, 305, 367–371, 2004.

Sarmiento, J. L. and Gruber, N.: Sinks for anthropogenic carbon, Phys. Today, 55, 30–36, 2002.

Sarmiento, J. L. and Gruber, N.: Ocean Biogeochemical Dynamics, Princeton Univ. Press, 526 pp., 2006.

Sarmiento, J. L., Orr, J. C., and Siegenthaler, U.: A perturbation simulation of CO_2 uptake in an ocean general circulation model, J. Geophys. Res., 97, 3621–3645, 1992.

Sarmiento, J. L., Gloor, M., Gruber, N., Beaulieu, C., Jacobson, A. R., Mikaloff Fletcher, S. E., Pacala, S., and Rodgers, K.: Trends and regional distributions of land and ocean carbon sinks, Biogeosciences, 7, 2351–2367, doi:10.5194/bg-7-2351-2010, 2010.

Schuster, U., McKinley, G. A., Bates, N., Chevallier, F., Doney, S. C., Fay, A. R., González-Dávila, M., Gruber, N., Jones, S., Krijnen, J., Landschützer, P., Lefèvre, N., Manizza, M., Mathis, J., Metzl, N., Olsen, A., Rios, A. F., Rödenbeck, C., Santana-Casiano, J. M., Takahashi, T., Wanninkhof, R., and Watson, A. J.: An assessment of the Atlantic and Arctic sea-air CO_2 fluxes, 1990–2009, Biogeosciences, 10, 607–627, doi:10.5194/bg-10-607-2013, 2013.

Sitch, S., Smith, B., Prentice, I. C., Arneth, A., Bondeau, A., Cramer, W., Kaplan, J. O., Levis, S., Lucht, W., Sykes, M. T., Thonicke, K., and Venevsky, S.: Evaluation of ecosystem dynamics, plant geography and terrestrial carbon cycling in the LPJ dynamic global vegetation model, Glob. Change Biol., 9, 161–185, doi:10.1046/j.1365-2486.2003.00569.x, 2003.

Sitch, S., McGuire, A. D., Kimball, J., Gedney, N., Gamon, J., Engstrom, R., Wolf, A., Zhuang, Q., Clein, J. S., and McDonald, K. C.: Assessing the carbon balance of circumpolar arctic tundra using remote sensing and process modeling, Ecol. Appl., 17, 213–234, 2007a.

Sitch, S., Cox, P. M., Collins, W. J., and Huntingford., C.: Indirect radiative forcing of climate change through ozone effects on the land-carbon sink, Nature, 448, 791–794, doi:10.1038/nature06059, 2007b.

Sitch, S., Huntingford, C., Gedney, N., Levy, P. E., Lomas, M., Piao, S., Betts, R., Ciais, P., Cox, P., Friedlingstein, P., Jones, C. D., Prentice, I. C., and Woodward, F. I.: Evaluation of the terrestrial carbon cycle, future plant geography, and climate-carbon cycle feedbacks using 5 Dynamic Global Vegetation Models (DGVMs), Glob. Change Biol., 14 1–25, doi:10.1111/j.1365-2486.2008.01626.x, 2008.

Smith, B., Prentice, I. C., and Sykes, M. T.: Representation of vegetation dynamics in the modelling of terrestrial ecosystems: comparing two contrasting approaches within European climate space, Global Ecol. Biogeogr., 10, 621–637, 2001.

Sokolov, A. P., Kicklighter, D. W., Melillo, J. M., Felzer, B. S., Schlosser, C. A., and Cronin, T. W.: Consequences of considering carbon-nitrogen interactions on the feedbacks between climate and the terrestrial carbon cycle, J. Climate, 21, 3776–3796, doi:10.1175/2008JCLI2038.1, 2008.

Stocker, B. D., Feissli, F., Strassmann, K. M., Spahni, R., and Joos, F.: Past and future carbon fluxes from land use change, shifting cultivation and wood harvest, Tellus B, 66, 23188, doi:10.3402/tellusb.v66.23188, 2014.

Stephens, B. B., Gurney, K. R., Tans, P. P., Sweeney, C., Peters, W., Bruhwiler, L., Ciais, P., Ramonet, M., Bousquet, P., Nakazawa, T., Aoki, S., Machida, T., Inoue, G., Vinnichenko, N., Lloyd, J., Jordan, A., Heimann, M., Shibistova, O., Langenfelds, R. L., Steele, L. P., Francey, R. J., and Denning, A. S.: Weak northern and strong tropical land carbon uptake from vertical profiles of atmospheric CO_2, Science, 316, 1732–1735, 2007.

Sweeney, C., Gloor, E., Jacobson, A. R., Key, R. M., McKinley, G., Sarmiento, J. L., and Wanninkhof, R.: Constraining global air-sea gas exchange for CO_2 with recent bomb ^{14}C measurements, Global Biogeochem. Cycl., 21, GB2015, doi:10.1029/2006GB002784, 2007.

Takahashi, T., Sutherland, S. C., Wanninkhof, R., Sweeney, C., Feely, R. A., Chipman, D., Hales, B., Friederich, G., Chavez, F., Sabine, C., Watson, A., Bakker, D. C. E., Schuster, U., Metzl, N., Yoshikawa-Inoue, H., Ishii, M., Midorikawa, T., Nojiri, Y., Kortzinger, A., Steinhoff, T., Hoppema, M., Olafsson, J., Arnarson, T. S., Tilbrook, B., Johannessen, T., Olsen, A., Bellerby, R., Wong, C. S., Delille, B., Bates, N. R., and de Baar, H. J. W.: Climatological mean and decadal changes in surface ocean pCO_2, and net sea-air CO2 flux over the global oceans, SOCOVV Symposium Volume, Deep Sea Res.-Pt. II, 810, 554–577, 2009.

Tans, P. P., Fung, I. Y., and Takahashi, T.: Observational constraints on the global atmospheric CO_2 budget, Science, 247, 1431–1439, doi:10.1126/science.247.4949.1431, 1990.

Thornton, P. E., Lamarque, J. F., Rosenbloom, N. A., and Mahowald, N. M.: Influence of carbon-nitrogen cycle coupling on land model response to CO_2 fertilization and climate variability, Global Biogeochem. Cy., 21, GB4018, doi:10.1029/2006GB002868, 2007.

Thornton, P. E., Doney, S. C., Lindsay, K., Moore, J. K., Mahowald, N., Randerson, J. T., Fung, I., Lamarque, J.-F., Feddema, J. J., and Lee, Y.-H.: Carbon-nitrogen interactions regulate climate-carbon cycle feedbacks: results from an atmosphere-ocean general circulation model, Biogeosciences, 6, 2099–2120, doi:10.5194/bg-6-2099-2009, 2009.

Tjiputra, J. F., Assmann, K., and Heinze, C.: Anthropogenic carbon dynamics in the changing ocean, Ocean Science, 6, 605–614, 2010.

Tucker, C. J., Slayback, D. A., Pinzon, J. E., Los, S. O., Myneni, R. B., and Taylor, M. G.: Higher northern latitude normalized difference vegetation index and growing season trends from 1982 to 1999, Int. J. Biometeorol., 45, 184–190, 2001.

Valentini, R., Arneth, A., Bombelli, A., Castaldi, S., Cazzolla Gatti, R., Chevallier, F., Ciais, P., Grieco, E., Hartmann, J., Henry, M., Houghton, R. A., Jung, M., Kutsch, W. L., Malhi, Y., Mayorga, E., Merbold, L., Murray-Tortarolo, G., Papale, D., Peylin, P., Poulter, B., Raymond, P. A., Santini, M., Sitch, S., Vaglio Laurin, G., van der Werf, G. R., Williams, C. A., and Scholes, R. J.: A full greenhouse gases budget of Africa: synthesis, uncertainties, and vulnerabilities, Biogeosciences, 11, 381–407, doi:10.5194/bg-11-381-2014, 2014.

Van der Molen, M. K., Dolman, A. J., Ciais, P., Eglin, T., Gobron, N., Law, B. E., Meir, P., Peters, W., Phillips, O. L., Reichstein, M., Chen, T., Dekker, S. C., Doubková, M., Friedl, M. A., Jung, M., van den Hurk, B. J. J. M., de Jeu, R. A. M., Kruijt, B., Ohta, T., Rebel, K. T., Plummer, S., Seneviratne, S. I., Sitch, S., Teuling, A. J., van der Werf, G. R., and Wang, G.: Drought and ecosystem carbon cycling, Agr. Forest Meteorol., 151, 765–773, doi:10.1016/j.agrformet.2011.01.018, 2011.

Vitousek, P. M. and Howarth, R. W.: Nitrogen limitation on land and in the sea: How can it occur?, Biogeochemistry, 13, 87–115, 1991.

Wang, Y. P., Law, R. M., and Pak, B.: A global model of carbon, nitrogen and phosphorus cycles for the terrestrial biosphere, Biogeosciences, 7, 2261–2282, doi:10.5194/bg-7-2261-2010, 2010.

Wanninkhof, R.: Relationship between wind speed and gas exchange over the ocean, J. Geophys. Res., 97, 7373–7382, 1992.

Wanninkhof, R., Park, G. -H., Takahashi, T., Sweeney, C., Feely, R., Nojiri, Y., Gruber, N., Doney, S. C., McKinley, G. A., Lenton, A., Le Quéré, C., Heinze, C., Schwinger, J., Graven, H., and Khatiwala, S.: Global ocean carbon uptake: magnitude, variability and trends, Biogeosciences, 10, 1983–2000, doi:10.5194/bg-10-1983-2013, 2013.

Woodward, F. I. and Lomas, M. R.: Vegetation-dynamics-simulating responses to climate change, Biological Reviews, 79, 643–670, 2004.

Woodward, F. I., Smith, T. M., Emanuel, W. R.: A global land primary productivity and phytogeography model. Global Biogeochem. Cy., 9, 471–490, 1995.

Zaehle, S. and Friend, A. D.: Carbon and nitrogen cycle dynamics in the O-CN land surface model, I: Model description, site- scale evaluation and sensitivity to parameter estimates, Global Biogeochem. Cy., 24, GB1005, doi:10.1029/2009GB003521, 2010.

Zaehle, S. and Dalmonech, D.: Carbon – nitrogen interactions on land at global scales: current understanding in modeling climate biosphere feedbacks, Current Opinion in Environmental Sustainability, 3, 311–320, 2011.

Zaehle, S., Friedlingstein, P., and Friend, A. D.: Terrestrial nitrogen feedbacks may acccelerate future climate change, Geophys. Res. Lett., 37, L01401, doi:10.1029/2009GL041345, 2010.

Zaehle, S., Ciais, P., Friend, A. D., and Prieur, V.: Carbon benefits of anthropogenic reactive nitrogen offset by nitrous oxide emissions, Nat. Geosci., 4, 601–605, doi:10.1038/ngeo1207, 2011.

Zaehle, S., Medlyn, B. E., De Kauwe, M. G., Walker, A. P., Dietze, M. C., Hickler, T., Luo, Y., Wany, Y.-P., El-Masri, B., Thornton, P., Jain, A., Wang, S., Warlind, D., Weng, E., Parton, W., Iversen, C. M., Gallet-Budynek, A., McCarthy, H., Finzi, A., Hanson, P. J., Prentice, I. C., Oren, R., and Norby, R. J.: Evaluation of eleven terrestrial carbon-nitrogen cycle models against observations from two temperate Free-Air CO_2 Enrichment Studies, New Phytologist, 202, 803–822, doi:10.1111/nph.12697, 2014.

Zeng, N.: Glacial-interglacial atmospheric CO_2 change – The glacial burial hypothesis, Adv. Atmos. Sci., 20, 677–673, 2003.

Zeng, N., Mariotti, A., and Wetzel, P.: Terrestrial mechanisms of interannual CO_2 variability, Global Biogeochem. Cy., 19, GB1016, doi:10.1029/2004gb002273, 2005.

Zhang, Q., Wang, Y. P., Matear, R. J., Pitman, A. J., and Dai, Y. J.: Nitrogen and phosphorous limitations significantly reduce future allowable CO_2 emissions, Geophys. Res. Lett, 41, 632–637, doi:10.1002/2013GL058352, 2014.

Zhu, Z., Bi, J., Pan, Y., Ganguly, S., Anav, A., Xu, L., Samanta, A., Piao, S., Nemani, R. R., and Myneni, R. B.: Global Data Sets of Vegetation Leaf Area Index (LAI)3g and Fraction of Photosynthetically Active Radiation (FPAR)3g Derived from Global Inventory Modeling and Mapping Studies (GIMMS) Normalized Difference Vegetation Index (NDVI3g) for the Period 1981 to 2011, Remote Sens., 5, 927–948, 2013.

Zscheischler, J., Mahecha, M. D., von Buttlar, J., Harmeling, S., Jung, M., Rammig, A., Randerson, J. T., Schoelkopf, B., Seneviratne, S. I., Tomelleri, E., Zaehle, S., and Reichstein, M.: A few extreme events dominate global interannual variability in gross primary production, Environ. Res. Lett., 9, 035001, doi:10.1088/1748-9326/9/3/035001, 2014.

Chapter 5: Changes in dry season intensity is a key driver of regional NPP trends

5.1.1 Introducion

One of the effects of global warming is the acceleration of the hydrological cycle (Durack et al. 2013). This not only means greater water fluxes (Precipitation and evapotranspiration) but also more extreme seasonality (Chou et al. 2013). An additional effect is the increase of extreme climatic events, for example over recent decades several droughts occurred, such as the drought in the western USA of 2000–2004 (McDowell et al., 2008; Anderreg et al., 2012) and the 2003 summer heatwave in Europe (Ciais et al., 2005).

Soil moisture controls plant productivity, thus long-term changes in climate or extreme events may lead to changes in net primary productivity (NPP) and vegetation biomass. Nevertheless, the effects of changes in seasonal water availability on annual NPP and biomass over the globe remain remarkably undetermined. Particularly, because the focus of most drought indices is annual, which may obscure changes at a seasonal scale.

The objective of this chapter is to explore the relationship between changing seasonal dryness and vegetation productivity at a global scale over recent decades (1989-2005), over the 20th century and over this century.

5.1.2 Methods

Datasets: We used three different observational precipitation products, Evapotranspiration (ET) from the land-flux merged product (which contains data from 24 different ET estimates), ET from the TRENDY and CMIP5 models as well as NPP and vegetation biomass, Vertical Optical Depth (VOD) from satellite and NPP, ET and precipitation (P) from 10 long-term ecological research (LTER) sites and 16 Fluxnet sites.

Timeframe: We analysed three time periods. 1) 1989-2005 based on observational datasets, 2) 1901-2005 based on TRENDY and CMIP5 models and 3) 2006-2099 based on CMIP5 models.

Drought indices: We used two novel seasonal indices, the dry season length and the dry season intensity. The first was defined as the number of months per year where ET was higher than P, while the second is the cumulative value of ET-P as long as ET is higher than P.

Analysis: we compare the trend in dry season intensity (DSI) against by dry season length (DSL); this gave an estimate of the change in dryness by ecosystem type. We then compared the change in seasonality by ecosystem (DSI, wet season intensity (WSI) and annual E-P) to study the trend in seasonal and annual water fluxes. We then established the relationship between changing DSI and the trend in NPP and biomass. All the analysis was conducted for the same three time periods.

5.1.3 Results

We found that the trend in DSI increases linearly with DSL ($p=3e-23$, $r^2=0.67$). This slope means that over these 17 years (1989-2005) the dry season became more severe over arid and semi-arid ecosystems, but decreased in intensity over the wet regions. Over the dry regions this was driven mostly by an increase in the DSL, while in the wet regions the main driver was a higher P over the dry season.

Our results also showed that the trend in the dry and wet season tends to be opposite. This meant that at an annual scale E-P changes are 10 times smaller than at a seasonal scale. This implies that the widespread use of aggregated annual drought indices may be misrepresenting the changes in the hydrological cycle.

We linked the changes in DSI to the trend in NPP and biomass. We found that seasonal increase in dryness leads to a reduction in both NPP and biomass over the dry ecosystems and vice versa. In other words, seasonal DSI trends controls annual NPP trends. The mechanism behind this is the fact that DSI trends impact wet season NPP, while changes in the wet season had no link to dry season NPP. Therefore an increase in dryness has a much larger impact on vegetation productivity than an excess of water.

We presented the paper as it was submitted, but we moved the supplementary information into the main text it, to aid the visualization of the results. In adittion we moved the methodology from the end of the paper (as requested by the journal) to the middle of the paper, to make for an easier reading.

Changes in dry season intensity is a key driver of regional NPP trends

Murray-Tortarolo, Guillermo[1*]; Friedlingstein, Pierre[1]; Sitch, Stephen[2]; Seneviratne, Sonia[3]; Fletcher, Imogen[1]; Mueller, Brigitte[3,4]; Greve, Peter[3]; Anav, Alessandro[1]; Liu, Yi[5], Ahlström, Anders[6]; Huntingford, Chris[7]; Levis, Sam[8]; Levy Peter[9]; Lomas, Mark[10]; Poulter, Benjamin[11]; Viovy, Nicholas[12]; Zaehle, Sonke[13]; Zeng, Ning[14].

1) College of Engineering, Mathematics and Physical Sciences, University of Exeter, United Kingdom.
2) Collage of Life Sciences, University of Exeter, United Kingdom.
3) The Institute for Atmospheric and Climate Science, ETH Zürich, 8057 Zürich, Switzerland.
4) Environment Canada, Climate Research Division, Toronto M3H 5T4, Canada.
5) ARC Centre of Excellence for Climate Systems Science & Climate Change Research Centre, University of New South Wales, Sydney, New South Wales, Australia.
6) Lund University, Sölvegatan 12, SE–223 62 Lund
7) Centre for Ecology and Hydrology, Benson Lane, Wallingford OX10 8BB, UK
8) National Center for Atmospheric Research, Boulder, Colorado, USA
9) Centre for Ecology and Hydrology, Bush Estate, Penicuik, Midlothian EH26 0QB, UK
10) Department of Animal & Plant Sciences, University of Sheffield, Sheffield S10 2TN, UK
11) Laboratoire des Sciences du Climat et de l'Environnement, CEA CNRS UVSQ, 91191 Gif-sur-Yvette, France
12) Max Planck Institute for Biogeochemistry, P.O. Box 10 01 64, 07701 Jena, Germany
13) Department of Atmospheric and Oceanic Science, University of Maryland, College Park, MD 20740, USA
14) Karlsruhe Institute of Technology, Garmisch-Partenkirchen, Germany

Rising temperatures are expected to modify the global hydrological cycle, altering patterns of precipitation (P) and evapotranspiration (E)[1,2]. Seasonal variations in soil moisture, which affect the structure and function of global biomes, may therefore change with global warming[3]. Here we use a seasonal index, the dry season intensity, to estimate regional trends in water availability and link them to trends in annual net primary productivity (NPP) and biomass. We include an ensemble of 24 E datasets, results from 9 Dynamic Global Vegetation Models (DGVMs) and 16 Earth System Models (ESMs). Our analysis is conducted over three time-periods, 1) 1989-2005, 2) 1901-2005 and 3) the 21st Century. Results show a wetness (E-P) asymmetry in dry ecosystems, with dry seasons becoming drier and wet seasons wetter. These trends are projected to continue into the future with evidence that they are driven by climate change, however the impact of decadal variability cannot be excluded over the 1989-2005 period. Results show a negative correlation between the trend in the dry season intensity and the trends in annual biomass from satellite data and NPP from DGVMs at all time periods. Annual NPP in dry ecosystems is particularly sensitive to the length and intensity of the dry season, whereas an increase in precipitation during the wet season has little effect. We conclude that changes in the water availability over the dry season affect vegetation throughout the whole year, driving changes in regional NPP. Moreover, these results suggest that the widespread usage of drought indices aggregated at annual scales is insufficient for understanding the link between water availability and the land carbon cycle.

Global temperatures have risen over the last century due to anthropogenic greenhouse gas emissions. As a consequence of warming, fluxes of water in the atmosphere have increased, altering patterns of precipitation (P) and evapotranspiration (E)[3]. This has important effects on the water cycle[4-8], although long-term global trends in hydrological variables are difficult to distinguish from decadal variability[4–8], partly due to the uncertainty of the underlying observational datasets[9,10]. Nonetheless, some regional (or latitudinal) trends can be identified[11,12], and a global increase in the range between dry vs. wet season precipitation has been reported[2], particularly over the tropics[13].

Soil moisture controls plant photosynthesis, influences growth and mortality, and thus affects NPP and biomass[5,14,15]. There are several examples of this mechanistic relationship: The 2003 heat-wave and drought in Europe was responsible for a steep decline in NPP[16]; over the Amazon the dry season has increased leading to more fires and lower NPP[17]; and climate-driven drought was responsible for the continuous decrease in NPP over the Mongolian steppe[18]. Nevertheless, the effects of changes in seasonal water availability on annual NPP and biomass over the globe remain remarkably undetermined. This is partially due to a lack of observational data, but also because commonly employed drought indices may not necessarily best relate to changes in land biogeochemistry (e.g. Standard precipitation index –SPI- or Palmer Drought Severity Index –PDSI-) (Figure S1)[19].

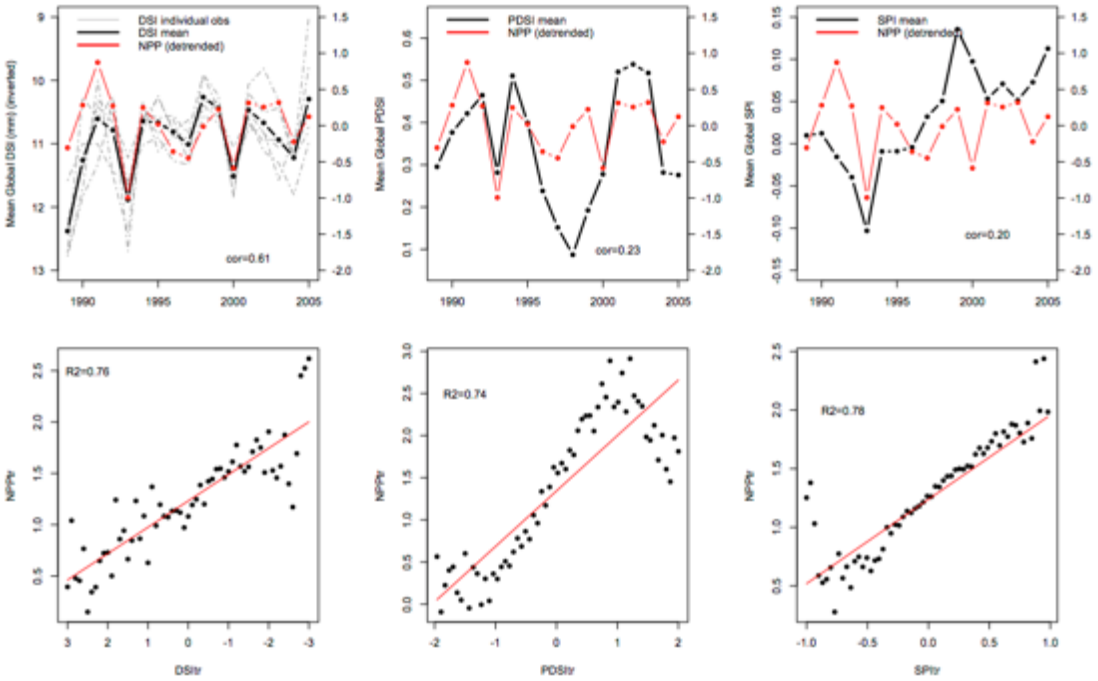

Figure S1. Timeseries of annual NPP and three global averaged drought indices DSI (left), PDSI (middle) and SPI (right) (top) and linear regression of trends for the same indices against binned NPP trends (bottom). Values for the temporal correlation and R^2 are given. While trends in all indices capture the trend in NPP correctly, there are clear differences in their ability to reproduce the IAV of NPP, with DSI showing the highest correlation.

The concept of dry season is common in the literature, yet there is no single definition. Some studies use a fixed time period to delimit dry seasons (e.g. driest or 6 month period)[20], while other definitions assume dry season length varies and are based on climate thresholds (e.g. the number of months that account for less than 30% of the rainfall)[17]. In order to investigate the link between changes in the availability of water contained in the land surface and NPP, we consider two seasonal indices based on net water fluxes, i.e. the difference between E and P. The first index is the dry season length (DSL), which is defined as the cumulative number of months in which E is larger than P over a year. The second index is the dry season intensity (DSI), defined as the cumulative value of E minus P during months when E is higher than P. The DSI is similar to the maximum climatological water deficit (MCWD) as defined by Mahli et al.[21], and applied for Amazonia, but rather than using calendar years, we allow for dry season to go over the end of a calendar year. Unlike the MCWD, we also allow E to vary, rather than fixing it at 100 mm / month, and we calculate it at a global scale. Both DSL and DSI are computed using observed

precipitation (mean of three products: CRU3.1[22], CPC[23] and GPCP[24]) and a product synthesizing E estimates from various sources[7].

Methods

Data

We use observed monthly precipitation (P) data from CRU3.1[22], CPC[23] and GPCP[24] for the two periods, 1989-2005 and 1901-2005. For the period 1989-2005, we use monthly evapotranspiration (E) from the landflux-merged product[7], which represents the ensemble of 24 different E datasets, and is the closest data available to observations. For the century timescale, 1901-2005, we use modeled monthly NPP and E from an ensemble of 9 DGVMs from the S2 (CO_2 + Climate) and S1 (CO_2 only) simulations of the TRENDY inter-comparison project[33] and also an ensemble from 16 ESMs from CMIP5[34]. The 0.25° annual passive microwave satellite-based vegetation optical depth (VOD) global product from 1989 to 2005 is used. VOD is an indicator of vegetation water content of aboveground biomass and able to capture long-term biomass changes over various land cover types at the global scale[18]. Monthly P, E and NPP for the period 2006-2100 were extracted from an ensemble of 16 CMIP5 ESMs from simulations for the future greenhouse gas pathway scenarios RCP2.6 and RCP8.5 (Table S1, Table S2).

All data were regridded to a common 1º x 1º grid. In order to remove especially low productivity / desert areas, a mask is applied whereby grid cells where NPP is less than 5% of mean global NPP are excluded.

Table S1. List of TRENDY-models used for the calculation of E, P and NPP over 1901-2005.

DGVMs	E	NPP S2 (climate +C02)	NPP S1 (CO_2 only)	Biomass (C Veg)
CLM4CN	X	X	X	X
HYLAND	X	X	X	X
LPJ	X	X	X	X
LPJ-GUESS	X	X	X	X
OCN	X	X	X	X
ORCHIDEE	X	X	X	X
SDGVM	X	X	X	X
TRIFFID	X	X	X	X
VEGAS	X	X	X	X

Table S2. List of CMIP5-models

ESMs	Historical Nat. 1901-2005	Historical 1901-2005	RCP2.6 2006-2100	RCP8.5 2006-2100
BCC-CSM1-1-M	n.a.	x	x	x
BCC-CSM1-1	x	x	x	x
BNU-ESM	x	x	x	x
CanESM2	x	x	x	x
CCSM4	x	x	x	x
GFDL-ESM2G	n.a.	x	x	x
GFDL-ESM2M	x	x	x	x
HadGEM2-ES	x	x	x	x
IPSL-CM5A-LR	x	x	x	x
IPSL-CM5A-MR	x	x	x	x
MIROC-ESM-CHEM	x	x	x	x
MIROC-ESM	x	x	x	x
MPI-ESM-LR	n.a.	x	x	x
MPI-ESM-MR	n.a.	x	x	x
NorESM1-ME	n.a.	x	x	x
NorESM1-M	x	x	x	x

Long-Term Ecological Research (Knapp and Smith, 2010): 10 sites, each sites contains unique methodology for the estimation of NPP (http://www.lternet.edu/node/144). We used data for the period 1989-1998 and calculated the NPP trend and DSI trend for each site. For the DSI calculation we used observed precipitation and ET from the landflux product for the nearest gridcell. We then calculated the trend in NPP for models and in VOD for the satellite for the same sites (nearest gridcell).

Fluxtowers (Anav et al. in progress): 16 sites, each site contains data for a period equal or shorter to 1990-2005, with an average of 6 years per site. GPP was calculated as the positive integral of the NEE flux for the summer months (JJA) for each year and we derived a linear trend. The DSI trend was computed for the same years (different for each site) based on the nearest grid. We then replicated the results with the DGVM NPP and Satellite VOD.

Dry season intensity and length

We used two indices of water availability:

- Dry Season Intensity (DSI) is computed as the time-integrated (in months) E minus P, for as long as the value is positive; when P>E, DSI becomes 0. Hence, as the number of consecutive months with water deficit increases, DSI becomes more positive. This is done allowing the integration to go across years, but DSI is defined as the maximum value for each year (i.e. in the event of two dry periods within a year). The same definition is used for Wet Season Intensity (WSI), but integrating while P is greater than E.
- Dry season length (DSL) is defined as the consecutive number of months where E>P (or when DSI is positive). There can be multiple dry seasons in one year. DSL is the sum across dry seasons for a given year.

Data analyses

DSI, DSL and WSI linear trends are calculated for each grid for the period 1989-2005 inclusive. In *Figure 1d*, the DSI trend is plotted against binned DSL values, by dividing DSL into 100 intervals (each size 3.65 days), so each point on the plot corresponds to the mean of all grids with the same DSL value. To calculate the error on the regression slope we run a bootstrap test randomly removing 20 per cent of the data and re-calculate its value; this procedure was replicated 1000 times. The results are plotted as “box and whiskers” format (*Figure 1e*). The same protocol is applied for the modeled data over the identical 17-year period, the 20th century and the two future scenarios.

For *Figure (left)* we calculate the range in the seasonal trends (WSI trend – DSI trend) and plot it by ecosystem type (arid: >6 months of DSL semi-arid: <6 and >3 months of DSL, and wet: <3 months of DSL). We also plotted the standard error as bars for each point. For *Figure (right)* we bin E-P trend over the dry season, wet season and annually against the DSL using the same procedure as in *Figure 1d* and plot a simple linear regressions for each. Values for the slope are shown.

For *Figure 3* the trend in NPP is calculated from the S2 run *(a*), and the biomass trends from the satellite product (*c*) for the period 1989-2005 for each

grid cell are plotted. Trends for both variables are binned by the DSI trends (*b* and *d*). The slope is calculated following the bootstrap procedure described above. We used the same procedure for the observed (TRENDY) and modeled climate (CMIP5) for the estimated effects of climate only (TRENDY S2 minusS1) over the whole century (1901-2005) and for the two future scenarios (2006-2100) (*Figure 3e*).

Finally for *Figure 4* we split the global annual NPP and season intensity into dry and wet seasons and calculate the trend for the period 1989-2005, plotting all possible data combinations as binned linear regressions. Each panel shows the global mean results.

For all figures m represents the slope of the linear regression and p the statistical significance.

Results and Discussion

The DSL closely corresponds to the distribution of global vegetation cover: evergreen (both broadleaf and needlleaf) forests coincide with areas of 0-3 months of dry season, dry forests and semi-arid ecosystems to those with 3-6 and arid ecosystems to those above 6 months **(Figure 1a**). DSL can be used as an index to aggregate ecosystems with similar phenological characteristics. DSI on the other hand represents an aridity gradient. Ecosystems that face the most severe water stress have the highest DSI values (**Figure 1b**). Sensitivity to drought (i.e. DSL) has been shown to be one of the main determinants of plant distribution in some tropical forests[25] and changes in the dry season intensity (DSI) can rapidly alter vegetation distribution.

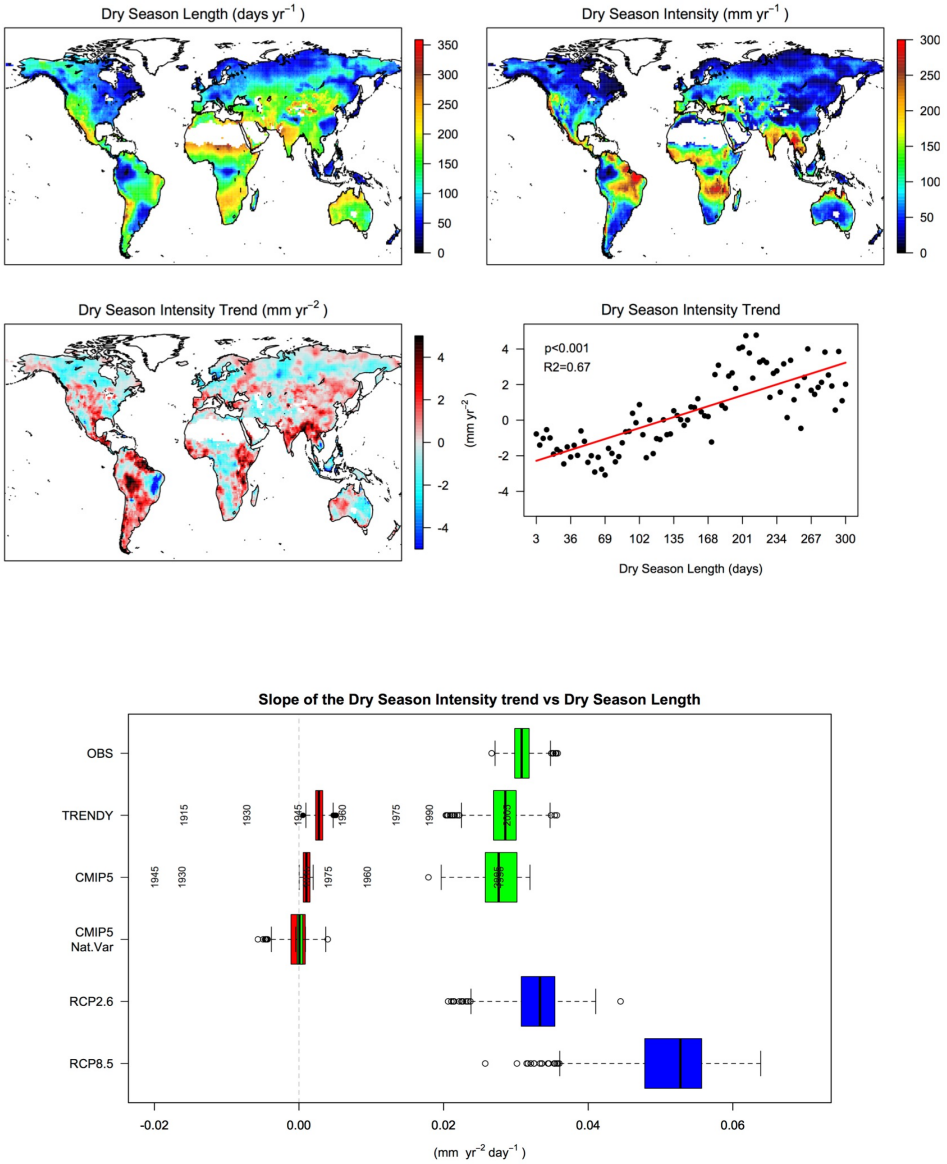

Figure 1. Annual average a) dry season length (days yr^{-1}) and b) dry season intensity (mm yr^{-1}) calculated during the period 1989-2005, c) Dry season intensity trend (mm yr^{-2}) during 1989-2005, d) binned dry season intensity trend plotted against dry season length, while the red line represents the linear regression through the data ($p<0.001$, $R^2=0.67$), e) median value for the regression slope of d) plus error, results from 1000 bootstrap simulations (box and whisker) for different datasets: observations, TRENDY-DGVMs, and CMIP5 ESMs (historical, natural forcing and two future RCPs). Green: 1989-2005, Red: 1901-2005, Blue: 2006-2100. In grey mean slope value for 15-years periods (last year).

When linear trends in DSI are calculated for the period 1989-2005 (for which more E estimates are available), clear regional patterns emerge (**Figure**

1c). We find an increase in DSI (i.e. it is getting drier) over Amazonia and many arid and semi-arid regions, including parts of temperate South-America, central USA and northern Mexico, the Mongolian steppe, eastern Africa, western Australia and eastern Asia. In contrast, a negative trend in DSI is found over the high northern latitudes, eastern Brazil and central Africa. Trends in DSI are correlated to trends in PDSI (r=0.75), soil moisture derived from the DGVMs (r=0.59) and soil moisture from satellite observations[26] (r=0.41), which shows consistency of the drying/wetting regions across the planet for this time period (Figure S2). This suggests that DSI can ultimately be used as a proxy of soil water availability and its trends, with the advantage of including ecologically meaningful units that clearly link to vegetation processes (i.e. change in NPP per mm of water deficit) and a better representation of the temporal evolution of NPP (Figure S1 and S2).

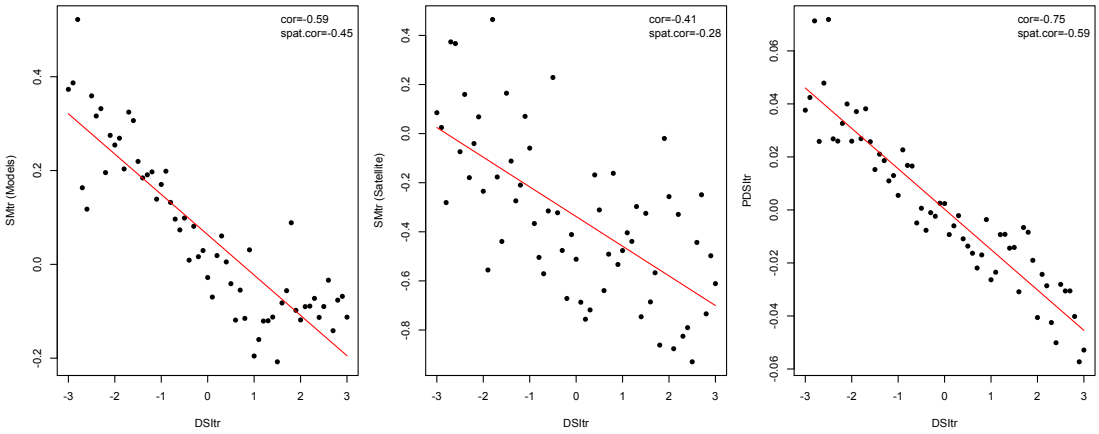

Figure S2. Binned relationship between the trend in DSI trend (1989-2005) and trends in soil moisture derived from models (left), soil moisture from satellite-retrievals (Dorigo et al. 2012) (middle) and PDSI trend (right). Values for the spatial and linear correlations are given. DSI trends closely resemble model-simulated soil moisture (SM) trends and PDSI trends, showing agreement of the wetting/drying regions globally.

The trend in DSI increases linearly with DSL (p=3e-23, r^2=0.67) (**Figure 1d 1989-2005**). This slope means that over these 17 years, the dry season became more severe over arid and semi-arid ecosystems, but decreased in intensity over the wet regions. However, because of the short timeframe this could be driven by the natural variability of the system. To rule this out we replicated the observed results using E calculated from 9 DGVMs to explore the

behavior of the system further back in the 20th century, as well as simulations from 16 CMIP5 models under natural and all (natural and anthropogenic combined) forcing. We plot the value for the slope and calculate its error based on 1000 bootstrap simulations using 80% of the data. For all cases a positive slope means that the dry season gets drier in regions of arid ecosystems than in areas where wet ecosystems are present. The same pattern was found in the observational-based products and models for the 17-year time period, with remarkably similar slope values (m=0.03 mm yr^{-2} day^{-1} of dry season) (**Figure 1e green**). Over the period 1901-2005 only a small change in intensity across ecosystems is observed, mostly driven by the last 30 years (**Figure 1e red**). However, when the century is split into 15-year intervals, the increased E-P imbalance during the dry season across wet and arid ecosystems becomes more evident in the 1989-2005 time-period. Over these 17 years the consistent trend in CMIP5 simulations under all forcing and the difference with the simulations under natural forcing suggest that the observed trend is unlikely to be driven by the natural variability of the Earth System but is rather an effect of anthropogenic climate change. The pattern is also similar for the two future scenarios: the less severe future scenario RCP2.6 (IPCC, 2014) revealed a similar slope to the present-day, in spite of temperature and precipitation stabilization at the end of the 21st century; while in the more extreme RCP8.5 scenario the slope was almost twice as strong (**Figure 1e blue**). Hence, both the recent observationally-based data and the model projections are found to display a similar tendency towards an increased DSI in regions with long DSL, although decadal variability could also play a role for the former given the limited length of the considered time period.

The change in DSI can be driven by an alteration of the DSL (change in length) or by a change on the distribution and magnitude of E and P during the dry season itself (change in the amplitude), or by both effects combined. To determine the possible causes of the change in DSI, we compare the DSL to its trend (change in length) and to the maximum monthly difference in E-P (change in amplitude) using the observational-based datasets for the period 1987-2005 (36). On average, DSL increased over the arid ecosystems, but they showed no change in the amplitude, indicating that the already short wet season has become even shorter, leading to higher water deficits during the dry season. In the semi-arid regions, DSL increased with decreased depth, but slightly higher

P occurred in the dry season. In the wet ecosystems we found no change in the length, but higher P than E during the dry season (Figure S3).

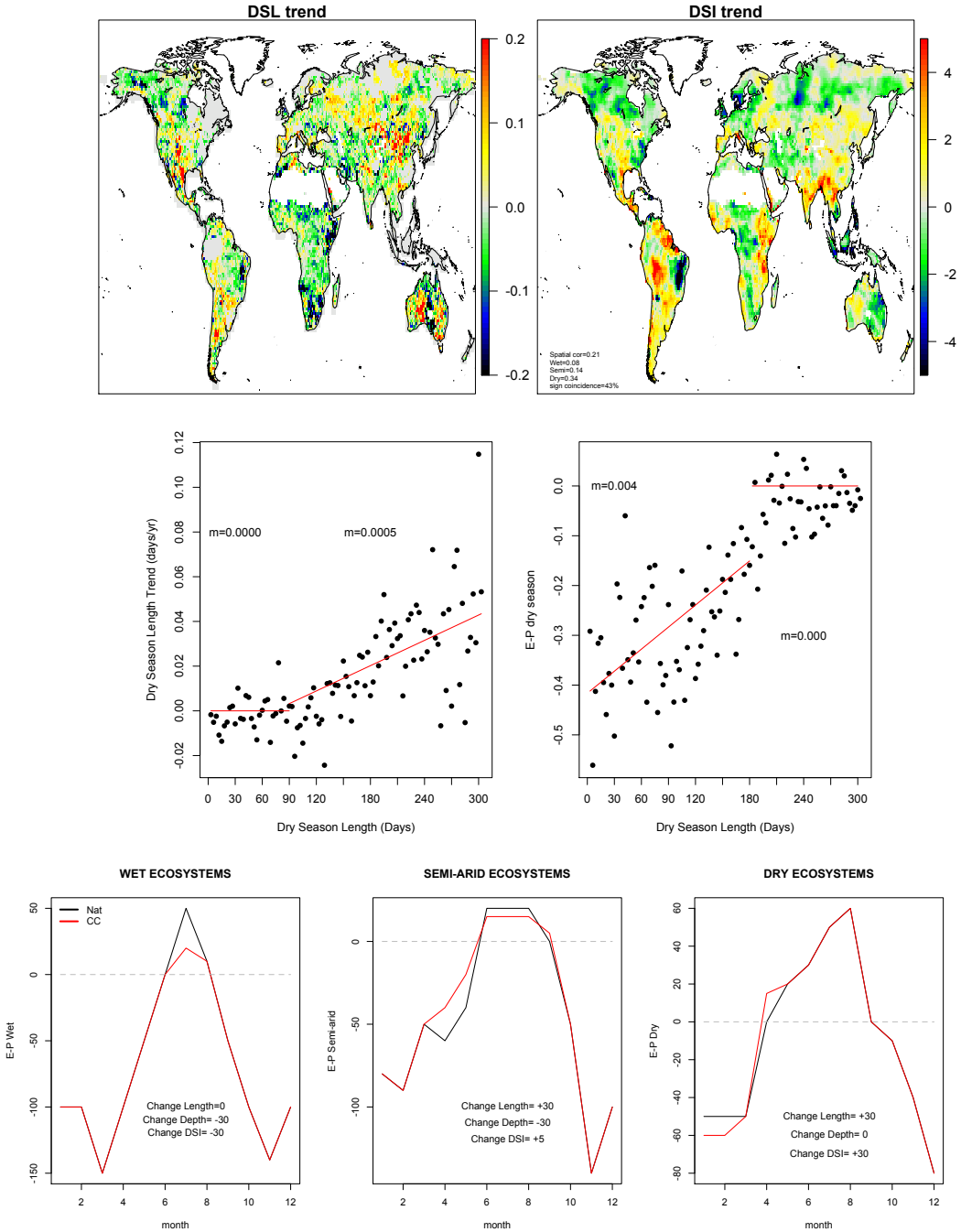

Figure S3. Top. Left: Dry season length trend. Right: Dry season intensity trend. **Middle.** Left: Change in the dry season length trend across ecosystems. Right: change in the depth (min P-E) of the season, dry ecosystem. **Bottom.** Change in length, depth and DSI by ecosystem type (wet, semi-arid and dry), with no climate change (as estimated from TRENDY for the period 1901-1915), black) and due to the effect of climate change (as estimated from TRENDY for the period 1989-2005). Changes in the dry season length are not always linked to changes in DSI. Globally those two trends have a spatial correlation of 0.21. For the wet ecosystems this relationship is only 0.08 and for the dry it is 0.034. It seems that the dry season in wet ecosystems remained equally longer, with decreased depth, leading to less intense DSI. In semi arid ecosystems both effects cancel each other out: longer dry seasons but decreased depth lead to

small changes in DSI. In the dry ecosystems the depth remained similar but we found longer dry seasons, which lead to an increase in DSI.

Variations in seasonality trends are also present during the wet season. However, arid and semi-arid ecosystems display an increase in seasonal range, while only small changes appear in the wet ecosystems. This explains why there is only a small difference across ecosystems when only annual E-P is used as an index. This increase in range between the dry (+0.003 mm/day) and the wet season (-0.0029 mm/day), translates to a zero-sum mean annual trend (-0.0001 mm/day) (**Figure 2, left panels**), potentially leading to the incorrect assessment that changes in E-P are generally small. In reality, we find that arid and semi-arid ecosystems face more extreme seasonality with more intense dry seasons, but they only display minor changes in annual mean E-P (**Figure right-hand column)**. This increased range has also been found by Kumar et al.[27] and by Cho et al.[2] at a global scale for precipitation and by Huntingford et al.[28] for temperature. However this is the first time this is explained by wet and arid regions.

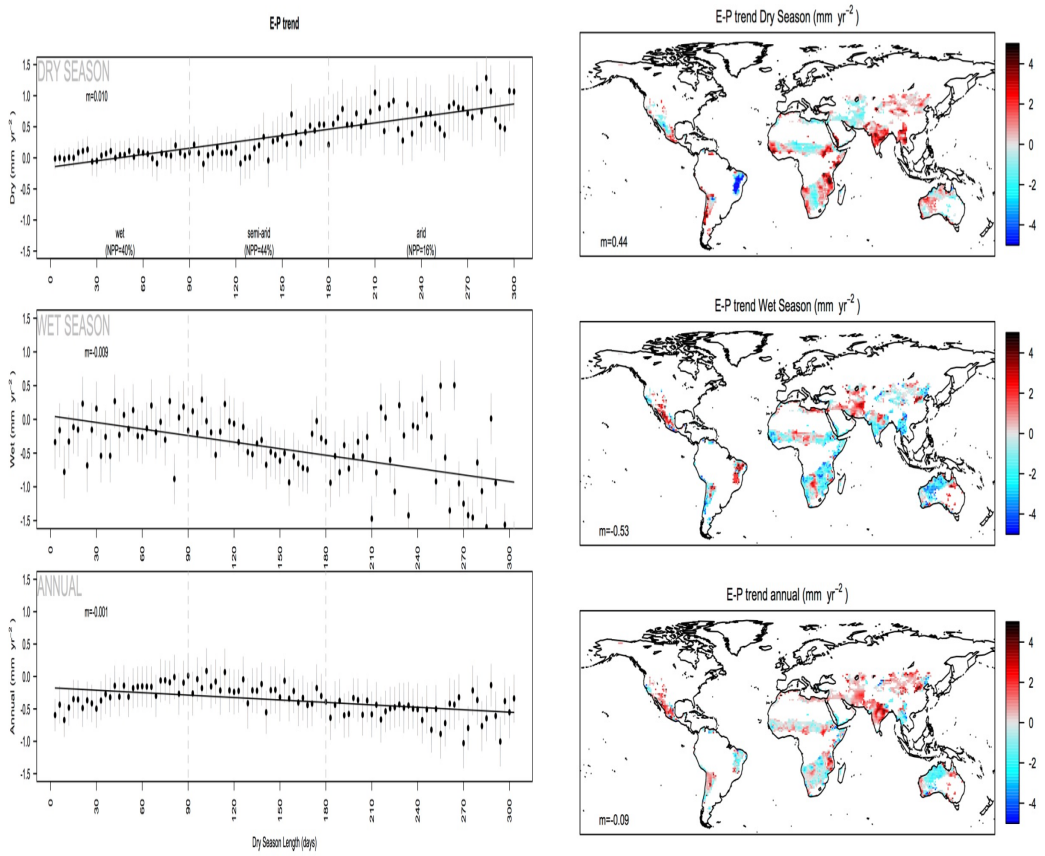

Figure 2. Left: E-P trend (mm yr^{-2}) binned by dry season length in the dry season (top), wet season (middle) and annual (bottom). Error bars (standard error) is shown as grey bars for each point. In parenthesis the percentage of NPP those ecosystems represent. A simple linear model was fitted to each plot and the slope value is presented (m), all slopes are statistically significant ($p<0.001$). Right: gridded E-P (mm yr^{-2}) trend by season in arid ecosystems, white areas represent other ecosystems.

As the dry season represents the maximum water deficifor vegetation, we hypothesize that this trend in dry season E-P imbalance between arid and wet ecosystems must also have an impact on vegetation productivity. We plotted the trend in NPP against the trend in DSI and found a high correlation between them (**Figure 3a**). We also found this linear relationship between DSI and modeled biomass and satellite-based vegetation changes (Vegetation Optical Depth (VOD) trends), for the period 1989-2005.

On the other hand, while NPP increased globally in all time periods (due to CO_2 fertilization), our results show smaller NPP trends and negative biomass trends in regions where DSI became more positive (**Figure 3bcd**). In other words, an increase in DSI leads to a decrease in vegetation productivity at a global scale but particularly over semi-arid and arid ecosystems. These results hold for different models, at smaller spatial scales (Figure S4) and when using observed data (Figure S5). This extends on the argument of Poulter et al.[29] showing a large contribution of arid and semi-arid ecosystems to the interannual variability of the C-cycle, driven by patterns we show above.

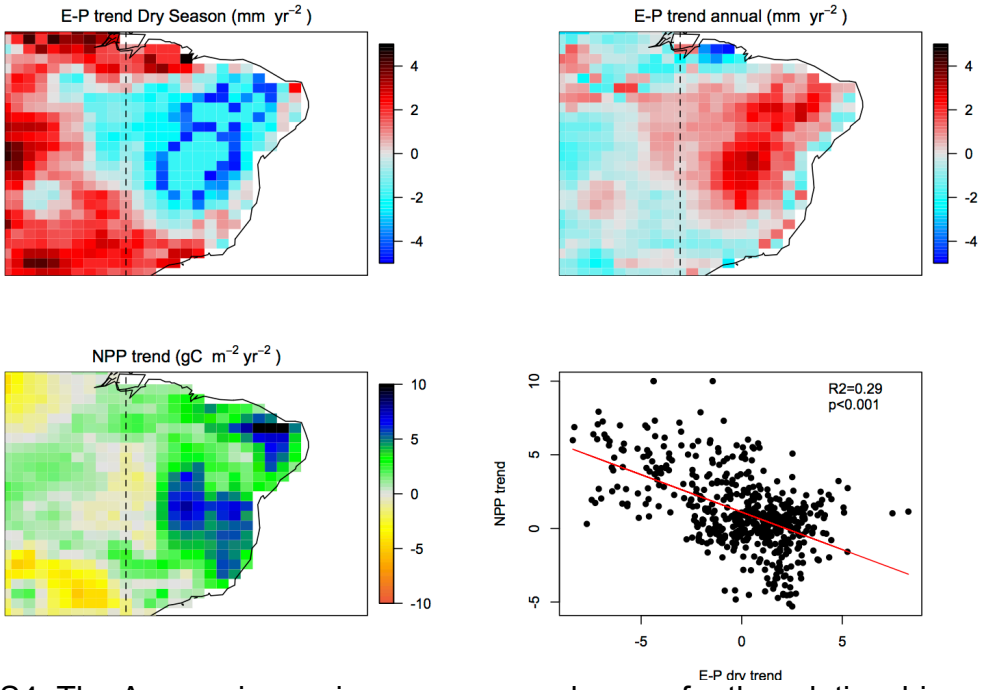

Figure S4. The Amazonian region as an example case for the relationship between DSI trend and annual NPP trend (1989-2005). The E-P trend for the dry season shows a clear link with annual NPP trends for the Amazon (i.e. increase productivity as it gets wetter). However, annual E-P shows an opposite trend (i.e. increase productivity when it is getting drier). This example shows how the dry season controls annual NPP. A similar analysis, linking cumulative water deficit (similar to our DSI see main paper) to NPP for the Amazon over the period 2005-2010, has been recently published by Doughty et al. (2015)[1]. The authors found that years with extreme CWD or DSI lead to increase three mortality and decreasing NPP.

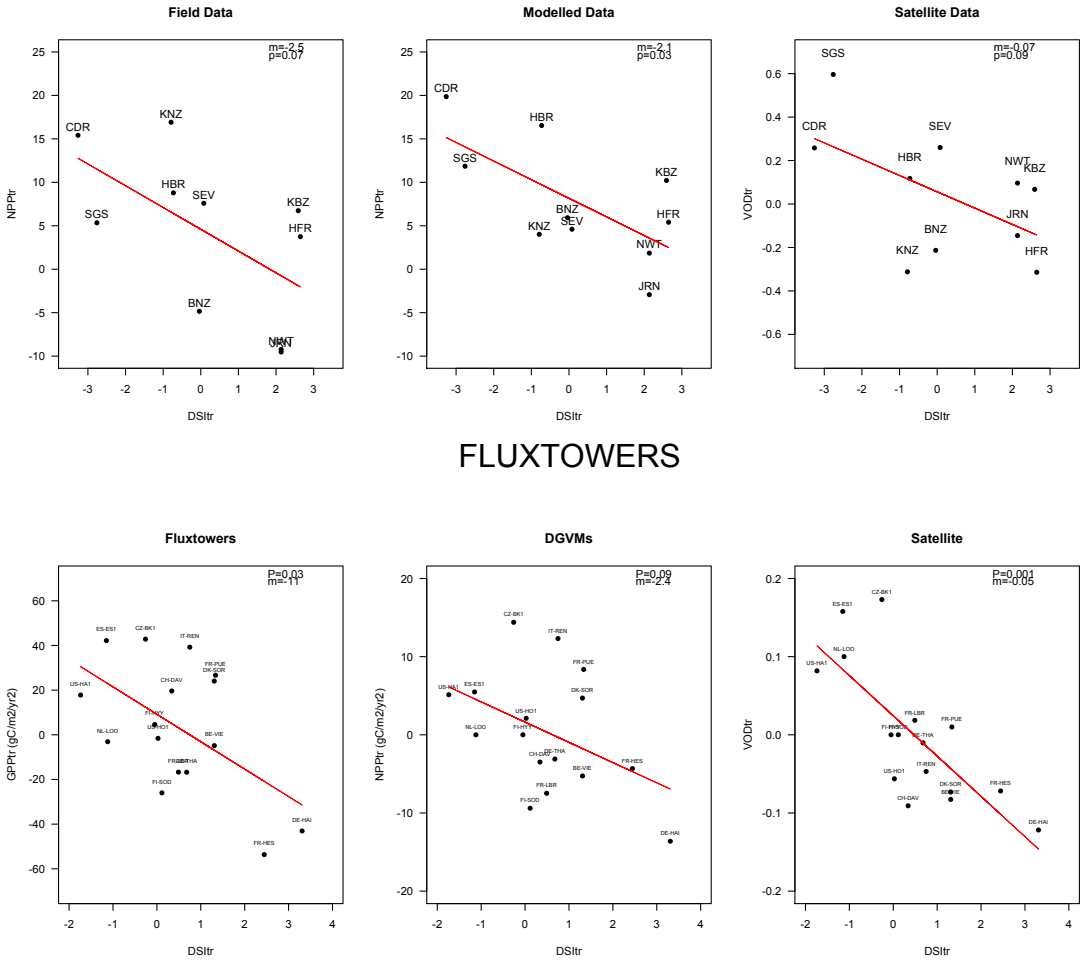

Figure S5. Linear regression between DSI trend (x-axis), observed GPP or NPP (left), modeled NPP (middle) and satellite VOD (right) trends for two different set of observations: LTER (up) and FLUXTOWERS (bottom). The same negative relationship we found at a global scale for DSI trends vs NPP trends was found at local scales using observed data.

Table S3. Changes in DSI and NPP in CMIP5-simulations under the emission scenario RCP2.6. We calculated mean DSI trend for the dry, semi-arid and arid ecosystem and multiply it by the relationship between NPP-DSI in RCP2.6 (Figure 3), we then extrapolate by the century and multiply by the area of each ecosystem type. The result is the change in NPP driven by DSI.
We then compare this value with the total change in NPP under RCP2.6 for 2005-2100.

Ecosystems	DSI trend (mm/yr)	NPP – DSI slope (gC/m2/mm)	Change in NPP due to DSI (gC/m2/yr)	Change in NPP due to DSI (gC/m2) 2005-2100	Area (10^12 m^2)	Total Change due to DSI
Arid	+1.1	- 0.22	- 0.24	-22.8	40	-912
Semi-Arid	+0.2	- 0.22	- 0.04	-3.8	54	-205
Wet	- 0.5	- 0.22	+ 0.11	10.45	45	+470

Total change in cumulative NPP by 2100=-646PgC (total NPP = 6175).
Reduction in NPP =10.45%

Table S4. Same as Table S3 but for RCP8.5

Ecosystems	DSI trend (mm/yr)	NPP – DSI slope (gC/m2/mm)	Change in NPP due to DSI (gC/m2/yr)	Change in NPP due to DSI (gC/m2) 2005-2100	Area (10^12 m)	Total Change due to DSI
Arid	+1.7	- 0.3	- 0.33	-31.3	40	-1240
Semi-Arid	+0.5	- 0.3	- 0.06	-5.7	54	-307
Wet	- 1.2	- 0.3	+ 0.15	14.25	45	+640

Total change in cumulative NPP by 2100=-905PgC (total NPP = 6775).
Reduction in NPP =13.35%

When analysing the models we found that the NPP-DSI slope was similar using observed and modeled DSI over the period 1989-2005 in both TRENDY (m=2.2 ± 0.4 $gCmm^{-1}$) and CMIP5 models (m=2.0 ± 0.6 $gCmm^{-1}$) (**Figure 3d green**). When the trend was simulated using CO_2-only simulations the slope was not different from zero (m=0.3 ± 0.5 $gCmm^{-1}$), but when removing the effect of CO_2 and leaving climate only the slope was similar to the observed one (m=2.5 ± 0. $gCmm^{-1}$5) (**Figure 3d climate-only)**. In other words, the effect of changing DSI in NPP is likely to be driven by climate change; so while the mean annual NPP trend is driven by the CO_2 fertilization effect, the regional variations in the NPP trend are governed by climate induced DSI trends. It is notable that this increasing effect of the hydrological over the land carbon cycle begins over the last 30 years, after which the land C-cycle sensitivity to the DSI trend is expected to remain at present-day levels for the next 100 years (**Figure 3d blue**). This implies that for the next 100 years, arid and semi-arid ecosystems will face more intense dry seasons, which alone would in turn lead to a NPP reduction of 230-310 gCm^{-2} for the arid and of 30-50 gCm^{-2} in the semi-arid ecosystems by 2100, depending on the future climate scenario This translates to a global reduction of 10-13% of total NPP by 2100 due to increased dryness (Table S3 and S4).

Our results indicate that DSI trends are closely link to annual NPP trends. This is consistent across datasets coming from multiple sources (satellite, direct measurements, fluxtowers, DGVMs, ESMs), at multiple time-scales (recent decades, past century and 21st century) and at different spatial scales (local, regional and global) and it is likely to be caused by climate change. An increase in the water deficit over the dry season is likely to have a large impact on annual NPP, particularly in dry ecosystems and DSI is likely to be a fundamental constrain for future NPP.

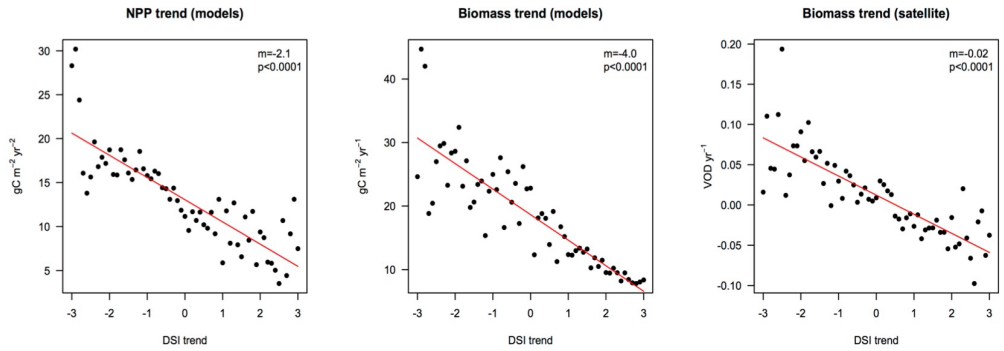

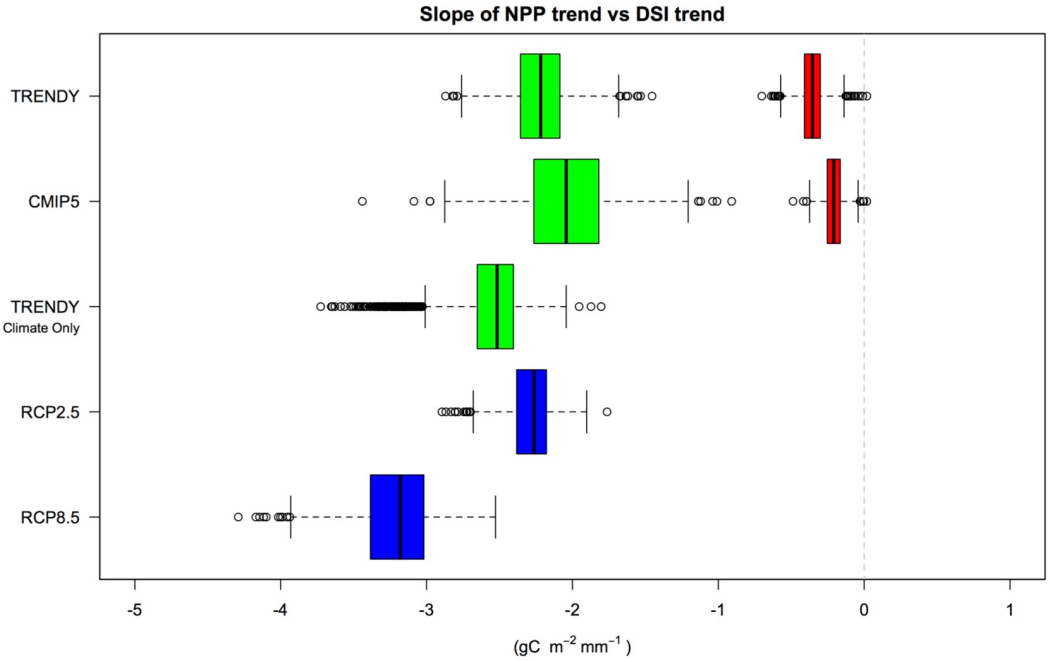

Figure 3. a) Binned modeled NPP trend (gC m^{-2} yr^{-2}), b) Binned modeled biomass trend (KgC m^{-2} yr^{-1}) c) Binned satellite biomass trend (VOD yr^{-1}) vs. DSI trend (x-axis). The negative slope indicates a higher DSI trend lead to a decrease in NPP or biomass trends. This was consistent across datasets. d) Median slope values plus error for NPP trend vs Dry Season trend for: TRENDY-DGVMs, CMIP5-ESMs (historical and two RCPs) and TRENDY-Climate-Only. Green: 1989-2005, Red: 1901-2005, Blue: 2006:2100. All plots have 100 bins. The value for the slope (m) is presented for a, b and c.

To explore why the dry season effect on NPP drives its annual trend (that is dry season behavior might also influence the other season), we split NPP between wet and dry seasons and compare it with the change in wet and dry season intensity during that time. We found that wet season intensity (WSI) trends are only linked to changes in NPP during the wet season, but not during the rest of the year (**Figure 4**). In contrast, the effect of changing dryness in the dry season appears in both seasons. This means that changes in DSI also affect productivity in the wet season. We propose two possible mechanisms for this process: The first one is that increasingly dry soils take longer to recover, leading to shorter effective growing seasons and longer time periods with closed stomata. This in turns leads to C starvation and reduces C reserves, leaf area index and NPP, which in the long-term also reduces biomass growth. The second possible mechanism is an increase in mortality as a consequence of hydraulic failure, which in turn leads to decreasing NPP[30-31]. On the other hand, changes in the wet season are not carried through to the dry season, mainly because excess water is not stored and is likely lost as river runoff. Cadule et al.[32] found a similar pattern when comparing wet and dry years across the planet. Therefore an increase in dryness has a much larger impact on vegetation productivity than an excess of water both seasonally and annually.

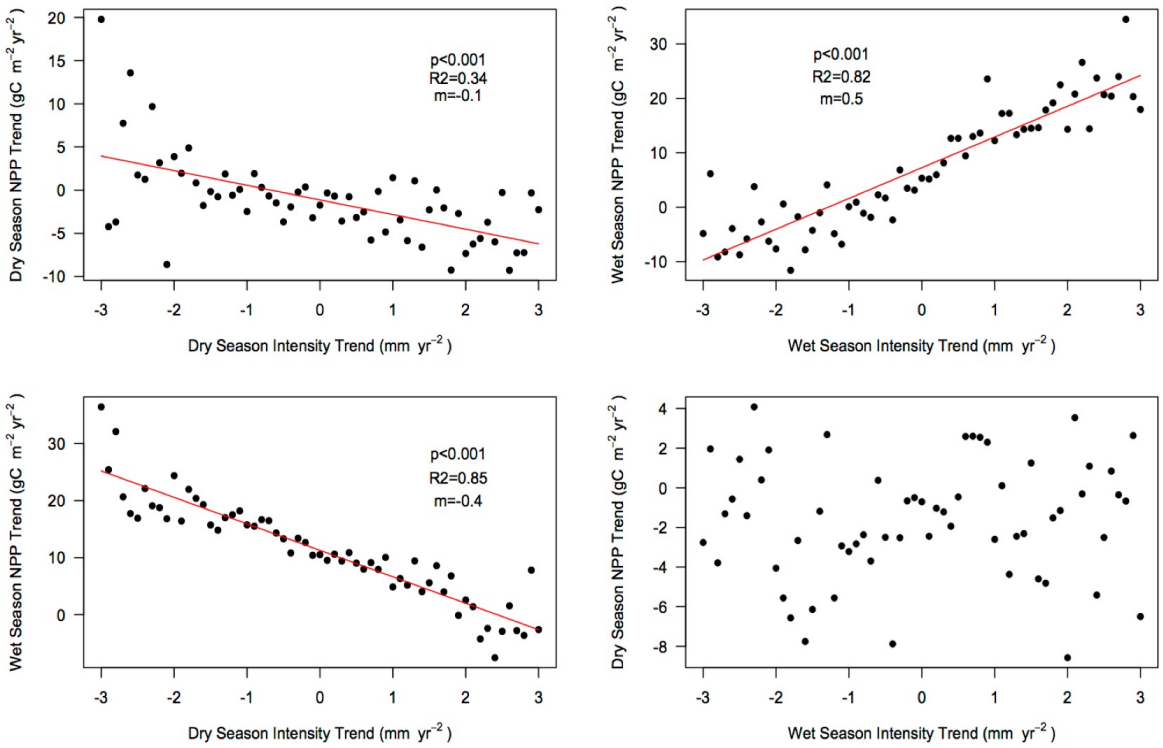

Figure 4. Top left: dry season NPP trend (gC m^{-2} yr^{-2}) against dry season water intensity trend (mm yr^{-2}). Top right: wet season NPP trend against wet season water intensity trend. On the bottom: the same effect but across seasons**.** The value for the slope is presented in each panel (m).

We conclude that changes in water availability over the dry season affect vegetation throughout the whole year, driving trends in net primary productivity globally at different time scales (past, present and future under climate change). Our seasonal index, the dry season intensity, gives a strong estimate of expected evolution of NPP using simple calculations derived from a basic water-balance. Moreover, we show evidence that the widespread use of drought indices aggregated at annual scales is insufficient for understanding the linkages between water availability and the land carbon cycle, as the effects of changes in specific seasons might be lost on an annual scale. Finally, our results suggest that the strength of the carbon-climate feedback might intensify in the future, reducing natural offsetting of fossil fuel emissions through vegetation capture of atmospheric CO_2 as a consequence of increased seasonality and dryness intensity.

REFERENCES

1. Held, I. & Soden, B. Robust Responses of the Hydrological Cycle to Global Warming. *J. Clim.* **19,** (2006).
2. Allen, M. R. & Ingram, W. J. Constraints on future changes in climate and the hydrologic cycle. *Nature* **419,** 224–232 (2002).
3. Chou, C. *et al.* Increase in the range between wet and dry season precipitation. *Nat. Geosci.* **6,** 263–267 (2013).
4. Greve, P *et al*. Global assessment of trends in wetting and drying over land. *Nat. Geosci.* **7**, 716–721 (2014)**.**
5. Reichstein, M. *et al.* Climate extremes and the carbon cycle. *Nature* **500,** 287–295 (2013).
6. Jung, M. *et al.* Recent decline in the global land evapotranspiration trend due to limited moisture supply. *Nature* **467,** 951–954 (2010).
7. Mueller, B. *et al.* Benchmark products for land evapotranspiration: LandFlux-EVAL multi-dataset synthesis. *Hydrol. Earth Syst. Sci.* **10,** 769–805 (2013).
8. Miralles, D. G. *et al.* El Niño–La Niña cycle and recent trends in continental evaporation. *Nat. Clim. Change* **4,** 122–126 (2014).
9. Peel, M. C. & McMahon, T. A. Continental Runoff: A quality-controlled global runoff data set. *Nature* **444,** E14–E14 (2006).
10. Seneviratne, S. I. Climate science: Historical drought trends revisited. *Nature* **491,** 338–339 (2012).
11. Sheffield, J., Wood, E. F. & Roderick, M. L. Little change in global drought over the past 60 years. *Nature* **491,** 435–438 (2012).
12. Zhang, X. *et al.* Detection of human influence on twentieth-century precipitation trends. *Nature* **448,** 461–465 (2007).
13. Feng, X., Porporato, A. & Rodriguez-Iturbe, I. Changes in rainfall seasonality in the tropics. *Nat. Clim. Change* **3,** 811–815 (2013).
14. Phillips, O. L., Aragão, L. E., Lewis, S. L., Fisher, J. B., Lloyd, J., López-González, G., ... & Andrade, A. (2009). Drought sensitivity of the Amazon rainforest. Science, 323(5919), 1344-1347

15. Nemani, R. R. *et al.* Climate-Driven Increases in Global Terrestrial Net Primary Production from 1982 to 1999. *Science* **300,** 1560–1563 (2003).
16. Ciais, P. *et al.* Europe-wide reduction in primary productivity caused by the heat and drought in 2003. *Nature* **437,** 529–533 (2005).
17. Zeng, N. *et al.* Causes and impacts of the 2005 Amazon drought. Environ. Res. Lett. **3** 014002 (2008).
18. Liu, Y. Y. *et al.* Changing Climate and Overgrazing Are Decimating Mongolian Steppes. *PLoS ONE* **8,** e57599 (2013).
19. Heim, R. R. A Review of Twentieth-Century Drought Indices Used in the United States. *Bull. Am. Meteorol. Soc.* **83,** 1149–1165 (2002).
20. Westerling, A. L., Hidalgo, H. G., Cayan, D. R. & Swetnam, T. W. Warming and Earlier Spring Increase Western U.S. Forest Wildfire Activity. *Science* **313,** 940–943 (2006).
21. Malhi, Y. *et al.* Exploring the likelihood and mechanism of a climate-change-induced dieback of the Amazon rainforest. *Proc. Natl. Acad. Sci.* **106,** 20610–20615 (2009).
22. Harris, I., Jones, P. d., Osborn, T. j. & Lister, D. h. Updated high-resolution grids of monthly climatic observations – the CRU TS3.10 Dataset. *Int. J. Climatol.* (2013). doi:10.1002/joc.3711
23. Higgins, R. W., Leetmaa, A., Xue, Y. & Barnston, A. Dominant Factors Influencing the Seasonal Predictability of U.S. Precipitation and Surface Air Temperature. *J. Clim.* **13,** 3994–4017 (2000).
24. Adler, R. F. *et al.* The Version-2 Global Precipitation Climatology Project (GPCP) Monthly Precipitation Analysis (1979–Present). *J. Hydrometeorol.* **4,** 1147–1167 (2003).
25. Engelbrecht, B. M. J. *et al.* Drought sensitivity shapes species distribution patterns in tropical forests. *Nature* **447,** 80–82 (2007).
26. Dorigo, W. *et al.* Evaluating global trends (1988–2010) in harmonized multi-satellite surface soil moisture. *Geo.Res.Let.* **39**, L18405 (2012)
27. Kumar, S., Lawrence, D. M., Dirmeyer, P. A. & Sheffield, J. Less reliable water availability in the 21st century climate projections. *Earths Future* **2,** 152–160 (2014).
28. Huntingford, C., Jones, P. D., Livina, V. N., Lenton, T. M. & Cox, P. M. No increase in global temperature variability despite changing regional patterns. *Nature* **500,** 327–330 (2013).
29. Poulter, B. *et al.* Contribution of semi-arid ecosystems to interannual variability of the global carbon cycle. *Nature* **509,** 600–603 (2014).
30. Adams, HD. *et al.* Temperature sensitivity of drought-induced tree mortality portends increased regional die-off under global-change-type drought. *PNAS* **17,** 7063–7066 (2009).
31. McDowell N. *et al.* Mechanisms of plant survival and mortality during drought: why do some plants survive while others succumb to drought?. *New Phytologist.* **178,** 719-739 (2008).
32. Cadule, P. *et al.* Benchmarking coupled climate-carbon models against long-term atmospheric CO_2 measurements. *Glob. Biogeochem. Cycles* **24,** GB2016 (2010).
33. Sitch, S. *et al.* Trends and drivers of regional sources and sinks of carbon dioxide over the past two decades. *Biogeosciences Discuss.* **10,** 20113–20177 (2013).
34. Taylor, K. E., Stouffer, R. J. & Meehl, G. A. An Overview of CMIP5 and the Experiment Design. *Bull. Am. Meteorol. Soc.* **93,** 485–498 (2011).

Acknowledgements

The lead author (GMT) thanks CONACYT-CECTI and the University of Exeter for their funding during his PhD Studies. The authors extend their thanks to the Short Term Scientific Mission (STSM) from the TERRABITES COST Action ES0805 for making this contribution possible. YL is the recipient of an Australian Research Council DECRA Fellowship (project number DE140100200). CH acknowledges the NERC National Capability fund.

CONCLUSIONS

CHAPTER 6: Conclusions

This chapter summaries the research of this thesis, the key findings, the limitations to the different analyses, the opportunities for further research and my novel contribution to my field of study.

6.1 Summary of the research

The work of my thesis comes from two different areas: model evaluation and process analysis. In the first part I evaluated the ability of DGVMs to reproduce observed data, and generate a new methodology for evaluating the phenology module of these models. I also give examples on how DGVMs can be evaluated over the tropics, where less data is available, using novel observations for different scales.

In the second part I analysed the relationship between NBP and NPP trends and recent changes in climate and atmospheric CO_2. Results show that globally NBP and NPP increased due to rising CO_2, but this was not homogeneously distributed across the globe. I showed that the decreasing trends in NPP over several regions were due to an increase in the dry season intensity and length.

6.2. Key findings

The main findings of my thesis can be separated into the same two parts: the ability of models to reproduce observed data (chapters and 3) and the analysis of processes that drive changes in land-C (chapters 4 and 5).

In chapter I found that all models overestimate the length of the growing season, driven by an earlier onset and later offset. As a consequence they also overestimate the trend in mean LAI. By comparing models that were forced with real climate (uncoupled) and forced with their own climate (coupled), it was determined that the misrepresentation of the phenology lies on the structure of the land component of the models.

Chapter 3 shows that modelled and observational variables of the land C cycle over the tropics are similar when comparing area means (at least over the past 20 years), however important differences on the temporal evolution and the estimation of NBP and NPP were found over certain ecosystems. In the case of Africa I showed that the modelled NBP trend is opposite to that simulated by atmospheric inversions, which was related to two regions (the

Sahel and the Congo Basin). For the case of Mexico, models and observations (satellite and field data) have a high spatial correlation, but disagree in the C stored over low-density vegetated areas. These results show that modelled NBP and NPP over semi-arid regions (e.g. grasslands, shrublands) needs to be improved for a more accurate representation in future scenarios, particularly since these regions are among the most susceptible to climate change accordingly to the most recent findings (Poulter et al. 2015; Ahlstrom et al. 2015).

The attribution of the trends in NBP over the last 20 years was the main focus of chapter 4. Here model results suggest NBP increased steadily primarily as a result of CO_2 fertilization on NPP over the last 20 years (1990-2009), however the trend was not homogeneously distributed across the globe, due to trends in the climate. Several regions where NBP decreased were identified (e.g. South Amazon, Mongolian Steppe or Southern USA) as a consequence of decrease in precipitation.

Chapter 5 continues where chapter 4 left off, linking changes in dryness to the trend in vegetation NPP. Here I found that, on average, arid ecosystems faced a longer and more intense dry season over the last 17 years (1989-2005), with the opposite is true for wet ecosystems. As a consequence climate lead to a decrease of regional annual NPP. This decreasing pattern would be obscured if using commonly annual aggregated water fluxes indices (e.g. PDSI or PSI), as the change in the wet and dry seasons tends to be counterbalance although their impact on NPP does not. Changes in the seasonality of water availability (dryness/wetness) are the key drivers of annual NPP at the regional scale.

6.3. Bringing the thesis together: evaluation and development

One question that arises from the thesis is how both parts are linked together, this is how model evaluation can help improve the models and lead to better understanding of the processes driving land C. From the first two chapters – model evaluation- two important conclusions arise: 1) models tend to overestimate the length and trend of the growing season over the NH and 2) the C budget over semi-arid regions. Both of this findings can help improve the models and has done so already.

On the first hand our findings on LAI had already help improved phenology on several models such as LPJ (Forkel et al., 2015) and SSiB4-TRIFFID (Zhang et al., 2014). The integration of these findings and the novel satellite data into the DGVMs has lead to a deeper understanding on the controls of phenology over the NH. For example for the model LPJ, Forkel et al. (2015) showed that its not only temperature, but also water availability what controls the long-term trend of LAI in the NH. For the case of the model TRIFFID, the implementation of interactive forage and foliage improved the representation of the phenology and showed that vegetation distribution and competition are key factors controlling LAI (Zhang et al., 2014). While additional work is needed to improve the DGVMs phenology module, it is also noteworthy that all models reproduce a consistent greening trend over the NH.

On the second hand our work showed that models tend to overestimate the C stocks over semi-arid regions. This is a fundamental finding because recent changes in the global C-cycle are driven by the response of semi-arid ecosystems to climate (Ahlstrom et al., 2015; Poulter et al., 2015). From our fingins in chapter 4, it seems that when the climatic signal is strong enough and consistent over time (i.e. the increase in DSI over tropical South America), all models display a similar response in the C-balance (i.e. a decrease in NBP trend). However, in regions where the signal is not strong enough or not consistent across different years (i.e. changes in DSI over Southern USA) models do not agree on the regional response (Figure 6.1). Our findings that DSI exert a strong control on annual NPP, may help improving model response to drought and climate change, as we have shown a similar pattern for multiple datasets coming from different sources (field data, satellite, DGVMs, ESMs). The effect of accumulated stress climatic signals -for example DSI- on the vegetation (i.e. the effect of continuous or prolonged dryness on vegetation

mortality) may help improving the drought response in the models as suggested by our findings, but comparison with other vegetation estimates (e.g. satellite biomass) is imperative to have reliable results.

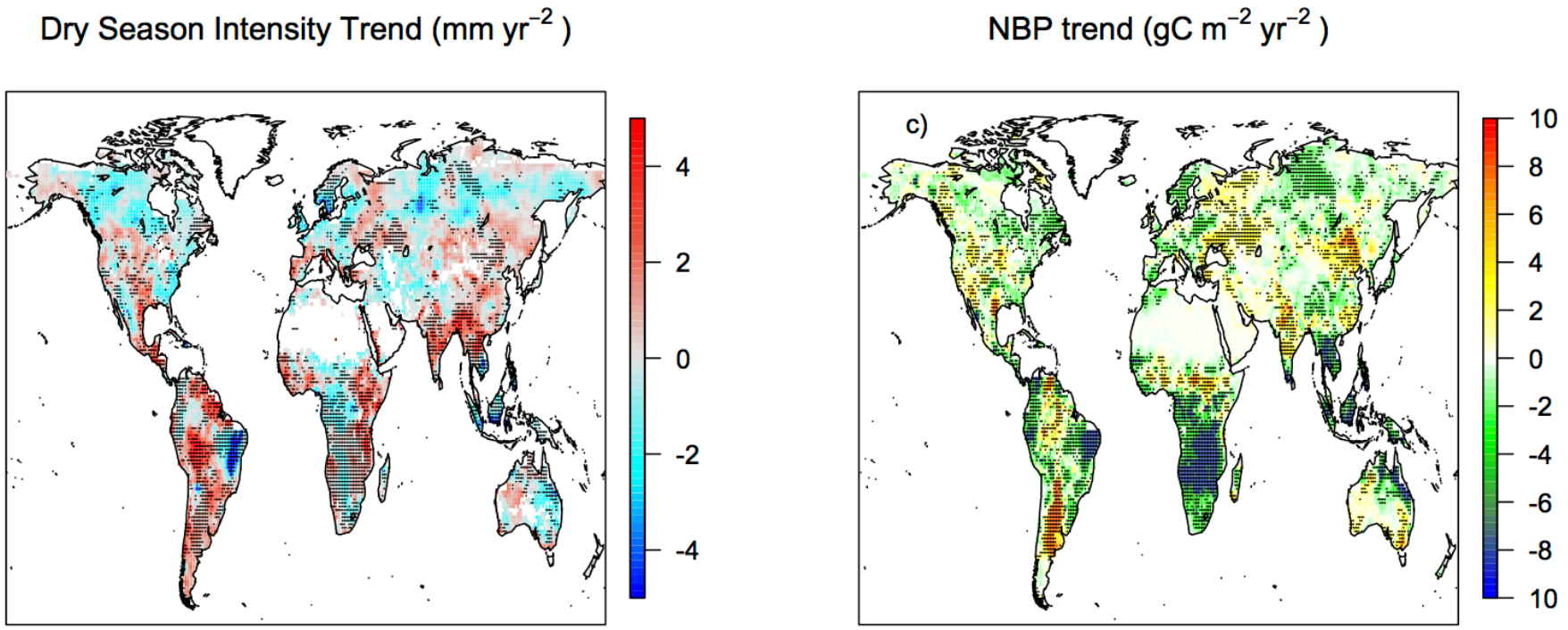

Figure 6.1 Model agreements for the DSI trend (left) and NBP trend (right) over the period 1990-2009 for an ensemble of 9 DGVMs. Stippling represents regions where 66% of the models agree on the sign of the trend. Regions where the climatic signal is strong show high model agreement, which translates into a strong signal and model agreement on the land-C balance.

6.4. Limitations of this study and opportunities for developing future research

I can find at least three important limitations to the studies presented in this thesis: 1) the omission of Land Use Change (LUC) as a driver, the poor representation of fire and nitrogen cycle in the DGVMs, 2) the need for more comparisons with field observations to conduct a more in-depth model evaluation and 3) the short time window analysed for most chapter, which disregard the role that decadal variability may play in the Earth-System.

6.4.1 Missing Processes in the DGVMs used here

DGVMs have developed a great deal since their first versions in the 1980s-1990s, however several important processes are either missing or not fully evaluated in the latest generation of DGVMs. Three particularly important processes are the effect of LUC, fire dynamics and a full nitrogen cycle.

The DGVMs used in this thesis do not include LUC –except for those used on the analysis on the C-cycle of Mexico-, a process that can account for a flux of C to the atmosphere of similar magnitude to annual NEP (Hurtt et al., 2013). Managed ecosystems represent at least 40% of the total land (Ramankuty and Foley, 1999), which means that for most regions of the globe (e.g. central Africa, USA, Europe, India) the estimates of NEP are higher than the actual carbon stored in reality. This was clear in Chapter 3, where the mean NEP for Africa in the models was higher than the atmospheric inversions (that do take into account LUC). Nontheless other chapter (e.g. LAI trends, drought trends) are most likely not to be affected by LUC and the same spatial and temporal patterns would emerge if LUC were included.

The new runs for TRENDY now include some representation of LUC (named S3) where all models have been forced by historical changes in crop and pastures, hence considering LUC (LeQuéré et al., 2014). However, the fate of carbon after land conversion and the description of croplands and pastures are still relatively crude in most models.

In some particular years (e.g. high ENSO) fire can return the same amount of C that is normally fixed by NEP (van der Werf et al., 2010). In other words, it can quickly change an ecosystem from being a sink into a source. As a result fire interannual variability (IAV) is captured in the IAV of atmospheric CO_2.

Most models lack a fire module. Hence, they implicitily account for fire as part of the heterotropical respiration, whose IAV is driven by other factors.

Another fundamental missing piece is the interaction between the C and the nitrogen cycles (Ciais et al., 2013; Fernandez-Martinez et al., 2014; Wider et al., 2015). Nitrogen concentration in the leaves is an important limitation for photosynthesis and places with little nitrogen availability may have a smaller GPP than modelled based on the C cycle alone (Fernandez-Martinez et al., 2014). Only a few models include a full representation of the N cycle (Zaehle et al., 2011; Clais et al., 2013). Other nutrients, such as phosphorus and potassium may also play a similar role, but the inclusion of these elements in DGVM is much less mature than nitrogen (Wieder et al., 2015).

Finally, ecosystem level processes such as forest gap dynamics, plant mortality, or forest re-growth and succession are not explicitly included in most DGVMs, which could also lead to discrepancies with observed data (Michaletz et al., 2014). Different DGVMs groups are trying to include and evaluate the processes mentioned above, a task that will likely continue over several years, representing a fundamental opportunity for future research.

6.4.2 Lack of comparison with field-observed data

Nowadays it is clear that DGVMs need to be evaluated against observed data to improve their performance. The availability of new products, such as satellite observations (Liu et al., 2015) or atmospheric inversions (Pelyin et al., 2012) represents a great opportunity to start benchmarking the models. On the other hand observed field data, particularly long-term ecological data (Knapp et al., 2001), the Free Air CO_2 enrichment experiments (Ainsworth and Long, 2004) and forest inventory plots (e.g. Rainfor; Brienen et al., 2015), yield great insight on ecosystem processes and provide direct measurments to test and evaluate the models.

There is an increasing need to evaluate models in order to improve their representation of different processes and nowadays there is already enough observations for most part of the globe to do so. An implementation of different evaluation benchmarks is needed and represents an important opportunity for future research, and although this is already ongoing (e.g. Kelley et al., 2013; Cadule et al., 2013; Blyth et al., 2010) efforts are still needed to implement it.

6.4.3 The impacts of decadal variability

One fundamental part of analysing any Earth-System process is that different drivers act at multiple time scales (Prentice et al., 2013). Our understanding of seasonal and inter-annual cycle on NPP, NEP and NBP has increased a great deal over the last 30 years, likewise for the long-term trend over the century. However there is high uncertainty over the change in the drivers over intermediate time periods (decadal time-scale). This means that decadal changes in the carbon cycle may not be properly addressed when analysing one or two decades, as it is the case of my thesis. This implicates that the interpretation of some regional trends that appear in one direction, could potentially shift when analysed over longer time periods. In other words, the response of vegetation over the last 30 years may be partly driven by climate variability rather than only by climate change. As more global observational data is available for longer series of time, a re-analysis of the processes driving NBP and NPP is needed; particularly, linking the vegetation C cycle and the hydrological cycle.

6.5 Novel contribution to the field of study

The analysis developed in this thesis contributes to the field of study in two ways. The first one is the creation of novel methodologies for the evaluation of DGVMs. Chapter provides a simple benchmark to evaluate the phenology of different DGVMs or different model versions, providing numeric estimates for the performance of the models in reproducing observed satellite data. Furthermore the same methodology can be applied using different observational data at multiple scales. This benchmarking method has been used by other to evaluate and improve their own models (e.g. Zhang et al. 2015 or Forkel et al. 2015). The results from Chapter 3 showed the need to improve models over semi-arid and arid ecosystems (e.g. grasslands, shrublands); however the main contribution of this chapter is the estimation of regional budgets for the C cycle, a fundamental piece of information for stakeholders and policy makers. For the particular case of Mexico, we estimated that the country was a sink of C over the last 60 years, which is opposite to all other available estimates.

The second main contribution of my research is the analysis of processes affecting the C cycle. Chapter 4 provides a background study to

identify the main driver of regional NBP and NPP trends, with the addition of providing estimates for global land C fluxes, fundamental to our understanding of the C cycle. Following this study, I analysed in-depth the regions where simulated NPP decreased (chapter 5) and found that it was driven by an increase in the dry season length and intensity. This is the first time, as far as I know, that changes in annual NPP are explained by changes in seasonal water fluxes. Furthermore, I showed that arid ecosystems are likely to face more extreme conditions, with decline in NPP in the future. This builds upon recently published papers showing that dryness and drought may play a bigger role in regulating the land C cycle that previously expected (e.g. Poulter et al. 2014, Doughthy et al. 2015, Ahlstrom et al. 2015).

REFERENCES

Adler, R.F.; Huffman, G.J.; Chang, A.; Ferraro, R.; Xie, P.-P.; Janowiak, J.; Rudolf, B.; Schneider, U.; Curtis, S.; Bolvin, D.; Gruber, A.; Susskind, J.; Arkin, P.; Nelkin, E. 2003. The Version-2 Global Precipitation Climatology Project. GPCP. Monthly Precipitation Analysis. 1979–Present.. J. Hydrometeorol. 4, 1147–1167. doi:10.1175/1525-7541

Ahas, R.; Jaagus, J.; Aasa, A. 2000. The phenological calendar of Estonia and its correlation with mean air temperature. Int. J. Biometeorol. 44, 159–166.

Ahl, D.E.; Gower, S.T.; Burrows, S.N.; Shabanov, N.V.; Myneni, R.B.; Knyazikhin, Y. 2006. Monitoring spring canopy phenology of a deciduous broadleaf forest using MODIS. Remote Sens. Environ. 104, 88–95.

Ahlström, A.; Raupach, M.R.; Schurgers, G.; Smith, B.; Arneth, A.; Jung, M.; Reichstein, M.; Canadell, J.G.; Friedlingstein, P.; Jain, A.K.; Kato, E.; Poulter, B.; Sitch, S.; Stocker, B.D.; Viovy, N.; Wang, Y.P.; Wiltshire, A.; Zaehle, S.; Zeng, N. 2015. The dominant role of semi-arid ecosystems in the trend and variability of the land CO2 sink. Science 348, 895–899. doi:10.1126/science.aaa1668

Ainsworth, E.A.; Long, S.P. 2005. What have we learned from 15 years of free-air CO2 enrichment. FACE.? A meta-analytic review of the responses of photosynthesis, canopy properties and plant production to rising CO2. New Phytol. 165, 351–372. doi:10.1111/j.1469-8137.2004.01224.x

Anav, A.; Gualdi, S.; Polcher, J.; Navarra, A. Effects of Land Surface-Vegetation on the Boreal Summer Surface Climate of a GCM. J. Climate 2007, 20, 225–278.

Alianza MREDD+. 2013. Mapa y base de datos sobre la distribución de la biomasa aérea de la vegetación leñosa en México.Woods Hole Research Center, USAID, CONAFOR, CONABIO, Proyecto México Noruega. México.

Allen, C.D.; Macalady, A. ; Chenchouni, H.; Bachelet, D.; McDowell, N.; Vennetier, M.; Kitzberger, T.; Rigling, A.; Breshears, D. ; Hogg, E.H.; Gonzalez, P.; Fensham, R.; Zhang, Z.; Castro, J.; Demidova, N.; Lim, J.-H.; Allard, G.; Running, S.W.; Semerci, A.; Cobb, N.;2010. A global overview of drought and heat-induced tree mortality reveals emerging climate change risks for forests. For. Ecol. Manag. 259, 660–684. doi:10.1016/j.foreco.2009.09.001

Allen, M. R.; and P. A. Stott. 2003. Estimating signal amplitudes in optimal fingerprinting: Part I. Theory'. Climate Dynamics 21, 477– 491.

Allen, M. R.; and S. F. B. Tett. 1999. Checking for model consistency in optimal fingerprinting, Climate Dynamics 15, 419–434.

Allen, M.R.; Ingram, W.J. 2002. Constraints on future changes in climate and the hydrologic cycle. Nature 419, 224–232. doi:10.1038/nature01092

Anav, A.; Friedlingstein, P.; Kidston, M.; Bopp, L.; Ciais, P.; Cox, P.; Jones, C.; Jung, M.; Myneni, R.; Zhu, Z. 2013. Evaluating the Land and Ocean Components of the Global Carbon Cycle in the CMIP5 Earth System Models. J. Clim. 26, 6801–6843. doi:10.1175/JCLI-D-12-00417.1

Anav, A.; Menut, L.; Khvorostyanov, D.; Viovy, N. A comparison of two canopy conductance parameterizations to quantify the interactions between surface ozone and vegetation over Europe. J. Geophys. Res. 2012, 117, G03027.

Anderegg, L.D.L.; Anderegg, W.R.L.; Abatzoglou, J.; Hausladen, A.M.; Berry, J.A. 2013. Drought characteristics' role in widespread aspen forest mortality across Colorado, USA. Glob. Change Biol. 19, 1526–1537. doi:10.1111/gcb.12146

Andres, R. J.; Boden, T. A.; Bréon, F.-M.; Ciais, P.; Davis, S.; Erickson, D.; Gregg, J. S.; Jacobson, A.; Marland, G.; Miller, J.; Oda, T.; Olivier, J. G. J.; Raupach, M. R.; Rayner, P.; and Treanton, K. 2012. A synthesis of carbon dioxide emissions from fossil-fuel combustion, Biogeosciences, 9, 1845-1871, doi:10.5194/bg-9-1845-2012

Angert, A.; Biraud, S.; Bonfils, C.; Henning, C. C.; Buermann, W.; Pinzon, J.; Tucker, C. J. and I. Fung. 2005. Drier summers cancel out the CO2 uptake enhancement induced by warmer springs, PNAS, 102. 31. 10823-10827.

Arora, V.K.; Boer, G.J.; Friedlingstein, P.; Eby, M.; Jones, C.D.; Christian, J.R.; Bonan, G.; Bopp, L.; Brovkin, V.; Cadule, P.; Hajima, T.; Ilyina, T.; Lindsay, K.; Tjiputra, J.F.; Wu, T. 2013. Carbon–Concentration and Carbon–Climate Feedbacks in CMIP5 Earth System Models. J. Clim. 26, 5289–5314. doi:10.1175/JCLI-D-12-00494.1

Arora, V.K.; Scinocca, J.F.; Boer, G.J.; Christian, J.R.; Denman, K.L.; Flato, G.M.; Kharin, V.V.; Lee, W.G.; Merryfield, W.J. 2011. Carbon emission limits required to satisfy future representative concentration pathways of greenhouse gases. Geophys. Res. Lett., 38.

Assmann, K. M.; Bentsen, M.; Segschneider, J.; and Heinze, C. 2010. An isopycnic ocean carbon cycle model, Geoscientific Model Development, 3, 143-167,.

Atlas, R.; R. N. Hoffman, J. Ardizzone, S. M. Leidner, J. C. Jusem, D. K. Smith, and D. Gombos. 2011. A Cross-Calibrated Multiplatform Ocean Surface Wind Velocity Product for Meteorological and Oceanographic Applications, B Am Meteorol Soc, 92(2. 157-157.

Aumont, O.; and Bopp, L. 2006. Globalizing results from ocean in situ iron fertilization studies, Global Biogeochem. Cycl., 20.

Bacastow, R.B. 1976. Modulation of atmospheric carbon dioxide by the Southern Oscillation. Nature 261: 116-118.

Badeck, F.-W.; Bondeau, A.; Böttcher, K.; Doktor, D.; Lucht, W.; Schaber, J.; Sitch, S. 2004. Responses of spring phenology to climate change. New Phytol. 162, 295–309. doi:10.1111/j.1469-8137.2004.01059.x

Baker, T. R.; O. L. Phillips, Y. Malhi, S. Almeida, L. Arroyo, A. Di Fiore, T. Erwin, N. Higuchi, T. J. Killeen, S. G. Laurance, W. F. Laurance, S. L. Lewis, A. Monteagudo, D. A. Neill, P. Nunez Vargas, N. C. A. Pitman, J. N. M. Silva & R. Vasquez Martinez. 2004. Increasing biomass in Amazonian forest plots. Philosophical Transactions of the Royal Society B: Biological Sciences, 359, 353-365.

Ballantyne, A.P.; C. B. Alden, J. B. Miller, P. P. Tans & J. W. C. White. 2012. Increase in observed net carbon dioxide uptake by land and oceans during the past 50 years, Nature, 488, doi:10.1038/nature11299

Barichivich, J.; Briffa, K.R.; Myneni, R.B.; Osborn, T.J.; Melvin, T.M.; Ciais, P.; Piao, S.; Tucker, C.; 2013. Large-scale variations in the vegetation growing season and annual cycle of atmospheric CO2 at high northern latitudes from 1950 to 2011. Glob. Change Biol. 19, 3167–3183. doi:10.1111/gcb.12283

Batjes, N. h. 1996. Total carbon and nitrogen in the soils of the world. Eur. J. Soil Sci. 47, 151–163. doi:10.1111/j.1365-2389.1996.tb01386.x

Battle, M.; M. L. Bender, P. P. Tans, J. W. C. White, J. T. Ellis, T. Conway, and R. J. Francey. 2000. Global carbon sinks and their variability inferred from atmospheric O2 and d13C, Science, 287, 2467–2469.

Beaulieu, C.; Sarmiento, J.L.; Mikaloff Fletcher, S.E.; Chen, J.; and D. Medvigy. 2012. Identification and characterization of abrupt changes in the land uptake of carbon, Global Biogeochemical Cycles, 26, GB1007, doi:10.1029/2010GB004024.

Beck, S.A. and S. J. Goetz. 2011. Satellite observations of high northern latitude vegetation productivity changes between 1982 and 2008: ecological variability and regional differences, Environ. Res. Lett. 6, doi:10.1088/1748-9326/6/4 /045501

Bentsen, M.; Bethke, I.; Debernard, J.B.; Iversen, T.; Kirkevåg, A.; Seland, Ø.; Drange, H.; Roelandt, C.; Seierstad, I.A.; Hoose, C.; Kristjánsson, J.E. 2012. The Norwegian Earth System Model, NorESM1-M – Part 1: Description and basic evaluation. Geosci. Model Dev. 5, 2843-2931,

Berterretche, M.; Hudak, A.T.; Cohen, W.B.; Maiersperger, T.K.; Gower, S.T.; Dungan, J. 2005. Comparison of regression and geostatistical methods for mapping Leaf Area Index. LAI. with Landsat ETM+ data over a boreal forest. Remote Sens. Environ. 96, 49–61. doi:10.1016/j.rse.2005.01.014

Betts, R.A.; Boucher, O.; Collins, M.; Cox, P.M.; Falloon, P.D.; Gedney, N.; Hemming, D.L.; Huntingford, C.; Jones, C.D.; Sexton, D.M.H.; Webb, M.J. 2007. Projected increase in continental runoff due to plant responses to increasing carbon dioxide. Nature 448, 1037–1041. doi:10.1038/nature06045

Betts, R.A.; Cox, P.M.; Lee, S.E.; Woodward, F.I. 1997. Contrasting physiological and structural vegetation feedback in climate change simulations. Nature, 387, 796-799.

Bhatt, U.S.; D.A. Walker, M.K. Raynolds, J.C. Comiso, H.E. Epstein, G. Jia, R. Gens, J.E. Pinzon, et al. 2010. Circumpolar Arctic tundra vegetation change is linked to sea ice decline. Earth Interactions 14: 1-20.

Blyth, E.; Gash, J.; Lloyd, A.; Pryor, M.; Weedon, G.P.; Shuttleworth, J. 2009. Evaluating the JULES Land Surface Model Energy Fluxes Using FLUXNET Data. J. Hydrometeorol. 11, 509–519. doi:10.1175/2009JHM1183.1

Bonan, G.; Levis, S.; Sitch, S.; Vertenstein, M.; Oleson, K.W. 2003. A dynamic global vegetation model for use with climate models: concepts and

description of simulated vegetation dynamics. Global Change Biol. 9, 1543–1566.

Bonan, G.B. 1993. Importance of leaf area index and forest type when estimating photosynthesis in boreal forests. Remote Sens. Environ. 43, 303–314. doi:10.1016/0034-4257(93.90072-6

Bondeau, A.; Smith, P.C.; Zaehle, S.; Schaphoff, S.; Lucht, W.; Cramer, W.; Gerten, D.; Lotze-Campen, H.; Müller, C.; Reichstein, M.; Smith, B. 2007. Modelling the role of agriculture for the 20th century global terrestrial carbon balance. Glob. Change Biol. 13, 679–706. doi:10.1111/j.1365-2486.2006.01305.x

Böning, C.W. et al. 2008. The response of the Antarctic Circumpolar Current to recent climate change. Nature Geoscience, 1(12. pp.864-869.

Botta, A.; Viovy, N.; Ciais, P.; Friedlingstein, P. 2000. A global prognostic scheme of leaf onset using satellite data. Global Change Biol., 6, 709–726.

Bounoua, L.; Collatz, G.J.; Los, S.O.; Sellers, P.J; Dazlich, D.A.; Tucker, C.J.; Randall, D.A. Sensitivity of climate to changes in NDVI. 2000. J. Climate, 13, 2277–2292.

Bousquet, P.; P. Peylin, P. Ciais, P. Friedlingstein, C. Lequere, and P. Tans. 2000. Interannual CO2 sources and sinks as deduced by inversion of atmospheric CO2 data, Science, 290, 1342– 1346.

Boyd, P. and S.C. Doney. 2003: The impact of climate change and feedback process on the ocean carbon cycle. Ocean Biogeochemistry, ed. M. Fasham, Springer, 157-193.

Boyd, P.W. 2011. Beyond ocean acidification. Nature Geoscience, 4(5. 273-274.

Bréda, N.J.J. 2003. Ground-based Measurements of Leaf Area Index: A Review of Methods, Instruments and Current Controversies. J. Exp. Bot. 54, 2403–2417. doi:10.1093/jxb/erg263

Broecker, W.S.; Peng, T.-H.; Ostlund, G.; and M. Stuiver. 1985. The distribution of bomb radiocarbon in the ocean. J. Geophys. Res.; 90, 6953-6970

Brovkin, V. 2002. Climate-vegetation interaction. J. Phys., 4, 57–72.

Buermann, W.; Dong, J.; Zeng, X.; Myneni, R.B.; Dickinson, R.E. 2001. Evaluation of the Utility of Satellite-Based Vegetation Leaf Area Index Data for Climate Simulations. J. Clim. 14, 3536–3550. doi:10.1175/1520-0442(2001.014<3536:EOTUOS>2.0.CO;2

Buermann, W.; Lintner, B.R.; Koven, C.D.; Angert, A.; Pinzon, J.E.; Tucker, C.J. and I.Y. Fung. 2007. The changing carbon cycle at Mauna Loa observatory, PNAS, 104(11. 4249-4254.

Buermann, W.; Dong, J.; Zeng, X.; Myneni, R.B.; Dickinson, R.E. 2001. Evaluation of the utility of satellite-based leaf area index data for climate simulation. J. Climate, 14, 3536–3550.

Buitenhuis, E.T.; Rivkin, R.B.; Sailley, S.; and C. Le Quéré. 2010. Biogeochemical flues through microzooplankton, Global Biogeochemical Cycles, 24, GB4015, doi:10.1029/2009GB003601.

Búrquez, A.; Martínez-Yrízar, A.; Núñez, S.; Quintero, T.; Aparicio, A.; 2010. Aboveground biomass in three Sonoran Desert communities: Variability within and among sites using replicated plot harvesting. J. Arid Environ. 74, 1240–1247. doi:10.1016/j.jaridenv.2010.04.004

Cadule, P. , P. Friedlingstein, L. Bopp, S. Sitch, C. D. Jones, P. Ciais, S.L. Piao and P. Peylin. 2010. Benchmarking coupled climate-carbon models against long-term atmospheric CO2 measurements, Global Biogeochemical Cycles, doi:10.1029/2009GB003556

Cairns, M.A.; Olmsted, I.; Granados, J.; Argaez, J.; 2003. Composition and aboveground tree biomass of a dry semi-evergreen forest on Mexico's Yucatan Peninsula. For. Ecol. Manag. 186, 125–132. doi:10.1016/S0378-1127(03.00229-9

Canadell JG, Ciais P, Gurney K, Le Quéré C, Piao S, Raupach MR, Sabine CL. 2011. An international effort to quantify regional carbon fluxes. EOS 92: 81-82.

Canadell JG, Ciais P, Sabine C, Joos F. 2013. REgional Carbon Cycle Assessment and Processes. RECCAP. Special issue. Biogeosciences. http://www.biogeosciences.net/special_issue107.html.

Canadell JG, Pataki D, Gifford R, Houghton RA, Lou Y, Raupach MR, Smith P, Steffen W. 2007. Saturation of the terrestrial carbon sink. In: Terrestrial Ecosystems in a Changing World, Canadell JG, Pataki D, Pitelka L. eds. pp. 59-78. The IGBP Series. Springer-Verlag, Berlin Heidelberg, pp. 59-78.

Canadell, J.G.; Raupach, M.R.; Houghton, R.A. 2009. Anthropogenic CO2 emissions in Africa. Biogeosciences 6, 463–468. doi:10.5194/bg-6-463-2009

Carvalhais, N.; Forkel, M.; Khomik, M.; Bellarby, J.; Jung, M.; Migliavacca, M.; Mu, M.; Saatchi, S.; Santoro, M.; Thurner, M.; Weber, U.; Ahrens, B.; Beer, C.; Cescatti, A.; Randerson, J.T.; Reichstein, M. 2014. Global covariation of carbon turnover times with climate in terrestrial ecosystems. Nature 514, 213–217. doi:10.1038/nature13731

Carvalhais, N.; Forkel, M.; Khomik, M.; Bellarby, J.; Jung, M.; Migliavacca, M.; Mu, M.; Saatchi, S.; Santoro, M.; Thurner, M.; Weber, U.; Ahrens, B.; Beer, C.; Cescatti, A.; Randerson, J.T.; Reichstein, M.;2014. Global covariation of carbon turnover times with climate in terrestrial ecosystems. Nature 514, 213–217. doi:10.1038/nature13731

Cayan, D.R.; Das, T.; Pierce, D.W.; Barnett, T.P.; Tyree, M.; Gershunov, A. 2010. Future dryness in the southwest US and the hydrology of the early 21st century drought. Proc. Natl. Acad. Sci. 107, 21271–21276. doi:10.1073/pnas.0912391107

Challenger, A. 1998. Utilización y conservación de los ecosistemas terrestres de México. Pasado, presente y futuro. Conabio, IBUNAM y Agrupación Sierra Madre, México.

Chapin, F.S.; Matson, P.A.; Vitousek, P. 2011. Principles of Terrestrial Ecosystem Ecology. Springer Science & Business Media.

Chapin, F.S.; Woodwell, G.M.; Randerson, J.T.; Rastetter, E.B.; Lovett, G.M.; Baldocchi, D.D.; Clark, D.A.; Harmon, M.E.; Schimel, D.S.; Valentini, R.;

Wirth, C.; Aber, J.D.; Cole, J.J.; Goulden, M.L.; Harden, J.W.; Heimann, M.; Howarth, R.W.; Matson, P.A.; McGuire, A.D.; Melillo, J.M.; Mooney, H.A.; Neff, J.C.; Houghton, R.A.; Pace, M.L.; Ryan, M.G.; Running, S.W.; Sala, O.E.; Schlesinger, W.H.; Schulze, E.-D. 2006. Reconciling Carbon-cycle Concepts, Terminology, and Methods. Ecosystems 9, 1041–1050. doi:10.1007/s10021-005-0105-7

Charlson, R.J.; Lovelock, J.E.; Andreae, M.O.; Warren, S.G. 1987. Oceanic phytoplankton, atmospheric sulphur, cloud albedo and climate. Nature, 326, 655–661.

Charney, J.; Quirk, W.J.; Chow, S.-H.; Kornfield, J.1977. A comparative study of the effects of albedo change on drought in semi-arid regions. J. Atmos. Sci., 34, 1366–1385.

Chase, T.N.; Pielke, R.; Kittel, T.; Nemani, R.; Running, S. 1996. Sensitivity of a general circulation model to global changes in leaf area index. J. Geophys. Res., 101, 7393–7408.

Chen, J.M.; Cihlar, J. 1996. Retrieving leaf area index of boreal conifer forests using Landsat TM images. Remote Sens. Environ. 55, 153–162. doi:10.1016/0034-4257(95.00195-6

Chevallier, F.; et al. 2010. CO2 surface fluxes at grid point scale estimated from a global 21-year reanalysis of atmospheric measurements. J. Geophys. Res.; 115, D21307, doi:10.1029/2010JD013887.

Chou, C.; Chiang, J.C.H.; Lan, C.-W.; Chung, C.-H.; Liao, Y.-C.; Lee, C.-J. 2013. Increase in the range between wet and dry season precipitation. Nat. Geosci. 6, 263–267. doi:10.1038/ngeo1744

Christidis, N.; Stott, P.; Brown, S.; Karoly, D.; Caesar J. 2007. Human contribution to the lengthening of the growing season during 1950–99. J. Clim., 20, 5441–5454.

Churkina, G.; Schimel, D.; Braswell, B.; Xiao, X. 2005. Spatial analysis of growing season length control over net ecosystem exchange. Global Change Biol., 11, 1777–1787.

Ciais, P.; Tans, P.P.; Trolier, M.; White, J. W. C.; and R. J. Francey. 1995. A large northern hemisphere terrestrial CO2 sink indicated by the 13C/12C ratio of atmospheric CO2, Science, 269, 1098-1102, doi:10.1126/science.269.5227.1098.

Ciais, P.; C. Sabine, G. Bala, L. Bopp, V. Brovkin, J. Canadell, A. Chhabra, R. DeFries, J. Galloway, M. Heimann, C. Jones, C. Le Quéré, R.B. Myneni, S. Piao and P. Thornton, 2013: Carbon and Other Biogeochemical Cycles. In: Cli- mate Change 2013: The Physical Science Basis. Contribution of Working Group I to the Fifth Assessment Report of the Intergovernmental Panel on Climate Change [Stocker, T.F.; D. Qin, G.-K. Plattner, M. Tignor, S.K. Allen, J. Boschung, A. Nauels, Y. Xia, V. Bex and P.M. Midgley. eds..]. Cambridge University Press, Cambridge, United Kingdom and New York, NY, USA.

Ciais, P.; Piao, S.-L.; Cadule, P.; Friedlingstein, P.; Chédin, A. 2009. Variability and recent trends in the African terrestrial carbon balance. Biogeosciences 6, 1935–1948. doi:10.5194/bg-6-1935-2009

Ciais, P.; Reichstein, M.; Viovy, N.; Granier, A.; Ogée, J.; Allard, V.; Aubinet, M.; Buchmann, N.; Bernhofer, C.; Carrara, A.; Chevallier, F.; De Noblet, N.; Friend, A.D.; Friedlingstein, P.; Grünwald, T.; Heinesch, B.; Keronen, P.; Knohl, A.; Krinner, G.; Loustau, D.; Manca, G.; Matteucci, G.; Miglietta, F.; Ourcival, J.M.; Papale, D.; Pilegaard, K.; Rambal, S.; Seufert, G.; Soussana, J.F.; Sanz, M.J.; Schulze, E.D.; Vesala, T.; Valentini, R. 2005. Europe-wide reduction in primary productivity caused by the heat and drought in 2003. Nature 437, 529–533. doi:10.1038/nature03972

Clark, D.B.; L.M. Mercado, S. Sitch, C.D. Jones, N. Gedney, M.J. Best, M. Pryor, G.G. Rooney, R.L.H. Essery, E. Blyth, O. Boucher, P.M. Cox, and R.J. Harding. 2011. The Joint UK Land Environment Simulator. JULES. Model description, Part 2: Carbon fluxes and vegetation, Geosci. Model Dev.; 4(3. 701-722.

Collatz, G.J.; Ball, J.T.; Grivet, C.; Berry, J.A. 1991. Physiological and environmental regulation of stomatal conductance, photosynthesis and transpiration: a model that includes a laminar boundary layer. Agric. For. Meteorol. 54, 107–136. doi:10.1016/0168-1923(91.90002-8

Collins, W.J.; Bellouin, N.; Doutriaux-Boucher, M.; Gedney, N.; Halloran, P.; Hinton, T.; Hughes, J.; Jones, C.D.; Joshi, M.; Liddicoat, S.; Martin, G.; O'Connor, F.; Rae, J.; Senior, C.; Sitch, S.; Totterdell, I.; Wiltshire, A.; Woodward, S. 2011. Development and evaluation of an Earth-system model–HadGEM2. Geosci. Model Dev., 4, 1051-1075.

Conway, T.J.; P.M. Lang, and K.A. Masarie. 2011. Atmospheric Carbon Dioxide Dry Air Mole Fractions from the NOAA ESRL Carbon Cycle Cooperative Global Air Sampling Network, 1968-2010, Version: 2011-06-21, Path: ftp://ftp.cmdl.noaa.gov/ccg/co2/flask/event/.

Cox, P. 2001. Description of the “TRIFFID” dynamic global vegetation model. Hadley Centre Technical Note 24.

Cox, P.M.; Betts, R.A.; Jones, C.D.; Spall, S.A.; Totterdell, I.J. 2000. Acceleration of global warming due to carbon-cycle feedbacks in a coupled climate model. Nature 408, 184–187. doi:10.1038/35041539

Cox, P.M.; Pearson, D.; Booth, B.B.; Friedlingstein, P.; Huntingford, C.; Jones, C.D.; Luke, C.M. 2013. Sensitivity of tropical carbon to climate change constrained by carbon dioxide variability. Nature 494, 341–344. doi:10.1038/nature11882

Dai, A. 2013. Increasing drought under global warming in observations and models. Nat. Clim. Change 3, 52–58. doi:10.1038/nclimate1633

Dai, Z.; Birdsey, R.A.; Johnson, K.D.; Dupuy, J.M.; Hernandez-Stefanoni, J.L.; Richardson, K. 2014. Modeling carbon stocks in a secondary tropical dry forest in the Yucatan Peninsula, Mexico. Water. Air. Soil Pollut. 225, 1–15. doi:10.1007/s11270-014-1925-x

De Jong, B.; Anaya, C.; Masera, O.; Olguín, M.; Paz, F.; Etchevers, J.; Martínez, R.D.; Guerrero, G.; Balbontín, C.; 2010. Greenhouse gas emissions between 1993 and 2002 from land-use change and forestry in Mexico. For. Ecol. Manag. 260, 1689–1701. doi:10.1016/j.foreco.2010.08.011

De Jong, R.; Verbesselt, J.; Zeileis, A.; Schaepman, M. 2013. Shifts in Global Vegetation Activity Trends. Remote Sens. 5, 1117–1133. doi:10.3390/rs5031117

Dee, D. P.; et al. 2011., The ERA-Interim reanalysis: configuration and performance of the data assimilation system, Q J Roy Meteor Soc, 137(656. 553-597.

Defries, R.S.; Houghton, R.A.; Hansen, M.C.; Field, C. B.; Skole, D.; and J. Townshend. 2002. Carbon emissions from tropical deforestation and regrowth based on satellite observations from the 1980s and 1990s, P. Natl. Acad. Sci. USA, 99, 14256-14261.

Denman, K. et al. 2007, 'Couplings Between Changes in the Climate System and Biogeochemistry' in IPCC, Climate Change 2007: The Physical Science Basis, Contribution of Working Group I to the Fourth Assessment Report of the Intergovernmental Panel on Climate Change [Solomon, S.; D. Qin, M. Manning, Z. Chen, M. Marquis, K. Averyt, M. Tignor and H. Miller. eds..], Cambridge University Press, Cambridge, United Kingdom and United States.

Dentener, F.; Stevenson, D.; Ellingsen, K.; van Noije, T.; Schultz, M.; Amann, M.; Atherton, C.; Bell, N.; Bergmann, D.; Bey, I.; Bouwman, L.; Butler, T.; Cofala, J.; Collins, B.; Drevet, J.; Doherty, R.; Eickhout, B.; Eskes, H.; Fiore, A.; Gauss, M.; Hauglustaine, D.; Horowitz, L.; Isaksen, I. S. A.; Josse, B.; Lawrence, M.; Krol, M.; Lamarque, J. F.; Montanaro, V.; Muller, J. F.; Peuch, V. H.; Pitari, G.; Pyle, J.; Rast, S.; Rodriguez, J.; Sanderson, M.; Savage, N. H.; Shindell, D.; Strahan, S.; Szopa, S.; Sudo, K.; Van Dingenen, R.; Wild, O.; and Zeng, G. 2006. The 5 global atmospheric environment for the next generation, Environ. Sci. Technol.; 40, 3586–3594, doi:10.1021/es0523845.

Diaz, S.; Cabido, M. 1997. Plant functional types and ecosystem function in relation to global change. J. Veg. Sci. 8, 463–474. doi:10.2307/3237198

Diaz, S.; Cabido, M.; Casanoves, F. 1998. Plant functional traits and environmental filters at a regional scale. J. Veg. Sci. 9, 113–122. doi:10.2307/3237229

Dickinson, R.E.; Henderson-Sellers, A; Kennedy, P.J. 1993. Biosphere-Atmosphere Transfer Scheme. BATS. Version 1e as coupled to the NCAR community climate model. NCAR Technical Note, NCAR/TN-387+ STR, National Center for Atmospheric Research, Boulder, CO.

Dirmeyer, P.A.; Shukla, J. 1994. Albedo as a modulator of climate response to tropical deforestation. J. Geophys. Res., 99, 20863–20877.

Dolman, A.J.; Shvidenko, A.; Schepaschenko, D.; Ciais, P.; Tchebakova, N.; Chen, T.; van der Molen, M.K.; Belelli Marchesini, L.; Maximov, T.C.; Maksyutov, S.; Schulze, E.-D. 2012. An estimate of the terrestrial carbon budget of Russia using inventory-based, eddy covariance and inversion methods. Biogeosciences 9, 5323–5340. doi:10.5194/bg-9-5323-2012

Doney, S. C.; I. Lima, J. K. Moore, K. Lindsay, M. J. Behrenfeld, T. K. Westberry, N. Mahowald, D. M. Glover, and T. Takahashi. 2009. Skill metrics for confronting global upper ocean ecosystem-biogeochemistry models against field and remote sensing data. J. Mar. Syst. 76, 95–112.

Doney, S. C.; I. Lima, R. A. Feely, D. M. Glover, K. Lindsay, N. Mahowald, J. K. Moore, and R. Wanninkhof. 2009. Mechanisms governing interannual variability in upper-ocean inorganic carbon system and air-sea CO2 fluxes: physical climate and atmospheric dust. Deep-Sea Res.; Part II, 56, 640–655.

Dorigo, W.A.; Scipal, K.; Parinussa, R.M.; Liu, Y.Y.; Wagner, W.; de Jeu, R.A.M.; Naeimi, V. 2010. Error characterisation of global active and passive microwave soil moisture datasets. Hydrol Earth Syst Sci 14, 2605–2616. doi:10.5194/hess-14-2605-2010

Doughty, C.E.; Metcalfe, D.B.; Girardin, C.A.J.; Amezquita, F.F.; Cabrera, D.G.; Huasco, W.H.; Silva-Espejo, J.E.; Araujo-Murakami, A.; da Costa, M.C.; Rocha, W.; Feldpausch, T.R.; Mendoza, A.L.M.; da Costa, A.C.L.; Meir, P.; Phillips, O.L.; Malhi, Y. 2015. Drought impact on forest carbon dynamics and fluxes in Amazonia. Nature 519, 78–82.

Douville, H.; Chauvin, F.; Broqua, H. I2001. nfluence of soil moisture on the Asian and African monsoons. Part I: Mean monsoon and daily precipitation. J. Climate, 14, 2381–2403.

Dufresne, J.-L.; Foujols, M.-A.; Denvil, S.; Caubel, A.; Marti, O.; Aumont, O.; Balkanski, Y.; Bekki, S.; Bellenger, H.; Benshila, R.; Bony, S.; Bopp, L. 2013. Climate change projections using the IPSL-CM5 Earth System Model: from CMIP3 to CMIP5. Clim. Dynam., 40, 2123-2165

Dunne, J.P.; John, J.G.; Shevliakova, E.; Stouffer, R.J.; Krasting, J.P.; Malyshev, S.L.; Milly, P.C.D.; Sentman, L.T.; Adcroft, A.J. Cooke, W.; Dunne, K.A.; et al. 2013. GFDL's ESM2 global coupled climate-carbon Earth System Models. Part II: Carbon system formation and baseline simulation characteristics. J Climate, 26, 2247–2267.

Durack, P.J.; Wijffels, S.E.; Matear, R.J. 2012. Ocean Salinities Reveal Strong Global Water Cycle Intensification During 1950 to 2000. Science 336, 455–458. doi:10.1126/science.1212222

Engelbrecht, B.M.J.; Dalling, J.W.; Pearson, T.R.H.; Wolf, R.L.; Gálvez, D.A.; Koehler, T.; Tyree, M.T.; Kursar, T.A. 2006. Short dry spells in the wet season increase mortality of tropical pioneer seedlings. Oecologia 148, 258–269. doi:10.1007/s00442-006-0368-5

Enting, I.G.; Rayner, P.J.; Ciais, P. 2012. Carbon Cycle Uncertainty in REgional Carbon Cycle Assessment and Processes. RECCAP.. Biogeosciences 9, 2889–2904. doi:10.5194/bg-9-2889-2012

Epule, E.T.; Peng, C.; Lepage, L.; Chen, Z. 2013. The causes, effects and challenges of Sahelian droughts: a critical review. Reg. Environ. Change 14, 145–156. doi:10.1007/s10113-013-0473-z

Euskirchen, E.S.; McGuire, A.D.; Kicklighter, D.W.; Zhuang, Q.; Clein, J.S.; Dargaville, R.J.; Dye, D.G.; Kimball, J.S.; McDonald, K.C.; Melillo, J.M.; Romanovsky, V.E.; Smith, N.V. 2006. Importance of recent shifts in soil thermal dynamics on growing season length, productivity, and carbon sequestration in terrestrial high-latitude ecosystems. Global Change Biol., 12, 731–750.

Falkowski, P. G.; Ziemann, D.; Kolber, Z. & Bienfang, P. K. 1991. Role of eddy pumping in enhancing primary production in the ocean. Nature 352, 55-58.

Fan, S.; Gloor, M.; Mahlmam, J.; Pacala, S.; Sarmiento, J.; Takahashi, T.; and P. Tans. 1998. A large terrestrial carbon sink in North America implied by atmospheric and oceanic carbon dioxide data and models, Science, 282, 442-446.

Fang, H.; Jiang, C.; Li, W.; Wei, S.; Baret, F.; Chen, J.M.; Haro, J.G.; Liang, S.; Liu, R.; Myneni, R.B.; Pinty, B.; Xiao, Z.; Zhu Z. 2013. Characterization and intercomparison of global moderate resolution leaf area index. LAI. products: Analysis of climatologies and theoretical uncertainties. J. Geophys. Res., 118.

FAO/IIASA/ISRIC/ISSCAS/JRC, 2012. Harmonized World Soil Database. version 1.2..

Farquhar, G.D.; Sharkey, T.D. 1982. Stomatal Conductance and Photosynthesis. Annu. Rev. Plant Physiol. 33, 317–345. doi:10.1146/annurev.pp.33.060182.001533

Fay, A. R.; and G. A. McKinley. 2013. Global trends in surface ocean pCO2 from in situ data, Global Biogeochem. Cycles, 27, 541–557, doi:10.1002/gbc.20051.

Fearnside, P.M. 2000. Global Warming and Tropical Land-Use Change: Greenhouse Gas Emissions from Biomass Burning, Decomposition and Soils in Forest Conversion, Shifting Cultivation and Secondary Vegetation. Clim. Change 46, 115–158. doi:10.1023/A:1005569915357

Felzer, B.S.; Cronin, T.W.; Melillo, J.M.; Kicklighter, D.W.; Schlosser, C.A.; Dangal, S.R.S. 2011. Nitrogen effect on carbon-water coupling in forests, grasslands, and shrublands in the arid western United States. J. Geophys. Res. Biogeosciences 116, 03023.

Feng, X.; Porporato, A.; Rodriguez-Iturbe, I. 2013. Changes in rainfall seasonality in the tropics. Nat. Clim. Change 3, 811–815. doi:10.1038/nclimate1907

Fernández-Martínez, M.; Vicca, S.; Janssens, I.A.; Sardans, J.; Luyssaert, S.; Campioli, M.; Chapin Iii, F.S.; Ciais, P.; Malhi, Y.; Obersteiner, M.; Papale, D.; Piao, S.L.; Reichstein, M.; Rodà, F.; Peñuelas, J. 2014. Nutrient availability as the key regulator of global forest carbon balance. Nat. Clim. Change 4, 471–476. doi:10.1038/nclimate2177

Field, C.B.; Jackson, R.B.; Mooney, H.A. 1995. Stomatal responses to increased CO2: implications from the plant to the global scale. Plant Cell Environ. 18, 1214–1225. doi:10.1111/j.1365-3040.1995.tb00630.x

Foley, J.A.; DeFries, R.; Asner, G.P.; Barford, C.; Bonan, G.; Carpenter, S.R.; Chapin, F.S.; Coe, M.T.; Daily, G.C.; Gibbs, H.K.; Helkowski, J.H.; Holloway, T.; Howard, E.A.; Kucharik, C.J.; Monfreda, C.; Patz, J.A.; Prentice, I.C.; Ramankutty, N.; Snyder, P.K. 2005. Global Consequences of Land Use. Science 309, 570–574. doi:10.1126/science.1111772

Foley, J.A.; Levis, S.; Costa, M.H.; Cramer, W.; Pollard, D. Incorporating dynamic vegetation cover within global climate models. 2000, Ecol. Appl., 10, 1620-1632.

Foley, J.A.; Prentice, I.C.; Ramankutty, N.; Levis, S.; Pollard, D.; Sitch, S.; Haxeltine, A. 1996. An integrated biosphere model of land surface

processes, terrestrial carbon balance, and vegetation dynamics. Global Biogeochem. Cy., 10, 603-628.

Forkel, M.; Carvalhais, N.; Schaphoff, S.; v. Bloh, W.; Migliavacca, M.; Thurner, M.; Thonicke, K. 2014. Identifying environmental controls on vegetation greenness phenology through model-data integration. Biogeosciences Discuss. 11, 10917–11025. doi:10.5194/bgd-11-10917-2014

Friedl, M.A.; Schimel, D.S.; Michaelsen, J.; Davis, F.W.; Walker, H. 1994. Estimating grassland biomass and leaf area index using ground and satellite data. Int. J. Remote Sens. 15, 1401–1420. doi:10.1080/01431169408954174

Friedlingstein, P.; Cox, P.; Betts, R.; Bopp, L.; von Bloh, W.; Brovkin, V.; Cadule, P.; Doney, S.; Eby, M.; Fung, I.; Bala, G.; John, J.; Jones, C.; Joos, F.; Kato, T.; Kawamiya, M.; Knorr, W.; Lindsay, K.; Matthews, H.D.; Raddatz, T.; Rayner, P.; Reick, C.; Roeckner, E.; Schnitzler, K.-G.; Schnur, R.; Strassmann, K.; Weaver, A.J.; Yoshikawa, C.; Zeng, N. 2006. Climate–Carbon Cycle Feedback Analysis: Results from the C4MIP Model Intercomparison. J. Clim. 19, 3337–3353. doi:10.1175/JCLI3800.1

Friedlingstein, P.; Fung, I.; Holland, E.; John, J.; Brasseur, G.; Erickson, D.; Schimel, D. 1995. On the contribution of CO2 fertilization to the missing biospheric sink. Glob. Biogeochem. Cycles 9, 541–556. doi:10.1029/95GB02381

Friedlingstein, P.; Houghton, R.A.; Marland, G.; Hackler, J.; Boden, T.A.; Conway, T.J.; Canadell, J.G.; Raupach, M.R.; Ciais, P.; Quéré, C.L. 2010. Update on CO2 emissions. Nat. Geosci. 3, 811–812. doi:10.1038/ngeo1022

Friedlingstein, P.; Meinshausen, M.; Arora, V.K.; Jones, C.D.; Anav, A.; Liddicoat, S.K.; Knutti, R. 2013. Uncertainties in CMIP5 Climate Projections due to Carbon Cycle Feedbacks. J. Clim. 27, 511–526. doi:10.1175/JCLI-D-12-00579.1

Friedlingstein, P.; R.A. Houghton, G. Marland, J. Hackler, T.A. Boden, T.J. Conway, J.G. Canadell, M.R. Raupach, P. Ciais and C. Le Quere. 2011. Update on CO2 emissions, Nature Geosciences, 3, 811-812.

Friend, A.D.; Lucht, W.; Rademacher, T.T.; Keribin, R.; Betts, R.; Cadule, P.; Ciais, P.; Clark, D.B.; Dankers, R.; Falloon, P.D.; Ito, A.; Kahana, R.; Kleidon, A.; Lomas, M.R.; Nishina, K.; Ostberg, S.; Pavlick, R.; Peylin, P.; Schaphoff, S.; Vuichard, N.; Warszawski, L.; Wiltshire, A.; Woodward, F.I. 2014. Carbon residence time dominates uncertainty in terrestrial vegetation responses to future climate and atmospheric CO2. Proc. Natl. Acad. Sci. 111, 3280–3285. doi:10.1073/pnas.1222477110

Galbraith, D.; P. E. Levy, S. Sitch, C. Huntingford , P. Cox, M. Williams, P. Meir. 2010. Multiple mechanisms of Amazonian Forest biomass losses in three Dynamic Global Vegetation Models under climate change, New Phytologist, 187(3. 647-665

Ganguly, S.; Nemani, R.R.; Zhang, G.; Hashimoto, H.; Milesi, C.; Michaelis, A.; Wang, W.; Votava, P.; Samanta, A.; Melton, F.; Dungan, J.L.; Vermote, E.; Gao, F.; Knyazikhin, Y.; Myneni, R.B. 2012. Generating global Leaf Area Index from Landsat: Algorithm formulation and demonstration. Remote Sens. Environ. doi:10.1016/j.rse.2011.10.032

Gao, F.; Morisette, J.T.; Wolfe, R.E.; Ederer, G.; Pedelty, J.; Masuoka, E.; Myneni, R.; Tan, B.; Nightingale, J. 2008. An Algorithm to Produce Temporally and Spatially Continuous MODIS-LAI Time Series. IEEE Geosci. Remote Sens. Lett. 5, 60–64.

Garcia-Moya, Montanes-Castro. 1992. Saline grassland near Mexico City. C, in: Primary Productivity of Grass Ecosystems of the Tropics and Sub-Tropics. Chapman and Hall, London.; pp. 70–99.

Gatti, L.V.; Gloor, M.; Miller, J.B.; Doughty, C.E.; Malhi, Y.; Domingues, L.G.; Basso, L.S.; Martinewski, A.; Correia, C.S.C.; Borges, V.F.; Freitas, S.; Braz, R.; Anderson, L.O.; Rocha, H.; Grace, J.; Phillips, O.L.; Lloyd, J. 2014. Drought sensitivity of Amazonian carbon balance revealed by atmospheric measurements. Nature 506.

Gedney, N.; Cox, P.M.; Betts, R.A.; Boucher, O.; Huntingford, C.; Stott, P.A. 2006. Detection of a direct carbon dioxide effect in continental river runoff records, Nature, 439, 835-838.

Gent, P. R.; G. Danabasoglu,. 2011. Response to Increasing Southern Hemisphere Winds in CCSM4. Journal of Climate, Vol. 24, Iss. 19, pp. 4992?4998.

Giorgi, F.; Marinucci M.R.; Bates, G.T. 1993. Development of a second generation regional climate model. RegCM2.. I. Boundary-layer and radiative transfer processes. Mon Weather Rev., 121, 2794–2813

Girard, C.M. 1982. Estimation of phenological stages and physiological states of grasslands from remote-sensing data. Vegetatio 1982, 48, 219–226.

Gloor, M.; Gatti, L.; Brienen, R.; Feldpausch, T.R.; Phillips, O.L.; Miller, J.; Ometto, J.P.; Rocha, H.; Baker, T.; de Jong, B.; Houghton, R.A.; Malhi, Y.; Aragão, L.E.O.C.; Guyot, J.-L.; Zhao, K.; Jackson, R.; Peylin, P.; Sitch, S.; Poulter, B.; Lomas, M.; Zaehle, S.; Huntingford, C.; Levy, P.; Lloyd, J. 2012. The carbon balance of South America: a review of the status, decadal trends and main determinants. Biogeosciences 9, 5407–5430. doi:10.5194/bg-9-

Goll, D.S.; Brovkin, V.; Parida, B.R.; Reick, C.H.; Kattge, J.; Reich, P.B.; van Bodegom, P.M.; Niinemets, Ü. 2012. Nutrient limitation reduces land carbon uptake in simulations with a model of combined carbon, nitrogen and phosphorus cycling. Biogeosciences 9, 3547–3569. doi:10.5194/bg-9-3547-2012

Gomez-Peralta, D.; Oberbauer, S.F.; McClain, M.E.; Philippi, T.E. 2008. Rainfall and cloud-water interception in tropical montane forests in the eastern Andes of Central Peru. For. Ecol. Manag. 255, 1315–1325. doi:10.1016/j.foreco.2007.10.058

Gonzalez, P.; Tucker, C.J.; Sy, H. 2012. Tree density and species decline in the African Sahel attributable to climate. J. Arid Environ. 78, 55–64. doi:10.1016/j.jaridenv.2011.11.001

Green, E.P.; Mumby, P.J.; Edwards, A.J.; Clark, C.D.; Ellis, A.C. 1997. Estimating leaf area index of mangroves from satellite data. Aquat. Bot. 58, 11–19. doi:10.1016/S0304-3770(97.00013-2

Greve, P.; Orlowsky, B.; Mueller, B.; Sheffield, J.; Reichstein, M.; Seneviratne, S.I. 2014. Global assessment of trends in wetting and drying over land. Nat. Geosci. 7, 716–721. doi:10.1038/ngeo2247

Grover, H.D.; Musick, H.B. 1990. Shrubland encroachment in southern New Mexico, U.S.A.: An analysis of desertification processes in the American southwest. Clim. Change 17, 305–330. doi:10.1007/BF00138373

Gruber, N. 2011. Warming up, turning sour, losing breath: Ocean biogeochemistry under global change. Phil. Trans. R. Soc. A, 369, 1980-1996, doi:10.1098/rsta.2011.0003.

Gruber, N.; et al. 2009. Oceanic sources, sinks, and transport of atmospheric CO2, Global Biogeochemical Cycles, 23, GB1005, doi:10.1029/2008GB003349.

Gruber, N.; Galloway, J.N. 2008. An Earth-system perspective of the global nitrogen cycle. Nature 451, 293–296. doi:10.1038/nature06592

Gruber, N.; Keeling, C.D.; Bates, N.R. 2002. Interannual Variability in the North Atlantic Ocean Carbon Sink. Science 298, 2374–2378. doi:10.1126/science.1077077

Gruber, N.; Lachkar, Z.; Frenzel, H.; Marchesiello, P.; Munnich, M.; McWilliams, J.; Nagai, T.; and Plattner, G.-K. 2011. Eddy-induced reduction of biological production in Eastern Boundary Upwelling Systems, Nat. Geosci.; 4, 787–792, doi:10.1038/ngeo1273.

Guan, D.; Liu, Z.; Geng, Y.; Lindner, S.; and K Hubacek. 2012. The gigatonne gap in China's carbon dioxide inventories, Nature Climate Change, doi: 10.1038/NCLIMATE1560

Guenther, A.; Karl, T.; Harley, P.; Wiedinmyer, C.; Palmer, P. I.; Geron, C. 2006. Estimates of global terrestrial isoprene emissions using MEGAN. Model of Emissions of Gases and Aerosols from Nature.. Atmos. Chem. Phys., 6, 3181–3210.

Gurney, K.R.; Eckels, W.J. 2011. Regional trends in terrestrial carbon exchange and their seasonal signatures. Tellus B 63, 328–339. doi:10.1111/j.1600-0889.2011.00534.x

Hänninen, H.; Tanino, K. 2011. Tree seasonality in a warming climate. Trends Plant Sci., 16, 412–416.

Harris, I.; Jones, P. d.; Osborn, T. j.; Lister, D. h; 2013. Updated high-resolution grids of monthly climatic observations – the CRU TS3.10 Dataset. Int. J. Climatol. n/a–n/a. doi:10.1002/joc.3711

Hayes, D.J.; Turner, D.P.; Stinson, G.; McGuire, A.D.; Wei, Y.; West, T.O.; Heath, L.S.; de Jong, B.; McConkey, B.G.; Birdsey, R.A.; Kurz, W.A.; Jacobson, A.R.; Huntzinger, D.N.; Pan, Y.; Post, W.M.; Cook, R.B. 2012. Reconciling estimates of the contemporary North American carbon balance among terrestrial biosphere models, atmospheric inversions, and a new approach for estimating net ecosystem exchange from inventory-based data. Glob. Change Biol. 18, 1282–1299. doi:10.1111/j.1365-2486.2011.02627.x

Hein, L.; De Ridder, N. 2006. Desertification in the Sahel: a reinterpretation. Glob. Change Biol. 12, 751–758. doi:10.1111/j.1365-2486.2006.01135.x

Held, I.; Soden, B.;2006. Robust Responses of the Hydrological Cycle to Global Warming. J. Clim. 19.

Hicke, J.A. 2005. NCEP and GISS solar radiation data sets available for ecosystem modeling: Description, differences, and impacts on net primary production. Global Biogeochemical Cycles, 19(GB2006.: doi:10.1029/2004GB002391.

Hickler, T.; Prentice, I.C.; Smith, B.; Sykes, M.T.; and Zaehle, S. 2006. Implementing plant hydraulic architecture within the LPJ Dynamic Global Vegetation Model. Global Ecology and Biogeography 15: 567-577.

Hickler, T.; Smith, B.; Prentice, I.C.; Mjöfors, K.; Miller, P.; Arneth, A.; Sykes, M.T. 2008. CO2 fertilization in temperate FACE experiments not representative of boreal and tropical forests. Glob. Change Biol. 14, 1531–1542. doi:10.1111/j.1365-2486.2008.01598.x

Higgins, R.W.; Leetmaa, A.; Xue, Y.; Barnston, A. 2000. Dominant Factors Influencing the Seasonal Predictability of U.S. Precipitation and Surface Air Temperature. J. Clim. 13, 3994–4017. doi:10.1175/1520-0442(2000.013<3994:DFITSP>2.0.CO;2

Houghton, R.A. 2010. How well do we know the flux of CO2 from land-use change? Tellus B, 62, 337-351, doi:10.1111/j.1600-0889.2010.00473.x

Houghton, R.A.; House, J.I.; Pongratz, J.; van der Werf, G.R.; DeFries, R.S.; Hansen, M.C.; Le Quéré, C.; Ramankutty, N. 2012. Carbon emissions from land use and land-cover change. Biogeosciences 9, 5125–5142. doi:10.5194/bg-9-5125-2012

Hourdin, F.; Musat, I.; Bony, S.; Braconnot, P.; Codron, F.; Dufresne, J.-L.; Fairhead, L.; Filiberti, M. A.; Friedlingstein, P.; Grandpeix, J.-Y.; et al. 2006. The LMDZ4 general circulation model: climate performance and sensitivity to parametrized physics with emphasis on tropical convection. Clim. Dynam. , 19, 3445–3482.

Hughes, R.F.; Kauffman, J.B.; Jaramillo, V.J.; 1999. Biomass, carbon, and nutrient dynamics of secondary forests in a humid tropical region of méxico.1999. Ecology 80, 1892–1907. doi:10.1890/0012-9658

Huntingford, C.; Jones, P.D.; Livina, V.N.; Lenton, T.M.; Cox, P.M. 2013. No increase in global temperature variability despite changing regional patterns. Nature 500, 327–330. doi:10.1038/nature12310

Huntingford, C.; Stott, P. A.; Allen, M. R. and Lambert, F. H. 2006. Incorporating model uncertainty into attribution of observed temperature change. Geophysical Research Letters, 33, L05710. 10.1029/2005GL024831

Hurtt, G.; Chini, L.; Frolking, S.; Betts, R.; Feddema, J.; Fischer, G.; Fisk, J.; Hibbard, K.; Houghton, R.; Janetos, A.; Jones, C.; Kindermann, G.; Kinoshita, T.; Klein Goldewijk, K.; Riahi, K.; Shevliakova, E.; Smith, S.; Stehfest, E.; Thomson, A.; Thornton, P.; van Vuuren, D.; Wang, Y. 2011. Harmonization of land-use scenarios for the period 1500–2100: 600 years of global gridded annual land-use transitions, wood harvest, and resulting secondary lands. Clim. Change 109, 117–161. doi:10.1007/s10584-011-0153-2

Hurtt, G.; Chini, L.; Frolking, S.; Betts, R.; Feddema, J.; Fischer, G.; Fisk, J.; Hibbard, K.; Houghton, R.; Janetos, A.; Jones, C.; Kindermann, G.;

Kinoshita, T.; Klein Goldewijk, K.; Riahi, K.; Shevliakova, E.; Smith, S.; Stehfest, E.; Thomson, A.; Thornton, P.; van Vuuren, D.; Wang, Y. 2011. Harmonization of land-use scenarios for the period 1500–2100: 600 years of global gridded annual land-use transitions, wood harvest, and resulting secondary lands. Clim. Change 109, 117–161. doi:10.1007/s10584-011-0153-2

Iivonen, S.; Kaakinen, S.; Jolkkonen, A.; Vapaavuori, E.; Linder, S. 2006. Influence of long-term nutrient optimization on biomass, carbon, and nitrogen acquisition and allocation in Norway spruce. Can. J. For. Res. 36, 1563–1571. doi:10.1139/x06-035

Jain, A.K. and X. Yang. 2015. Modeling the Effects of Two Different Land Cover Change Data Sets on the Carbon Stocks of Plants and Soils in Concert With CO2 and Climate Change, Global Biogeochemical Cycles ,19, doi:10.1029/2004GB002349.

Janssens, I. A. et al. 2003. Europe's terrestrial biosphere absorbs 7 to 12% of European anthropogenic CO2 emissions. Science 300, 1538–1542.

Jasso, R. 2014. Crecimiento, biomasa y carbono arbóreo en un gradiente altitudinal en bosques templados. Tesis de Maestría, Posgrado en Ciencias Biológicas, UNAM.

Jeansson, E.; A. Olsen, T. Eldevik, I. Skjelvan, A.M. Omar, S.K. Lauvset, J.E.Ø. Nilsen, R.G.J. Bellerby, T. Johannessen, and E. Falck. 2011. The Nordic Seas carbon budget: Sources, sinks, and uncertainties, Global Biogeochemical Cycles, 25, 4010, doi:10.1029/2010GB003961.

Jeong, S.-J.; Ho, C.-H.; Gim, H.-J.; Brown, M.E. 2011. Phenology shifts at start vs. end of growing season in temperate vegetation over the Northern Hemisphere for the period 1982–2008. Glob. Change Biol. 17, 2385–2399. doi:10.1111/j.1365-2486.2011.02397.x

Jeong, S.-J.; Ho, C.-H.; Gim, H.J.; Brown, M.E. 2011. Phenology shifts at start vs. end of growing season in temperate vegetation over the Northern Hemisphere for the period 1982–2008. Global Change Biol., 17, 2385–2399.

Jönsson, A.M.; Schröder, M.; Lagergren, F.; Anderbrandt, O. & Smith, B. 2015. Guess the impact of Ips typographus – an ecosystem modelling approach for simulating spruce bark beetle outbreaks. Agricultural and Forest Meteorology, in press.

Jung, M. et al. 2007. Uncertainties of modeling gross primary productivity over Europe: A systematic study on the effects of using different drivers and terrestrial biosphere models. Global Biogeochemical Cycles, 21(GB4021.: doi:10.1029/2006GB002915.

Jung, M.; Reichstein, M.; Bondeau, A. 2009. Towards global empirical upscaling of FLUXNET eddy covariance observations: validation of a model tree ensemble approach using a biosphere model. Biogeosciences 6, 2001–2013. doi:10.5194/bg-6-2001-2009

Jung, M.; Reichstein, M.; Ciais, P.; Seneviratne, S.I.; Sheffield, J.; Goulden, M.L.; Bonan, G.; Cescatti, A.; Chen, J.; de Jeu, R.; Dolman, A.J.; Eugster, W.; Gerten, D.; Gianelle, D.; Gobron, N.; Heinke, J.; Kimball, J.; Law, B.E.; Montagnani, L.; Mu, Q.; Mueller, B.; Oleson, K.; Papale, D.; Richardson, A.D.; Roupsard, O.; Running, S.; Tomelleri, E.; Viovy, N.; Weber, U.;

Williams, C.; Wood, E.; Zaehle, S.; Zhang, K. 2010. Recent decline in the global land evapotranspiration trend due to limited moisture supply. Nature 467, 951–954. doi:10.1038/nature09396

Jung, M.; Reichstein, M.; Margolis, H.A.; Cescatti, A.; Richardson, A.D.; Arain, M.A.; Arneth, A.; Bernhofer, C.; Bonal, D.; Chen, J.; Gianelle, D.; Gobron, N.; Kiely, G.; Kutsch, W.; Lasslop, G.; Law, B.E.; Lindroth, A.; Merbold, L.; Montagnani, L.; Moors, E.J.; Papale, D.; Sottocornola, M.; Vaccari, F.; Williams, C. 2011. Global patterns of land-atmosphere fluxes of carbon dioxide, latent heat, and sensible heat derived from eddy covariance, satellite, and meteorological observations. J. Geophys. Res. Biogeosciences 116, G00J07. doi:10.1029/2010JG001566

Kalnay, E.; et al. 1996. The NCEP/NCAR 40-year reanalysis project, B Am Meteorol Soc, 77(3. 437-471.

Kang, H.-S.; Xue, Y.; Collatz, G.J. 2007. Impact assessment of satellite-derived leaf area index datasets using a general circulation model: Seasonal variability. J. Climate, 20, 993–1015.

Kattge, J. et al. 2011. TRY – a global database of plant traits, Global Change Biology, 17(9. 2905-2935.

Keeling C.; Whorf T,P. 2005. Atmospheric CO2 records from sites in the SIO sampling network. In Trends: A compendium of data on global change. Carbon Dioxide Information Analysis Center, Oak Ridge National Laboratory, U.S. Department of Energy, Oak Ridge, Tenn.; U.S.A.

Keeling, C.D.; Bacastow, R.B.; Bainbridge, A.E.; Ekdahl Jr, C.A.; Guenther, P.R.; Waterman, L.S. and J.F.S. Chin. 1976. Atmospheric carbon dioxide variations at Mauna Loa observatory, Hawaii, Tellus, 28(6. 538 – 551.

Keeling, C.D.; Whorf, T.P.; Wahlen, M.; Van Der Plicht, J. 1995. Interannual extremes in the rate of rise of atmospheric carbon dioxide since 1980. Nature 375, 666–670.

Keeling, C.D.; Chin, J.F.S.; Whorf, T.P. 1996. Increased activity of northern vegetation in inferred from atmospheric CO2 measurements. Nature, 382, 146–149.

Keenan T, García R, Friend AD, Zaehle S, Gracia C, Sabaté S. 2009. Improved understanding of drought controls on seasonal variation in Mediterranean forest canopy CO2 and water fluxes through combined in situ measurements and ecosystem modelling. Biogeosciences, 6:1423-44.

Khatiwala, S.; T. Tanhua, S. Mikaloff; Fletcher, M. Gerber, S. C. Doney, H. D. Graven, N. Gruber, G. A. McKinley, A. Murata, A. F. Ríos, C. L. Sabine, and J. L. Sarmiento. 2012. Global ocean storage of anthropogenic carbon, Biogeosciences Discuss.; 9, 8931-8988

Kim, T.-W.; Lee, K.; Najjar, R.G.; Jeong, H.-D.; Jeong, H.J. 2011. Increasing N Abundance in the Northwestern Pacific Ocean Due to Atmospheric Nitrogen Deposition. Science 334, 505–509. doi:10.1126/science.1206583

Kimball, J.; McDonald, K.; Running, S.; Frolking S. 2004. Satellite radar remote sensing of seasonal growing seasons for boreal and subalpine evergreen forests. Remote Sens. Environ, 90, 243–258.

Kimball, J.; McDonald, K.; Running, S.; Frolking, S. 2004. Satellite radar remote sensing of seasonal growing seasons for boreal and subalpine evergreen forests. Remote Sens. Environ, 90, 243–258.

King, A.W.; Andres, R.J.; Davis, K.J.; Hafer, M.; Hayes, D.J.; Huntzinger, D.N.; de Jong, B.; Kurz, W.A.; McGuire, A.D.; Vargas, R.; Wei, Y.; West, T.O.; Woodall, C.W. 2015. North America's net terrestrial CO2 exchange with the atmosphere 1990–2009. Biogeosciences 12, 399–414. doi:10.5194/bg-12-399-2015

King, A.W.; Hayes, D.J.; Huntzinger, D.N.; West, T.O.; Post, W.M. 2012. North American carbon dioxide sources and sinks: magnitude, attribution, and uncertainty. Front. Ecol. Environ. 10, 512–519. doi:10.1890/120066

Knapp, A.K.; Smith, M.D. 2001. Variation Among Biomes in Temporal Dynamics of Aboveground Primary Production. Science 291, 481–484. doi:10.1126/science.291.5503.481

Knorr, W.; Prentice, I.C.; House, J.I.; Holland, E.A. 2005. Long-term sensitivity of soil carbon turnover to warming. Nature 433, 298–301. doi:10.1038/nature03226

Knyazikhin, Y.; Martonchik, J.V.; Diner, D.J.; Myneni, R.B.; Verstraete, M.; Pinty, B.; Gobron, N. 1998. Estimation of vegetation canopy leaf area index and fraction of absorbed photosynthetically active radiation from atmosphere-corrected MISR data. J. Geophys. Res. 103, PP. 32,239–32,256. doi:199810.1029/98JD02461

Koven, C.D.; Ringeval, B.; Friedlingstein, P.; Ciais, P.; Cadule, P.; Khvorostyanov, D.; Krinner, G.; Tarnocai, C. 2011. Permafrost Carbon-Climate Feedbacks Accelerate Global Warming. Proc. Natl. Acad. Sci. 108, 14769–14774. doi:10.1073/pnas.1103910108

Krinner, G.; Viovy, N.; de Noblet-Ducoudré, N.; Ogée, J.; Polcher, J.; Friedlingstein, P.; Ciais, P.; Sitch, S.; Prentice, I.C. 2005. A dynamic global vegetation model for studies of the coupled atmosphere-biosphere system. Glob. Biogeochem. Cycles 19. doi:10.1029/2003GB002199

Kumar, S.; Lawrence, D.M.; Dirmeyer, P.A.; Sheffield, J.; 2014. Less reliable water availability in the 21st century climate projections. Earths Future 2, 152–160. doi:10.1002/2013EF000159

Lagergren, F.; Jönsson, A.M.; Blennow, K. & Smith, B. 2015. Implementing storm damage in a dynamic vegetation model for regional applications in Sweden. Ecological Modelling.

Lambert, F.H.; Gillett, N.P.; Stone, D.A. and Huntingford, C. 2005 Attribution studies of observed land precipitation changes with nine coupled model, Geophysical Research Letters 32, Art Num: L18704.

Landsberg, J.J.; Waring, R.H. 1997. A generalised model of forest productivity using simplified concepts of radiation-use efficiency, carbon balance and partitioning. For. Ecol. Manag. 95, 209–228. doi:10.1016/S0378-1127(97.00026-1

Large, W. G.; and S. Yeager. 2004: Diurnal to decadal global forcing for ocean and sea-ice models: The data sets and flux climatologies. NCAR Tech. Rep. TN-460_STR, 105 pp.

Lathière, J.; Hauglustaine, D.A.; Friend, A.D.; De Noblet-Ducoudré, N.; Viovy, N.; Folberth, G.A. 2006. Impact of climate variability and land use changes on global biogenic volatile organic compound emissions. Atmos. Chem. Phys., 6, 2129-2146.

Lawrence DM, Oleson KW, Flanner MG , Thornton PE, Swenson SC, Lawrence PJ, Zeng X, Yang Z-L, Levis S, Sakaguchi K, Bonan GB, and Slater AG. 2011. Parameterization improvements and functional and structural advances in version 4 of the Community Land Model. Journal of Advances in Modeling Earth Systems, 3, doi: 10.1029/2011MS000045.

Lawrence, D.M.; Slingo, J.M. 2004. An annual cycle of vegetation in a GCM. Part II: Global impacts on climate and hydrology. Clim. Dynam., 22, 107–122.

Le Quéré , C.; S.P. Harrison, I.C. Prentice, E.T. Buitenhuis, O. Aumont, L. Bopp, H. Claustre, L. Cotrim da Cunha, R. Geider, X. Giraud, C. Klaas, K. Kohfeld, L. Legendre, M. Manizza, T. Platt, R.B. Rivkin, S. Sathyendranath, J. Uitz, A.J. Watson, D. Wolf-Gladrow, 2005. Ecosystem dynamics based on plankton functional types for global ocean biogeochemistry models. Global Change Biology Vol. 11. 11. p. 2016-2040, doi: 10.1111/j.1365-2486.2005.001004.x

Le Quéré C, Raupach MR, Canadell JG, Marland G, Bopp L, Ciais P, Conway TJ, Doney SC, Feely RA, Foster P, et al. 2009. Trends in the sources and sinks of carbon dioxide, Natural Geosciences 2(12.: 831-836

Le Quéré, C.; Andres, R.J.; Boden, T.; Conway, T.; Houghton, R.A.; House, J.I.; Marland, G.; Peters, G.P.; van der Werf, G.R.; Ahlström, A.; Andrew, R.M.; Bopp, L.; Canadell, J.G.; Ciais, P.; Doney, S.C.; Enright, C.; Friedlingstein, P.; Huntingford, C.; Jain, A.K.; Jourdain, C.; Kato, E.; Keeling, R.F.; Klein Goldewijk, K.; Levis, S.; Levy, P.; Lomas, M.; Poulter, B.; Raupach, M.R.; Schwinger, J.; Sitch, S.; Stocker, B.D.; Viovy, N.; Zaehle, S.; Zeng, N. 2013. The global carbon budget 1959–2011. Earth Syst. Sci. Data 5, 165–185. doi:10.5194/essd-5-165-2013

Le Quéré, C.; Moriarty, R.; Andrew, R.M.; Peters, G.P.; Ciais, P.; Friedlingstein, P.; Jones, S.D.; Sitch, S.; Tans, P.; Arneth, A.; Boden, T.A.; Bopp, L.; Bozec, Y.; Canadell, J.G.; Chevallier, F.; Cosca, C.E.; Harris, I.; Hoppema, M.; Houghton, R.A.; House, J.I.; Jain, A.; Johannessen, T.; Kato, E.; Keeling, R.F.; Kitidis, V.; Klein Goldewijk, K.; Koven, C.; Landa, C.S.; Landschützer, P.; Lenton, A.; Lima, I.D.; Marland, G.; Mathis, J.T.; Metzl, N.; Nojiri, Y.; Olsen, A.; Ono, T.; Peters, W.; Pfeil, B.; Poulter, B.; Raupach, M.R.; Regnier, P.; Rödenbeck, C.; Saito, S.; Salisbury, J.E.; Schuster, U.; Schwinger, J.; Séférian, R.; Segschneider, J.; Steinhoff, T.; Stocker, B.D.; Sutton, A.J.; Takahashi, T.; Tilbrook, B.; van der Werf, G.R.; Viovy, N.; Wang, Y.-P.; Wanninkhof, R.; Wiltshire, A.; Zeng, N. 2014. Global carbon budget 2014. Earth Syst. Sci. Data Discuss. 7, 521–610. doi:10.5194/essdd-7-521-2014

Le Quéré, C.; T. Takahashi, C. E. Buitenhuis, C. Rödenbeck, and S. Sutherland. 2010. Impact of climate change and variability on the global oceanic sink of CO2. Global Biogeochem. Cycles, 24, GB4007

Levy ,P.E; Cannell M; Friend A. 2004. Modelling the impact of future changes in climate, CO2 concentration and land use on natural ecosystems and the terrestrial carbon sink. Global Environmental Change, 14, 21-30.

Lewis, S. L.; G. Lopez-Gonzalez, B. Sonké, K. Affum-Baffoe, T. R. Baker, L. O. Ojo, O. L. Phillips, J. M. Reitsma, L. White, J. A. Comiskey, M.-N. D. K, C. E. N. Ewango, T. R. Feldpausch, A. C. Hamilton, M. Gloor, T. Hart, A. Hladik, J. Lloyd, J. C. Lovett, J.-R. Makana, Y. Malhi, F. M. Mbago, H. J. Ndangalasi, J. Peacock, K. S. H. Peh, D. Sheil, T. Sunderland, M. D. Swaine, J. Taplin, D. Taylor, S. C. Thomas, R. Votere & H. Wöll. 2009. Increasing carbon storage in intact African tropical forests. Nature, 457, 1003-1006.

Lewis, S.L.; J. Lloyd, S. Sitch, E. T. A. Mitchard & W. F. Laurance. 2009. Changing Ecology of Tropical Forests: Evidence and Drivers, Annu. Rev. Ecol. Evol. Syst.; 40:529–49

Linderholm, H.W. 2006. Growing season changes in the last century. Agric. For. Meteorol. 137, 1–14. doi:10.1016/j.agrformet.2006.03.006

Lindsay, K.; Bonan, G.B.; Doney, S.C.; Hoffman, F.M.; Lawrence, D.M.; Long, M.C.; Mahowald, N.M.; Moore, J.K.; Randerston, J.T.; Thornton, P.E. 2013. Preindustrial Control and 20th Century Carbon Cycle Experiments with the Earth System Model CESM1.

Liu, Y.Y.; Evans, J.P.; McCabe, M.F.; de Jeu, R.A.M.; van Dijk, A.I.J.M.; Dolman, A.J.; Saizen, I. 2013. Changing Climate and Overgrazing Are Decimating Mongolian Steppes. PLoS ONE 8, e57599. doi:10.1371/journal.pone.0057599

Liu, Y.Y.; Parinussa, R.M.; Dorigo, W.A.; De Jeu, R.A.M.; Wagner, W.; van Dijk, A.I.J.M.; McCabe, M.F.; Evans, J.P. 2011. Developing an improved soil moisture dataset by blending passive and active microwave satellite-based retrievals. Hydrol Earth Syst Sci 15, 425–436. doi:10.5194/hess-15-425-2011

Lovelock, J. 1987. The Ages of Gaia: A Biography of Our Living Earth, 2nd ed. OUP Oxford.

Lovenduski, N. S.; N. Gruber, S. C. Doney, and I. D. Lima. 2007. Enhanced CO2 outgassing in the Southern Ocean from a positive phase of the Southern Annular Mode. Global Biogeochemical Cycles 21:2, doi:10.1029/2006GB002900.

Lucht, W.; Prentice, I.C.; Myneni, R.B.; Sitch, S.; Friedlingstein, P.; Cramer, W.; Bousquet, P.; Buermann, W.; Smith, B. 2002. Climatic Control of the High-Latitude Vegetation Greening Trend and Pinatubo Effect. Science 296, 1687–1689. doi:10.1126/science.1071828

Lucht, W.; Prentice, I.C.; Myneni, R.B.; Sitch, S.; Friedlingstein, P.; Cramer, W.; Bousquet, P.; Buermann, W.; Smith, B. 2002. Climatic control of the high-latitude vegetation greening trend and Pinatubo effect. Science, 296, 1687–1689.

Luo, Y.Q et al. 2012. A framework of benchmarking land models, Biogeosciences Discusss.; 9, 1899-1944, 2012.

Maignan, F.; Bréon, F.-M.; Chevallier, F.; Viovy, N.; Ciais, P.; Garrec, C.; Trules, J.; Mancip, M. 2011. Evaluation of a Global Vegetation Model using time series of satellite vegetation indices. Geosci. Model Dev. 4, 1103–1114.

Malhi, Y.; Aragão, L.E.O.C.; Galbraith, D.; Huntingford, C.; Fisher, R.; Zelazowski, P.; Sitch, S.; McSweeney, C.; Meir, P. 2009. Exploring the likelihood and mechanism of a climate-change-induced dieback of the Amazon rainforest. Proc. Natl. Acad. Sci. 106, 20610–20615. doi:10.1073/pnas.0804619106

Malhi, Y.; Grace, J. 2000. Tropical forests and atmospheric carbon dioxide. Trends Ecol. Evol. 15, 332–337. doi:10.1016/S0169-5347(00.01906-6

Manning, A.C.; Keeling, R.F. 2006. Global oceanic and land biotic carbon sinks from the Scripps atmospheric oxygen flask sampling network. Tellus B 58, 95–116. doi:10.1111/j.1600-0889.2006.00175.x

Mao, J; Shi, X.; Thornton, P.E.; Piao, S.; Wnag, X. 2012. Causes of spring vegetation growth trends in the northern mid–high latitudes from 1982 to 2004. Environ. Res. Lett. , 7, 014010 doi:10.1088/1748-9326/7/1/014010.

Mao, J.; Shi, X.; Thornton, P.; Hoffman, F.; Zhu, Z.; Myneni, R. 2013. Global Latitudinal-Asymmetric Vegetation Growth Trends and Their Driving Mechanisms: 1982–2009. Remote Sens. 5, 1484–1497. doi:10.3390/rs5031484

Martinez-Yrizar, A.; Maass, J.M.; Perez-Jimenez, L.A.; Sarukhan, J. 1996. Net primary productivity of a tropical deciduous forest ecosystem in western Mexico. J. Trop. Ecol. 12, 169–175. doi:10.1017/S026646740000938X

Masera, O.R.; Cerón, A.D.; Ordóñez, A. 2001. Forestry Mitigation Options for Mexico: Finding Synergies between National Sustainable Development Priorities and Global Concerns. Mitig. Adapt. Strateg. Glob. Change 6, 291–312. doi:10.1023/A:1013327019175

Matear, R. J.; A. Lenton, 2008: Impact of Historical Climate Change on the Southern Ocean Carbon Cycle. J. Climate, 21, 5820–5834. doi: http://dx.doi.org/10.1175/2008JCLI2194.1

Matsumoto, K. and N. Gruber. 2005. How accurate is the estimation of anthropogenic carbon in the ocean? An evaluation of the DC* method, Global Biogeochemical Cycles, 19, GB3014, doi:10.1029/2004GB002397.

Matsumoto, K.; Ohta, T.; Irasawa, M.; Nakamura, T.; 2003. Climate change and extension of the Ginkgo biloba L. growing season in Japan. Glob. Change Biol. 9, 1634–1642. doi:10.1046/j.1365-2486.2003.00688.x

McDowell, N.; Pockman, W.T.; Allen, C.D.; Breshears, D.D.; Cobb, N.; Kolb, T.; Plaut, J.; Sperry, J.; West, A.; Williams, D.G.; Yepez, E.A.; 2008. Mechanisms of plant survival and mortality during drought: why do some plants survive while others succumb to drought? New Phytol. 178, 719–739. doi:10.1111/j.1469-8137.2008.02436.x

McDowell, N.G. 2011. Mechanisms Linking Drought, Hydraulics, Carbon Metabolism, and Vegetation Mortality, Plant Physiology, 155, 1051-1059

McGillicuddy, D. J. et al. 1998. Influence of mesoscale eddies on new production in the Sargasso Sea. Nature 394, 263_266.

McGuire, A.D.; Sitch, S.; Clein, J.S.; Dargaville, R.; Esser, G.; Foley, J.; Heimann, M.; Joos, F.; Kaplan, J.; Kicklighter, D.W.; Meier, R.A.; Melillo, J.M.; Moore, B.; Prentice, I.C.; Ramankutty, N.; Reichenau, T.; Schloss, A.; Tian, H.; Williams, L.J.; Wittenberg, U. 2001. Carbon balance of the terrestrial biosphere in the Twentieth Century: Analyses of CO2, climate

and land use effects with four process-based ecosystem models. Glob. Biogeochem. Cycles 15, 183–206. doi:10.1029/2000GB001298

McKinley, G. a. et al. 2006. North Pacific carbon cycle response to climate variability on seasonal to decadal timescales. Journal of Geophysical Research, 111(C7. pp.1-22.

McKinley, G. a. et al. 2011. Convergence of atmospheric and North Atlantic carbon dioxide trends on multidecadal timescales. Nature Geoscience, 4(9. pp.606-610.

McNeil, B. I. and Matear, R. J. 2013. The non-steady state oceanic CO2 signal: its importance, magnitude and a novel way to detect it, Biogeosciences, 10, 2219-2228, doi:10.5194/bg-10-2219-2013.

Menzel, A.; Fabian, P. 1999. Growing season extended in Europe. Nature, 397, 659.

Mercado, L. M.; N. Bellouin, S. Sitch, O. Boucher, C. Huntingford and P. M. Cox. 2009. Impact of Changes in Diffuse Radiation on the Global Land Carbon Sink. Nature, 458. 7241. 1014.

Miralles, D.G.; van den Berg, M.J.; Gash, J.H.; Parinussa, R.M.; de Jeu, R.A.M.; Beck, H.E.; Holmes, T.R.H.; Jiménez, C.; Verhoest, N.E.C.; Dorigo, W.A.; Teuling, A.J.; Johannes Dolman, A. 2014. El Niño–La Niña cycle and recent trends in continental evaporation. Nat. Clim. Change 4, 122–126. doi:10.1038/nclimate2068

Mitchell, T.D.; Jones, P.D. 2005. An improved method of constructing a database of monthly climate observations and associated high-resolution grids. Int. J. Climatol., 25, 693–712.

Moore, B.; Braswell, B.H. 1994. The lifetime of excess atmospheric carbon dioxide. Glob. Biogeochem. Cycles 8, 23–38. doi:10.1029/93GB03392

Morales, P.; Hickler, T.; Rowell, D.P.; Smith, B.; Sykes, M.T. 2007. Changes in European ecosystem productivity and carbon balance driven by regional climate model output. Glob. Change Biol. 13, 108–122. doi:10.1111/j.1365-2486.2006.01289.x

Mueller, B.; Hirschi, M.; Jimenez, C.; Ciais, P.; Dirmeyer, P.A.; Dolman, A.J.; Fisher, J.B.; Jung, M.; Ludwig, F.; Maignan, F.; Miralles, D.; McCabe, M.F.; Reichstein, M.; Sheffield, J.; Wang, K.C.; Wood, E.F.; Zhang, Y.; Seneviratne, S.I. 2013. Benchmark products for land evapotranspiration: LandFlux-EVAL multi-dataset synthesis. Hydrol. Earth Syst. Sci. Discuss. 10, 769–805. doi:10.5194/hessd-10-769-2013

Murray-Tortarolo, G.; Anav, A.; Friedlingstein, P.; Sitch, S.; Piao, S.; Zhu, Z. 2013. Evaluation of DGVMs in reproducing satellite derived LAI over the Northern Hemisphere. Part I: Uncoupled DGVMs. Remote Sensing 4,701-759

Myneni, R.B.; Keeling, C.D.; Tucker, C.J.; Asrar, G.; and R.R. Nemani. 1997. Increased plant growth in the northern high latitudes from 1981 to 1991, Nature, 386, 698-702, doi:10.1038/386698a0

Myneni, R.B.; Ramakrishna, R.; Nemani, R.; Running, S.W. 1997. Estimation of global leaf area index and absorbed par using radiative transfer models. Geosci. Remote Sens. IEEE Trans. On 35, 1380 –1393. doi:10.1109/36.649788

Myneni, R.B.; Hoffman, S.; Knyazikhin, Y.; Privette, J. L.; Glassy, J.; Tian, Y.; Wang, Y.; Song, X.; Zhang, Y.; Smith, G.; et al. 2002. Global products of vegetation leaf area and fraction absorbed PAR from year one of MODIS data. Remote Sens. Environ., 83, 214–231.

Navar, J.; Rodriguez-Flores, F. de J.; Dominguez-Calleros, P.A.; Perez-Verdin, G. 2014. Diversity-Productivity Relationship in the Northeastern Tamaulipan Thornscrub Forest of Mexico. Int. J. Ecol. 2014, e196073. doi:10.1155/2014/196073

Nemani, R.R.; Keeling, C.D.; Hashimoto, H.; Jolly, W.M.; Piper, S.C.; Tucker, C.J.; Myneni, R.B.; Running, S.W. 2003. Climate-Driven Increases in Global Terrestrial Net Primary Production from 1982 to 1999. Science 300,

New MG, Hulme M, Jones PD. 2000. Representing twentieth-century space-climate variability, Part II, Development of 1901-1996 monthly grids of terrestrial surface climate. Journal of Climate, 13, 2217-2238

Norby, R.J.; DeLucia, E.H.; Gielen, B.; Calfapietra, C.; Giardina, C.P.; King, J.S.; Ledford, J.; McCarthy, H.R.; Moore, D.J.P.; Ceulemans, R.; De Angelis, P.; Finzi, A.C.; Karnosky, D.F.; Kubiske, M.E.; Lukac, M.; Pregitzer, K.S.; Scarascia-Mugnozza, G.E.; Schlesinger, W.H.; Oren, R. 2005. Forest response to elevated CO2 is conserved across a broad range of productivity. Proc. Natl. Acad. Sci. U. S. A. 102, 18052–18056. doi:10.1073/pnas.0509478102

Norby, R.J.; Warren, J.M.; Iversen, C.M.; Medlyn, B.E.; and R. E. McMurtrie. 2010. Co2 enhancement of forest productivity constrained by limited nitrogen availability. PNAS, 107, 19368-19373.

Oleson, K.W.; Lawrence, D.M.; B, G.; Flanner, M.G.; Kluzek, E.; J, P.; Levis, S.; Swenson, S.C.; Thornton, E.; Feddema, J.; Heald, C.L.; Lamarque, J.; Niu, G.; Qian, T.; Running, S.; Sakaguchi, K.; Yang, L.; Zeng, X.; Zeng, X. 2010. Technical Description of version 4.0 of the Community Land Model. CLM..

Oleson, K.W.; Bonan, G.B. 2000. The effects of remotely sensed plant functional type and leaf area index in simulations of boreal forest surface fluxes by the NCAR land surface model. J. Hydrometeor., 1, 431–446.

Olivier, J.G.J.; Janssens-Maenhout, G.; J.A.H.W. Peters. 2012. Trends in global CO2 emissions, 2012 report, Background Studies, PBL Netherlands Environmental Assessment Agency, 40 pp.

Pacala, S. W. et al. 2001. Consistent land- and atmosphere-based US carbon sink estimates, Science 292, 2316–2320.

Pacala, S.; Birdsey, R.; Bridgham, S.; Conant, R.; Davis, K.; Houghton, R.; Jenkins, J.; Johnston, M.; Marland, G.; Paustian, K.; 2007. The North American Carbon Budget Past and Present, in: The First State of the Carbon Cycle Report. SOCCR. The North American Carbon Budget and Implications for the Global Carbon Cycle. A Report by the U.S. Climate Change Science Program and the Subcommittee on Global Change Research. National Oceanic and Atmospheric Administration, National Climatic Data Center, Asheville, NC, USA, pp. 29–36.

Pan, Y.; Birdsey, R.A.; Fang, J.; Houghton, R.; Kauppi, P.E.; Kurz, W.A.; Phillips, O.L.; Shvidenko, A.; Lewis, S.L.; Canadell, J.G.; Ciais, P.; Jackson, R.B.; Pacala, S.W.; McGuire, A.D.; Piao, S.; Rautiainen, A.;

Sitch, S.; Hayes, D.; 2011. A Large and Persistent Carbon Sink in the World's Forests. Science 333, 988–993. doi:10.1126/science.1201609

Pappas, C.; Fatichi, S.; Leuzinger, S.; Wolf, A.; Burlando, P. 2013. Sensitivity analysis of a process-based ecosystem model: Pinpointing parameterization and structural issues. J. Geophys. Res. Biogeosciences 118, 505–528. doi:10.1002/jgrg.20035

Pausas, J.G.; Ribeiro, E. 2013. The global fire–productivity relationship. Glob. Ecol. Biogeogr. 22, 728–736. doi:10.1111/geb.12043

Pearson, P.N.; Palmer, M.R. 2000. Atmospheric carbon dioxide concentrations over the past 60 million years. Nature 406, 695–699. doi:10.1038/35021000

Peel, M.C.; McMahon, T.A. 2006. Continental Runoff: A quality-controlled global runoff data set. Nature 444, E14–E14. doi:10.1038/nature05480

Petroff, A.; Mailliat, A.; Amielh, M.; Anselmet, F. 2008. Aerosol dry deposition on vegetative canopies. Part 1: Review of present knowledge. Atmos. Environ., 42, 3625–3653.

Peylin, P.; Law, R.M.; Gurney, K.R.; Chevallier, F.; Jacobson, A.R.; Maki, T.; Niwa, Y.; Patra, P.K.; Peters, W.; Rayner, P.J.; Rödenbeck, C.; van der Laan-Luijkx, I.T.; Zhang, X. 2013. Global atmospheric carbon budget: results from an ensemble of atmospheric CO2 inversions. Biogeosciences 10, 6699–6720. doi:10.5194/bg-10-6699-2013

Piao, S. L.; P. Friedlingstein, P. Ciais, L. M. Zhou, and A. P. Chen. 2006. Effect of climate and CO2 changes on the greening of the Northern Hemisphere over the past two decades, Geophys. Res. Lett.; 33,

Piao, S.; Fang, J.; Ciais, P.; Peylin, P.; Huang, Y.; Sitch, S.; Wang, T. 2009. The carbon balance of terrestrial ecosystems in China. Nature 458, 1009–1013. doi:10.1038/nature07944

Piao, S.; Friedlingstein, P.; Ciais, P.; Viovy, N.; and J. Demarty. 2007. Growing season extension and its impact on terrestrial carbon cycle in the Northern Hemisphere over the past 2 decades, Global Biogeochemical Cycles, 21, GB3018, doi:10.1029/2006GB002888.

Piao, S.; Sitch, S.; Ciais, P.; Friedlingstein, P.; Peylin, P.; Wang, X.; Ahlström, A.; Anav, A.; Canadell, J.G.; Cong, N.; Huntingford, C.; Jung, M.; Levis, S.; Levy, P.E.; Li, J.; Lin, X.; Lomas, M.R.; Lu, M.; Luo, Y.; Ma, Y.; Myneni, R.B.; Poulter, B.; Sun, Z.; Wang, T.; Viovy, N.; Zaehle, S.; Zeng, N. 2013. Evaluation of terrestrial carbon cycle models for their response to climate variability and to CO2 trends. Glob. Change Biol. 19, 2117–2132. doi:10.1111/gcb.12187

Piao, S.L.; Ciais, P.; de Noblet-Ducoudre, Cadule, P.; Viovy, N.; and T. Wang. 2009. Spatiotemporal patterns of terrestrial carbon cycle during the 20th century, Global Biogeochem. Cy. 23, GB4026, doi:10.1029/2008GB003339.

Piao, S.L.; Ito, A.; Li, S.G.; Huang, Y.; Ciais, P.; Wang, X.H.; Peng, S.S.; Nan, H.J.; Zhao, C.; Ahlström, A.; Andres, R.J.; Chevallier, F.; Fang, J.Y.; Hartmann, J.; Huntingford, C.; Jeong, S.; Levis, S.; Levy, P.E.; Li, J.S.; Lomas, M.R.; Mao, J.F.; Mayorga, E.; Mohammat, A.; Muraoka, H.; Peng, C.H.; Peylin, P.; Poulter, B.; Shen, Z.H.; Shi, X.; Sitch, S.; Tao, S.; Tian,

H.Q.; Wu, X.P.; Xu, M.; Yu, G.R.; Viovy, N.; Zaehle, S.; Zeng, N.; Zhu, B. 2012. The carbon budget of terrestrial ecosystems in East Asia over the last two decades. Biogeosciences 9, 3571–3586. doi:10.5194/bg-9-3571-2012

Pielke, R.A.; Avissar, R.; Raupach, M.; Dolman, A.J.; Zeng, X.; Denning, A.S. 1998. Interactions between the atmosphere and terrestrial ecosystems: influence on weather and climate. Global Change Biol., 4, 461–475.

Pitman, A.J. 2003. The evolution of, and revolution in, land surface schemes designed for climate models. Int. J. Climatol., 23, 479–510.

Poulter, B.; Frank, D.; Ciais, P.; Myneni, R.B.; Andela, N.; Bi, J.; Broquet, G.; Canadell, J.G.; Chevallier, F.; Liu, Y.Y.; Running, S.W.; Sitch, S.; van der Werf, G.R. 2014. Contribution of semi-arid ecosystems to interannual variability of the global carbon cycle. Nature 509, 600–603. doi:10.1038/nature13376

Poulter, B.; Frank, D.; Hodson, E.L.; Lischke, H. and Zimmermann, N.E. 2011. Impacts of land cover and climate data selection on understanding terrestrial carbon dynamics and the CO2 airborne fraction. Biogeosciences, 8: 2027-2036.

Poulter, B.; Heyder, U.; Cramer, W. 2009. Modeling the Sensitivity of the Seasonal Cycle of GPP to Dynamic LAI and Soil Depths in Tropical Rainforests. Ecosystems 12, 517–533. doi:10.1007/s10021-009-9238-4

Poulter, B.; N. Pederson, H. Liu, Z. Zhu, R. D'Arrigo, P. Ciais, N. Davi, D. Frank, C. Leland, R. Myneni, S. Piao, and T. Wang. 2013. Recent trends in Inner Asian forest dynamics to temperature and precipitation indicate high sensitivity to climate change. Agricultural and Forest Meteorology 178-179:31-45.

Prentice I. C.; G.D. Farquhar, M.J.R. Fasham, M.L. Goulden, M. Heimann, V.J. Jaramillo, H.S. Kheshgi, C. Le Quere, R.J. Scholes, D.W.R. Wallace Contributing Authors D. Archer, M.R. Ashmore, O. Aumont, D. Baker, M. Battle, M. Bender, L.P. Bopp, P. Bousquet, K. Caldeira, P. Ciais, P.M. Cox, W. Cramer, F. Dentener, I.G. Enting, C.B. Field, P. Friedlingstein, E.A. Holland, R.A. Houghton, J.I. House, A. Ishida, A.K. Jain, I.A. Janssens, F. Joos, T. Kaminski, C.D. Keeling, R.F. Keeling, D.W. Kicklighter, K.E. Kohfeld, W. Knorr, R. Law, T. Lenton, K. Lindsay, E. Maier-Reimer, A.C. Manning, R.J. Matear, A.D. McGuire, J.M. Melillo, R. Meyer, M. Mund, J.C. Orr, S. Piper, K. Plattner, P.J. Rayner, S. Sitch, R. Slater, S. Taguchi, P.P. Tans, H.Q. Tian, M.F. Weirig, T. Whorf, A. Yool. 2001.. The carbon cycle and atmospheric carbon dioxide. In. Climate Change 2001: The Scientific Basis. eds Houghton J.T. et al. Cambridge Univ. Press, New York

Prentice, I.C.; Bondeau, A.; Cramer, W.; Harrison, S.P.; Hickler, T.; Lucht, W.; Sitch, S.; Smith, B.; Sykes, M.T. 2007. Dynamic Global Vegetation Modeling: Quantifying Terrestrial Ecosystem Responses to Large-Scale Environmental Change, in: Canadell, J.G.; Pataki, D.E.; Pitelka, L.F. Eds. Terrestrial Ecosystems in a Changing World, Global Change — The IGBP Series. Springer Berlin Heidelberg, pp. 175–192.

Prentice, I.C.; Kelley, D.I.; Foster, P.N.; Friedlingstein, P.; Harrison, S.P.; Bartlein, P.J. 2011. Modeling fire and the terrestrial carbon balance. Glob. Biogeochem. Cycles 25, 13 PP. doi:201110.1029/2010GB003906

Prince, S.D. 1991. A model of regional primary production for use with coarse resolution satellite data. Int. J. Remote Sens. 12, 1313–1330. doi:10.1080/01431169108929728

Quaife, T. et al. 2008. Impact of land cover uncertainties on estimates of biospheric carbon fluxes. Global Biogeochemical Cycles, 22, GB4016.: doi:10.1029/2007GB003097.

Raddatz, T.; Reick, C.H.; Knorr, W.; Kattge, J.; Roeckner, E. Schnur, R.; Schnitzler, K.-G.; Wetzel, P.; Jungclaus, J. 2007. Will the tropical land biosphere dominate the climate-carbon cycle feedback during the twenty-first century? Clim. Dynam., 29, 565-574.

Ramankutty, N.; Foley, J.A. 1999. Estimating historical changes in global land cover: Croplands from 1700 to 1992. Glob. Biogeochem. Cycles 13, 997–1027. doi:10.1029/1999GB900046

Randerson, J.T.; Hoffman, F.M.; Thornton, P.E.; Mahowald, N.M.; Lindsay, K.; Lee, Y.-H.; Nevison, C.D.; Doney, S.C.; Bonan, G.; Stöckli, R.; Covey, C.; Running, S.W.; Fung, I.Y. 2009. Systematic assessment of terrestrial biogeochemistry in coupled climate–carbon models. Glob. Change Biol. 15, 2462–2484. doi:10.1111/j.1365-2486.2009.01912.x

Rea, J.; Ashley, M. 1976. Phenological evaluations using Landsat-1 sensors. Int. J. Biometeorol 1976, 20, 240–248

Reich, P.B.; Hobbie, S.E.; Lee, T.; Ellsworth, D.S.; West, J.B.; Tilman, D.; Knops, J.M.H.; Naeem, S.; Trost, J. 2006. Nitrogen limitation constrains sustainability of ecosystem response to CO2. Nature 440, 922–925. doi:10.1038/nature04486

Reich, P.B.; Hobbie, S.E.; Lee, T.D. 2014. Plant growth enhancement by elevated CO2 eliminated by joint water and nitrogen limitation. Nat. Geosci. 7, 920–924. doi:10.1038/ngeo2284

Reich, P.B.; Oleksyn, J. 2004. Global patterns of plant leaf N and P in relation to temperature and latitude. Proc. Natl. Acad. Sci. U. S. A. 101, 11001–11006. doi:10.1073/pnas.0403588101

Reichstein, M.; Bahn, M.; Ciais, P.; Frank, D.; Mahecha, M.D.; Seneviratne, S.I.; Zscheischler, J.; Beer, C.; Buchmann, N.; Frank, D.C.; Papale, D.; Rammig, A.; Smith, P.; Thonicke, K.; van der Velde, M.; Vicca, S.; Walz, A.; Wattenbach, M. 2013. Climate extremes and the carbon cycle. Nature 500, 287–295. doi:10.1038/nature12350

Richardson, A.D.; Anderson, R.S.; Arain, M.A.; Barr, A.G.; Bohrer, G.; Chen, G.; Chen, J.M.; Ciais, P.; Davis, K.J.; Desai, A.R.; Dietze, M.C.; Dragoni, D.; Garrity, S.R.; Gough, C.M.; Grant, R.; Hollinger, D.Y.; Margolis, H.A.; McCaughey, H.; Migliavacca, M.; Monson, R.K.; Munger, J.W.; Poulter, B.; Raczka, B.M.; Ricciuto, D.M.; Sahoo, A.K.; Schaefer, K.; Tian, H.; Vargas, R.; Verbeeck, H.; Xiao, J.; Xue, Y. 2011. Terrestrial biosphere models need better representation of vegetation phenology: results from the North American Carbon Program Site Synthesis. Glob. Change Biol. 18, 566–584. doi:10.1111/j.1365-2486.2011.02562.x

Richardson, A.D.; Black, T.A.; Ciais, P.; Delbart, N.; Friedl, M.A.; Gobron, N.; Hollinger, D.Y.; Kutsch, W.L.; Longdoz, B.; Luyssaert, S.; et al. 2010. Influence of spring and autumn phenological transitions on forest ecosystem productivity. Philos. T. R. Soc. B., 365, 3227–3246.

Rodhe, H. 1990. A comparison of the contribution of various gases to the greenhouse effect. Science 248, 1217–1219. doi:10.1126/science.248.4960.1217

Roy, T.; L. Bopp,M. Gehlen, B. Schneider, P. Cadule, T.L. Frölicher, J. Segschneider, J. Tjiputra, C.Heinze, and F. Joos. 2011. Regional Impacts of Climate Change and Atmospheric CO2 on Future Ocean Carbon Uptake: A Multimodel Linear Feedback Analysis, J. Climate, 24, 2300-2318.

Running, S.W.; Coughlan, J.C. 1988. A general model of forest ecosystem processes for regional applications I. Hydrologic balance, canopy gas exchange and primary production processes. Ecol. Model. 42, 125–154. doi:10.1016/0304-3800

Running, S.W.; Nemani, R.R.; Heinsch, F.A.; Zhao, M.; Reeves, M.; Hashimoto, H. 2004. A Continuous Satellite-Derived Measure of Global Terrestrial Primary Production. BioScience 54, 547–560. doi:10.1641/0006-3568

Sabine. C.S.; R. A. Feely, N. Gruber, R. M. Key, K. Lee, J. L. Bullister, R. Wanninkhof, C. S. Wong, D. W. R. Wallace, B. Tillbrook, F. J. Millero, T.-H. Peng, A. Kozyr, T. Ono, and A. F. Rios. 2004. The oceanic sink for anthropogenic CO2. Science, 305, 367-371.

Sarmiento, J.L. and N. Gruber. 2002. Sinks for anthropogenic carbon. Physics Today. 55, 30-36.

Sarmiento, J.L.; Gloor, M.; Gruber, N.; Beaulieu, C.; Jacobson, A.R.; Mikaloff Fletcher, S.E.; Pacala, S.; Rodgers, K. 2010. Trends and regional distributions of land and ocean carbon sinks. Biogeosciences 7, 2351–2367. doi:10.5194/bg-7-2351-2010

Sarmiento, J.L.; Hughes, T.M.C.; Stouffer, R.J.; Manabe, S. 1998. Simulated response of the ocean carbon cycle to anthropogenic climate warming. Nature 393, 245–249. doi:10.1038/30455

Sarmiento, JL, and N. Gruber. 2006. Ocean Biogeochemical Dynamics, Princeton Univ. Press, 526pp.

Schulz, J.-P.; Dümenil, L.; Polcher, J.; Schlosser, C.A.; Xue, Y. 1998. Land surface energy and moisture fluxes: Comparing three models. J. Appl. Meteor, 37, 288–307.

Schuster, U.; Mckinley, G. A.; Bates, N. R.; Chevallier, F.; Doney, S. C.; Fay, A. R.; Gruber, N.; et al. 2013.. An assessment of the Atlantic and Arctic sea-air CO2 fluxes, 2000-2009. Biogeosciences, 10, 607–627. doi:10.5194/bg-10-607-2013.

Schuur, E.A.G.; Bockheim, J.; Canadell, J.G.; Euskirchen, E.; Field, C.B.; Goryachkin, S.V.; Hagemann, S.; Kuhry, P.; Lafleur, P.M.; Lee, H.; Mazhitova, G.; Nelson, F.E.; Rinke, A.; Romanovsky, V.E.; Shiklomanov, N.; Tarnocai, C.; Venevsky, S.; Vogel, J.G.; Zimov, S.A. 2008. Vulnerability of Permafrost Carbon to Climate Change: Implications for the Global Carbon Cycle. BioScience 58, 701–714. doi:10.1641/B580807

Sellers, P.J.; Randall, D.A.; Betts, A.K.; Hall, F.G.; Berry, J.A.; Collatz, G.J.; Denning, A.S.; Mooney, H.A.; Nobre, C.A.; Sato, N.; et al. 1997. Modeling the exchanges of energy, water, and carbon between continents and the atmosphere. Science, 275, 502–509.

Sellers, P.J.; Randall, D.A.; Collatz, G.J.; Berry, J.A.; Field, C.B.; Dazlich, D.A.; Zhang, C.; Collelo, G.D.; Bounoua, L. 1996. A revised land surface parameterization. SiB2. for atmospheric GCMs, Part I : Model Formulation. J. Climate, 9, 676–705.

SEMARNAT, 2002. Evaluacion de la degradacion de suelo causada por el hombre en la Republica Mexicana.

Seneviratne, S.I. 2012. Climate science: Historical drought trends revisited. Nature, 491, 338–339. doi:10.1038/491338a

Sheffield, J.; Wood, E.F.; Roderick, M.L. 2012. Little change in global drought over the past 60 years. Nature 491, 435–438. doi:10.1038/nature11575

Shukla, J.; Mintz, Y. 1982. Influence of land-surface evapotranspiration on the Earth's climate. Science, 215, 1498–1501.

Sitch, S.; C. Huntingford, N. Gedney, P. E. Levy, M. Lomas, S. Piao, R. Betts, P. Ciais, P. Cox, P. Friedlingstein, C. D. Jones, I. C. Prentice, F. I. Woodward. 2008. Evaluation of the terrestrial carbon cycle, future plant geography, and climate-carbon cycle feedbacks using 5 Dynamic Global Vegetation Models. DGVMs.. Global Change Biology,14 1-25,doi:10.1111/j.1365-2486.2008.01626.x

Sitch, S.; Friedlingstein, P.; Gruber, N.; Jones, S.D.; Murray-Tortarolo, G.; Ahlström, A.; Doney, S.C.; Graven, H.; Heinze, C.; Huntingford, C.; Levis, S.; Levy, P.E.; Lomas, M.; Poulter, B.; Viovy, N.; Zaehle, S.; Zeng, N.; Arneth, A.; Bonan, G.; Bopp, L.; Canadell, J.G.; Chevallier, F.; Ciais, P.; Ellis, R.; Gloor, M.; Peylin, P.; Piao, S.L.; Le Quéré, C.; Smith, B.; Zhu, Z.; Myneni, R. 2015. Recent trends and drivers of regional sources and sinks of carbon dioxide. Biogeosciences 12, 653–679. doi:10.5194/bg-12-653-2015

Sitch, S.; P. M. Cox, W. J. Collins, C. Huntingford. Indirect radiative forcing of climate change through ozone effects on the land-carbon sink. 2007. Nature , doi:10.1038/nature06059.

Smith, B.; Prentice, I.C.; Sykes, M.T. 2001. Representation of vegetation dynamics in the modelling of terrestrial ecosystems: comparing two contrasting approaches within European climate space. Glob. Ecol. Biogeogr. 10, 621–637. doi:10.1046/j.1466-822X.2001.t01-1-00256.x

Smith, N.V.; Saatchi, S. S.; Randerson, J.T. 2004. Trends in high northern latitude soil freeze and thaw cycles from 1988 to 2002. J. Geophys. Res., 109.

Sokolov, A.P.; Kicklighter, D.W.; Melillo, J.M.; Felzer, B.S.; Schlosser, C.A.; Cronin, T.W. 2008. Consequences of Considering Carbon–Nitrogen Interactions on the Feedbacks between Climate and the Terrestrial Carbon Cycle. J. Clim. 21, 3776–3796. doi:10.1175/2008JCLI2038.1

Stephens, B.B.; Gurney, K.R.; Tans, P.P.; Sweeney, C.; Peters, W.; Bruhwiler, L.; Ciais, P.; Ramonet, M.; Bousquet, P.; Nakazawa, T.; Aoki, S.; Machida, T.; Inoue, G.; Vinnichenko, N.; Lloyd, J.; Jordan, A.; Heimann, M.;

Shibistova, O.; Langenfelds, R.L.; Steele, L.P.; Francey, R.J.; Denning, A.S.; 2007. Weak Northern and Strong Tropical Land Carbon Uptake from Vertical Profiles of Atmospheric CO2. Science 316, 1732–1735. doi:10.1126/science.1137004

Sterl, A.; Severijns, C.; Dijkstra, H.; Hazeleger, W.; Oldenborgh, G.J. van, Broeke, M. van den, Burgers, G.; Hurk, B. van den, Leeuwen, P.J. van, Velthoven, P. van. 2008. When can we expect extremely high surface temperatures? Geophys. Res. Lett. 35, 5 PP. doi:200810.1029/2008GL034071

Stier, P.; Feichter, J.; Kinne, S.; Kloster, S.; Vignati, E.; Wilson, J.; Ganzeveld, L.; Tegen, I.; Werner, M.; Balkanski, Y.; et al. 2005. The aerosol-climate model ECHAM5-HAM. Atmos. Chem. Phys., 5, 1125-1156.

Stöckli, R.; Vidale, P.L. 2004. European plant phenology and climate as seen in a 20-year AVHRR land-surface parameter dataset. Int. J. Remote Sens., 25, 3303–3330.

Sud, Y.C.; Fennessy, M.J. 1982. A study of the influence of surface albedo on July circulation in semi-arid regions using the GLAS GCM. J. Climatol., 2, 105–125.

Sud, Y.C.; Shukla, J.; Mintz, Y. 1988. Influence of land surface roughness on atmospheric circulation and precipitation: A sensitivity study with a general circulation model. J. Appl. Meteor., 27, 1036–1054.

Suni, T.; Berninger, F.; Markkanen, T.; Keronen, P.; Rannik, Ü.; Vesala T. 2003. Interannual variability and timing of growing-season CO2 exchange in a boreal forest. J. Geophys. Res., 108.

Suzuki, R.; Nomaki, T.; Yasunari, T. 2003. West-east contrast of phenology and climate in northern Asia revealed using a remotely sensed vegetation index. Int. J. Remote Sens., 47, 126–138.

Sweeney, C.; Gloor, E.; Jacobson, A. R.; Key, R. M.; McKinley, G.; Sarmiento, J. L.; and Wanninkhof, R. 2007. Constraining global air-sea gas exchange for CO2 with recent bomb 14C measurements, Global Biogeochem. Cycl.; 21, GB2015, doi:10.1029/2006GB002784.

Tans, P.P.; I.Y. Fung, and T. Takahash., 1990. Observational constraints on the global atmospheric CO2 budget. Science, 247, 1431-1439, doi:10.1126/science.247.4949.1431.

Taylor, K.E.; Stouffer, R.J.; Meehl, G.A. 2011. An Overview of CMIP5 and the Experiment Design. Bull. Am. Meteorol. Soc. 93, 485–498. doi:10.1175/BAMS-D-11-00094.1

Thonicke, K.; Venevsky, S.; Sitch, S.; Cramer, W. 2001. The role of fire disturbance for global vegetation dynamics: coupling fire into a Dynamic Global Vegetation Model. Glob. Ecol. Biogeogr. 10, 661–677. doi:10.1046/j.1466-822X.2001.00175.x

Thornton PE and Rosenbloom NA. 2005. Ecosystem model spin-up: Estimating steady state conditions in a coupled terrestrial carbon and nitrogen cycle model. Ecological Modelling 189:25-48.

Thornton PE.; et al. 2009. Carbon-nitrogen interactions regulate climate-carbon cycle feedbacks: Results from an atmosphere-ocean general circulation model, Biogeosciences, 6, 2099–2120.

Thornton, P.E.; Lamarque, J.-F.; Rosenbloom, N.A.; Mahowald, N.M.; 2007. Influence of carbon-nitrogen cycle coupling on land model response to CO2 fertilization and climate variability. Glob. Biogeochem. Cycles 21, GB4018. doi:10.1029/2006GB002868

Tian, Y.; Dickinson, R.E.; Zhou, L.; Myneni, R.B.; Friedl, M.; Chaaf, C.B.; Carroll, M.; Gao, F. 2004. Land boundary conditions from MODIS data and consequences for the albedo of a climate model. Geophys. Res. Lett., 31, L05504.

Tjiputra, J.F.; K. Assmann, and C. Heinze,.2010, Anthropogenic carbon dynamics in the changing ocean, Ocean Science, 6, 605–614, www.ocean-sci.net/6/605/2010/

Trenberth, K.E.; Dai, A.; van der Schrier, G.; Jones, P.D.; Barichivich, J.; Briffa, K.R.; Sheffield, J.; 2014. Global warming and changes in drought. Nat. Clim. Change 4, 17–22. doi:10.1038/nclimate2067

Tucker, C.J.; Slayback, D.A.; Pinzon, J.E.; Los, S.O.; Myneni, R.B. & Taylor, M.G. 2001. Higher northern latitude normalized difference vegetation index and growing season trends from 1982 to 1999. International Journal of Biometeorology 45: 184-190.

Valentini, R.; Arneth, A.; Bombelli, A.; Castaldi, S.; Cazzolla Gatti, R.; Chevallier, F.; Ciais, P.; Grieco, E.; Hartmann, J.; Henry, M.; Houghton, R.A.; Jung, M.; Kutsch, W.L.; Malhi, Y.; Mayorga, E.; Merbold, L.; Murray-Tortarolo, G.; Papale, D.; Peylin, P.; Poulter, B.; Raymond, P.A.; Santini, M.; Sitch, S.; Vaglio Laurin, G.; van der Werf, G.R.; Williams, C.A.; Scholes, R.J. 2014. A full greenhouse gases budget of Africa: synthesis, uncertainties, and vulnerabilities. Biogeosciences 11, 381–407. doi:10.5194/bg-11-381-2014

Van den Hurk, B.J.J.M.; Viterbo, P. 2003. S.O. Impact of leaf area index seasonality on the annual land surface evaporation in a global circulation model. J. Geophys. Res., 108, 4191, doi:10.1029/2002JD002846.

Van der Molen, M.K.; A.J Dolman, P. Ciais, T. Eglin, N. Gobron, B.E. Law, P. Meir, W. Peters, O.L. Phillips, M. Reichstein, T. Chen, S.C. Dekker, M. Doubková, M.A. Friedl, M. Jung, B.J.J.M van den Hurk, R.A.M. de Jeu, B. Kruijt, T. Ohta, K.T. Rebel, S. Plummer, S.I. Seneviratne, S. Sitch, A.J. Teuling, G.R. van der Werf, G. Wang, 2011. Drought and ecosystem carbon cycling, Agricultural and Forest Meteorology, 151(7, 765-773 DOI: 10.1016/j.agrformet.2011.01.018

Van der Werf, G.R.; Randerson, J.T.; Giglio, L.; Collatz, G.J.; Mu, M.; Kasibhatla, P.S.; Morton, D.C.; DeFries, R.S.; Jin, Y.; van Leeuwen, T.T.; 2010. Global fire emissions and the contribution of deforestation, savanna, forest, agricultural, and peat fires. 1997–2009.. Atmos Chem Phys Discuss 10, 16153–16230. doi:10.5194/acpd-10-16153-2010

Vitousek, P.M.; Aber, J.D.; Howarth, R.W.; Likens, G.E.; Matson, P.A.; Schindler, D.W.; Schlesinger, W.H.; Tilman, D.G.' 1997. Human Alteration of the Global Nitrogen Cycle: Sources and Consecuences. Ecol. Appl. 7, 737–750. doi:10.1890/1051-0761(1997.007[0737:HAOTGN]2.0.CO;2

Vitousek, P.M.; and R. W. Howarth. 1991. Nitrogen limitation on land and in the sea: How can it occur? Biogeochemistry, 13, 87-115.

Volodin, E.M.; Dianskii, N.A.; Gusev, A.V. 2010. Simulating present day climate with the INMCM4.0 coupled model of the atmospheric and oceanic general circulations. Izv. Ocean. Atmos. Phys., 46, 414–431.

Wang, D.; Heckathorn, S.A.; Wang, X.; Philpott, S.M. 2012. A meta-analysis of plant physiological and growth responses to temperature and elevated CO2. Oecologia 169, 1–13. doi:10.1007/s00442-011-2172-0

Wang, Y.; Woodcock, C.E.; Buermann, W.; Stenberg, P.; Voipio, P.; Smolander, H.; Häme, T.; Tian, Y.; Hu, J.; Knyazikhin, Y.; Myneni, R.B. 2004. Evaluation of the MODIS LAI algorithm at a coniferous forest site in Finland. Remote Sens. Environ. 91, 114–127. doi:10.1016/j.rse.2004.02.007

Wanninkhof, R.; Park, G. H.; Takahash.T, Sweeney, C.; Feely, R.; Nojiri, Y.; Gruber, N.; Doney, S.; et al. 2013. Global Ocean Carbon Uptake: Magnitude, Variability and Trends. Biogeosciences, 10, 1983-2000. doi: 10.5194/bg-10-1983-2013.

Wanninkhof, R. 1992. Relationship between wind speed and gas exchange over the ocean, J. Geophys. Res., 97, 7373-7382.

Watanabe, S.; Hajima, T.; Sudo, K.; Nagashima, T.; Takemura, T.; Okajima, H.; Nozawa, T.; Kawase, H.; Abe, M.; Yokohata, T.; Ise, T.; Sato, H.; Kato, E.; Takata, K.; Emori, S.; Kawamiya, M. 2011. MIROC-ESM 2010: model description and basic results of CMIP5-20c3m experiments. Geosci. Model Dev., 4, 845-872.

Westerling, A.L.; Hidalgo, H.G.; Cayan, D.R.; Swetnam, T.W. 2006. Warming and Earlier Spring Increase Western U.S. Forest Wildfire Activity. Science 313, 940–943. doi:10.1126/science.1128834

White, M.A.; Thornton, P.E.; Running, S.W. 1997.. A continental phenology model for monitoring vegetation responses to interannual climatic variability. Global Biogeochem. Cy. 1997, 11, 217–234.

Wieder, W.R.; Cleveland, C.C.; Smith, W.K.; Todd-Brown, K. 2015. Future productivity and carbon storage limited by terrestrial nutrient availability. Nat. Geosci. 8, 441–444. doi:10.1038/ngeo2413

Williams, C.A.; Hanan, N.P.; Neff, J.C.; Scholes, R.J.; Berry, J.A.; Denning, S.A.; Baker, D.F. 2007. Africa and the global carbon cycle. Carbon Balance Manag. 2, 1–13. doi:10.1186/1750-0680-2-3

Woodward FI, Lomas MR. 2004. Vegetation-dynamics- simulating responses to climate change. Biological Reviews, 79, 643-670.

Woodward FI, Smith TM, Emanuel WR. 1995. A global land primary productivity and phytogeography model. Global Biogeochemical Cycles, 9, 471-490.

Woodward, F.I.; 1998. Vegetation-climate feedbacks in a greenhouse world. Philos. Trans. R. Soc. B Biol. Sci. 353, 29–39. doi:10.1098/rstb.1998.0188

Wu, T.; Li, W.; Ji, J.; Xin, X.; Li, L.; Wang, Z.; Zhang, Y.; Li, J.; Zhang, F.; Wei, M.; Shi, X.; et al.2013. Global carbon budgets simulated by the Beijing Climate Center Climate System Model for the last century. J. Geophys. Res., 118, doi:10.1002/jgrd.50320

Xu, L.; Myneni, R.B.; Chapin Iii, F.S.; Callaghan, T.V.; Pinzon, J.E.; Tucker, C.J.; Zhu, Z.; Bi, J.; Ciais, P.; Tømmervik, H.; Euskirchen, E.S.; Forbes,

B.C.; Piao, S.L.; Anderson, B.T.; Ganguly, S.; Nemani, R.R.; Goetz, S.J.; Beck, P.S.A.; Bunn, A.G.; Cao, C.; Stroeve, J.C. 2013. Temperature and vegetation seasonality diminishment over northern lands. Nat. Clim. Change advance online publication. doi:10.1038/nclimate1836

Yang, W.; Tan, B.; Huang, D.; Rautiainen, M.; Shabanov, N.V.; Wang, Y.; Privette, J.L.; Huemmrich, K.F.; Fensholt, R.; Sandholt, I.; Weiss, M.; Ahl, D.E.; Gower, S.T.; Nemani, R.R.; Knyazikhin, Y.; Myneni, R.B. 2006. MODIS leaf area index products: from validation to algorithm improvement. IEEE Trans. Geosci. Remote Sens. 44, 1885 –1898. doi:10.1109/TGRS.2006.871215

Yocom, L.L.; Fulé, P.Z.; Brown, P.M.; Cerano, J.; Villanueva-Díaz, J.; Falk, D.A.; Cornejo-Oviedo, E. 2010. El Niño–Southern Oscillation effect on a fire regime in northeastern Mexico has changed over time. Ecology 91, 1660–1671. doi:10.1890/09-0845.1

Zaehle, S, and Dalmonech, D. 2011. Carbon – nitrogen interactions on land at global scales: current understanding in modeling climate biosphere feedbacks, Current Opinion in Environmental Sustainability, 3:311-320.

Zaehle, S.; Friedlingstein, P.; Friend, A.D. 2010. Terrestrial nitrogen feedbacks may accelerate future climate change. Geophys. Res. Lett. 37, 5 PP. doi:201010.1029/2009GL041345

Zaehle, S.; Friend, A.D. 2010. Carbon and nitrogen cycle dynamics in the O-CN land surface model: 1. Model description, site-scale evaluation, and sensitivity to parameter estimates. Glob. Biogeochem. Cycles 24, n/a–n/a. doi:10.1029/2009GB003521

Zampieri, M.; D'Andrea, F.; Vautard, R.; Ciais, P.; de Noblet-Ducoudré, N.; Yiou, P. 2009. Hot European Summers and the Role of Soil Moisture in the Propagation of Mediterranean Drought. J. Climate, 22, 4747–4758.

Zeng, N. 2003. Glacial-interglacial atmospheric CO2 change - The glacial burial hypothesis, Advances in Atmospheric Sciences, 20(5. 677-673.

Zeng, N.; A. Mariotti, and P. Wetzel. 2005. Terrestrial mechanisms of interannual CO2 variability, Global Biogeochemical Cycles

Zeng, N.; Qian, H.; Roedenbeck, C.; Heimann, M. 2005. Impact of 1998–2002 midlatitude drought and warming on terrestrial ecosystem and the global carbon cycle. Geophys. Res. Lett. 32, n/a–n/a. doi:10.1029/2005GL024607

Zhang, P.; Anderson, B.; Barlow, M.; Tan, B.; Myneni, R.B.; 2004. Climate-related vegetation characteristics derived from Moderate Resolution Imaging Spectroradiometer. MODIS. leaf area index and normalized difference vegetation index. J. Geophys. Res. Atmospheres 109. doi:10.1029/2004JD004720

Zhang, X.; Zwiers, F.W.; Hegerl, G.C.; Lambert, F.H.; Gillett, N.P.; Solomon, S.; Stott, P.A.; Nozawa, T. 2007. Detection of human influence on twentieth-century precipitation trends. Nature 448, 461–465. doi:10.1038/nature06025

Zhang, X.; Friedl, M.A.; Schaaf, C.B.; Strahler, A.H.; Hodges, J.C.F.; Gao, F.; Reed, B.C.; Huete A. 2003. Monitoring vegetation phenology using MODIS. Remote Sens. Environ. 2003, 84, 471–475.

Zhang, Z.; Xue, Y.; MacDonald, G.; Cox, P.M.; Collatz, G.J. 2015. Investigation of North American vegetation variability under recent climate: A study using the SSiB4/TRIFFID biophysical/dynamic vegetation model. J. Geophys. Res. Atmospheres 120, 2014JD021963. doi:10.1002/2014JD021963

Zhou, L.; Tian, Y.; Myneni, R.B.; Ciais, P.; Saatchi, S.; Liu, Y.Y.; Piao, S.; Chen, H.; Vermote, E.F.; Song, C.; Hwang, T. 2014. Widespread decline of Congo rainforest greenness in the past decade. Nature 509, 86–90. doi:10.1038/nature13265

Zhou, L.; Kaufmann, R.K.; Tian, Y.; Myneni, R.B.; Tucker, C.J. 2003. Relation between interannual variations in satellite measures of northern forest greeness and climate between 1982 and 1999. J. Geophys. Res., 108, 4004, doi:10.1029/2002JD002510.

Zhou, L.; Tucker, C.J.; Kaufmann, R.K.; Slayback, D.; Shabanov, N.V.; Myneni, R.B. 2001. Variations in northern vegetation activity inferred from satellite data of vegetation index during 1981 to 1999. J. Geophys. Res., 106, 20069–20083.

Zhu, Z.; Bi, J.; Pan, Y.; Ganguly, S.; Anav, A.; Xu, L.; Samanta, A.; Piao, S.; Nemani, R.R.; Myneni, R.B. 2013. Global Data Sets of Vegetation Leaf Area Index. LAI.3g and Fraction of Photosynthetically Active Radiation. FPAR.3g Derived from Global Inventory Modeling and Mapping Studies. GIMMS. Normalized Difference Vegetation Index. NDVI3g. for the Period 1981 to 2011. Remote Sens., 5, 927-948.